Studies investigating the preparation of solid core drug delivery systems for oral delivery of γ-globulin *via* supercritical fluid processing technology

Adejumoke Lara Ajiboye

A thesis submitted in partial fulfilment of the requirements of the University of Greenwich for the degree of Doctor of Philosophy

November 2018

University of Greenwich

School of Science

Chatham Maritime

Kent, ME4 4TB, UK

DECLARATION

I certify that the work contained in this thesis, or any part of it has not been accepted in substance for any previous degree awarded to me, and it is not concurrently being submitted for any degree other than that of Doctor of Philosophy being studied at the University of Greenwich. I also declare that this work is the result of my own investigations, except where otherwise identified by references and that the contents are not the outcome of any form of misconduct.

Signature (Candidate):

Date:

Signature (Supervisor):

Date:

ACKNOWLEDGEMENTS

I would like to express my gratitude to my supervisors, Dr Vivek Trivedi and Professor John Mitchell for their encouragement, guidance and constructive criticism all through my research work. I would like to acknowledge the help provided by Dr Bruce Alexander towards the CD measurements, along with other members of the School of Science for giving me the opportunity to improve my scientific skills.

I am very grateful to my other research colleagues particularly Uttom Nandi, for making this research journey quite pleasant. Special thanks to Morgane and Teddy for their help with the protein adsorption and desorption studies.

I am thankful for the support provided by my friends and family both financially and emotional encouragement.

ABSTRACT

The rising interest in protein therapeutics has led to the growing research in the development of novel carrier systems particularly for oral delivery. However, several physicochemical and biological barriers pose as a challenge for the use of biomolecules as oral drug therapies. Solid core drug delivery systems (SCDDS) allow for immobilization of these molecules on a solid surface to improve and maintain their stability, followed by the enteric coating to achieve targeted/sustained release. Furthermore, supercritical fluid technology (SCFT) as a processing technique may be explored to ensure that the integrity of immobilized molecules is not compromised during the formulation process. The aim of this research was to develop a SCDDS for the oral delivery of peptide/protein-based drugs, using inorganic/organic particles as core, gamma globulin (γ-globulin) as a model drug, fatty acid (FA) as a shell material and SCFT as the processing method.

The adsorption of γ-globulin was successfully evaluated with experiments involving particles formulated using polycaprolactone (PCL) and Eudragit® S100 (ES100), and commercially obtained silica known as MSU-H, Syloid AL-1 FP (S_{AL}), Syloid XDP-3150 (S_{XDP}), and Syloid 244 FP (S_{FP}). For silica particles, protein adsorption followed the descending trend of S_{FP} > S_{XDP} > MSU-H >S_{AL}. The variations in adsorbed γ-globulin between these particles were largely related to their differences in surface porosity and pore sizes, with minimal effect from a change in pH. On the other hand, electrostatic interactions between the adsorbent surface and the adsorbing molecules were suggested to largely influence γ-globulin immobilization on PCL-ES100 systems. SCDDS was successfully formulated by FA coating of protein-adsorbed S_{FP} and S_{XDP} particles (2:1 silica: FA ratio), and MSU-H (1:1 ratio) *via* melt deposition technique by supercritical carbon-dioxide ($scCO_2$) processing. A pH-induced release of γ-globulin was observed with the SCDDS formulations where protein release was not obtained in simulated gastric fluid but achieved in alkaline media.

CONTENTS

ABBREVIATIONS

Symbol	***Description***
γ−globulin	*Gamma-globulin*
ABPR	*Automatic back pressure regulator*
ALL	*Acute lymphoblastic leukaemia*
API	*Active pharmaceutical ingredient*
BET	*Brauner-Emmett-Teller*
BJH	*Barrett-Joyner-Halenda*
CD	*Circular dichroism*
DPPD	*Recombinant purified protein derivative*
DDS	*Drug delivery systems*
DLS	*Dynamic light scattering*
DSC	*Differential scanning calorimetry*
F1	*Dissimilarity factor*
F2	*Similarity factor*
FAs	*Fatty acids*
Fc	*Fragment crystallisable*
FDA	*Food and Drug Administration*
FTIR	*Fourier Transform Infrared*
G.I.	*Gastro-intestinal*
HIV	*Human immunodeficiency virus*
I.E.P	*Iso-electric point*
IgG	*Immunoglobulin G*

LCP	*Left circularly polarized*
LDV	*Laser Doppler Velocimetry*
M.W	*Molecular weight*
MSN	*Mesostructured nanoparticle*
PB	*Phosphate buffer*
PCL	*Polycaprolactone*
PCL-ES100	*Polycaprolactone-Eudragit® S100*
PEG	*Polyethylene glycol*
PEM	*Photoelastic modulator*
PF127	*Pluronic F127*
PZC	*Point of zero charge*
RCP	*Right circularly polarized*
Rh	*Rhesus*
RV	*Reaction vessel*
S_{AL}	*Syloid AL1-FP silica*
S_{FP}	*Syloid 244FP silica*
S_{XDP}	*Syloid XDP-3150 silica*
SSA	*Specific Surface area*
SCDDS	*Solid core drug delivery systems*
SCF	*Supercritical fluid*
SCFT	*Supercritical fluid technology*
SDS	*Sodium dodecyl sulfate*
SEM	*Scanning electron microscopy*

SMEDDS	*Self-emulsifying drug delivery systems*
TNF	*Tumour necrosis factor*
UV-Vis	*Ultraviolet-Visible*

LIST OF TABLES

List of Figures

Chapter 1

Introduction

Recent advances in conventional medicine have been majorly directed towards the use of biologically originated drugs including proteins and peptides for the treatment of infections and diseases. Although there have been significant successes in this area, the delivery and processing of these molecules still pose a huge challenge to researchers. Due to the fragility of the biologics, most formulations on the market only allow for a parenteral delivery route with frequent administration leading to a number of disadvantages including poor patient compliance [1]. Therefore, there is a need to design novel systems that contribute significantly to the future prospect for the oral delivery of these molecules. This research presents a study investigating the design of delivery systems that allow for the safe passage of protein to the upper intestine without compromising their integrity.

This chapter presents a brief overview on the use of protein therapeutics and their delivery systems, in addition to limitations associated with protein delivery and strategies that can be undertaken to develop novel delivery systems including the use of supercritical fluid technology (SCFT).

1.1. Proteins and Peptides

A peptide is made of a chain of amino acids that are linked together by amide or peptide bonds [2]. The formation of an amide bond is presented in Figure 1.1 which is a covalent chemical linkage between the carboxyl group of one amino acid molecule and the amino group of another [3].

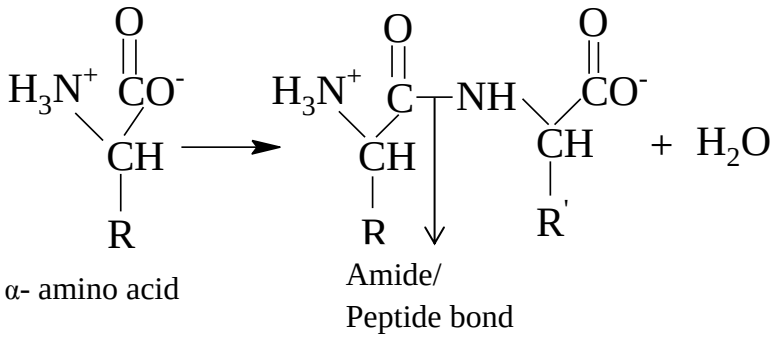

Figure 1.1: Formation of an amide bond [3]

Proteins are referred to as polypeptides that contain more than 50 amino acid units, with most comprising of 100 to 300 amino acid residues [4]. The single amino acid sequence chain is known as the primary structure of the protein. The polypeptide chains further interact with each other by hydrogen bonding between the amide protons and carbonyl oxygens to form secondary structures commonly known as α-helix or β-pleated sheets. The folding of the polypeptide chain to form three dimensional shapes is regarded to as the protein's tertiary structure while the quaternary structure refers to the arrangement of two or more chains that coexist [4].

The properties of peptides and proteins are influenced by its amino acid constituents, particularly on the nature of the side chains [4]. Group of proteins within a cell usually define the cell's health and functions. Proteins are termed according to their vast range of functions in the body, and they can include hormones, antibodies, enzymes, cell structural components, and biological messengers [5, 6]. The three-dimensional structure of the protein plays an important role in sustaining its biological activity; unwanted changes to the protein structure can lead to a loss or reduction of their biological activity [7].

As mentioned above, a polypeptide chain can fold to form a three-dimensional tertiary structure. The folding is stabilized by various interactions including covalent, and hydrogen bonds, electrostatic attractions, and hydrophobic (Van der Waals) interactions. Protein denaturation occurs when these stabilizing bonds are broken leading to the unfolding and random conformation of the protein. Denaturation can occur because of one or more of the following reasons [8, 9]:

- pH: variations to the environmental pH alter the charges on side chains of amino acid residues. This causes a disruption in the electrostatic interactions and hydrogen bonding that help to maintain the structure of protein.
- Organic solvents: many solvents including alcohols can denature proteins by interfering with the hydrophobic interactions between the nonpolar side chains of amino acids. This is because these substances consist of functional groups that can favourably bind with the hydrophobic protein residues.
- Reagents: for example, urea can result in the unfolding of the protein by the preferential formation of hydrogen bonds between the carbonyl group of urea and the amides from the protein backbone contributing to the breaking of intra-backbone hydrogen bonds.

- Detergents: chemicals such as sodium dodecyl sulfate (SDS), link with the nonpolar groups of the protein thereby interfering with the normal hydrophobic interactions and destabilizing its structure.
- Temperature: increase in temperature is associated with a rise in molecular motion leading to an unfolding and refolding in non-native conformation.

Although the fragility of the protein structure poses major drawbacks to its use as a therapeutic agent, there are still many advantages associated with protein therapeutics. The use of protein as a drug therapy is discussed in the section below.

1.1.1. Use of peptides and proteins in medicine

Currently, there are over 40 peptide and protein drugs in the global market with nearly 270 peptides in the clinical phase and 400 peptides in advanced preclinical phase testing [2]. An outline of the existing peptide drug classes with their targets and clinical activity is presented in Table 1.1 below.

Table 1.1: A summary of current peptide drug classes [10]

Target	Clinical activity	Peptide class example
26S proteasome	Multiple myeloma	Bortezomib
ACTH receptor	Diagnostic agent for cortisol syndrome	Cosyntropin
Angiotensin II receptor	Anti-hypertension	Saralasin
Bacterial cell wall synthesis	Antibiotic (Gram-positive)	Vancomycin
Bradykinin B2 receptor	Hereditary angioedema	Icatibant
Calcitonin receptor	Osteoporosis	Calcitonin
Cholecystokinin-B receptor	Diagnostic agent of gastric function	Pentagastrin
Corticotropin releasing hormone receptor	Diagnostic agent for Cushing's or ectopic adrenocorticotropic hormone syndrome	Corticorelin
Cyclophilin protein	Immunosuppressant	Cyclosporin
Follicle-stimulating hormone receptor	Fertility treatment	Urofollitropin
Glucagon receptor	Hypoglycaemia	Glucagon
Glucagon-like peptide 1 receptor	Type 2 Diabetes mellitus	Exenatide
Glucagon-like peptide 2 receptor	Short bowel syndrome	Teduglutide
Glycoprotein (GP) IIb/IIIa	Risk reducing of myocardial infarction	Eptifibatide
Gonadotropin-releasing hormone receptor	Sex hormone-responsive cancers	Buserelin

Glycoprotein 41 Human immunodeficiency virus (GP41 HIV) envelope protein	Anti-HIV	Enfuvirtide
Growth-hormone-releasing hormone receptor	Diagnostic agent for growth hormone deficiency	Somatorelin
Guanylate cyclase 2C	Irritable bowel syndrome	Linaclotide
Histone deacetylase	T-cell lymphoma	Romidepsin
Neurokinin 1 receptor	Oesophageal variceal bleeding	Vapreotide
N-type calcium channels	Chronic pain	Ziconotide
Nucleotide-binding oligomerization domain-containing protein 2	Osteosarcoma	Mifamurtide
Oxytocin receptor	Postpartum bleeding	Carbetocin
Parathyroid hormone receptor	Osteoporosis	Teriparatide
Secretin receptor	Diagnostic aid for pancreatic exocrine dysfunction and gastrinoma	Secretin (human)
Somatostatin receptor	Neuroendocrine tumours	Somatostatin

The growing interest in the use of these molecules as therapeutic agents is because of their biologically favourable properties, which include higher target specificity and affinity, and an enhanced pharmacological potency when compared to other established small- molecular weight drugs usually derived from chemical synthesis. In addition, peptides/proteins are typically well-tolerated and less likely to cause immune responses because of their innate physiological importance [11, 12]. There are also possible financial benefits with respect to novel intellectual property generation because of the uniqueness in structure and functionality of their biological product [13].

Protein therapeutics can be established for different purposes including their use as a substitute for a deficient or irregular protein *e.g.* Insulin for the management of diabetes [13, 14]. Enzyme replacement therapy, where, patients with no or reduced capacity to produce certain enzymes can be given protein therapeutics to perform specific functions efficiently. These include the use of *Lactaid* for patients with primary adult lactase deficiency [15], and *Creon* as a pancreatic enzyme (lipase, amylase and protease) replacement therapy in diseases like cystic fibrosis and pancreatitis [13]. Similarly, haemophiliacs A and B can be treated by substituting blood-clotting factors such as factor VIII (*e.g. Bioclate*) and IX (*e.g. Benefix*) respectively [16, 17].

Protein therapeutics can also be used as supplements to enhance the activity of normal existing protein pathways [13]. One example is the use of recombinant erythropoietin (*e.g. Epogen*, *Procrit*) to stimulate the production of erythrocytes in the bone marrow for patients

suffering from anaemia [13, 18]. An increase in the number of erythrocytes or red blood cells leads to a rise in oxygen levels and the alleviation of associated hypoxic-related symptoms like fatigue [13, 18]. This type of therapy can also be used to provide an entirely new or different function in the body [13]. This includes application of the enzyme L-asparaginase (*Elspar*) in the treatment of paediatric acute lymphoblastic leukaemia (ALL). Asparaginase works by rapidly decreasing the extracellular pools of asparagine by converting it into L-aspartic acid and ammonia, which results in the inhibition of protein synthesis in leukemic cells. As these cancerous cells are highly dependent on this source of asparagine for their growth, inhibition consequently leads to nutritional insufficiency and apoptotic cell death [19].

Protein therapeutics can also act as inhibitors of a molecule or organism [13]. This includes the use of immune-regulator Etanercept (*Enbrel*) in the treatment of inflammatory arthritis and psoriasis [20]. Etanercept is a dimeric fusion protein made of recombinant soluble tumour necrosis factor (TNF) receptor and fragment crystallisable (Fc) region of human immunoglobulin G1 (IgG1). The TNF receptor region of the regulator binds surplus TNF in the plasma, whereas the Fc region of the regulator marks the attached TNF for destruction. The cells of the immune system identify the Fc region then endocytose and destroy the bound molecule [20]. Another area in protein therapy is the use of the biomolecules as carrier systems for other therapeutic agents such as a radionuclide, cytotoxic drug, or protein effector [13]. For example, in the application of B-lymphocyte CD20 surface antigen as a recognition system for the delivery of apoptotic agents (*Tositumomab*) coupled with radioactive iodine-131 (Bexxar I-131) to B-cells for cytotoxic radiation [21].

The applications of protein therapeutics are diverse and include diagnostics (*e.g.* recombinant purified protein derivative (DPPD)) [22], vaccination (*Sipuleucel-T*; *Provenge*) [23], the management of autoimmune diseases (*e.g.* Anti-Rhesus (Rh) immunoglobulin G; *Rhophylac*) [24] and the protection against foreign bodies (*e.g*. *Gardasil*) [25].

The examples previously stated cover a range of applications for protein therapeutics, which is expected to rapidly increase based on the number of biomolecules currently in development as pharmaceutical therapeutics. Nevertheless, there are still important factors to consider for an emerging protein therapy as discussed in section 1.1.2.

1.1.2. Limitations in protein and peptide therapeutics

Although the peptide and protein therapeutic market has advanced significantly in past decades, a number of drawbacks restricting their use still exist. Their high hydrophilicity and physical and chemical instability are some of the limitations encountered in the development of protein therapeutics [26]. Even though some proteins, for example insulin, have been delivered successfully to the body, they are still associated with disadvantages like the need for frequent administration, cold storage requirements, and the invasive technique of administration. Therefore, further developments in their parenteral formulations or exploration into other routes of delivery (*e.g.* oral) is highly important [27]. This section focuses on the oral delivery of protein/peptides and its limitations.

Oral delivery is the favoured route of drug administration for most patients and usually results in the highest level of compliance due to its non-invasive nature, simplicity and ease of administration [28, 29]. Moreover, the development of controlled release systems for therapeutic agents can further improve patient compliance by reducing dosage frequency [30]. An oral delivery of protein therapeutics is not considered a primary choice despite the large number of biomolecules being discovered as pharmaceutical actives every year [31]. This is largely due to issues associated with oral administration, including:

Variable physiological factors of the gastro-intestinal (G.I) tract can have detrimental effects on the stability of the formulation *e.g.* hydrolysis of proteins and peptides because of the acidic environment in the stomach [32]. Furthermore, the presence of digestive enzymes like trypsin, carboxypeptidase and chymotrypsin secreted from the pancreas into the small intestine in the G.I. tract can result in the enzymatic degradation of the ingested therapeutic [32]. The intestinal epithelial membrane also poses a major challenge to the absorption of biomolecules upon oral administration. Drug molecules are normally absorbed either *via* the transcellular or paracellular pathway (as presented in Figure 1.2). The transcellular absorption usually occurs by means of passive diffusion, carrier-mediated transport, or vesicular transport while the paracellular occurs *via* passage through intercellular spaces [33, 34]. The phospholipid nature of the bilayer easily allows for absorption of lipid-soluble molecules whilst preventing the passive diffusion of hydrophilic, charged, and large molecules [35]. Typically, the bulky size and hydrophilic properties of peptides and proteins inhibit them from diffusing through the cell membrane, restricting their transport *via* diffusion through the

paracellular pathway. Similarly, absorption through the intercellular spaces remains limited due to tight junctions in between cells [35, 36].

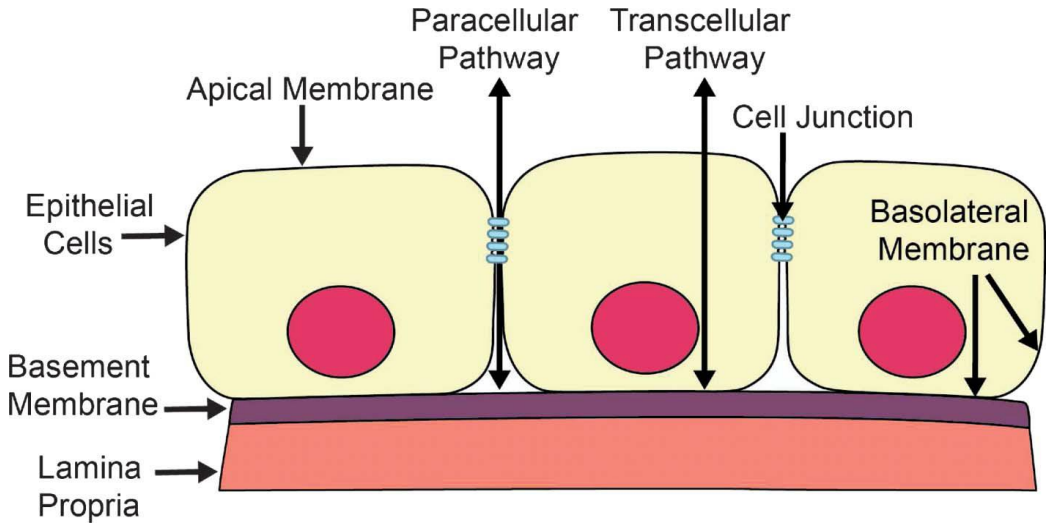

Figure 1.2: Pathways across the epithelial barrier [37].

Another significant limitation to the absorption of protein and peptide drugs after oral administration is the efflux pump known as the P-glycoprotein. It can transport the ingested biomolecules back into the intestinal lumen resulting in a low drug bioavailability [38].

Further to these barriers, the bioavailability of absorbed macromolecules can also be significantly reduced by possible first-pass metabolism that occurs in the liver [2]. Unlike parenteral delivery that allows direct passage to the systemic circulation, drugs absorbed through the intestinal epithelial are primarily directed to the liver *via* the hepatic portal vein. Following transport to the liver, a large proportion of the drug is metabolized by hepatic enzymes thus reducing the amount that emerges to the circulatory system and subsequent target sites [39]. Hence, alternative routes for the oral absorption of proteins and peptides have also been explored including pathways *via* gut-associated lymphoid tissue (*i.e.* Peyer's patches) [2, 40]. The follicle-associated epithelium overlying Peyer's patches is characterized by the presence of specialized M cells that are able to allow for the transcytosis of macromolecules across the lymphatic system. Drug transport through the lymphatic system means that their entry into blood circulation is now directed *via* the thoracic duct and not through the liver. Therefore, hepatic first-pass metabolism will be largely avoided [2, 40]. However, it is worth considering that the ideal physicochemical properties including charge, size, and hydrophobicity that will allow for optimal absorption *via* this pathway are still not

clearly defined in current literature. Additionally, there is conflicting data on the extent to which drug uptake can successfully occur by Peyer's patches [40].

Even though there are numerous obstacles to protein and peptide drug absorption *via* oral administration, still considerable work has been done to overcome these limitations and few of those are discussed in section 1.1.3.

1.1.3. Overcoming limitations in protein and peptide therapeutics

Various approaches have been applied to improve the oral bioavailability of protein/peptide-based drugs over the years which could be classified into the following categories:

- Enzyme inhibitors: One of the major issues with oral administration is the enzymatic degradation which can be overcome using enzyme inhibitors such as aprotinin (*e.g.* *Trasylol*). Aprotinin works by inhibiting serum proteases particularly trypsin, chymotrypsin and plasmin, thereby reducing the enzymatic degradation and increasing bioavailability of the administered drug molecule [41]. Even though enzyme inhibitors have been proven to help improve protein/peptide oral absorption, they are associated with a number of disadvantages. To begin with, they can interrupt the regular absorption of dietary peptides and may prompt toxic shock after the sustained use [42]. It is thought that these inhibitors can also cause the body to escalate the production of proteases, thereby resulting in hypertrophy and hyperplasia of the pancreas. Moreover, these products may also be toxic and damaging to the G.I. tract after prolonged use [43]. Alternatively, a change to the pH can result in enzyme inhibition. Most enzymes in the stomach are only active at low pH while those in the intestines work at a higher pH. Therefore, an increase in pH may inhibit the activity of the enzymes in the stomach whereas a decrease in pH will inhibit the intestinal enzymes [43- 46]. For example, oral intake of antacids such as sodium bicarbonate not only have a temporary inhibitory effect on gastric pH but can also result in the alkali denaturation of pepsin (proteolytic enzyme) present in the stomach at the time of ingestion [44]. This enzyme neutralization effect is however dependent on the extent of pH increase as it has been shown that an optimal point needs to be achieved before denaturation can occur (*e.g.* above pH 4.5 for pepsin) [44].
- Absorption enhancers: The hydrophilic nature of therapeutic proteins/peptides is a known impediment to their absorption which can be improved using absorption enhancers in the formulation [47- 49]. The ideal enhancer should be nontoxic at its

active concentration, allow for a rapid permeation, and its effect on the cells should be reversible [47- 49]. A common example in this category is chitosan. Chitosan is a muco-adhesive, biocompatible polymer that promotes the absorption of hydrophilic drug molecules. The polymer works when protonated by increasing paracellular permeability across the mucosal epithelia, although it is limited by its ability to diffuse across the mucus layer [47- 49].

- Structural modifications: Chemical changes to the structure of the therapeutic biomolecule can help to improve its oral bioavailability. For example, the covalent linkage of polyethylene glycol (PEG) to therapeutic polypeptides, commonly known as PEGylation. This process can result in an increased resistance to digestive enzymes, reduced systemic clearance, and an increased intestinal absorption [50, 51]. Although structural modification is theoretically useful to improve the biopharmaceutical characteristics of a drug, it should not lead to undesirable effects (such as loss of biological activity) on the pharmacologic properties of the drug [52].
- Carrier systems: The use of carrier systems for the delivery of proteins and peptides can allow for targeted transport to specific sites in the G.I. tract, protection against degradation, and controlled release rate [53]. Further examples of drug delivery systems and their use in protein therapy are discussed in section 1.2.

1.2. Drug delivery systems (DDS)

The use of carrier systems, particularly the micro- and nano- scale structures for the delivery of biological molecules has rapidly increased over the years as these can successfully maximize the efficacy of the therapeutic molecules [54]. Examples of DDS that have been studied for the delivery of proteins and peptides are discussed below:

1.2.1 Hydrogels

Hydrogels are three dimensional polymeric networks prepared by chemical or physical crosslinking. Hydrogels are hydrophilic, and have the capacity to imbibe large amounts of water or biological fluid, thus making them attractive for the encapsulation of hydrophilic proteins [55]. There are numerous applications of these systems as biomolecule carriers, *e.g.* studies by Wood, Stone and Peppas showed that hydrogels can be suitable for the oral delivery of biomolecules due to their excellent biocompatibility and encapsulation capacity [56]. Hydrogels can also be physiologically responsive where the swelling can be dictated by the changes in physiological conditions (*e.g.* pH, ionic strength, and temperature) [57].

Vakkalanka, Brazel, and Peppas successfully investigated the synthesis of temperature and pH sensitive copolymer/terpolymer hydrogels using *N*-isopropylacrylamide (NIPAAm) and methacrylic acid (MAA)/ 2-hydroxyethyl methacrylate (HEMA), NIPAAm, and acrylic acid (AA), for the delivery of streptokinase [58]. Regardless of the beneficial properties of hydrogels, the high porosity and water content of these systems means drug release can occur very rapidly thereby restricting the design of controlled release systems [59].

1.2.2 Self-emulsifying drug delivery systems (SMEDDS)

SMEDDS are isotropic mixtures of oil, surfactant, co-surfactant, and the therapeutic molecule which form fine oil-in-water (o/w) emulsions under gentle agitation. Formation of micro/nano- emulsions helps to present the drug in a solubilised form and resulting small droplet size provide large interfacial surface area for absorption of the therapeutic drug. The presence of lipids in the system also helps to improve absorption and consequently results in the enhanced bioavailability of the therapeutic molecule [60]. Other advantages of this system include easy preparation, thermodynamic stability and an increased drug loading capacity [61].

Li, *et al* successfully developed nano-emulsions coated with alginate/chitosan as oral insulin delivery systems. There were significantly prolonged hypoglycaemic effects after oral administration of the coated nano-emulsions compared to subcutaneous insulin. Li, *et al* suggested that this phenomenon may be due to the muco-adhesive properties of the polymer coating which led to a prolonged retention time in the G.I. tract. Although this study showed promising results in terms of protein stability, further work need to be carried out to improve the loading efficiency of protein in these systems [62].

1.2.3 Liposomes

Liposomes are colloidal vesicles made of phospholipid bilayer consisting of unimers comprising hydrophilic head and hydrophobic tail. In an aqueous environment, the bilayer is oriented so that the hydrophobic parts are inside the bilayer while the hydrophilic parts face outwards interacting with water molecules [63- 65]. This carrier system can be used to encapsulate wide range of drugs including cytotoxic drugs, genetic materials, antimicrobial drugs, and proteins, to efficiently deliver them to their target sites [31].

Liposomes have received significant attention as drug carriers due to their ability to improve the permeability of hydrophilic bio-macromolecules across cell membrane, protect and

stabilize labile drugs and provide an opportunity for controlled release [66]. These can also be designed to allow for a triggered release of the loaded drugs in response to specific changes (such as pH and temperature) at their target sites [67]. Gradauer, *et al* designed liposomes-based peptide delivery system that was coated with the muco-adhesive thiomer chitosan to enhance their absorption upon oral administration [68]. The peptide loaded liposomes were coated with either chitosan-thioglycolic acid or an S-protected version of the same polymer. Coated systems were shown to effectively penetrate the intestinal mucus layer. S-protected liposomes provided better permeation and reduction in P-glycoprotein efflux pump activities than the corresponding unprotected thiomer, possibly due to higher reactivity of S-protected thiol groups [68]. The results of this study were quite promising but the use of thiomer in the oral delivery systems need to be further investigated as their muco-adhesive properties can be limited by the natural mucus turnover [69].

1.2.4 Stimuli- responsive polymers

The use of stimuli-responsive polymers in the design of DDS have been explored due to their ability to release encapsulated drugs at the appropriate time and target site in response to specific physiological triggers. The use of these systems can result in more accurate and programmable drug delivery. Stimuli- responsive polymers can include pH, temperature, or light sensitive polymers, and glucose responsive polymers [70]. Other advantages of these polymer-based DDS can include; simple preparation technique (although this may not be seen in all cases), prolonged release of incorporated drug, reduced side-effects, enhanced stability of the incorporated drug, and improved patient compliance [71].

Capurso and Fahmy formulated pH-responsive polymeric micro-particles for the oral delivery of interleukin-10 (IL-10) [72]. The micro-particles were composed of an aqueous gelatine core surrounded by the coating of pH- responsive polymer Eudragit® FS30D. The aqueous core of the micro-particles allowed for the encapsulation of hydrophilic peptides whereas the coating protected the drug contents from the low pH in the stomach. *In vitro* tests showed that the micro-particles retained their encapsulated contents at acidic pH, with a release of the drug at neutral pH. Further *in vivo* tests such as particle bio-distribution and toxicity tests need to be carried out to understand the potential side-effects of these delivery systems [72].

Away from the carrier systems listed above, this research will focus on the design of solid core delivery systems using inorganic particles or polymeric nanoparticles for the oral delivery of proteins.

1.3 Solid core drug delivery systems (SCDDS)

SCDDS involves the immobilization of the therapeutic drug molecule on the surface of a solid, followed by the coating of this drug core to achieve targeted/sustained release [73, 74]. In this work, SCDDS was designed by immobilizing protein molecules onto a solid core made of either inorganic particles or polymeric-composite nanoparticles, followed by enteric coating of the solid core. The immobilization of proteins onto a solid surface has been shown to improve their stability and maintain their biological activity [75- 80]. For example, the adsorption of enzymes on mesoporous silica results in improved thermal stability in comparison to free native enzymes [77]; The denaturation of lysozyme was prevented by immobilizing the molecule onto mesoporous molecular sieves [78]; Immobilization of cytochrome c onto mesoporous molecular sieves led to its retention of its redox activity for several months [80].

As previously stated, this work involves the immobilization of a protein onto a solid core in addition to the enteric coating of the core. The following sections provide brief discussion on the materials and processes involved in the design of the SCDDS.

1.3.1 Silica

Inorganic materials such as carbon, gold, iron oxide and silica have been studied to act as delivery vehicles for therapeutic molecules due to their reduced susceptibility to microbial attack and excellent stability [81]. Mesoporous silica are one of the commonly researched carrier materials because these are readily available, tuneable, non-toxic, and allow for surface functionalization with compounds such as alkoxysilanes/ halosilanes [82, 83]. Silica gel are solid substances comprising porous structures with hundreds of void channels (mesopores) that can absorb or adsorb reasonably large amounts of biomolecules. Their distinctive properties; such as high surface area, large pore volume, and tuneable pore size with a narrow distribution make them readily suitable for various controlled release applications [84- 89].

As presented in the Figure 1.3, silica gel is a polymer that consists of tetrahedral silicon atoms connected through oxygen atoms (siloxane Si-O-Si) with functional hydroxyl (OH) groups on the surface. The surface plays an important role in defining the way silica interacts with the adsorbing molecule which can include the formation of hydrogen, ionic and/or covalent bonds [90, 91].

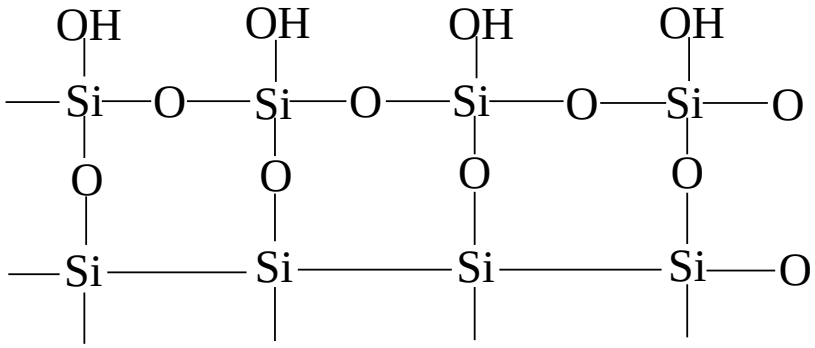

Figure 1.3: Structure of silica gel

Several studies investigating the use of these mesoporous particles for drug delivery have been carried out by various research groups [84- 89]. Examples include: The application of silica-based systems for controlled release drug delivery has been established by Kwon, *et al* [84] and Radin, Chen, and Ducheyne [85]. Klichko, *et al* investigated the use of mesostructured silica for optical drug delivery [86]. These inorganic materials have also been designed into implants for drug delivery [87, 89]. Fu, *et al* demonstrated that mesoporous silica particles can allow the design of non-toxic drug delivery systems (DDS) for the oral delivery route [92]. This research will focus on the design of SCDDS applying silica materials as the solid core.

1.3.2 Fatty Acids (FAs)

FAs are an important component of lipids found in animals, plants and microorganisms. They are known as carboxylic acids attached to long aliphatic chains consisting of carbon atoms typically between 4 and 28. The chain starts with a methyl group and ends with the carbon attached to the carboxylic acid group. Most natural FAs are even-numbered (palmitic, stearic and oleic acids) because of their mode of biosynthesis but odd numbered FAs also exist [93-95]. FAs can be classified into two groups known as saturated and unsaturated [95]. Figure 1.4 shows examples of saturated, monounsaturated, and polyunsaturated FAs.

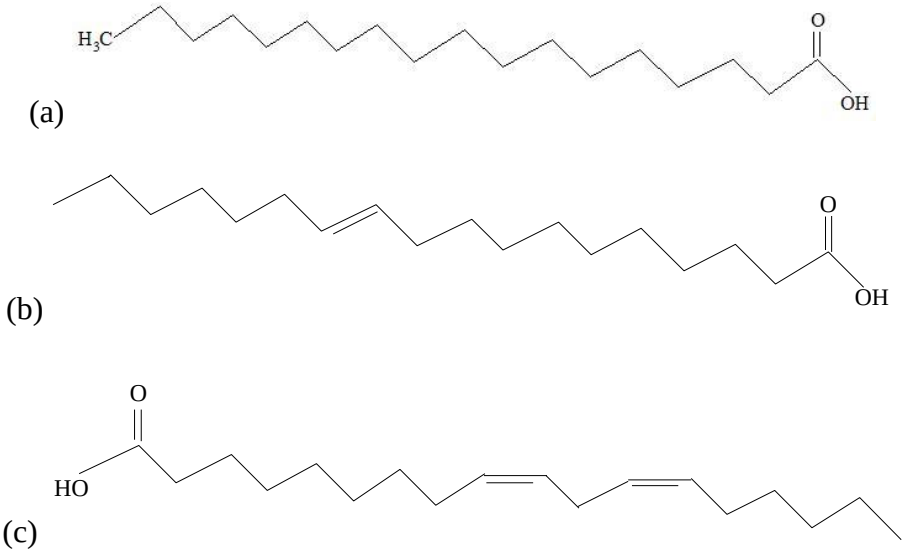

Figure 1.4: Structure of (a) Stearic acid (n-Octadecanoic acid) [saturated FA], (b) Vaccenic acid (*cis*-11-octadecenoic acid) [monounsaturated FA], and (c) Linoleic acid (*cis*, *cis*-9,12-octadecadienoic acid) [polyunsaturated FA].

The carbon-carbon interactions of the hydrocarbon chain for saturated FAs exist as single bonds while those for unsaturated form either one (monounsaturated) or more (polyunsaturated) double bonds [95]. The degree of unsaturation (amount of double bonds) and length of the hydrocarbon chain influences the physical and chemical properties of the FAs. For example, in comparison to their corresponding straight chain FAs, the presence of double bonds in branched chain FAs leads to a reduction in melting point. Also relative to short chain FAs, longer chain acids are much less soluble in aqueous solutions [94, 95].

In the design of SCDDS for this work, the protein-adsorbed core particle will be coated with a selection of saturated FAs. The properties of FAs used in this work are listed in Table 1.2. FAs are commonly used in the pharmaceutical industry including in the design of DDS. Biocompatibility, low toxicity and their inert nature are some of the advantages that make FAs attractive for drug delivery. Moreover, saturated FAs are also capable of providing sufficient enteric coating for targeted delivery to the specific site in the G.I. system [97, 98].

Table 1.2: Properties of FAs used in this study

	Myristic acid	Palmitic acid	Stearic acid
Molecular formula [94, 95]	$C_{14}H_{28}O_2$	$C_{16}H_{32}O_2$	$C_{18}H_{36}O_2$
Molecular weight (g/mol) [94, 95]	228.38	256.43	284.48
Boiling point °C (mm Hg) [96]	250.5 (100)	271.5 (100)	361 (760)
Melting point °C [96]	53 - 54	62 - 63	69 - 72
Density g/cm^3 (°C) [96]	0.8622 (54)	0.8527 (62)	0.847 (70)
Viscosity mPa sec (°C) [96]	5.83 (70)	7.80 (70)	9.87 (70)

1.4 Polymeric nanoparticles

This work aims to investigate the ability of polymeric nanoparticles to act as suitable core materials for the adsorption of protein in the design of SCDDS. This section gives a brief summary on the polymers used in the formation of the nanoparticles.

Nanoparticles are usually defined as particles between 0.1 and 100 nm. They are derived from different types of materials and designed to carry range of substances in a controlled and targeted manner [99]. Nanoparticles including polymeric micelles, dendrimers, and other polymeric nanoparticles are composed of biodegradable polymers and co-polymers. Drug molecules can be entrapped within the particle, physically adsorbed on the surface, or chemically linked to the surface of the particles [54]. Polymeric nanoparticles can allow enhanced stability and protection of the encapsulated drug molecule and provide controlled and targeted delivery [100]. The use of polymeric nanoparticles for the delivery of therapeutic molecules has been widely investigated; Chuang *et al.* successfully designed a pH-responsive nanoparticle for oral insulin delivery using chitosan and poly-γ-glutamic acid conjugated with ethylene glycol tetra acetic acid (γPGA–EGTA) [101]; Campardelli, Reverchon and Della-Porta investigated the use of polymeric nanoparticles for the controlled delivery of proteins by encapsulating bovine serum albumin in particles made of poly (lactic acid) (PLA) and poly (glycolic acid) (PLGA) [102]. Although, these systems show promising results with respect to targeting and preserving the integrity of attached drug molecule but drawbacks such as burst

release are still a significant concern [101-103]. Thus, there is a need to improve the design of these particles to allow for an enhanced controlled release.

1.4.1 Polycaprolactone (PCL)

PCL is a semi-crystalline polyester that is hydrophobic and biocompatible. It is synthesized by the ring opening polymerization of the cyclic monomer ε-caprolactone as shown in Figure 1.5 [104].

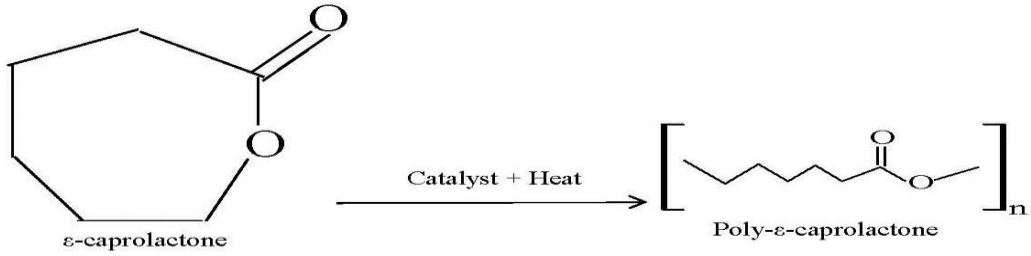

Figure 1.5: Synthesis of Poly-ε-caprolactone

The biodegradability of this polymer makes it attractive to researchers for the design of drug delivery vehicles. PCL is degraded by hydrolysis of its ester linkages under the normal human physiological conditions to give components with minimal or no toxicity. When compared to other polymers (*e.g.* polylactides) the biodegradation of PCL is slow, hence it can be highly suitable for the design of controlled-release delivery systems [105-108]. The glass transition temperature (T_g) of -60 °C and low melting point (59-64 °C) of PCL allows for the easy fabrication of delivery systems at reasonably low temperatures [107]. Furthermore, PCL has an excellent blend compatibility with other polymers which facilitates tailoring of desired properties like degradation kinetics, hydrophilicity, and muco-adhesion. PCL is known to be compatible with synthetic polymers *e.g.* poly ethylene glycol (PEG) and poly ethylene oxide (PEO), and natural polymers *e.g.* starch and chitosan [104, 109, 110].

In the last decades, these polymers have been a key area of interest in the development of controlled DDS particularly for biologics such as proteins and peptides [111]. The delivery systems formulated with PCL or PCL blends have shown to be useful in varied conditions. For example, while developing PCL microspheres for vaccine delivery, Jameela, *et al* showed that PCL has good permeability to proteins [112]. Furthermore, when compared to poly (lactic acid) PLA and poly glycolic acid (PGA), the polymer degrades very slowly and does not give rise to an acidic environment which can negatively affect the antigenicity of the vaccine [112]. Observations by Youan, *et al* provided data demonstrating that PCL delivery

systems are unaffected by simulated gastric fluid. Hence, these systems could give some protection to the encapsulated peptide from proteolytic destruction in the stomach, allowing the entrapped drugs to pass unharmed into the intestine for presentation to the gut-associated lymphoid system [113].

In this work, PCL and PCL-Eudragit® composite particles were designed and their ability to act as solid core for model therapeutic protein was also investigated.

1.4.2 Eudragit®

Eudragit® comprises a series of biocompatible copolymers made by the free-radical polymerization of acrylic and methacrylic acids or their esters. The functional properties of the final copolymer are determined by the choice of acrylic acid or methacrylic acid derivative and their relative ratios. Although, these materials are not biodegradable, they have been widely accepted as materials for the design of DDS owing to rapid clearance from the systemic circulation by the mononuclear phagocytic system [114, 115]. Table 1.3 shows the grades of Eudragit® currently available for the design of drug delivery vehicles [116]. A number of these grades have been successfully investigated for their use as materials for the design of nano/micro-particles/microspheres [117, 118] or enteric coating for DDS [119].

Table 1.3: Eudragit® grades and their physical properties [116]

	Average molecular mass (g/mole)	**Glass transition temperature (°C)**
Eudragit® S 100	~ 125 000	> 130
Eudragit® L 100	~ 125 000	> 130
Eudragit® L 100-55	~ 320 000	96
Eudragit® FS 30 D	~ 280 000	43 (as solid)
Eudragit® NM 30 D	~ 600 000	9 (as solid)
Eudragit® NE 30 D	~ 750 000	6 (as solid)
Eudragit® E 100	~ 47 000	45
Eudragit® RL 100	~ 32 000	63
Eudragit® RS 100	~ 32 000	58

Figure 1.6 presents the chemical structure of Eudragit® and the functional groups.

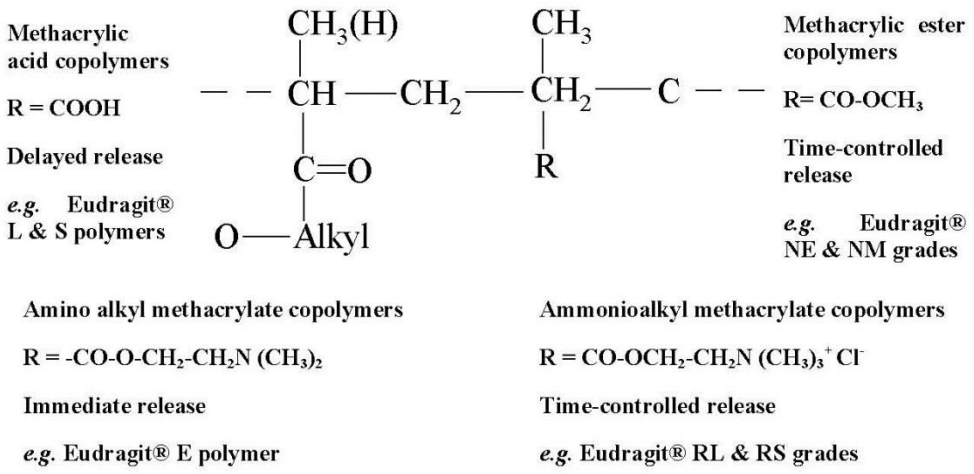

Figure 1.6: Structural unit of Eudragit® polymer and functional groups [116]

A range of anionic Eudragit® grades (*e.g.* methacrylic acid copolymers) are available for the design of enteric drug delivery carriers. These anionic copolymers have carboxyl groups in variable ratios as functional units, for example the ratio of free carboxyl groups to the ester groups is 1:2 for Eudragit® S 100 (ES100). Solubility of the anionic copolymers occurs due to structural changes associated with the ionization of the carboxyl group [114, 116]. For this work, composite nanoparticles were designed using PCL and Eudragit® polymers. ES100 was selected due to its desirable solubility property. ES100 is a methacrylic copolymer that dissolves above neutral pH (≥ 7.0) and is insoluble in acidic medium [116]. This is particularly important in the design of oral enteric formulations as ES100 is not soluble in gastric pH therefore, it can delay drug release in the stomach and protect the loaded/adsorbed contents from the acidic pH. Selective solubility of this polymer at high pH will also mean that it can provide targeted release in intestinal fluid. The design of PCL-Eudragit® composite materials has been established for the encapsulation of drug molecules. For example, Seremeta *et al.* successfully controlled the burst-effect of PCL particles by introducing Eudragit® RS100 polymers into the particulate system [115].

1.5 Supercritical fluids

The need to develop sustainable processes particularly in the production of drug delivery systems has led to the rising interest in the use of environmental friendly solvent alternatives such as ionic liquids, and supercritical or dense phase fluids. A supercritical fluid (SCF) can be defined as a substance above its critical pressure and temperature [120, 121]. Table 1.4 presents examples of common supercritical solvents and their physical properties [122].

Table 1.4: Examples of supercritical solvents and their physical properties [122]

Compound	Critical temperature, T_c (°C)	Critical pressure, P_c (bar)	Critical density (g/cm^3)
Water	374.1	220.5	0.322
Ammonia	132.5	112.8	0.235
Methanol	239.4	81.0	0.272
Ethane	32.2	48.8	0.203
Ethanol	243.0	63.8	0.276
Nitrogen	-147.0	34.0	0.314

SCFs exist as single phase above their critical point with distinctive properties that are unlike those of either liquids or gases under standard conditions. These properties are intermediate to those of liquid and gases *i.e.* gas-like viscosity and diffusivity of the SCF solvent with almost zero surface tension give them excellent transport properties, while liquid-like density provides higher solvent power. It is worth noting that these properties can also be easily tuned by varying pressure and temperature, as opposed to conventional organic solvents which have minimal effect of temperature and remain unchanged with pressure [120, 122].

Carbon-dioxide (CO_2) is one of the most commonly used SCF partly due to its relatively low critical temperature and pressure (T_c = 31.1, and P_c = 73.8 bar) which is ideal for processing thermosensitive materials [122, 123]. In addition, supercritical CO_2 ($scCO_2$) has further advantages of being inexpensive, nontoxic, and non-flammable. Moreover, the retrieval of final products and elimination of CO_2 can be done easily without the need of extra steps [123]. The relationship between temperature, pressure and the formation of SCF can be explained using phase diagrams as presented in Figure 1.7 [123].

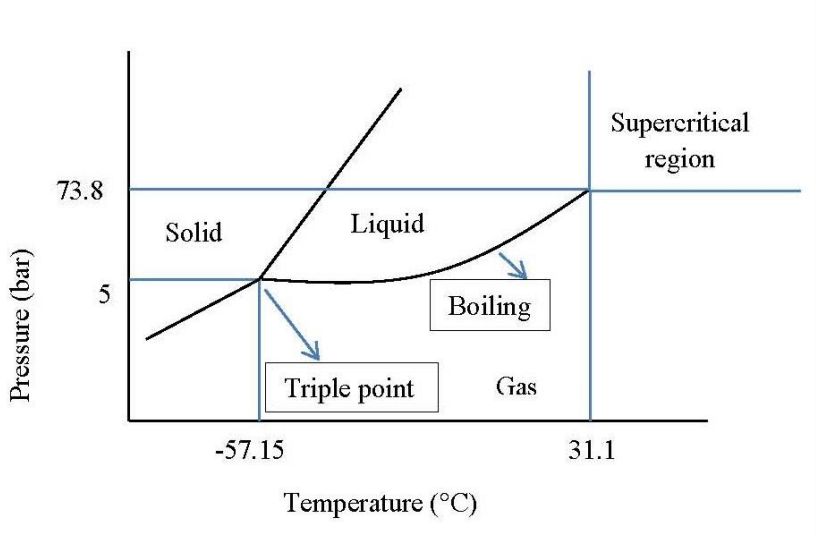

Figure 1.7: Phase diagram for carbon-dioxide

The supercritical region can be found by following the boiling curve on the phase diagram and is easily distinguishable by the lack of distinction between phases unlike a triple point where all three phases (solid, liquid and gas) exist at the same point [123].

Supercritical fluid technology (SCFT) is a novel DDS formation technique that employs the use of a SCF such as $scCO_2$ [124]. Current pharmaceutical applications of SCFT in the development of DDS include: drug extraction and analysis, particle and polymorph engineering, solubility enhancement of a poorly soluble drug, and coating of delivery vehicles [124]. Few of these are briefly discussed in the following section according to the role of SCFs in the process.

1.5.1 Applications of supercritical fluid technology

SCFs particularly $scCO_2$ can be employed as solvent, anti-solvent, or plasticizer to prepare DDS. The following section discusses various application of $scCO_2$ according to its role.

- Rapid expansion of supercritical solution (RESS)

This process utilises SCF as a solvent where the first step entails the saturation of a solute in the SCF at a high pressure, followed by depressurization through a heated nozzle. Depressurization leads to precipitation of the solute resulting in the formulation of small particles with uniform sizes. RESS is a promising technique for the formation of uniform micro-particles, for example Huang *et al* successfully designed ultrafine spherical particles of aspirin using $scCO_2$ as a processing solvent [125]. This technique can be suitable for heat sensitive compounds as the RESS process is usually undertaken at moderate temperatures [125, 126]. In general, RESS produces final products with minimal or no contaminants as it does not require any other organic solvent in the process. This is true mostly for non-polar materials as polar substances are largely insoluble in SCF and may require the addition of a co-solvent [125, 126].

- Gas anti-solvent (GAS) processes

This technique utilises SCF as an anti-solvent and is an alternative encapsulation or recrystallization procedure for materials typically insoluble in SCF. Examples of supercritical processes that apply SCF as an anti-solvent include supercritical anti-solvent fractionation (SAS), gas anti-solvent precipitation (GAS), gas anti-solvent re-crystallization (GASR) and precipitation with a compressed fluid anti-solvent (PCA) [127].

During the anti-solvent process, the material is first dissolved in an organic solvent and then placed in a high-pressure vessel under supercritical conditions [128, 129]. The miscibility of

SCF with the solvent leads to reduction in solvation power of the organic solvent causing either precipitation or recrystallization of the solute. The major benefit of these techniques is that the solvent can also be efficiently eliminated during processing. Additionally, it is a clean and effective single-step process that requires mild operating conditions. Moreover, the solubility power of the SCF can be easily controlled by altering either temperature or pressure, therefore giving room for selective crystallization and control of particle morphology or crystalline forms [128, 129]. The use of $scCO_2$ as an anti-solvent in the formation of polymeric nanoparticles has been successfully studied by Kalani and Yunus [128]. An important limitation of this process is that the SCF must be miscible with the organic solvent, but the solute must be immiscible for it to be successfully applied [129].

- Particles from gas saturated solution (PGSS)

PGSS can be a possible solution to the issues associated with RESS and GAS. PGSS allows particle formation from specific substances by SCF acting as either solute or plasticizer. For example, dissolution of $scCO_2$ in a polymer either swells or lowers its melting point/glass transition temperature. PGSS can also be used for micronisation of suspensions and emulsions [127].

The dissolution of a dense gas in a solute reduces viscosity of the resulting melt. This highly SCF saturated melt can then be depressurized through a nozzle to form particles. Although the diameter of the nozzle is an important factor in controlling the particle morphology, nevertheless altering other processing parameters like temperature and pressure can also assist in controlling the particle size and distribution [123]. This process is particularly useful for polymers which can dissolve large amounts of SCF within their matrix resulting in the reduction of glass transition and/or melting temperatures [126].

This work includes some aspects of PGSS where the final FA coating method to produce SCDDS was performed using a melt deposition technique under $scCO_2$ conditions.

1.6 Gamma globulins (γ-globulins)

γ-globulin was used as a model drug in this work to study the suitability of SCDDS for oral delivery of proteins and peptides. The major protein constituents of blood plasma are albumin, globulins, and fibrinogen which make up about 99% of the total protein constituent [130, 131]. Globulins are globular proteins with relatively high molecular weight (*e.g.* 150-160 kDa for immunoglobulin G). Globulins are primarily classified based on their size and charge and include alpha (*e.g.* Alpha 1-antichymotrypsin), beta (*e.g.* plasminogen) and

gamma globulins (*e.g*. immunoglobulins). Alpha and beta globulins are produced mainly in the liver while γ-globulins are manufactured in the cells of the immune system. Among the three categories, γ-globulins are known to be less mobile in alkaline or electrically charged solutions while alpha is more mobile than the other two [130, 131]. The main role of alpha and beta globulins is in the transportation of enzymes and proteins in the body. On the other hand, γ-globulins largely act as antibody defence against antigen invasion [130, 131].

γ-globulins generally known as immunoglobulins (Ig) are glycoproteins which are produced by lymphocytes and plasma cells. They play a crucial role in eliciting immune response by specifically identifying and binding to antigens such as bacteria or viruses. There are five isotypes of immunoglobulins including IgG, IgM, IgA, IgD, and IgE based on the type of heavy chain found in the molecule *i.e*. gamma in IgG, mu in IgM, alpha in IgA, epsilon in IgE, and delta in IgD. The function of IgG, IgD, IgM, and IgA and IgE is listed in Table 1.5 [132, 133].

Table 1.5: Isotypes of immunoglobulin and their functions [133]

Isotype	Proposed function (s)
IgM	• Primary immune response • Commonly used to diagnose acute exposure to an immunogen or pathogen.
IgD	• Interacts with specific bacterial proteins resulting in B cell stimulation and activation.
IgA	• Essential at protecting mucosal surfaces from virus, toxins and bacteria by direct neutralization or prevention of binding to the mucosal surface • Makes up about 50 % of the protein in colostrum (the ‘first milk’) given to a neonate by the mother.
IgE	• Responsible for hypersensitivity and allergic reactions • Response to parasitic worm infections.
IgG	• Primarily responsible for the recognition, neutralization, and elimination of pathogens and toxic antigens

The differences in function and antigen responses of these antibodies are primarily due to the heavy chain structure variability. IgG is the main serum immunoglobulin with the longest half-life and IgE is present at the lowest concentrations with shortest half-life. The concentrations and half-lives of IgM, IgD, and IgA typically vary between both IgG and IgE [132, 133].

Ig is made of two heavy and two light polypeptide chains comprising of NH_2- and COOH-terminals for variable and constant amino acid regions respectively (Figure 1.8).

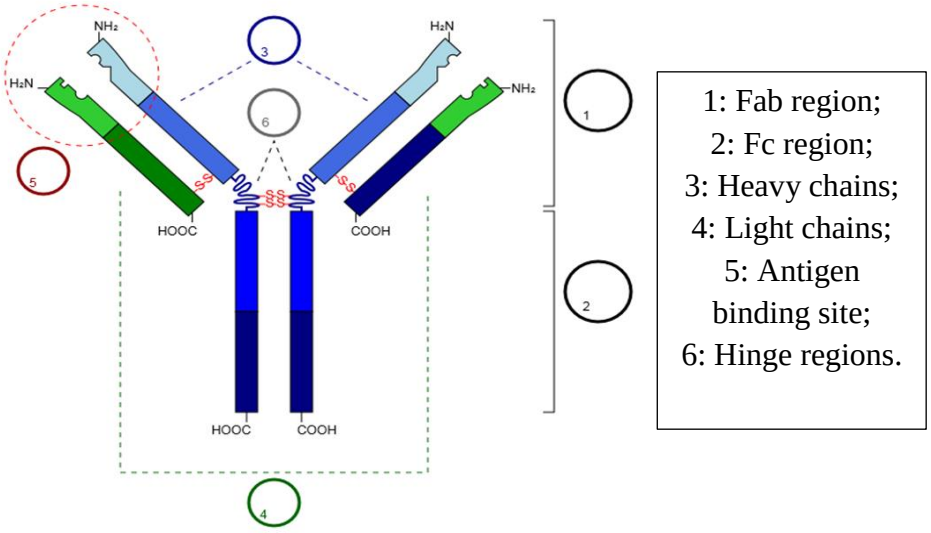

Figure 1.8: Structure of a monomer of immunoglobulin [134]

These heavy and light chains are held together by a mixture of non-covalent interactions and covalent inter-chain disulphide bonds, creating a bilaterally symmetric structure. The variable region of the polypeptide chains forms the antigen binding sites (Fab) while, the constant region of the heavy chains (Fc) is responsible for the binding of the antibodies to various surfaces and Fc receptors. Each Ig monomer holds two antigen-binding sites and is assumed to be bivalent [133, 135- 137].

The flexible hinge (found in IgG, IgA and IgD, but not IgM or IgE) region consist of disulphide bonds that connect the heavy chains which allows the distance between two antigen- binding sites to vary. The total average molecular mass of an IgG molecule is about 150 kDa with molecular masses of approximately 100 and 50 kDa per pair for the heavy and light chain respectively [133, 135-137].

Ig replacement therapy composed of mainly IgG is currently available for patients with primary immunodeficiency diseases involving the humoral immune system, and it is generally administered either intravenously (IVIG) or subcutaneously (SCIG). The appropriate use of Ig therapy can be life-saving but there is high prevalence of adverse reactions mainly due to the complexity of dosage regimen and injection/ infusion site reactions [138-140]. Therefore, there is a need to develop non-invasive routes that can minimise these adverse events.

1.7 Aim and objectives

The oral administration of therapeutic peptides and proteins is proposed to be associated with a number of benefits including eliminating the need for expensive invasive techniques and allowing for a reduced dosage frequency with regards to controlled release systems. However,

certain limitations such as barriers in the G.I. system (proteolytic enzymes, pH gradients, and low epithelial permeability) have a significant impact on the bioavailability of these bio-molecules in the body. The developmental process of bio-formulations is also impeded by the harsh conditions used in commonly known preparation techniques. In response to this problem, this research intends to investigate simple carrier systems (*i.e.* SCDDS) which can provide adequate enteric properties and a degree of steric hindrance to attached biomolecules. Consequently, this should ensure safe passage of the therapeutic peptide/ protein to the intestinal tract upon oral administration. This work will also study the application of novel procedures such as SCFT which can help in addressing few of the problems associated with biomolecular processing and in the development of delivery systems.

The aim of this research is to produce SCDDS using γ-globulin as the therapeutic drug, silica / PCL / PCL-ES100 particles as core material, FAs as a shell material and $scCO_2$ technology as a processing technique.

The objectives for this research are as follows:

a) Identification of suitable organic and inorganic core

Silica particles, PCL and PCL-ES100 particles will be investigated for their suitability to act as the solid core. The polymeric particles will be formulated *via* solvent emulsification evaporation where the development method will also include determination of the effect of temperature and $scCO_2$ on solvent evaporation, and the effect of polymer and surfactant concentration on particle formation.

b) Protein stability

To establish if its conformation will be affected by the adsorption process, changes to the secondary structure of γ-globulin will be measured in relation to time and pH under continuous stirring at room temperature.

c) Determination of adsorption/desorption behaviour of protein

The adsorption of γ-globulin onto selected core particles will be studied as a function of pH and protein concentration. Furthermore, desorption of immobilized γ-globulin molecules will be investigated at simulated intestinal conditions.

d) SCDDS preparation

Selected protein-adsorbed core particles will be coated by saturated FAs applying SCFT as processing technique.

e) *In-vitro* release studies and protein stability

Drug release studies from loaded enteric particles will be investigated at neutral pH, and in simulated gastric and intestinal fluid. The stability of released protein will also be analysed and compared with that of its native molecule.

1.8 Research question/ Hypothesis

This work intends to address the following question; 'What main factors predict the successful design of oral protein/ peptide drug formulations, and how can the application of SCDDS and novel preparation techniques such as SCFT ease this development process'. It is theorized that upon oral administration, the SCDDS will provide physical and chemical stability to the associated macromolecule against the environmental barriers (acidic pH and proteolytic enzymes) of the gastric system. Furthermore, the mild processing conditions associated with the use of SCFT will help to reduce any likelihood of structural changes to the bio-molecule.

Chapter 2

Materials and Methods

This chapter gives details on the list of reagents and standard methods employed to produce and characterise solid core drug delivery systems.

2A. Materials

Commercially purchased chemical reagents used in this work are listed in Table 2.1. All reagents were of analytical grade and used without any further purification. All were stored at room temperature at standard conditions except for γ-globulin which was stored at 4-8 °C. Deionized water was used throughout the study.

Table 2.1: Chemical reagents

Chemical Name	CAS no.	Batch no.	Source	Purity
Pluronic F-127	9003-11-6	027K0034	Sigma-Aldrich, UK	NA
Sodium dodecyl sulfate (SDS)	151-21-3	SLBH8870V	Sigma-Aldrich, UK	98.5%
Tween 80	9005-65-6	11215CC	Sigma-Aldrich, UK	NA
Sodium hydrogen phosphate	7558-79-4	10126289	Alfa Aesar, UK	98.0%
Potassium dihydrogen phosphate	7778-77-0	13C120034	VWR, UK	99.5%
Gamma globulin (γ-globulin) [M.W: 150 kDa; Mixture of IgG (80%), IgM (10%), and IgA (< 10%)]	9007-83-4	SLBQ4091V	Sigma-Aldrich, UK	≥99%
Sodium hydroxide	1310-73-2	1405869	Fisher Scientific, UK	99%
Hydrochloric acid	7647-01-0	1364174	Fischer scientific, UK	37% w/v
Syloid AL-1 FP silica (S_{AL})	7631-86-9	1000255368	Grace Davison, USA	NA
Syloid XDP-3150 silica (S_{XDP})	7546	1000253833	Grace Davison, USA	NA
Syloid 244FP silica (S_{FP})	7631-86-9	1000259186	Grace Davison, USA	NA

Mesostructured silica (MSU-H)	7631-86-9	MKBN6166V	Sigma-Aldrich, UK	NA
Polycaprolactone (PCL), Mw 45 000 Da	24980-41-4	H-001	Shenzhen ESUN, China	99.5%
Eudragit® S 100 (ES100)	NA	B141205008	Evonik Industries, UK	NA
Ethanol	64-17-5	1852958	Fisher scientific, UK	≥ 99.5% v/v
Acetone	67-64-1	1857114	Fisher scientific, UK	≥ 99% v/v
Dichloromethane (DCM)	75-09-2	1722966	Fisher scientific, UK	NA
Palmitic Acid	51-10-3	A0166845001	Acros organics, USA	98.0 %
Stearic Acid	57-11-4	A0215983	Acros organics, USA	97.0%
Myristic Acid	544-63-8	0001349933	Fluka analytical, UK	98.0%
Liquid CO_2	124-38-9	NA	BOC ltd, UK	99.9%

2B. Methods

This section discusses standard methods used throughout this study for the production and characterization of SCDDS.

2.1 Formulation of polymeric nanoparticles

This section describes the techniques and parameters used for the design of nanoparticles using PCL and composite nanoparticles using PCL and ES100 polymer.

2.1.1 Preparation of PCL nanoparticles

The nanoparticles were prepared through spontaneous emulsification technique adapted from the work reported by Prieto and Calvo [141]. The organic phase consisted of a homogenous solution of PCL in acetone and surfactant (Tween 80), while deionized water made up the aqueous phase. A summary of the PCL and Tween 80 components for the different nanoparticle formulations are listed in Tables 2.2 and 2.3 below.

Table 2.2: Overview of PCL formulations with different Tween 80 concentrations

	Formulation A	Formulation B
PCL concentration (%w/w acetone)	**Tween 80 concentration (%w/w emulsion)**	
0.6	0.07	0.14
1	0.07	0.14
2	0.07	0.14
4	0.07	0.14
6	0.07	0.14
8	0.07	0.14
10	0.07	0.14

Table 2.3: Overview of PCL formulations with different Tween 80 ratios

	Formulation C	Formulation D	Formulation E	Formulation F	Formulation G
PCL concentration (% w/w acetone)	**Tween 80 ratios (w/w polymer)**				
0.6	1:1	2:1	4:1	8:1	16:1
1	1:1	2:1	4:1	8:1	16:1
2	1:1	2:1	4:1	8:1	16:1
4	1:1	2:1	4:1	8:1	16:1
6	1:1	2:1	4:1	8:1	16:1
8	1:1	2:1	4:1	8:1	16:1
10	1:1	2:1	4:1	8:1	16:1

Generally, PCL was first dissolved in acetone (14.65 g) in a thermostatic water bath at 40 °C, before the addition of Tween 80 at the appropriate quantities. The contents in the tube were mixed together using a vortex mixer for 1 minute. After vortexing, 35.8 g of warm deionized water (40 ± 2 °C) was added and the tube was placed back on the vortex mixer for 5 minutes in order to form a homogenous emulsion. Solvent extraction was carried out immediately after emulsion was prepared.

2.1.2 Solvent extraction for PCL emulsions

The organic solvent was eliminated from the prepared PCL emulsions either using $scCO_2$ or at atmospheric pressure to produce aqueous nanoparticle dispersions. The resulting

nanoparticles were then collected from the aqueous medium by freeze-drying under vacuum at -55 °C using a ScanVac CoolSafe freeze dryer (LaboGene ApS, Denmark).

a) Supercritical fluid extraction of emulsion (SFEE)

SFEE was employed as a solvent extraction technique for PCL emulsions to allow for the efficient recovery of nanoparticles and possible formation of porous particles due to interactions between PCL and $scCO_2$. The experiments were performed in a Thar Technologies Inc. instrument (USA) as presented in Figure 2.1.

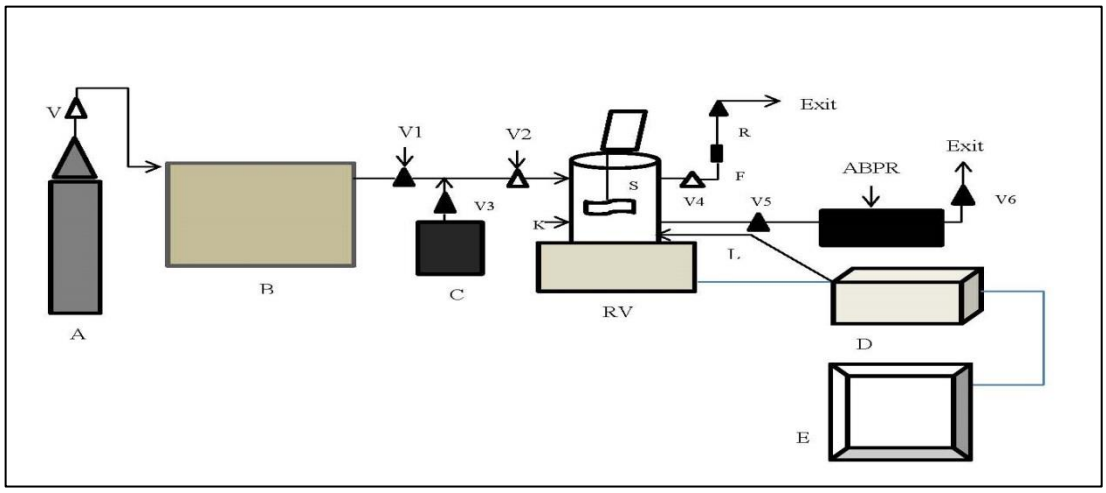

Figure 2.1: Schematic presentation of laboratory SCF instrument

As shown in Figure 2.1, the SCF instrument can be divided into three sections as follows;

1) CO_2 supply comprising of the liquid CO_2 cylinder (A), cooling unit (B), and liquid CO_2 pumping unit (C).
2) Reaction vessel (RV).
3) Control unit consisting of the automatic back pressure regulator (ABPR), controller (D) and display unit (E).

The cooling unit was made up of a thermostatically-controlled water bath to keep the pump heads and the CO_2 from the cylinder at 6 °C throughout its transit. The specifications of the CO_2 pump were as follows; high-pressure P-series pump manufactured by Thar technologies Inc. (USA) with maximum CO_2 flow rate and burst pressure of 50 g/minute and 690 bar respectively.

The RV (Thar Process Inc., USA) was the important part of the SCF instrument as all experiments took place in here. The temperature in the RV was thermostatically

monitored from the controller. The pressure in the vessel, rate of CO_2 entry and exit from the RV was assigned and monitored from the display unit. Additional control over the pressurization/ depressurization process was given by the ABPR attached to the vessel. Solvent extraction in $scCO_2$ was conducted in batch mode, where 25 g of formulated PCL emulsion was introduced in the RV pre-heated to 40 °C (±2 °C). The vessel was then closed, and liquid CO_2 was pumped until a pressure of 100 bar was achieved. The system was left to equilibrate under stirring for 15 minutes before continuously flushing it with fresh CO_2 for 1 hour. Initially, experiments were carried out at controlled $scCO_2$ flow rates of 1, 4 or 10 g/min to determine the solvent extraction efficiency of $scCO_2$. The system was then depressurized at a rate of 6 bar/ minute and the sample was removed from the RV. The acetone extraction efficiency was calculated using the weight difference before and after the procedure.

b) Solvent extraction at atmospheric pressure

Acetone extraction was also carried out at atmospheric pressure to generate efficiency data for comparison with SFEE technique. Experiments were conducted at 40 °C (±2 °C) in a thermostatic water bath (Fisher Scientific, UK) on 25 g of emulsion at a stirring rate of 300 rpm. The evaporation of acetone was determined at time 0, 1, 2, 3, 4 and 24 hours using weight difference similar to SFEE.

2.1.3 Preparation of PCL-ES100 nanoparticles

Like the preparation of PCL particles, aqueous dispersions of PCL-ES100 nanoparticles were prepared by solvent extraction of nano-emulsions. A summary of the polymer components for the prepared emulsions are listed in Table 2.4 below.

Table 2.4: Overview of PCL-ES100 emulsions

PCL:ES100 ratios	Amount of PCL (mg)	Amount of ES100 (mg)
1:2	50	100
1:3	50	150
1:4	50	200
1:5	50	250

In brief, required amounts of PCL and ES100 were first dissolved separately in 2 mls of dichloromethane (DCM) and ethanol respectively. This was followed by mixing of the

solutions by vortexing for 30 seconds after the addition of 0.2 ml of deionized water. After vortexing, the polymer suspension was added to 25 mls of ethanol in a beaker under stirring at 350 rpm and left to equilibrate for 120 seconds. Lastly, 25 mls of deionized water was added to the beaker of polymer suspension and ethanol. The resulting emulsion was left to further equilibrate under stirring at 350 rpm for 10 minutes. It was then transferred to a thermostatic water bath at 40 °C for approximately 8 to 12 hours to allow for the evaporation of the organic solvents (ethanol and DCM). Similar to the preparation of PCL nanoparticles, removal of the organic phase resulted in aqueous dispersion of PCL-ES100 composite nanoparticles. The particles were then recovered from the aqueous medium by freeze-drying as described in section 2.1.2.

2.2 Identification and characterization of core particles

Formulated PCL, PCL-ES100 nanoparticles and commercially purchased silica particles (Table 2.1) were characterized as follows to determine their suitability for the adsorption of γ-globulin.

2.2.1 Particle size and zeta-potential determination

The average particle sizes and polydispersity index (PDI) of PCL and PCL-ES100 particles were determined by dynamic light scattering using the Zetasizer Nano-ZS (Malvern Instruments Ltd, UK). The back-scattering detection was set at an angle of 175°. Aqueous dispersions obtained after organic solvent extraction were diluted in deionized water (1 in 4) and measurements were carried out in triplicate at room temperature (25 °C). The mean particle size was the average of three independent measurements.

The surface charge of the formulated particles was also determined by measuring the zeta potential (ζ-potential) of the aqueous nano-dispersions using Zetasizer Nano-ZS at 25 °C. The measurements were carried out using a folded capillary cell in triplicate on the same samples used for particle size measurements.

2.2.2 Specific surface area, pore size and pore volume determination

Experiments for Brunauer-Emmett-Teller (BET) specific surface area (SSA), pore size, and pore volume analysis were carried out on a Gemini 2380 instrument (Micromeritics Instrument Corporation, UK). BET surface area analysis was carried out on all core particles (silica and polymeric) using nitrogen sorption. The samples were degassed prior to the

measurements to get rid of any moisture or adsorbed gases. 30-60 mg of particles were weighed in the sample tube and degassed with nitrogen at 100 °C for silica and at 40 °C for PCL and PCL-ES100 for approximately 12 hours. Sample and reference tubes were then placed firmly inside the Gemini 2380 instrument and dipped in liquid nitrogen. The air in the tubes was displaced at the rate of 50-100 mmHg/min for 5 minutes, and full adsorption and desorption isotherms were obtained at relative pressure (P/Po) from 0.05 to 1.

The SSA of the particles was calculated with BET theory (equations 2.11 and 2.12) [142, 143] as described below using the isotherm adsorption/desorption data;

$$\frac{1}{\left[V(\frac{Po}{P}-1)\right]} = \frac{C-1}{VmC} \times \frac{P}{Po} + \frac{1}{VmC} \qquad \text{Equation 2.11}$$

Where, P= partial vapour pressure of adsorbate gas in equilibrium with surface at 77.4 K (boiling point of nitrogen) in pascals, Po= saturated pressure of adsorbate gas, in pascals, V= volume of gas adsorbed at standard temperature and pressure (STP), Vm= volume of gas adsorbed at STP to produce an apparent monolayer on the sample surface, in millilitres, and C= BET constant that is related to the strength of adsorption of the adsorbate gas on the powder sample.

A linear plot of 1/ [V (Po/P-1)] against P/Po results into the slope equal to C - 1/VmC and the intercept of 1/VmC as determined by linear regression analysis. The value for Vm is generated using these values, and SSA is calculated as shown in the equation below [143];

$$SA = \frac{Vm \times N \times a}{m \times 22400} \qquad \text{Equation 2.12}$$

Where, SA= specific surface area (m^2/g), N= Avogadro constant, a= effective cross-sectional area of one adsorbate molecule (m^2), m= mass of the sample (g), and 22400= volume occupied by one mole of the adsorbate gas at STP (ml).

Additionally, using the nitrogen sorption isotherm, the pore volume and distribution were determined by Barrett, Joyner and Halenda (BJH) model. BJH model uses the Kelvin equation (equation 2.13) to relate the amount of adsorbate gas removed from pores of the sample when the relative pressure (P/Po) is decreased from a high to low value [144].

$$\text{Pore radius} = \frac{4.15}{\log\left(\frac{P}{Po}\right)} + 3.54 \times \left(\frac{-5}{\ln\left(\frac{P}{Po}\right)}\right)^{0.333} \qquad \text{Equation 2.13}$$

2.2.3 Attenuated total reflectance- Fourier transform infrared (ATR-FTIR) spectroscopy

The ATR-FTIR spectra of core particles (silica and polymeric) were obtained using a Spectrum Two FTIR spectrometer (Perkin Elmer, UK). Approximately 1 to 2 mg of the particles were spread uniformly on the surface of a single reflection horizontal ATR accessory with a zinc selenide (ZnSe) crystal, and adequate pressure was exerted on the sample using the pressure-arm to ensure optimal contact. The spectra were collected from 4000 – 400 cm^{-1} range in transmission mode. Approximately 16 scans were collected for each spectrum with a spectrum resolution of 8 cm^{-1}.

2.2.4 Scanning Electron Microscopy (SEM)

SEM was performed in order to determine the shape and surface morphology of the core particles. SEM analysis was carried out using a Hitachi SU8030 microscope (Hitachi High-Technologies, UK) with an emission gun as its electron source, and resolution of 1.1 nm and 0.8 nm at 1 kV and 15 kV respectively. Approximately 1 mg of sample was placed on a SEM stub using a carbon adhesive and the extra loose particles were removed by an air blower. The sample was then coated with chromium under vacuum for approximately 5 minutes. Thereafter the stub was mounted onto the sample holder and placed inside the microscope for the collection of micrographs. Measurement parameters such as probe current, accelerating voltage, detector type (lower or upper), and working distance (distance between the stubs to the electron beam) were adjusted according to each sample to obtain the required micrograph.

2.2.5 Differential Scanning Calorimetry (DSC)

Thermal analysis for formulated polymeric nanoparticles was carried out using DSC Q2000 instrument (TA Instruments, UK) under nitrogen gas conditions. 3-5 mg of sample was placed in an aluminium pan which was then sealed using a crimper. The sealed pans were placed inside the DSC instrument and heated from 25 to 200 °C at a rate of 10 °C per minute. The thermo-grams obtained were analysed by Star Evaluation software.

2.3 Stability studies for γ-globulin

The stability of γ-globulin was measured by either monitoring the change in its secondary structure *via* CD spectroscopy or the absorption of UV-Vis by their peptide bonds *via* UV-Vis spectroscopy. This was to ensure that the integrity of the protein will not be compromised

during the adsorption process. Phosphate buffers of pH 5, 6, 7.4 and 9 were used to prepare 0.01 and 0.1 mg/ml concentrations of γ-globulin and stirred in a 10 ml volumetric flask at 250 rpm for 5 hours. UV-Vis and CD analysis were carried out after collecting samples at 0, 1, 2, 3, 4 and 5 hours to study the conformational changes due to continuous stirring at room temperature (23 ± 2 °C).

2.3.1 Preparation of phosphate buffer solutions

Phosphate buffers with a range of pH values between pH 5 and pH 9 were selected to better understand the effect of pH on γ-globulin immobilization onto core particles. The buffers were prepared by mixing 0.133 M disodium hydrogen phosphate (Na_2HPO_4) and 0.133 M potassium hydrogen phosphate (KH_2PO_4) as described in Table 2.5 [145]. The pH was adjusted when necessary using small aliquots of either hydrochloric (HCL) or sodium hydroxide (NaOH).

Table 2.5: Phosphate buffer preparation [145]

pH	Na_2HPO_4 (ml)	KH_2PO_4 (ml)
5	2.0	98.0
6	12.0	88.0
7.4	77.4	22.6
9	95.0	5.0

2.3.2 UV-Vis spectroscopy

UV-Vis analysis on γ-globulin solutions was performed with a Cary 100 UV-Vis spectrometer (Agilent Technologies, UK). Protein samples (0.1 and 0.01 mg/ml) were prepared in phosphate buffer at the desired pH and monitored for 5 hours using UV-Vis spectroscopy. Analysis was carried out using a matched pair of quartz cuvette of 10 mm optical path length. The spectra were recorded in the range of 200- 800 nm wavelength at 20 °C in order to collect absorbance values at 204 and 278 nm. All experiments were carried out in triplicate.

2.3.3 CD spectroscopy

Using a Chirascan qCD spectrometer (Agilent Technologies, USA), the CD spectra for γ-globulin solutions was obtained to study their secondary structure. 0.1 mg/ml protein solution was prepared in phosphate buffer at the desired pH. Analysis was carried out with a matched pair of rectangular quartz cells of 1 mm optical path length under nitrogen gas conditions. The

spectra of dissolved protein and matching fresh buffer solution were recorded as a measurement of four repeats in the range of 180-260 nm wavelengths at 20 °C with a time per-point of 2.5 seconds. The data for the protein was obtained by subtracting the spectrum of the buffer from that of the protein solution.

2.4 Iso-electric point (IEP) determination

The zeta-potential *vs* pH profiles of appropriate samples were obtained by performing titration experiments with a Malvern MPT-2 autotitrator (Malvern Instruments Ltd, UK). The IEP of γ-globulin, point of zero charge for pure silica and γ-globulin-adsorbed silica particles were determined at 25 °C using 0.3 M NaOH and HCl as titrants. 0.1% solutions/suspensions of γ-globulin/core/protein-adsorbed particles were prepared in water, and the samples were stirred for the whole duration of the experiment. Zeta-potential values were mostly measured between pH 1 to 12. The pH range and pH increments (between 1 and 2) were assigned to the instrument. The volume of acid or base needed to achieve the required pH value was calculated automatically by the titrator before taking a measurement. IEP was determined by plotting a graph of pH against obtained zeta-potential values.

2.5 Adsorption studies for γ-globulin

This section details standard methods used for the adsorption of γ-globulin onto suitable core particles (commercially purchased silica and formulated polymeric particles).

2.5.1 Maximum γ-globulin adsorption studies

The adsorption of γ-globulin on silica particles were performed at pH 5, 6, 7.4 and 9 while protein immobilization on PCL and PCL-ES100 systems was carried out in pH 5 and 6 phosphate buffer. Experiments were limited to pH 5 and 6 for polymeric systems due to their reduced stability at higher pH values. The protein solutions (0.5- 24 mg/ml) were prepared using phosphate buffers at the required pH (Table 2.5) and 10 ml of each solution was transferred into a volumetric flask. The specific amount (50- 400 mg) of core particle was then added to each flask and the contents were stirred at 250 rpm at room temperature (23 ± 2 °C). The experiment was limited to four hours in order to protect the integrity of the protein. After the specified time limit (4 and 2 hours for silica and polymeric systems respectively), the supernatant was collected, filtered and evaluated by UV-Vis analysis. The maximum amount of γ-globulin adsorbed on the particles (mg/g) was calculated as follows;

Provided there were no deviations from Beer-Lambert's law, the amount of γ-globulin in a specific volume (mg/ml) at time, t, was calculated from equation 2.14, which is derived from a linear regression plot of absorbance at 278 nm *vs* concentration of a set of known γ-globulin solutions (0.01 to 0.8 mg/ml).

$$y = 1.1189x + 0.0192 \qquad \text{Equation 2.14}$$

Where, y = absorbance at 278 nm, 1.1189 = slope, x = protein concentration (mg/ml), and 0.0192 = intercept.

The quantity of adsorbed protein (mg/g) was calculated using the following equation;

$$[C - Co] \times V \div A \qquad \text{Equation 2.15}$$

Where, C = initial protein concentration (mg/ml), Co = protein concentration (mg/ml) at time, t, V = volume of the sample (ml), and A = amount of adsorbent (g).

Following surface adsorption, freeze-dried γ-globulin-adsorbed particles were prepared using core particles at conditions that allowed for maximum γ-globulin immobilization. Protein solutions of 0.5, 1, 4, and 10 mg/ml concentration were prepared for γ-globulin adsorption on S_{AL}, PCL-ES100, MSU-H, and S_{XDP}/ S_{FP} respectively in phosphate buffer at the required pH. Amount of core particles as specified in section 2.5.2 was added to each of these solutions and the mixture was stirred at 250 rpm for 2 to 4 hours at 23 ± 2 °C. After the required time, particles were separated from the medium by centrifugation at 3780 rpm for 5 mins. The supernatant was decanted and the protein-adsorbed particles were freeze dried at -55 °C under vacuum using a ScanVac CoolSafe freeze dryer (LaboGene ApS, Denmark). The freeze-dried protein-adsorbed particles were further using BET and ATR-FTIR as described in section 2.2.2 and 2.2.3 respectively.

2.5.2 Kinetic adsorption measurements

The rate of protein adsorption against time was determined for each type of core particle at the concentration which resulted in maximum γ-globulin adsorption. Measurements were carried out using 0.5, 1, 8, 10, and 18 mg/ml γ-globulin concentrations for S_{AL}, PCL-ES100 (1:3 ratio), MSU-H, S_{XDP}, and S_{FP} particles respectively at pH 6 and 7.4 for silica particles and pH 5 for PCL-ES100. In eight separate volumetric flasks of 10 ml capacity, the protein solutions and required amounts of particle (50 mg PCL-ES100, 200 mg MSU-H and 400 mg

$S_{AL}/S_{XDP}/S_{FP}$) were stirred at 250 rpm and UV-Vis analysis was taken for a period covering 2 hours for PCL-ES100 and 4 hours for all silica particles using time points of 15, 30, 45, 60, 90, 120, 150 and 240 minutes. The experiments were conducted at room temperature (23 ± 2 °C) and absorbance values were recorded in triplicate. The amount of protein immobilized on the particles (mg/g) was calculated using Equation 3.12 and was plotted against time (minutes).

2.6 Drug release studies for uncoated particles

Protein release studies for uncoated γ-globulin-adsorbed core particles were performed at two different pH environments to understand the effect of pH on the rate of release. Experiments were carried out at 37 ± 2 °C in a temperature-controlled water bath in simulated intestinal fluid (SIF/ phosphate buffer pH 6.8) and in phosphate buffer pH 7.4 with or without surfactant. The SIF was prepared as described in section 2.6.1.

A fixed quantity of freeze-dried γ-globulin-adsorbed particles [100 mg for S_{FP} and S_{XDP}, 200 mg for MSU-H, and 250 mg for PCL-ES100 (1:3 ratio)] was placed into a beaker containing 20 to 50 mls of either SIF/ pH 7.4 buffer alone or buffer and 0.1% surfactant [sodium dodecyl sulfate (SDS)/Tween 80/pluronic F-127 (PF127)] . The contents were stirred at 250 rpm, and the amount (mg/ml) of γ-globulin desorbed from the core particles was determined by UV-Vis analysis after 5, 15, 30, 45, 60, 90, 120, 150, and 240 minutes for silica particles, and at 1, 2 and 3 hours for PCL-ES100 system. Approximately 4 mls of sample was removed from the beaker at each time-point and filtered before placing it into the spectrophotometer for analysis. The total desorption media volume was kept constant by the addition of 4 ml of fresh buffer after every withdrawal. All experiments were conducted in triplicate.

CD analysis of desorbed protein from the core particles was also carried out as per the method described in section 2.3.3 to establish the integrity of the secondary protein conformation.

2.6.1 Preparation of simulated intestinal fluid

SIF (phosphate buffer pH 6.8) was prepared by adding 50 mls of 0.2 M monobasic potassium phosphate and 22.4 ml of 0.2 M NaOH solutions in a 200 ml volumetric flask. Deionized water was used to make up the volume to 200 ml [145].

2.7 Coating of protein-adsorbed silica particles

The coating of γ-globulin_adsorbed silica particles was carried out in $scCO_2$ *via* the deposition of fatty acid melt onto these particles. The experiments were carried out in a RV (Thar Process Inc., USA) using parameters determined by Trivedi *et al* [73]. FAs and parameters used for this experiment are listed in Table 2.6.

Table 2.6: Parameters for particle coating [73]

Fatty acid	Pressure (bar)	Temperature (˚C)	Time (min)
Myristic acid (MA)	100	43	15
Palmitic acid (PA)	150	53	15
Stearic acid (SA)	150	60	15

For each coating experiments; a mixture of freeze-dried γ-globulin_adsorbed particles and FA (2:1 ratio for S_{FP} and S_{XDP}, 1:1 ratio for MSU-H) was placed in a beaker and introduced into the high-pressure vessel. Liquid CO_2 was introduced inside the cell by a high-pressure pump until the pre-determined pressure value (100 – 150 bar) was attained. The temperature of the vessel was maintained at 43- 60 °C depending on the FA. The contents of the beaker were left stirring at 100 rpm for the duration of the experiment (15 minutes). The system was depressurized after 15 minutes at a rate of 8 bar per minute and sample was removed from the vessel.

2.7.1 Drug release studies for coated particles

In-vitro release studies of γ-globulin from FA coated S_{FP}, S_{XDP}, and MSU-H particles were carried out in simulated gastric fluid [(SGF/ 0.1M HCl) pH 1.2], SIF (pH 6.8) and phosphate buffer pH 7.4. Additional experiments were performed in SGF to investigate the enteric properties of the shell formulation. Due to the sensitivity of γ-globulin and the small particulate nature of the formulated SCDDS, the conventional USP protocol for delayed release preparations was difficult to use. Therefore, the method was slightly altered and two beakers were used for the separate pH conditions instead of one. The required amount of SCDDS formulation (200 mg for S_{FP} and S_{XDP}, and 400 mg for MSU-H) was taken in two beakers containing 50 mls of 0.1% of PF127 in SGF/SIF/pH 7.4 buffer. Beaker A contained the SGF while beaker B had either SIF or phosphate pH 7.4 buffer. The contents of beaker A were stirred at 100 rpm for 2 hours before switching to beaker B. The readings were recorded

after 15, 60 and 120 minutes for beaker A and after 135, 180, 240, 360, and 420 minutes for beaker B. Approximately 4 mls of sample was removed at each time-point and filtered for UV-Vis analysis. The total release media was kept constant by replacing with 4 mls after each withdrawal. The experiments were carried out in triplicate in a thermostatic water bath at 37 ± 2 °C.

CD spectra for released protein molecules were carried out as described in section 2.3.3.

2.8 Protocol for determination of dissimilarity/ similarity factors

F1 (dissimilarity factor) and F2 (similarity factor) contrast was made between control (uncoated particles) and various coated preparations in both SIF and at pH 7.4. The following equations were used to obtain the required data for F1 and F2 [146];

$$F1 = \left\{\frac{[\sum |R_t - T_t|]}{[\sum R_t]}\right\} \times 100 \qquad \text{Equation 2.16}$$

$$F2 = 50 \times \log\{\left[1 + \left({}^{1}/_{n}\right)\sum (R_t - T_t)^2\right]^{-0.5} \times 100\} \qquad \text{Equation 2.17}$$

Where n = number of time points, R_t = % active pharmaceutical Ingredient (API) dissolved of reference product at time point x, T_t = % API dissolved of test product at time point x.

Chapter 3

Polymeric particle formulation and characterization of core particles

This section discusses the formulation and characterization of polymeric nanoparticles along with the physico-chemical analysis of commercially purchased silica particles.

3A. Polymeric particle formulation and characterization

The following sections provide a summary on the formulation of polymeric particles *via* solvent extraction of emulsions. The influence of processing parameters (*e.g.* polymer and surface concentration) on the preparation of nanoparticles is discussed with respect to particle size, size distribution and surface charge. Further physico-chemical characterization of the formulated particles *via* SEM, BET, and FTIR are also presented in this section.

3A.1 Aims and Objectives

The need to improve targeted delivery of therapeutic biomolecules into the body has led to an increased interest in the development of various DDS including polymeric nanoparticles. The adsorption/encapsulation of drug molecules on/in polymeric nanoparticles can provide enhanced stability to the associated drug and a controlled delivery to target organs [100]. Therefore, for the immobilization of γ-globulin, this work aimed to prepare polymeric particles using PCL alone or in a combination with ES100 polymer. In this study, spontaneous emulsification technique was employed as a processing technique for the formulation of nano-emulsions. Subsequently, aqueous particles were recovered after extraction of the organic solvent from the prepared biphasic system. The objectives of this work were to; (i) identify the ideal parameters (i.e. polymer and surfactant concentration) for the preparation of emulsions, (ii) establish a suitable technique for the extraction of organic solvent particularly focusing on the use of $scCO_2$, and (iii) physico-chemical characterization of formulated nanoparticles.

3A.2 Experimental

The methods for the preparation of PCL emulsions and extraction procedures are detailed in sections 2.1.1 and 2.1.2 respectively. PCL-ES100 particles were prepared as described in section 2.1.3. Procedures for particle size and zeta potential determination of aqueous particle dispersions are detailed in section 2.2.1. The surface characteristics of formulated polymeric particles were determined by nitrogen sorption measurements as described in section 2.2.2.

The method for SEM analysis and ATR-FTIR is detailed in sections 2.2.4 and 2.2.3 respectively. In addition, to further understand the interactions between PCL and ES100, thermal analysis was carried out on composite systems using DSC as detailed in section 2.2.5.

3A.3 Introduction

In spontaneous emulsification, droplet formation can occur by the addition of two immiscible or partly miscible liquids that are not in equilibrium typically without the excessive need of external energy (mechanical or thermal) [147]. The formation of nano-emulsions *via* spontaneous emulsification mechanism using a water-miscible solvent is an established method that allows for the generation of nano-sized droplets [148]. Nano-emulsions consist of droplet sizes ranging between 100 nm to 600 nm. They can be prepared using a small surfactant concentration and typically exhibit low oil-water interfacial tensions. The choice of organic and aqueous phases in spontaneous emulsification determines the droplet size and size distribution which depends on variables including bulk viscosity and surfactant concentration [148 - 150]. In this work, the organic phase consisted of a homogenous solution of the polymer in a water-miscible solvent with or without surfactant which is mixed with the aqueous phase to produce nano-emulsions.

Although emulsification of polymer mixtures is known to be an efficient method, particle recovery from resultant dispersion with conventional solvent extraction processes can lead to the presence of solvent residues and agglomerates, and lack of control on particle size and distribution [151]. Solvent extraction is typically performed by evaporation at atmospheric pressure or under vacuum at temperatures near or equal to the boiling point of the associated solvent. The extraction of organic solvent from the emulsion results in the formation of aqueous dispersions of the nanoparticles which can then be recovered by either centrifugation and/or evaporation of the aqueous vehicle [152]. In this work, polymeric nano-emulsions were formulated by spontaneous emulsification followed by organic solvent extraction at atmospheric pressure or using $scCO_2$. At first, the efficiency of the solvent extraction process at atmospheric or supercritical conditions was investigated, and then the effect of parameters including polymer and surfactant concentration on the particles' hydrodynamic diameter, PDI and zeta potential was also determined for both PCL and PCL-ES100 particles.

3A.4 Results and discussion

This section discusses the results obtained for the preparation and characterization of PCL and PCL-ES100 particles.

3.1 PCL nanoparticles

This section covers the formulation and characterization of PCL nanoparticles.

3.1.1 Solvent extraction for PCL emulsions

Solvent extraction is required to remove organic solvent form an emulsion to obtain an aqueous dispersion of fine particles. Ideally, the extraction technique should allow for maximum product yield and be quick, cheap, simple, and environmentally friendly with little or no toxic waste [153]. SFEE is a novel particle formation technique where it employs the solvating power of a SCF such as $scCO_2$ to rapidly extract the solvent or oil phase of an emulsion. The $scCO_2$ extraction process is highly selective for the rapid and efficient recovery of hydrophobic components due to its non-polarity and high diffusivity [152, 154-155]. The gas-like properties of $scCO_2$ allows it to rapidly diffuse into the sample, and its liquid-like behaviour helps in dissolving large quantities of the organic solvent to be extracted. The solvent and CO_2 mixture can be completely removed upon controlled depressurization [155]. The removal of the solvent leads to the precipitation of the solute resulting into an aqueous suspension containing nanoparticles. Particles can thereafter be recovered from the aqueous suspension by centrifugation and/or by evaporation of aqueous phase at room temperature [152]. Particles generated *via* the SFEE process have ordered size and morphology because the fast kinetics of the $scCO_2$ extraction prevents particle agglomeration. SFEE eliminates the presence of solvent residues and the mild operating conditions can also make this process favourable for thermo-sensitive materials [141, 155]. Solvent extraction for PCL nanoemulsions was investigated as follows using either SFEE technique or under atmospheric conditions.

Initially, the time and efficiency of acetone extraction at both atmospheric and supercritical conditions were evaluated and compared along with the optimum CO_2 flow rate for complete acetone extraction within an hour. The removal of acetone from the emulsions was found to be faster at supercritical conditions than at atmospheric pressure. The rate of acetone extraction from the organic phase during SFEE was evaluated at 40 ± 2 °C at 100 bar in $scCO_2$. These conditions (temperature and pressure) were selected to allow extraction below

the melting point (59- 64 °C) of PCL polymer which was important to avoid possible particle deformation due to the simultaneous melting of the polymer during extraction. Moreover, the miscibility of acetone with $scCO_2$ at 40 °C/ 100 bar is also known to be very good which is essential for the successful extraction of the solvent from nano-emulsion [156]. The flow rate of CO_2 was varied between 1, 4, and 10 g/min to determine the optimal rate for complete and fast acetone extraction. As presented in Figure 3.1, at a constant exposure time of 1 hour, the acetone extraction from the emulsion increases with an increasing flow rate of $scCO_2$ and, the complete removal of solvent was achieved at a CO_2 flow rate of 10 g/min.

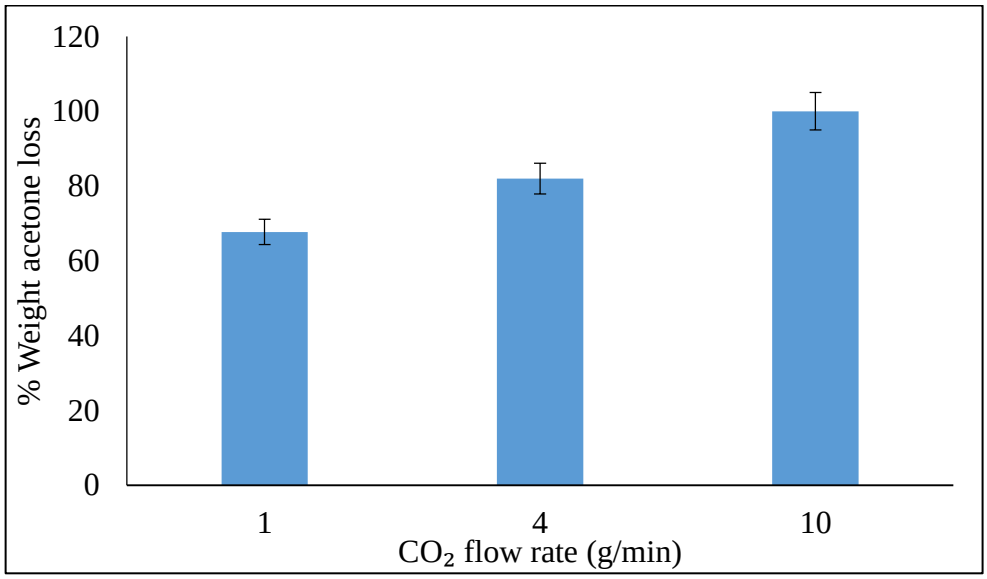

Figure 3.1: Acetone extraction *via* $scCO_2$ extraction

As discussed earlier, solvent extraction using $scCO_2$ takes place because of its ability to diffuse into the emulsion and preferentially mix with comparatively non-polar acetone. The rate of extraction is dependent on the availability of $scCO_2$ to acetone which evidently increases with the increasing flow rate of $scCO_2$. High CO_2 flow rates allow for comparatively large quantities of $scCO_2$ to be in contact with the emulsion and consequently the organic phase resulting into faster organic solvent extraction [157]. The primary mechanism of miscibility between acetone (Figure 3.2) and CO_2 is thought to be due to Lewis acid-base type interactions between acetone's carbonyl (C=O) group and CO_2 [158- 160]. Other mechanism such as dipole-dipole interactions between CO_2 and the carbonyl group can also be suggested as the reason for solubility of acetone in CO_2 [161].

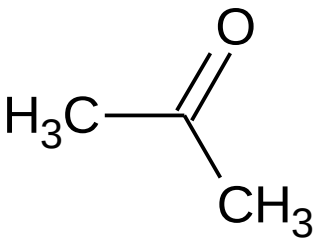

Figure 3.2: Structure of acetone

Acetone extraction at atmospheric pressure was also carried out at 40 ± 2 °C to obtain comparative data at the same temperature used in SFEE. As shown in Figure 3.3, the complete removal of acetone could only be obtained after 24 hours of continuous stirring at atmospheric pressure.

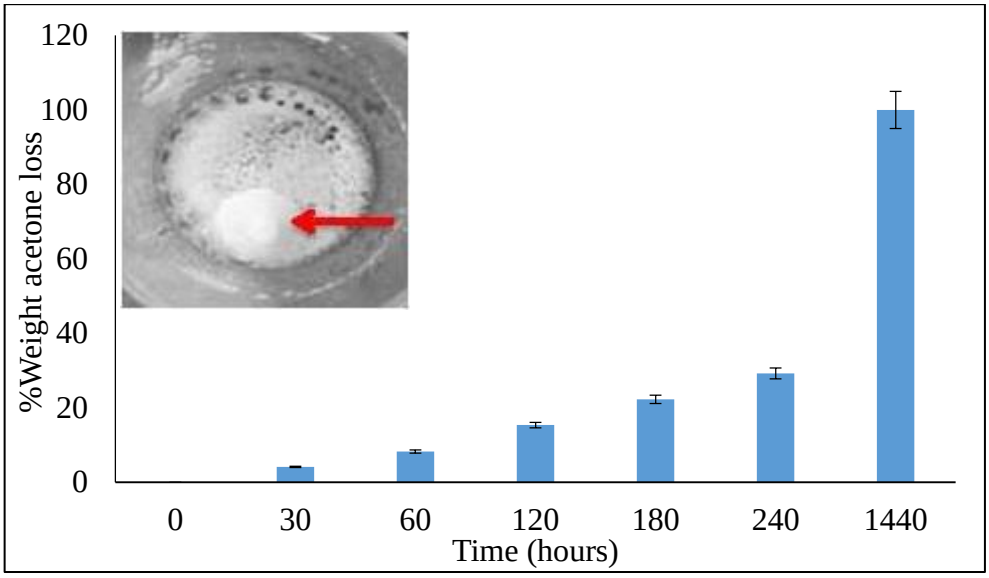

Figure 3.3: Acetone extraction at atmospheric pressure

Moreover, the extraction at atmospheric pressure also led to the agglomeration of particles (Figure 3.3, inset) consequently decreasing the total product yield. The gas-like viscosity of $scCO_2$ coupled with high diffusivity facilitates the rapid and efficient extraction of acetone without particle agglomeration in comparison to solvent extraction at atmospheric pressure at the same temperature [162]. Extraction at atmospheric conditions was therefore discontinued and SFEE was chosen as the preferred extraction method for the formation of PCL nanoparticles.

3.1.2 Influence of processing parameters on the formulation of PCL particles

This section discusses the parameters influencing the preparation of PCL nanoparticles *via* SFEE with respect to particle size and surface charge.

3.1.3 Effect of PCL concentration on particle size and charge

In general, an increase in polymer concentration led to increase in particle size (Figure 3.4). There was a gradual increase in particle size from approximately 190 nm at PCL 0.6% (w/w in acetone) to 356 nm at 10% concentration. These findings are in line with previous work done by Santos *et al* [163] and Kwon *et al* [164].

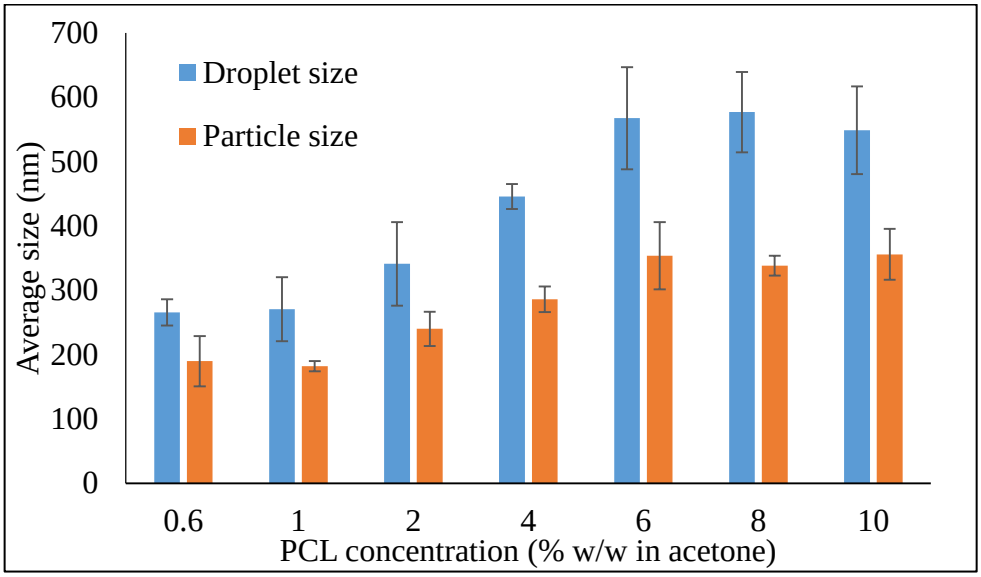

Figure 3.4: The effect of PCL concentration on the average sizes before and after SFEE

Primarily, it is assumed that nanoparticle formation occurs when both the organic and aqueous phases are in contact. The solvent diffuses from organic to aqueous phase and takes along some polymer chains which are still in solution. Thereafter, as the solvent spreads further into the aqueous phase, the accompanying polymer chains aggregate to form nanoparticles [165]. A rise in the polymer content in the organic phase consequently increases both its hydrophobic composition and viscosity which is relative to higher mass transfer resistance. Hence, this leads to a negative effect on the distribution efficiency of polymer-solvent composition in the external aqueous phase and the formation of larger nanoparticles [164, 165].

Figure 3.4 also shows a marked difference between the size before (droplet size) and after (particle size) acetone extraction. The droplets containing PCL before the elimination of acetone are always larger than the particles obtained after extraction. For example, at 0.6%, the size reduces from 266 nm before extraction to 190 nm after the removal of acetone. This could be due to the presence of voids in the polymer matrix of the emulsion droplets which then collapse upon the extraction of acetone. It is well known that free spaces within the polymer network caused by the presence of a solvent can cause particles to shrink and reduce in size after drying [166].

The PDI of formulated nanoparticles at various PCL concentrations is presented in Table 3.1.

Table 3.1: PDI and Z-potential of PCL particles before and after extraction by SFEE

PCL concentration (% w/w in acetone)	PDI ± SD before SFEE	PDI ± SD after SFEE	Z-potential (mV) ± SD after SFEE
0.6	0.13 ± 0.07	0.11 ± 0.10	-10 ± 1
1	0.19 ± 0.06	0.09 ± 0.07	-12 ± 1
2	0.09 ± 0.07	0.16 ± 0.08	-15 ± 2
4	0.17 ± 0.04	0.22 ± 0.04	-24 ± 1
6	0.23 ± 0.07	0.27 ± 0.04	-21 ± 0
8	0.21 ± 0.05	0.27 ± 0.02	-24 ± 1
10	0.21 ± 0.04	0.25 ± 0.02	-26 ± 1

In general, the PDI was very low for all formulations, confirming that the prepared nanoparticles are highly monodisperse and have narrow particle size distribution. A slight increase in PDI was observed with the increase in polymer concentration and particle size. This could be attributed to the increase in viscosity of the organic phase and possible coalescence of smaller droplets into larger droplets at higher concentrations resulting in comparatively broad particle size distribution [167- 168].

The particle surface charge was determined by carrying out zeta potential measurements using a Zetasizer (section 2.2.1). The Z-potential values of PCL nanoparticles prepared with different polymer concentrations are also presented in Table 3.1. Formulated PCL nanoparticles contain net negative surface charge which can be due to the localization of C=O

groups present in PCL at the surface of the nanoparticles. Table 3.1 also shows a shift in Z-potential values with an increasing polymer concentration. The change in Z-potential can be attributed to the shielding effect by the surfactant molecules at the interface due to interaction with PCL. Therefore, as the polymer content increases at a constant surfactant concentration, the number of Tween 80 molecules available at the interface decreases consequently resulting in a reduced shielding effect and leading to a change in Z-potential [169].

3.1.4 Effect of surfactant concentration

To investigate the effect of surfactant concentration on the particle size, PDI and surface charge, the surfactant content was doubled from 0.07 to 0.14 % (w/w emulsion) at a constant polymer concentration. The aqueous-to-organic phase ratio was maintained at 2.5:1 as before.

Similar to earlier observations, an increase in droplet sizes with the rise in polymer concentration was observed as shown in Figure 3.5 below;

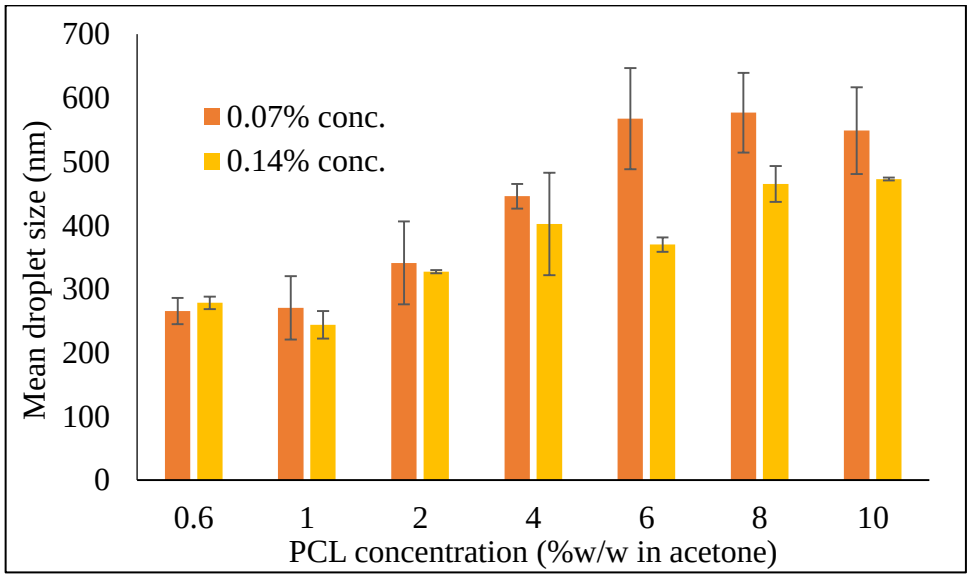

Figure 3.5: Droplet sizes of PCL emulsions made with 0.07 or 0.14% Tween 80

Furthermore, an increase in surfactant amount (0.14%) led to smaller droplet sizes when compared to samples prepared with 0.07% Tween 80. The size range obtained at 0.07% (266 ± 20 – 549 ± 68 nm) reduced to 278 (±10) – 473 (±2) nm at 0.14% Tween 80. This result was in line with the findings from the work done by Goloub and Pugh [170]. The positive effect of a higher Tween 80 concentration on droplet size can be easily related to its role in the emulsion. A low concentration of surfactant in the emulsion and consequently at the solvent-water interface would mean that there were not enough surfactant molecules to cover the

surface of drops, resulting in coalescence of droplets and increase in size. An increase in the surfactant concentration would therefore result in a higher number of surfactant molecules present at the interfacial layer promoting the formation of smaller droplets [171].

Similarly, there was a reduction in size after acetone extraction by SFEE, with the sizes increasing with the rise in PCL concentration as presented in Figure 3.6.

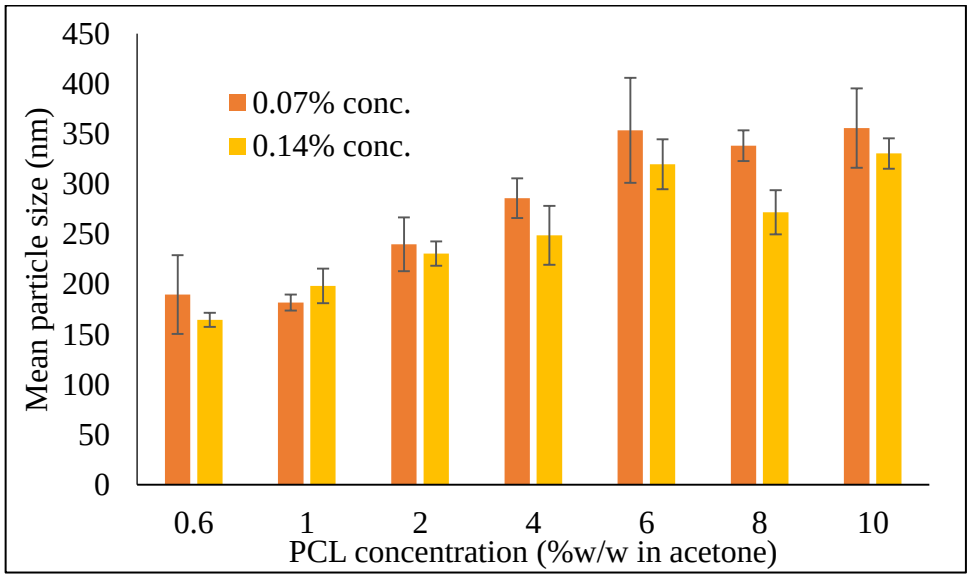

Figure 3.6: Size of PCL particles made with 0.07 or 0.14% Tween 80 after SFEE

Figure 3.6 also shows that higher surfactant concentration led to decrease in particle size and standard error. A particle size range of 165 ± 7 nm to 331 ± 15 nm was obtained at 0.14% Tween 80 in comparison to 190 ± 39 nm to 356 ± 40 nm at 0.07% concentration. This result was in accordance to that reported by Mu and Feng [172]. The reduction in size can be anticipated from the role of surfactant as an emulsion stabiliser during the formation of nanoparticles [173].

Similar to previous results, the PDI recorded for samples with higher surfactant concentration (Table 3.2) were very low (0.09 to 0.26) indicating that the formulated nanoparticles have narrow particle size distribution.

Table 3.2: PDI and Z-potential of PCL nanoparticles before and after SFEE for 0.14% Tween 80 samples

PCL concentration (% w/w in acetone)	PDI ± SD before SFEE	PDI ± SD after SFEE	Z-potential (mV) ± SD after SFEE
0.6	0.09 ± 0.03	0.11 ± 0.05	-14 ± 1
1	0.14 ± 0.05	0.19 ± 0.04	-17 ± 3
2	0.09 ± 0.04	0.14 ± 0.07	-19 ± 3
4	0.14 ± 0.08	0.19 ± 0.08	-22 ± 2
6	0.16 ± 0.06	0.22 ± 0.12	-25 ± 3
8	0.19 ± 0.04	0.26 ± 0.09	-29 ± 3
10	0.19 ± 0.06	0.24 ± 0.05	-29 ± 3

Z-potential measurements (Table 3.2) were also determined on the 0.14 % (w/w emulsion) Tween 80 samples to understand the effect of the increase in surfactant concentration on the surface charge density, and just like earlier results these values increased with the polymer concentration (-14 to -29 mV). However, Z-potential values for samples prepared with high surfactant content (0.14%) did not differ significantly in comparison to the 0.07% Tween 80 samples.

3.1.5 Effect of polymer to surfactant ratio on particle size

Previously, the PCL to Tween 80 w/w ratios ranged between 1.3:1 and 32:1 at 0.07 and 0.14% Tween 80. To further study the effect of varying surfactant/polymer content on nanoparticle size at a constant PCL concentration, the amount of Tween 80 was altered to prepare emulsions with polymer-to-surfactant weight ratios of 1:1, 2:1, 4:1, 8:1 and 16:1. The aqueous to organic phase ratio was kept constant to 2.5:1 for all preparations. Results obtained for droplet and particle sizes (Figures 3.7 and 3.8 respectively) were in line with previously discussed findings where at a constant polymer-to-surfactant weight ratio, increasing polymer concentration led to the formation of larger particles.

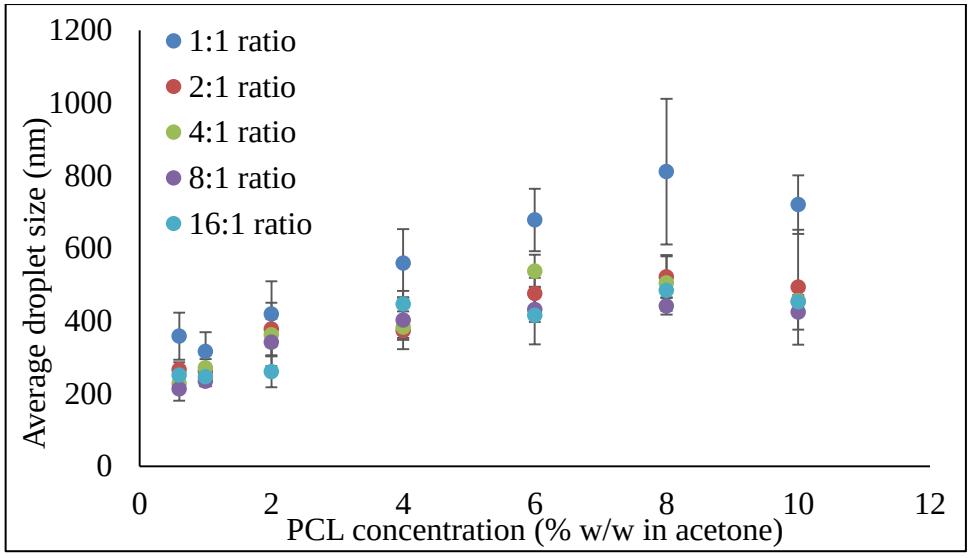

Figure 3.7: Mean emulsion droplet size at a varying PCL-to-Tween 80 ratio

Similarly, there was also a reduction in size observed after SFEE in comparison to droplet sizes before acetone extraction. For example, samples prepared with 0.6% PCL (2:1 PCL-Tween 80) led to the formation of 190 nm particles after the extraction of acetone from their resulting emulsion which contained droplets of 266 nm.

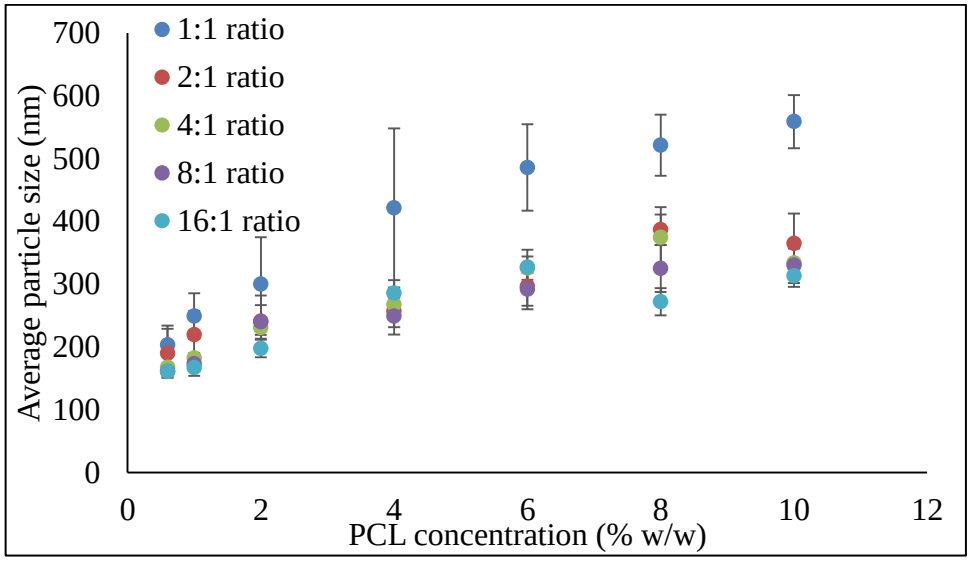

Figure 3.8: Mean particle size after SFEE at a varying PCL-to-Tween 80 ratio

Interestingly, 1:1 w/w ratio samples have noticeably higher particle size (> 500 nm) in comparison to the rest of the data sets. This could be attributed to the depletion effect from non-adsorbing Tween 80 micelles at such high surfactant concentration [174]. The presence of free micelles at high surfactant concentrations can cause increase in osmotic pressure in the

liquid surrounding the particles to an extent which can result in droplet/particle destabilization and aggregation [175].

It is also important to note that the error associated to the particles prepared with 1:1 w/w ratio is also very high in comparison to other formulations which suggest flocculation/aggregation of prepared particles. There were minimal changes in particle sizes at polymer-to-surfactant weight ratio from 16:1 to 2:1 w/w where sizes ranging from 150-350 nm with narrow distribution were reproducibly obtained. These results confirm that particles of different size and size distribution could be obtained by fine-tuning the preparation conditions such as polymer and surfactant content.

The PDI recorded (Appendix A.1) for these formulations ranged between 0.03 ± 0.02 to 0.37 ± 0.05 indicating that these particles have narrow size distribution. There was no trend observed with the change in polymer to surfactant w/w ratio. However, particles prepared with higher PCL concentrations (6 to 8 mg/ml) generally resulted in higher PDI values (>0.20) in comparison to lower PCL amounts. As previously discussed, this occurrence could be associated with the rise in viscosity of the organic phase as the amount of polymer dissolved in acetone increases. Also, there is the possibility for smaller droplets to merge into larger droplets at increased polymer concentrations resulting in comparatively broad particle size distribution [167, 168].

Generally, at a constant PCL to surfactant ratio there was a considerable increase in zeta-potential values (Appendix A.1) as the polymer concentration increased from 0.6 to 4%. This increase in surface charge was more evident at lower polymer/surfactant ratios. The zeta-potential value appeared to remain stable with increasing polymer concentration on particles prepared with high PCL/Tween 80 ratios. Furthermore, particles formulated with high polymer concentration (6 to 10%) always contained similar surface charge irrespective of the ratio between polymer and surfactant. The negative charge on these particles could be associated to the localization of C=O group present in PCL. Therefore, an increase in zeta-potential value can be expected with the rising polymer concentration and variations in shielding effect provided by surfactant molecules at the interface [169].

The PCL nanoparticles were further characterized as follows to evaluate their surface morphology and properties.

3.1.6 Structural and surface characterization of PCL particles

The following sections discuss investigations regarding the structural and surface characterization of PCL particles prior to the adsorption of γ-globulin.

3.1.7 Specific surface area and porosity for PCL particles

This section discusses data obtained for the surface characterization of PCL particles with regards to their porosity and SSA. The plot for adsorption and desorption of nitrogen molecules onto/from freeze-dried PCL particles is shown in Figure 3.9. The isotherm for PCL particles can be classed as an intermediate to the Brauner-Derming-Derming-Teller (BDDT) reversible *Type I* and *II* isotherms without the presence of a hysteresis loop indicating that these particles are nonporous in nature [176, 177].

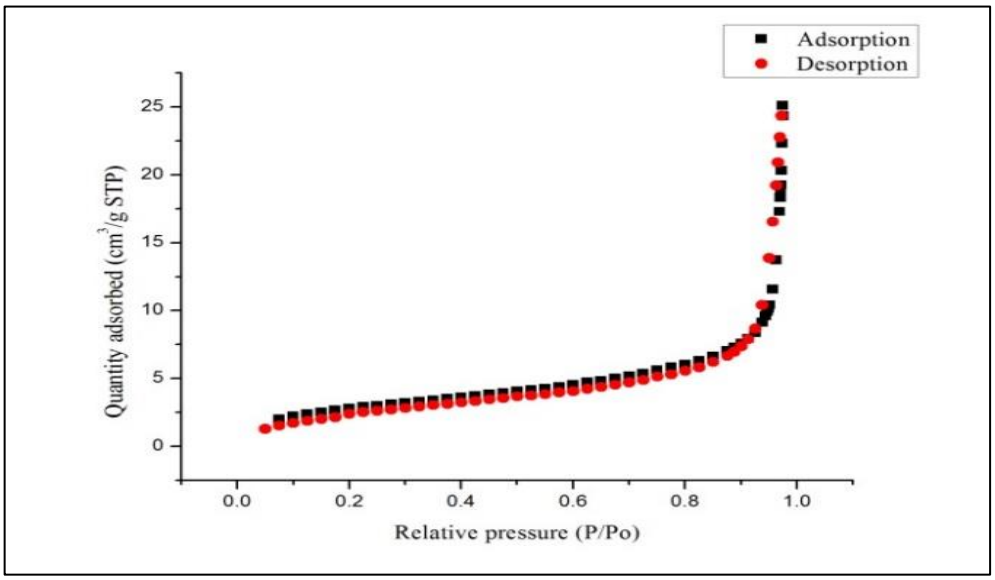

Figure 3.9: Nitrogen sorption isotherm for PCL particles at 1% w/w

The International Union of Pure and Applied Chemistry (IUPAC) classification of various types of physisorption isotherms are shown in Figure 3.10a. *Type I, II, III* and *VI* isotherms are commonly observed with non-porous particles, while the presence of hysteresis loop in *Type IV* and *V* is associated with porous materials [176- 178]. The adsorption hysteresis loop of *Type IV* and *V* isotherms can be classed into four types as presented in Figure 3.10b.

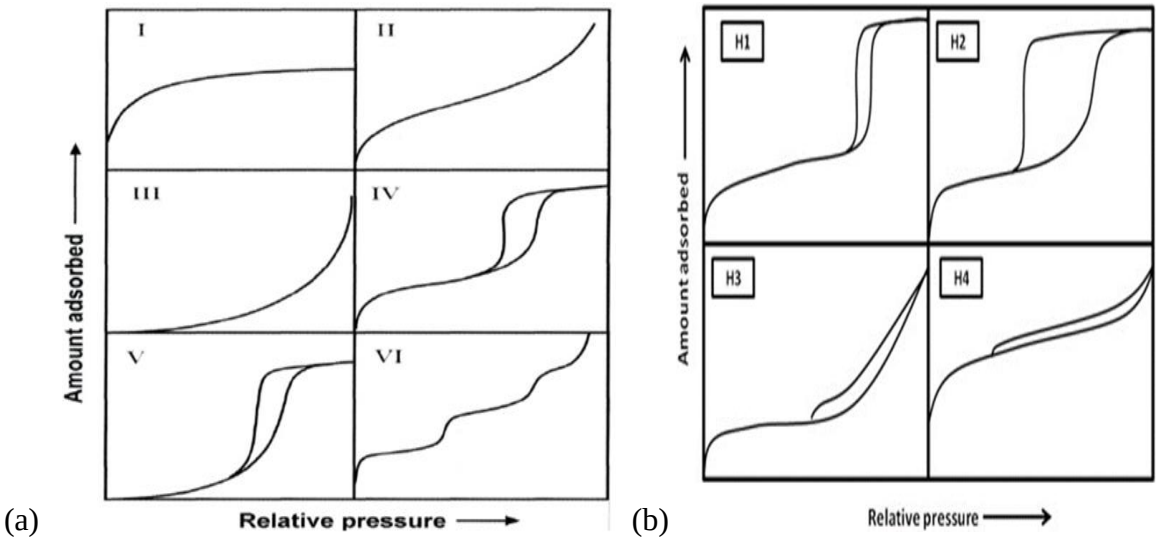

(a) (b)

Figure 3.10: Types of (a) physisorption isotherms, and (b) hysteresis loops

The shape of the hysteresis loop is widely known to correlate to pore structures including pore size distribution, pore geometry and connectivity, of mesoporous materials. Type H1 is usually related to porous materials that have agglomerates or distinct cylindrical-like pore channels of nearly uniform spheres, while Type H2 represents materials that are normally disordered where pore size distribution and pore shape is not well defined. The Type H3 loop is seen with aggregates of plate-like particles consisting of slit-shaped pores. Likewise, materials with narrow slit-like pores are linked to the Type H4 loop but its *Type I* isotherm character typically suggest that associated materials are microporous [176, 177].

The pore volume and diameter of the PCL particles (1% w/w acetone) as determined by BJH model were recorded as 0.04 ml/g and 19.1 nm respectively. There was no further change to the isotherm or improvement in the particle pore volume and size with the increase or decrease in polymer concentration. With regards to the BET, it is known that SSA can be influenced by the particle size with a likely decrease in the area as the size increases [179-181]. However, there was no significant difference in the SSA obtained for formulated particles with respect to particle sizes. For example, PCL particles prepared with 1, 4 and 6% w/w polymer resulted in particles of ascending sizes but had SSA of only 11, 13 and 7 m^2/g respectively. It is possible that the increase in size had almost no effect on SSA due to similarities in or lack of porosity in the PCL particles. The surface characteristics were further evaluated by SEM analysis as described in section 3.1.8.

3.1.8 Surface morphology and particle shape of PCL particles

SEM micrographs were collected using chromium-coated freeze-dried PCL nanoparticles in order to investigate the shape and surface morphology of these preparations and example of micrographs of particles prepared by SFEE are shown in Figure 3.11.

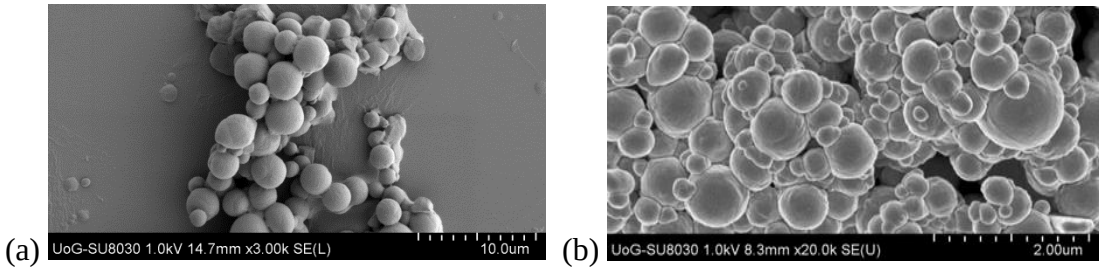

Figure 3.11: Example of SEM micrographs of PCL particles processed by SCF at (a) 0.6 and (b) 10 %w/w

From the micrographs, it can be observed that the particles are generally spherical and uniform. Additionally, there were no visible signs to indicate the presence of pores at the surface of these particles, thereby confirming the BET results that they are non-porous in nature. However, when compared to the size data obtained with DLS, the SEM micrographs show the presence of possible PCL micro-particles. The variations between SEM and DLS results could likely be linked to measurement limitations of the DLS instrument. During size analysis with the zetasizer, larger particles have a tendency to sediment faster, and therefore less likely to be detected by the instrument.

3.1.9 ATR-FTIR analysis of PCL particles

The structural features of the PCL particle surface were investigated by ATR-FTIR analysis and a representative spectrum is presented in Figure 3.12. As expected, there were no differences observed to the spectrum with an increase in PCL concentration. Typical IR bands relating to the stretching modes of functional groups in PCL can be observed at 1239 cm^{-1} (asymmetric C=O=C), 1293 cm^{-1} (C–O and C–C in crystalline phase), 1721 cm^{-1} (C=O), 2865 cm^{-1} (symmetric CH_2), and 2943 cm^{-1} (asymmetric CH_2). The bands representing CH_2 bending can be found at 1471, 1397, 1366 cm^{-1} [182, 183].

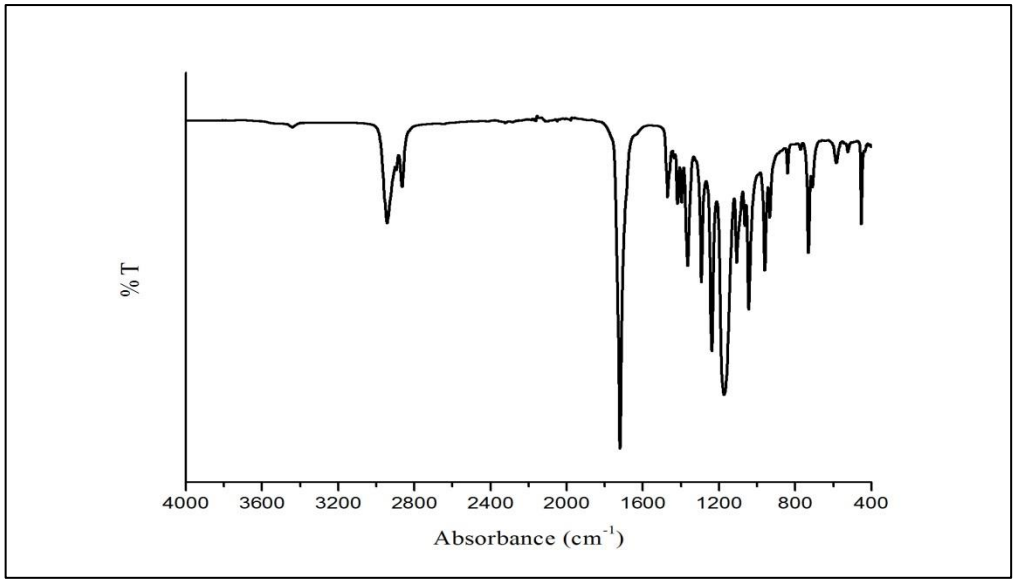

Figure 3.12: ATR-FTIR spectrum for PCL particles (1% w/w)

In addition to these polymeric systems, PCL and ES100 composite particles were also prepared and evaluated as discussed in the following sections.

3.2 PCL-ES100 particles

This section covers the formulation and characterization of PCL-ES100 particles.

3.2.1 Solvent extraction for PCL-ES100 particles

Unlike the PCL particles, solvent extraction of PCL-ES100 emulsion carried out at studied $scCO_2$ conditions (> 100 bar and 40 °C) did not result in a comparatively efficient method. The $scCO_2$ extraction resulted in 60-70% of residual solvent after 5 hours of stirring and continuous flushing with CO_2 at 10 g/min flow rate. This could be attributed to the fact that PCL-ES100 system consists of a mixture of solvents (ethanol and DCM) with a lower aqueous to organic phase ratio (~ 1:1). This consequently larger volume of solvent in comparison to PCL emulsion comprising only acetone with a 2.5:1 aqueous to organic phase ratio could require much longer time to achieve 100% extraction. However, polarity difference between ethanol and acetone must also be considered as preferential solubility of non-polar materials in $scCO_2$ is an important factor in the success and efficiency of the extraction process [125, 126]. A better interaction between CO_2 and acetone can be expected as acetone is less polar than ethanol [184], consequently leading to its complete removal from the emulsion. SFEE procedure with PCL-ES100 may be improved by increasing the solvating power of CO_2 through varying pressure, temperature, and/or flow rate [120, 121].

The complete removal of solvent from the organic phase of PCL-ES100 emulsions was achieved under atmospheric conditions at 40 °C in 8 to 12 hours and formulated particles were characterized as follows.

3.2.2 Influence of processing parameters on the formulation of PCL-ES100 particles

This section discusses the parameters influencing the preparation of PCL-ES100 nanoparticles *via* solvent evaporation of emulsions with respect to particle size and surface charge.

3.2.3 Effect of polymer ratio on particle size

PCL-ES100 nanoparticles were formulated with various ratios of PCL to ES100 polymer (1:2, 1:3, 1:4, and 1:5) to evaluate the effect of addition of ES100 to the polymeric system for protein delivery. The preferential solubility of ES100 at/ or above neutral pH (≥ 7) makes it desirable for the design of a DDS that can allow for targeted release of a drug in the lower G.I tract (small intestine) [116]. Therefore, they can potentially stabilize formulated SCDDS against acidic degradation in the stomach. There is also evidence that the presence of ES100 polymer in the PCL system can control the burst release effect typically seen with the latter [106].

The sizes for aqueous dispersions of PCL-ES100 particles after solvent extraction are presented in Figure 3.13.

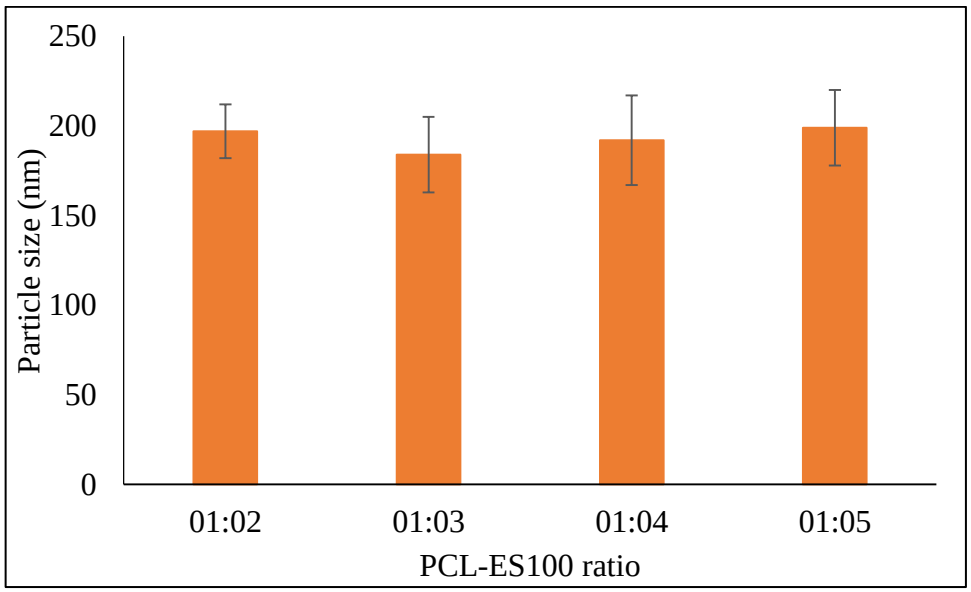

Figure 3.13: Hydrodynamic size of formulated PCL-ES100 nanoparticles

PCL-ES100 nanoparticles were successfully produced by solvent extraction of their resulting emulsion and unlike the PCL systems there is no correlation between size and increase in polymer content. The sizes ranged from 184 to 199 nm with the smallest particles obtained with 1:3 (PCL-ES00) ratio.

Similar to PCL particles, the PDI (Table 3.3) for these systems was also low indicating that they have narrow particle size distribution.

Table 3.3: PDI values for PCL-ES100 nanoparticles

PCL: ES100 ratio	**PDI**
1: 2	0.21 ± 0.02
1: 3	0.19 ± 0.03
1: 4	0.18 ± 0.03
1: 5	0.14 ± 0.03

Interestingly, addition of ES100 to the PCL systems led to the generation of particles with comparatively smaller range sizes *i.e*. going from approximately 170- 356 nm for pure PCL nanoparticles to 180- 199 nm for the composite systems. This trend was also observed by Seremeta, *et al* and it is suggested that the ES100 polymer acts like a surfactant creating a stabilizing effect on the resulting nano-emulsions to allow for the formation of smaller-sized particles [106]. Although, it is also worth considering that the polymer content for the PCL emulsions (0.089 to 1.415 g) exceeds that for PCL-ES100 systems (150 to 300 mg).

3.2.4. Effect of polymer ratio on surface charge

The zeta-potential values recorded for aqueous dispersions of PCL-ES100 particles after solvent extraction are presented in Table 3.4.

Table 3.4: Zeta-potential values for PCL-ES100 nanoparticles

PCL: ES100 ratio	Zeta-potential (mV)
1: 2	-36 ± 6
1: 3	-37 ± 6
1: 4	-39 ± 10
1: 5	-36 ± 6

Like the data obtained for their particle size, there was no correlation between the increasing polymer content and surface charge for PCL-ES100 systems. The zeta-potential values for these particles were similar ranging from -36 to -39 mV. The negative surface charge recorded could be attributed to the presence of localized C=O groups from either the PCL/ ES100 polymer or a combination of both at the particle surface.

The interactions between PCL and ES100 were further investigated by structural and surface analysis as described in the following sections.

3.2.5 Structural and surface characterization for PCL-ES100 particles

The following sections discuss analysis relating to the structural and surface characterization of PCL-ES100 particles before protein adsorption.

3.2.6. Specific surface area and porosity for PCL-ES100 particles

The BET isotherms for nitrogen sorption on PCL-ES100 particles at varying polymer ratios were obtained to study their porosity. As presented in Figure 3.14, the recorded BET isotherm can be classed as intermediate to the reversible *Type I* and *II* isotherms without the presence of a hysteresis loop thereby indicating non-porosity [176, 177]. Similar to the data observed with PCL particles, there was no change to the curvature of the isotherm with the varying polymer content used for the preparation of PCL-ES100 systems (Appendix A.2).

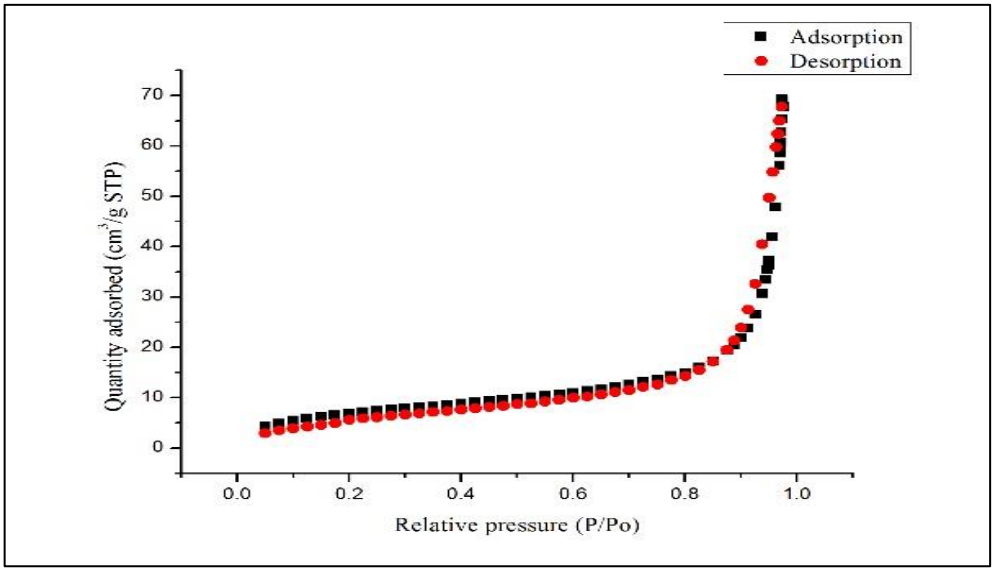

Figure 3.14: Nitrogen sorption isotherm for PCL-ES100 (1: 2 ratio) particles

A summary of the surface characteristics for PCL-ES100 particles at the varying polymer ratios is presented in Table 3.5 and aside from the results for 1:2 ratio, there is generally a slight increase in the SSA, pore volume and diameter with rising ES100 ratio.

Table 3.5: Summary of surface characteristics for PCL-ES100 particles

PCL-ES100 ratio	**1:2**	**1:3**	**1:4**	**1:5**
Quantity of nitrogen adsorbed (cm^3/g STP)	69	44	53	117
BET surface area (m^2/g)	26	20	26	33
BJH cumulative pore volume (ml/g)	0.10	0.06	0.08	0.18
BJH pore diameter (nm)	19.1	16.7	16.0	23.9

The quantity of adsorbed nitrogen at the ratio 1:5 is approximately 1.5 times higher than that of nanoparticles prepared with 1:2 ratio. This could simply be due to slight variation in particle size which also follows the same trend *i.e.* 1:5 > 1:2 > 1:4 > 1:3.

In addition to the particle sizes, an increase in ES100 content may also contribute to the differences observed in the particle characteristics. A study by Mahalingam and Krishnamoorthy investigating the development of camptothecin-loaded ES100 nanoparticles found an inverse relationship between SSA and the ES100 concentration used for particle preparation [179].

The surface characteristics of the formulated PCL-ES100 particles were further analysed by SEM as discussed in the following section.

3.2.7 Surface morphology and particle shape of PCL-ES100 particles

SEM was employed to visually study the surface morphology and particle shape of the prepared PCL-ES100 systems, and the micrograph collected is shown in Figure 3.15.

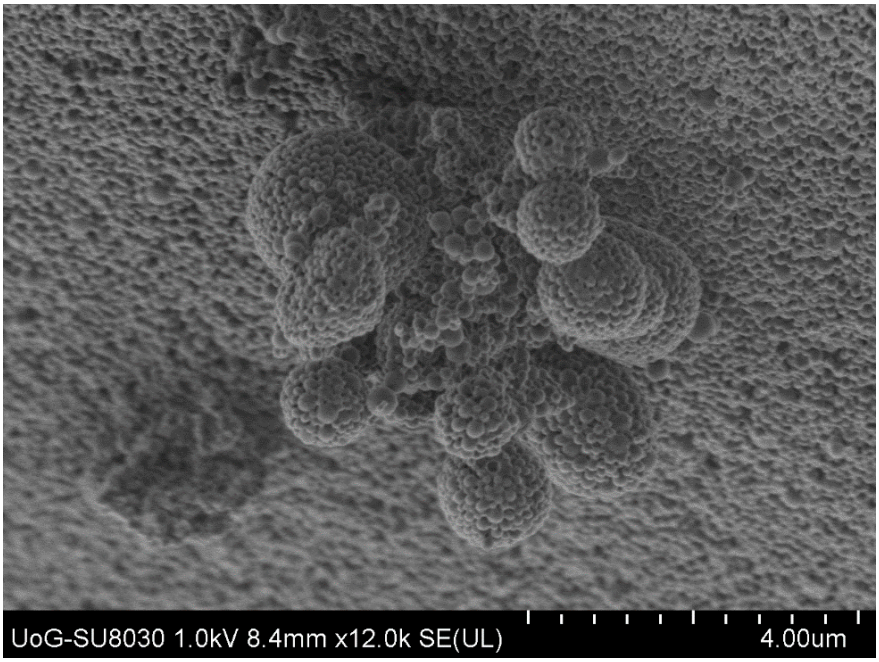

Figure 3.15: SEM micrograph for PCL-ES100 particles

Similar to PCL particles, the micrograph for the formulated PCL-ES100 systems show that they are spherical and have uniform size distribution. Although, the micrographs also suggest the presence of large agglomerates made up of the small individual PCL-ES100 particles which could have occurred either during the solvent extraction or drying steps.

The structure of the PCL-ES100 nanoparticles was also studied through ATR-FTIR analysis as discussed in section 3.2.8.

3.2.8 ATR-FTIR analysis of PCL-ES100 particles

The structural characteristics of formulated PCL-ES100 particles were studied by ATR-FTIR analysis and the spectra recorded are presented in Figure 3.16. As observed in Figure 3.16, the spectra for pure PCL and ES100 polymer are quite similar with respect to the types of functional groups present in their structure. While the groups present in PCL are identical to those previously described for the PCL nanoparticles, the spectra of ES100 show the characteristic carbonyl vibrations of its ester group at approximately 1726 cm^{-1} [106, 185].

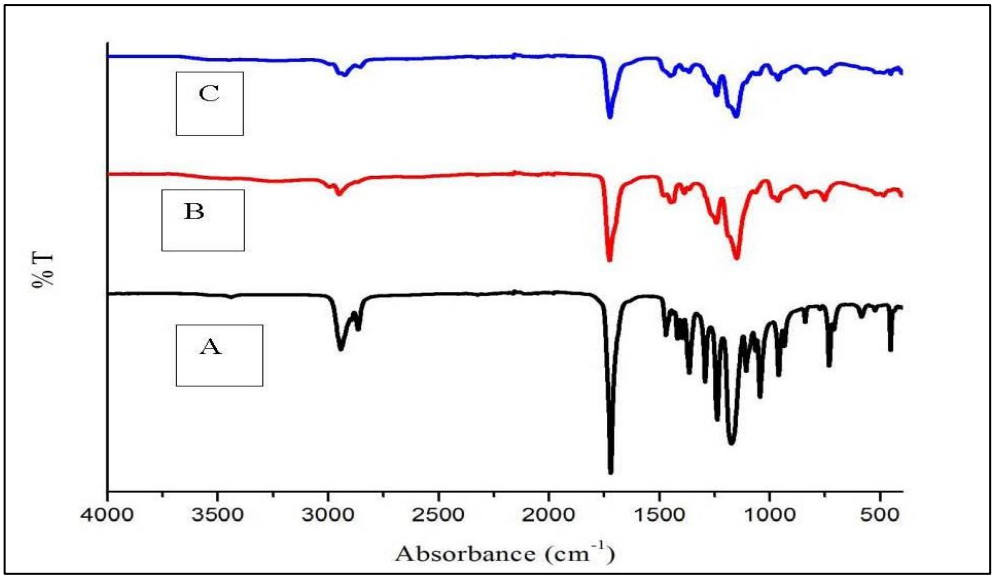

Figure 3.16: ATR-FTIR spectra for (A) PCL and (B) ES100 polymer, (C) PCL-ES100 (1: 2) nanoparticle

The spectrum recorded for PCL-ES100 nanoparticle was very similar to that of ES100 polymer showing lack of any major shift in wavenumber or functional groups. This suggests that the ES100 polymer is possibly acting as a surface coating for PCL particles rather than physically interacting with PCL when both materials are mixed together [186]. There was no change to their ATR-FTIR spectrum with the rising ES100 content for the PCL-ES100 systems (see Appendix A.3).

The interactions between PCL and ES100 were further investigated by thermal analysis as discussed in the following section.

3.2.9 Thermal analysis of PCL-ES100 particles

The thermal analysis of PCL-ES100 particles was carried out by DSC and thermogram recorded for polymer ratio 1:2 is shown in Figure 3.17. There was no difference observed with the varying PCL to ES100 ratios (Appendix A.4).

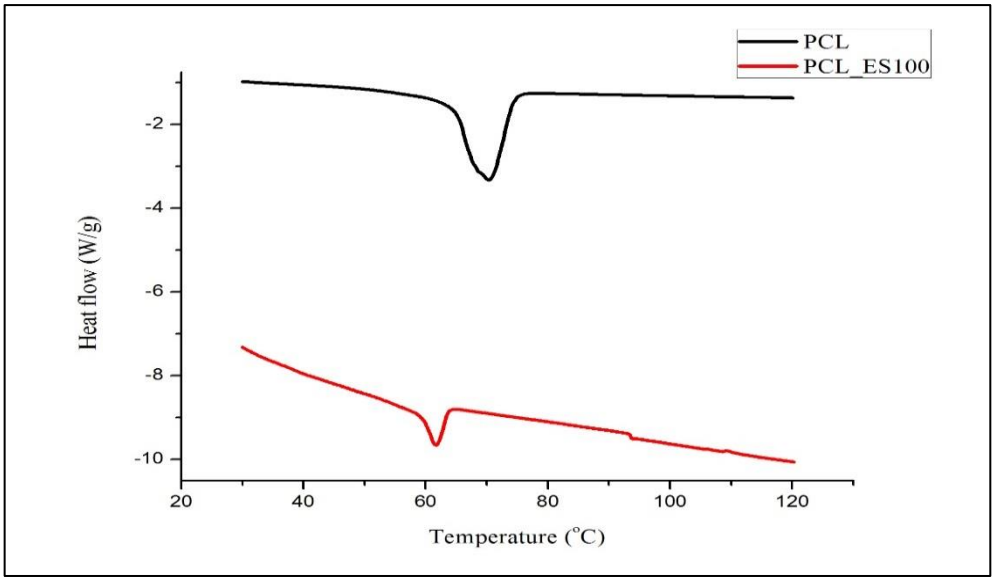

Figure 3.17: DSC thermograms for PCL polymer and PCL-ES100 (1:2)

As noted in Figure 3.17, the thermogram for untreated PCL showed an endothermic peak due to its crystalline nature at approximately 70 °C whereas a broad peak can be visible for ES100 polymer (Figure 3.18) at around 90 °C.

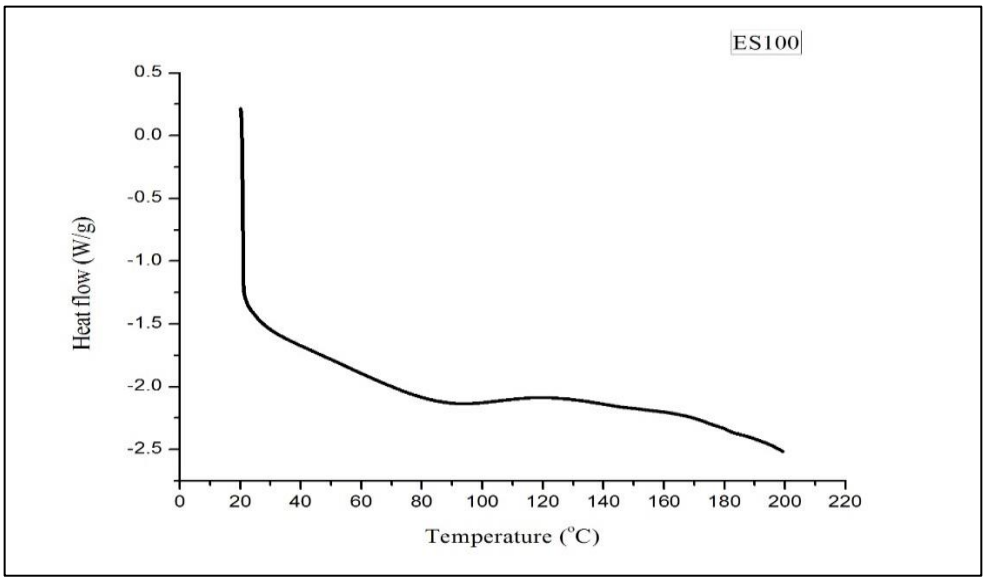

Figure 3.18: DSC thermogram for pure ES100

The recorded peak value for untreated PCL differs slightly from those quoted in literature (60-62 °C) which could possibly be as a result of a difference in purity of the analysed samples [187, 188]. For pure ES100 there were two endothermic peaks with the first (below ~ 100 °C) representing dehydration of the polymer. The second peak signifies possible start of the polymer degradation as the decomposition of ES100 above 200 °C is reported by various

groups in the past [189- 192]. Nevertheless, a melt peak at 62 °C (Figure 3.17) for PCL-ES100 particles confirms the presence of PCL in these systems. The slight shift in the melting temperature of PCL could be due to the presence of ES100 in the composite particles and may also suggest physical interactions between PCL and ES100.

The appropriateness for the prepared PCL and PCL-ES100 systems to allow for γ-globulin adsorption will be discussed in chapter 5.

3B. Characterization of silica particles

The following sections cover the surface and structural characterization of commercially purchased silica particles listed as S_{AL}, S_{XDP}, S_{FP}, and MSU-H in section 2A.

3B.1 Aims and Objectives

For the successful preparation of SCDDS, part of this work was largely focused on identifying suitable core particles for the immobilization of γ-globulin. Hence, in addition to formulated polymeric systems, four different types of silica particles were commercially purchased to determine their suitability for protein adsorption. The following work was carried out to better understand the structural and surface properties of these purchased materials. This included SEM, ATR-FTIR, and BET analysis of the silica particles.

3B.2 Experimental

S_{FP}, S_{XDP}, S_{AL} and MSU-H were characterized similar to PCL and PCL-ES100 particles. Methods related to BET, SEM, and ATR-FTIR analysis are detailed in sections 2.2.2, 2.2.4, and 2.2.3 respectively.

3B.3 Introduction

The growing interest in the use of solid core particles, particularly mesoporous silica materials, for drug delivery is attributed to their favourable properties including chemical and thermal stability, biocompatibility, and biodegradability [193]. In addition, the strong Si-O bond in silica makes them less likely to undergo degradation that can occur because of mechanical or thermal stress during DDS design [193]. The distinctive structure of mesoporous particles consisting of a solid framework with porous structures and large surface area can enable the effective absorption/immobilization of drug molecules, and the subsequent controlled release of absorbed/adsorbed drug at target organ sites in the body [193, 194]. Moreover, the particle size and surface properties of the mesoporous structures can be fine-tuned during their synthesis to improve drug loading capacity [193, 194]. Furthermore, the presence of silanol groups provides an opportunity for surface functionalization with different substances (such as stimuli-responsive materials) to enhance the targeted delivery of drug substances [193]. The structural and surface characterization of the silica particles of interest for this research is described as follows.

3B.4 Results and discussion

This section discusses the results obtained for the structural and surface characterization of S_{AL}, S_{XDP}, S_{FP}, and MSU-H particles.

3.3 Specific surface area and porosity for silica particles

The surface porosity of silica particles was investigated by nitrogen sorption experiments and the recorded BET isotherms are presented in Figure 3.19.

(a)

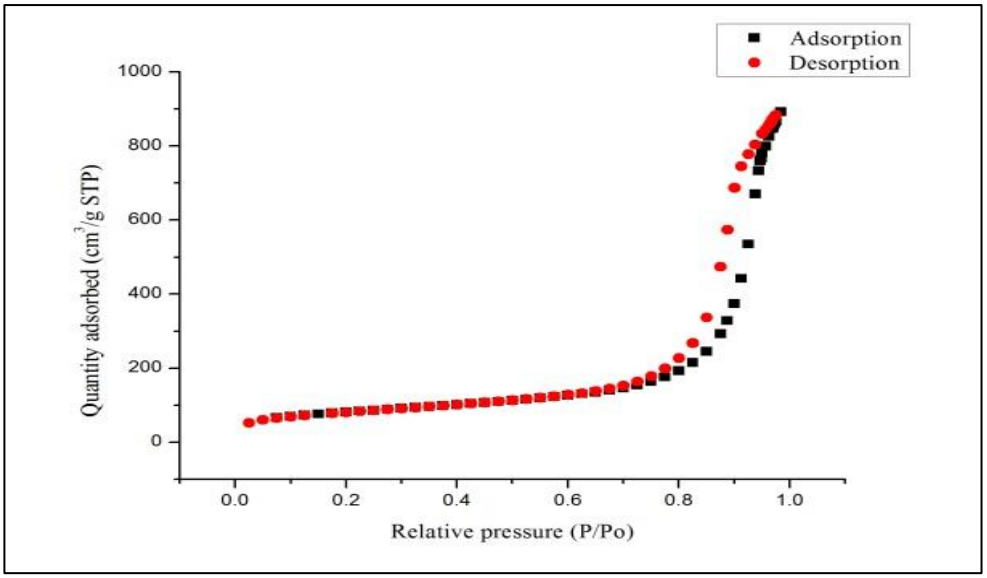

(b)

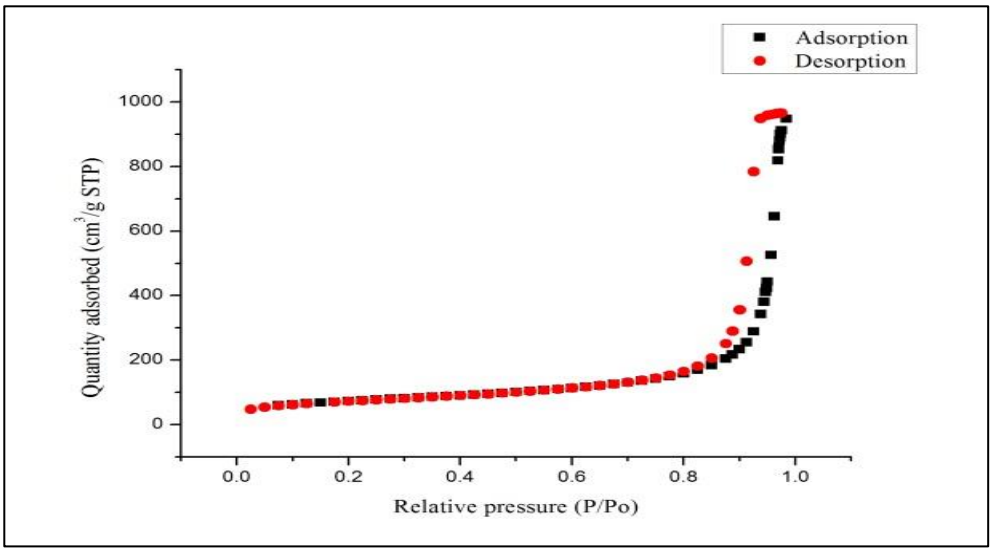

(c)

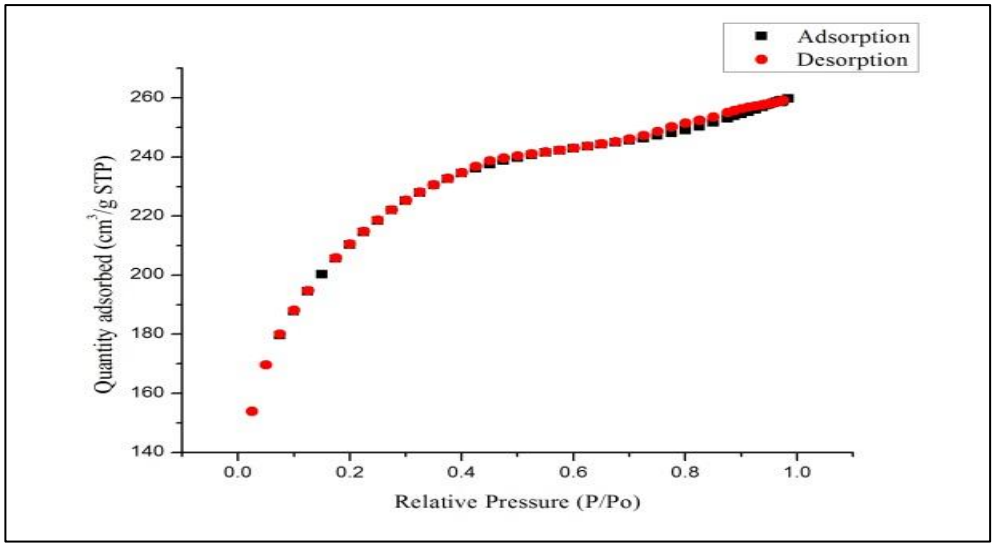

(d)

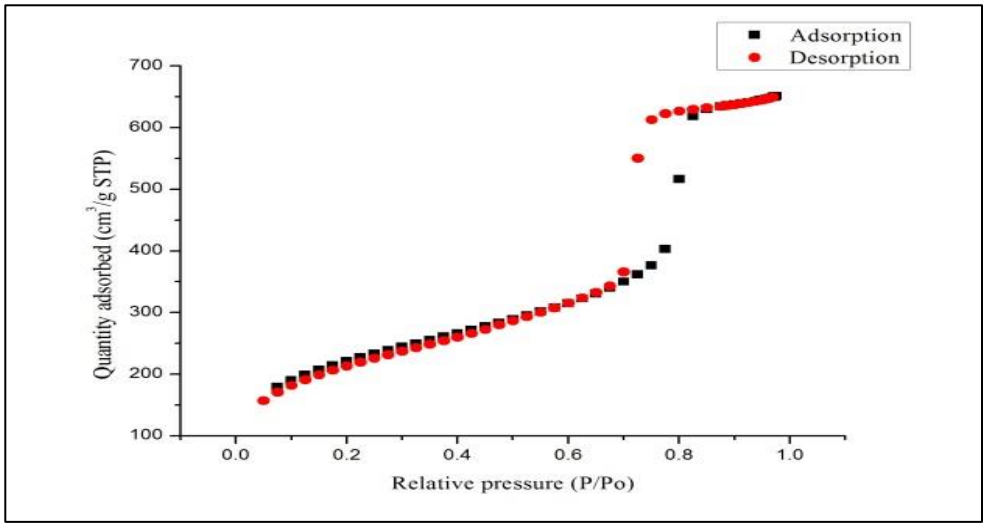

Figure 3.19: BET isotherms for (a) S_{FP}, (b) S_{XDP}, (c) S_{AL} , and (d) MSU-H particles

The isotherm for S_{FP}, S_{XDP} and MSU-H can be classed as a *Type IV* due to their characteristic H1 hysteresis loop (Figure 3.10), thus suggesting that they are mesoporous (pores of widths between 2 and 50 nm) in nature. Like the *Type II* isotherm, the first part of the *Type IV* curve signifies a monolayer-multilayer adsorption in nature [176, 177]. The shape of the hysteresis loop is widely known to correlate to pore structures including pore size distribution, pore geometry and connectivity, of mesoporous materials. Type H1 is usually related to porous materials that have agglomerates or distinct cylindrical-like pore channels of nearly uniform spheres [176, 177]. On the other hand, the lack of hysteresis and the reversible *Type II* isotherm for S_{AL} indicates that they are generally nonporous [176, 177]. Additionally, the amount of nitrogen adsorbed (260 cm^3/g STP) onto the surface of S_{AL} was lower than that recorded for S_{FP}, S_{XDP}, and MSU-H (892, 996, and 651 cm^3/g STP respectively) indicating

that the S_{AL} particles have a reduced adsorption capacity for nitrogen when compared to the other three materials.

The SSA calculated by BET theory along with the pore volume and diameter deduced by BJH model for these silica particles are presented in Table 3.6.

Table 3.6: Summary of surface characteristics for S_{FP}, S_{XDP}, S_{AL}, and MSU-H particles

Silica particle	S_{FP}	S_{XDP}	S_{AL}	MSU-H
Quantity of adsorbed nitrogen (cm^3/g STP)	892	996	260	651
BET surface area (m^2/g)	289	258	767	782
BJH cumulative pore volume (ml/g)	1.35	1.44	0.40	0.99
BJH pore diameter (nm)	19.1	22.2	2.5	5.7

The SSA for MSU-H and S_{AL} particles were similar at 782 and 767 m^2/g respectively whereas, the SSA of S_{FP} and S_{XDP} was comparable at 289 and 258 m^2/g respectively. The variations in the SSA resulted in a difference in the amount of adsorbed of nitrogen between the silica particles where higher quantities were adsorbed by both S_{FP} and S_{XDP} in comparison to MSU-H and S_{AL}. The pore sizes and volume followed an ascending trend of S_{AL} < MSU-H < S_{FP} < S_{XDP} which is also similar to that for the quantity of nitrogen adsorbed to the surface of the particles. The surface characteristics of the silica particles were further analysed as described in section 3.4.

3.4 Surface morphology and particle shape of silica particles

The micrographs collected for S_{FP} are presented in Figure 3.20 and indicate that they are irregularly shaped and exist as agglomerates with interlocking pores and large volume of void spaces. The presence of the pore structures in the micrograph confirms the results of BET individual BJH analysis. Micrographs also suggest that large agglomerates containing individual particles are of the size ranging from 100 to 162 nm.

(a) 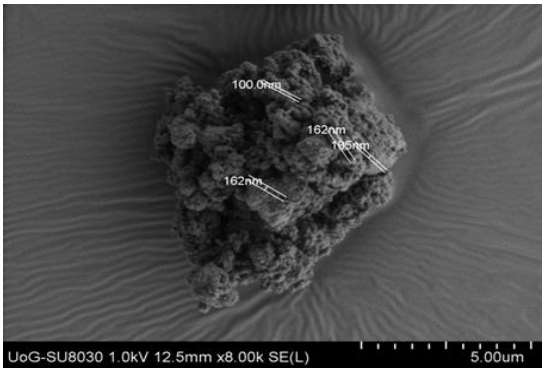

(b) 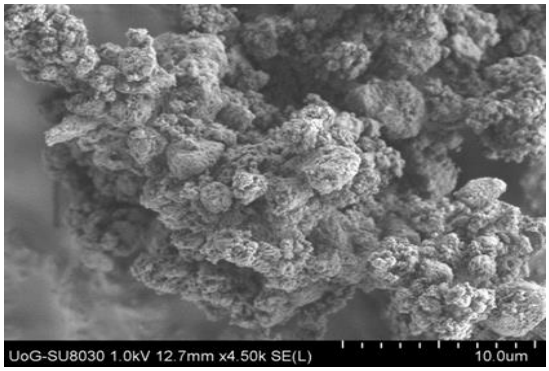

Figure 3.20: SEM micrographs for (a) S_{FP} particles at x8k (b) S_{FP} particles at x4.50k

The micrographs for S_{XDP} particles (Figure 3.21) show that they exist both as singular particles and as irregularly-shaped clusters with interlocking pore and void spaces in between the clusters. These images also confirm the BET results regarding the porous nature of the S_{XDP} particles. The findings suggest that these particles may vary in size from each other, with an estimated size range of 7 to 14 μm.

(a) 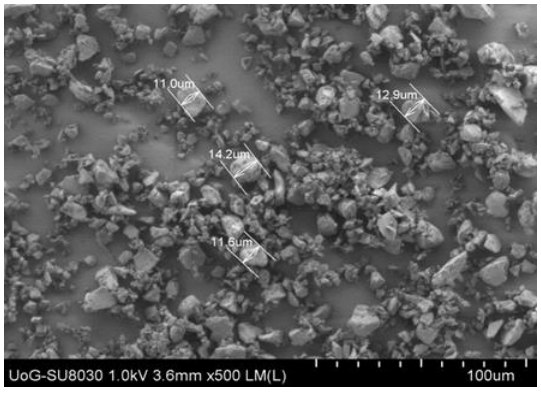

(b) 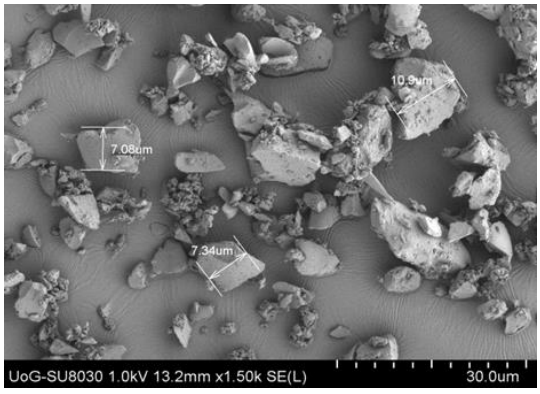

Figure 3.21: SEM micrographs for (a) S_{XDP} particles at x500 (b) S_{XDP} particles at x1.5k

Like the S_{FP} and S_{XDP} particles, the micrographs collected for S_{AL} (Figure 3.22) confirm the BET results that they are non-porous in nature as it shows that these particles exist independently from each other with no presence of aggregates or interlocking pores. Also, like the S_{FP} and S_{XDP} particles, these particles are irregularly-shaped. The estimated particle size range for S_{AL} was between 120 to 140 μm.

(a) 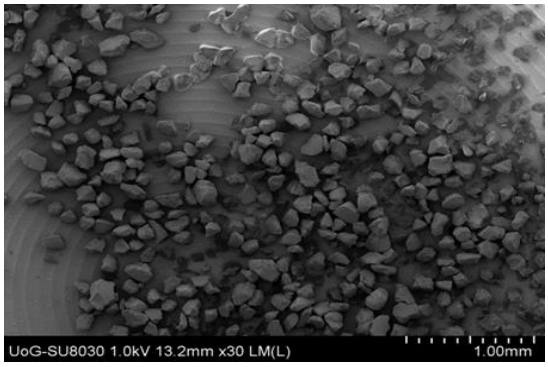

(b) 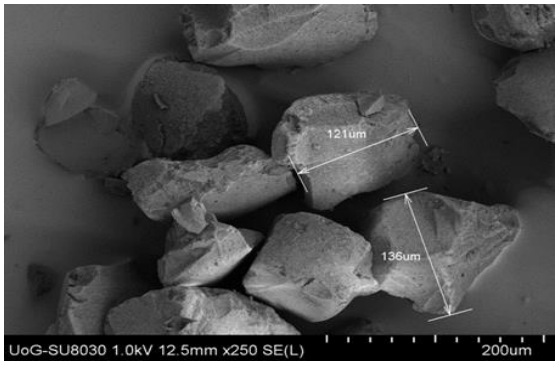

Figure 3.22: SEM micrographs for (a) S_{AL} particles at x30 and (b) S_{AL} particles at x250

The SEM micrographs for MSU-H particles (Figure 3.23) indicate that the particles are alike in structure and do not exist independently from each other. The MSU-H particles exist as clusters with signs of void spaces in between the particles. There is minimal variation in the measured particle sizes with the size ranging from 1 to 2 μm.

(a) 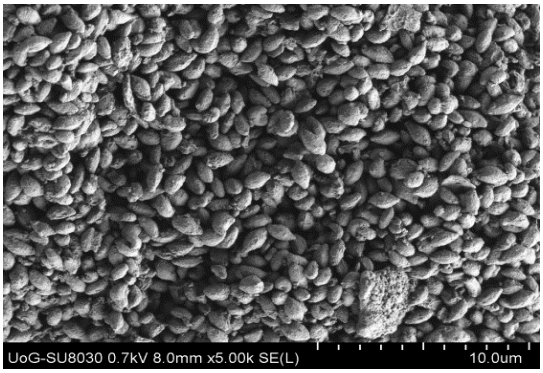

(b) 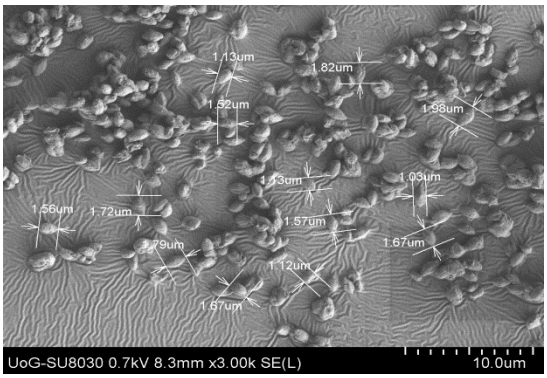

Figure 3.23: SEM micrographs for (a) MSU-H particles at x5k and (b) MSU-H particles at x1.5k

Further structural characterization of the silica particles was carried out by ATR-FTIR analysis and is discussed in section 3.5.

3.5 Structural analysis of silica particles

ATR-FTIR analysis was performed to study the structural properties of the silica particles and the spectra collected are presented in Figure 3.24.

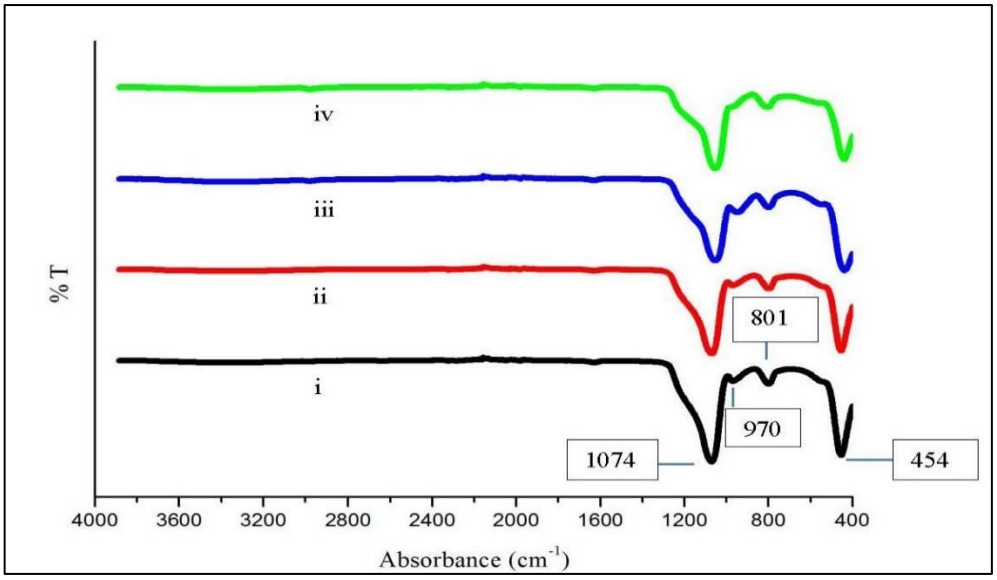

Figure 3.24: ATR-FTIR spectra for (i) S_{FP} (ii) S_{XDP} (iii) S_{AL} and (iv) MSU-H particles

As expected, no differences can be observed between these materials. The absorption bands near 1070 cm^{-1} relate to stretching vibrations of Si-O bonds, while bands near 970 cm^{-1} correspond to the presence of non-bonded $Si\text{-}O^{-}$. The bands at 800 cm^{-1} are also related to bending vibrations of Si-O bonds and that near 450 cm^{-1} is attributed to bending vibrations of O-Si-O bonds [195, 196]. The characterization of these silica materials indicate that they only differ significantly in their surface properties which will be further explored with the adsorption of protein in chapter 5.

3.6 Conclusion

Negatively-charged, spherical PCL and PCL-ES100 particles with uniform size distribution were successfully formulated by solvent extraction of emulsions under either $scCO_2$ or atmospheric conditions. The influence of polymer and surfactant content on particle size and charge was particularly important for the preparation of PCL particles. The structural and surface properties of the polymeric and silica particles were evaluated. In summary, the identical structures of silica particles were seen in ATR-FTIR spectra, while, the presence of ES100 and PCL in their resulting composite system was confirmed by ATR-FTIR and DSC. Based on the nitrogen sorption data, S_{FP}, S_{XDP} and MSU-H particles were determined to be mesoporous in nature while S_{AL}, PCL and PCL-ES100 particles are largely non-porous. Although MSU-H and S_{AL} particles had the highest surface area (m^2/g) when compared to S_{FP} and S_{XDP}, they also had the lowest pore volume and diameter in relation to both silica particles. The largest pore volumes and diameters were recorded for S_{XDP} and S_{FP} particles,

with only slight differences between them. PCL and PCL-ES100 systems had the lowest surface area and pore volume in comparison to the silica particles.

Following the data discussed in this chapter, these core particles (polymeric and silica) will now be investigated for the adsorption of protein as discussed in Chapter 5.

Chapter 4

Protein stability and Iso-electric point determination

This chapter covers preliminary stability studies for γ-globulin and investigations for the IEP of the protein.

4A. Protein stability

This section briefly discusses the analysis involved in monitoring the stability of γ-globulin before its adsorption on core particles.

4A.1 Aims and Objectives

Prior to the immobilization of protein on core particles, it was essential for this work to establish the pH and agitation stability of γ-globulin in the aqueous media. The following studies were carried out to provide better understanding of the stability and robustness of γ-globulin in a number of buffered solutions. This work also played an important role in determining the ideal processing parameters for protein in the development of SCDDS.

4A.2 Experimental

The methods involved in this section for the CD and UV analysis of γ-globulin are described in section 2.3.

4A.3 Introduction

Proteins have a constant active conformation with the unfolded state being non-functional. The secondary and tertiary structures of the protein molecule are considered to play an important role in maintaining its overall active state [135, 197- 198]. Any changes to their required/ native conformation may result in a decrease in biological activity and possible aggregation. Additionally, γ-globulins are classed as “soft” molecules that can easily undergo conformational transitions in response to environmental changes such as pH, hence monitoring conformational changes to the protein’s structure during DDS design is critical [135, 197- 198]. Procedures for monitoring secondary structure are mainly spectroscopic or physical techniques such as ATR-FTIR, CD, and UV-Vis analysis [198]. Few of the commonly used techniques are briefly discussed as follows;

(a) CD spectroscopy: this technique can be performed because polypeptides have optical properties and so can interact in different ways with right- and left- circularly polarized light [198, 199]. The optical characteristics of these molecules are due to the presence of asymmetric centres of their component amino acids (except for glycine). Conformational transitions of the protein are identified as changes in the difference in the absorption of left- and right- circularly polarized light by the protein molecules at the far-ultraviolet (UV) region (< 250 nm) [198, 199].

(b) UV-Vis spectroscopy: this technique is known to be the most convenient measure of protein stability. The absorption of UV by various functional groups such as the carbonyl group of peptide bonds (190-210 nm), disulfide bonds (250-300 nm), and aromatic amino acids (250-320 nm) of the protein molecules result in absorption peaks that can be used to monitor conformation transitions of the protein [198]. Although CD spectroscopy is far more relevant with respect to determining conformational changes of proteins, but major conformational changes can also be easily detected by UV-Vis spectroscopy.

(c) ATR-FTIR spectroscopy: this technique has the benefit of being able to monitor parts of the protein structure in the solid state [198]. Proteins contain peptide/amide bonds that can absorb infrared (IR) radiation allowing it to vibrate with bending and stretching motions [8, 200]. As it requires more energy to stretch a bond than to bend it, absorption bands for stretching vibrations are typically found in the 4000 to 1000 cm^{-1} wavenumber region (or "functional group region"), while bands for bending vibrations are typically found in the fingerprint region (approximately 1000- 400 cm^{-1}) [8, 200]. Among the absorption bands given by protein, the amide I band ranging from wavenumbers of 1600 to 1700 cm^{-1} (mainly due to C=O stretching vibrations) and amide II band (primarily because of N-H bending, and C-H stretching vibrations) found between 1500 to 1600 cm^{-1} are widely used to study conformational transitions of the protein molecule [201, 202]. For instance, because the absorption frequency of the amide I band depends on the three-dimensional configuration of the protein structure, it shows up typically at 1650 cm^{-1} for α-helix and at 1658 cm^{-1} for a random coil configuration [200].

ATR-FTIR and CD analysis were also carried out in this study to monitor any changes to γ-globulin conformation after immobilization on core particles and are discussed in chapter 5.

4A.4 Results and discussion

This section discusses the results for CD and UV-Vis analysis of γ-globulin at pH 5, 6, 7.4 and 9 for 5 hours under continuous stirring at room temperature (23 ± 2 °C).

4.1 UV-Vis spectroscopy

UV-Vis spectra γ-globulin has two distinct peaks in the wavelength range from 200 to 300 nm. The first absorption peak in the region of 200 to 240 nm reflects the structural conformation of the protein and results from the polypeptide backbone structure. The aromatic amino acid residues of the protein give rise to the second absorption peak in the region 250–300 nm [201]. Figure 4.1 presents a typical UV-Vis spectrum of γ-globulin which contains two distinct peaks at 204 and 278 nm. These were monitored during this study to observe any conformational changes in the structure of γ-globulin.

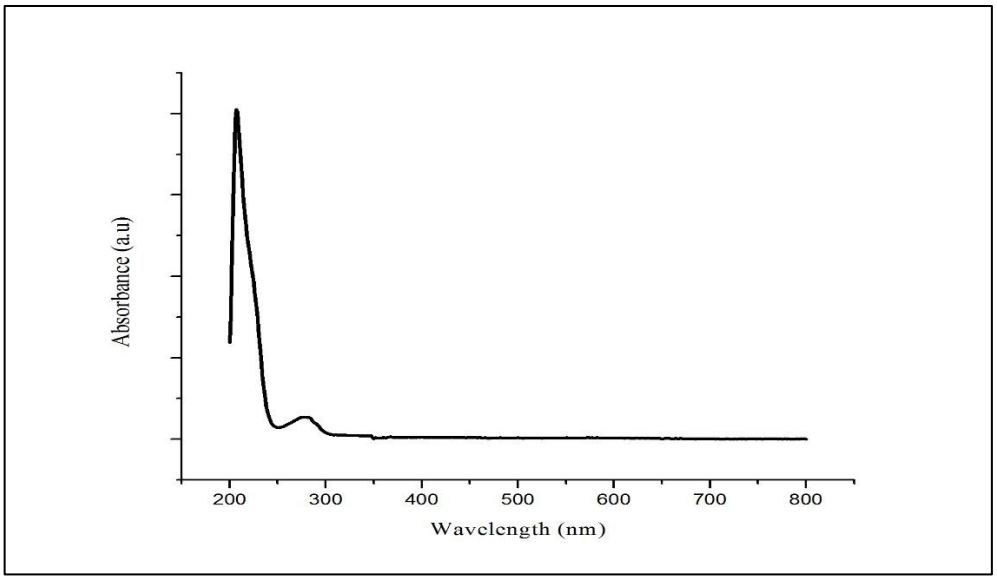

Figure 4.1: Typical UV-Vis spectrum for γ-globulin

The change of absorbance with time for γ-globulin in phosphate buffer pH 5 is presented in Figure 4.2.

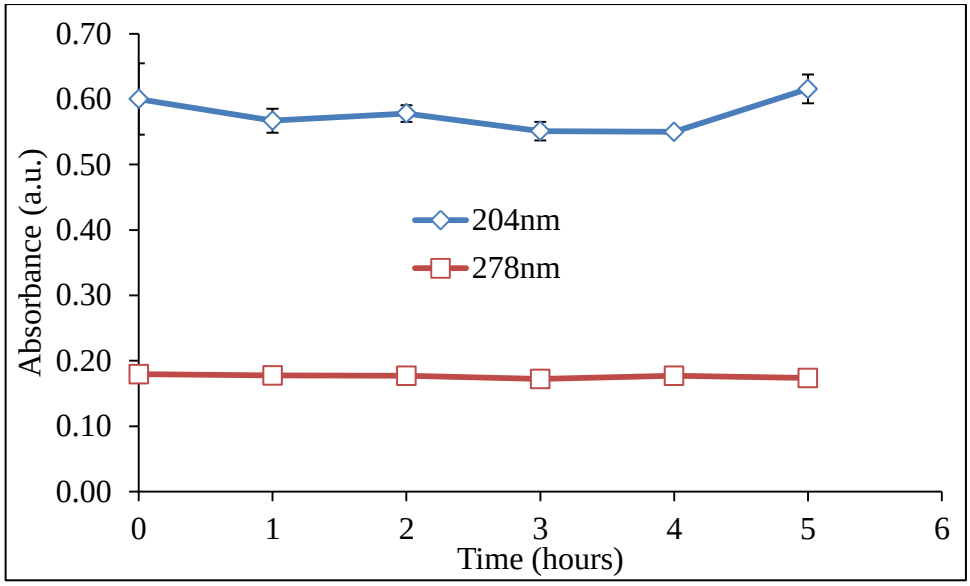

Figure 4.2: Plot of absorbance *vs* time for γ-globulin solution in pH 5

There was no change at 278 nm with continuous stirring of protein solution for up to 5 hours suggesting that the aromatic groups (such as phenylalanine, tyrosine and tryptophan) present within the macromolecular structure are still in place [201, 203]. Absorbance values (0.55 – 0.60 a.u.) also remained constant at 204 nm for the first 4 hours with a slight increase between 4 and 5 hours. The increase in absorbance may indicate possible conformational changes to the polypeptide backbone of the γ-globulin structure.

Minor changes to the absorbance values were also observed at both 204 and 278 nm for γ-globulin solution in pH 6 buffer (Figure 4.3). These may suggest that denaturation may occur to γ-globulin if left stirring at pH 6 for longer than 3 hours.

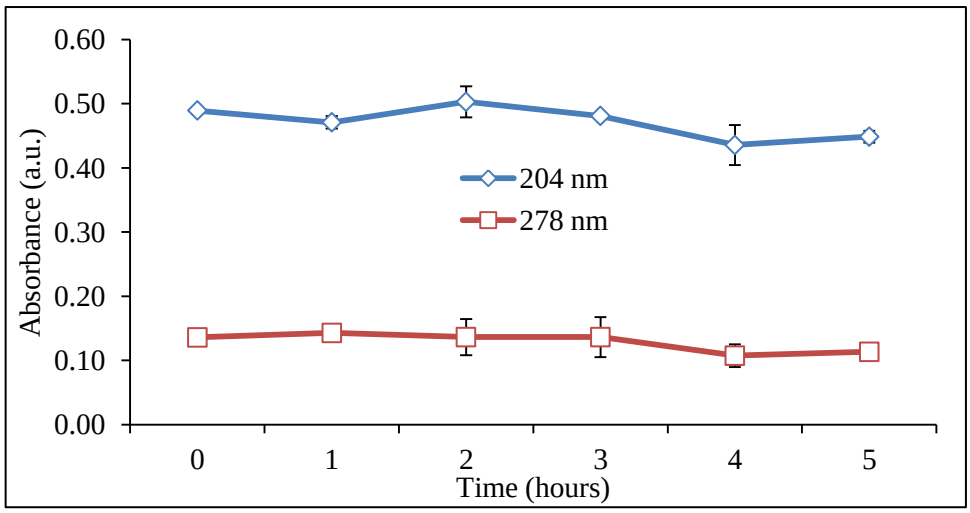

Figure 4.3: Plot of absorbance *vs* time for γ-globulin solution in pH 6

However, differences observed between the absorbance values for γ-globulin solution at pH 5 and 6 can also be attributed to the minute variations in the starting sample concentrations and may not necessarily signify denaturation.

The plot for absorbance against time for protein solution in pH 7.4 is presented in Figure 4.4. A gradual increase in the initial absorbance at 204 nm (0.56 ± 0.02 a.u.) was observed with continuous stirring for up to 5 hours (0.68 ± 0.01 a.u.). The values at 278 nm remained comparatively unchanged for the duration of the experiment.

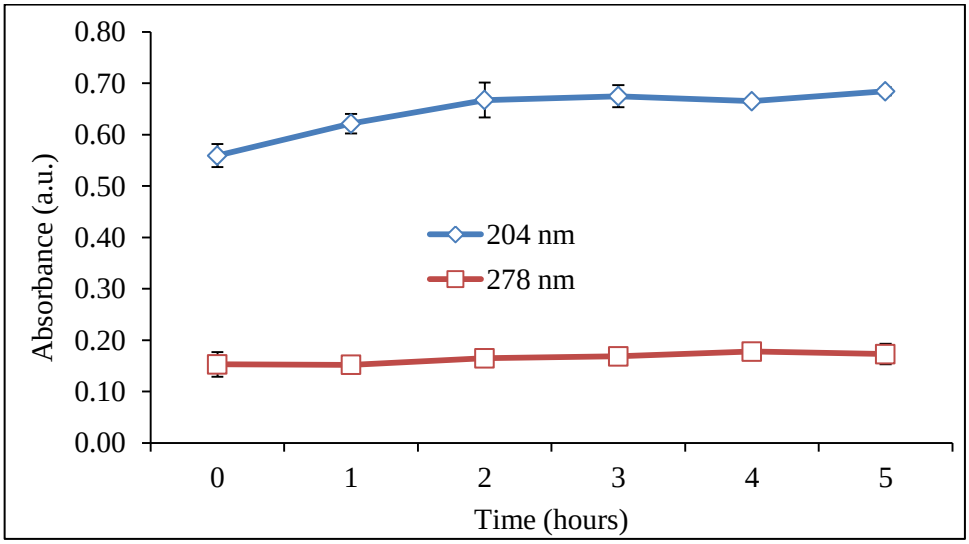

Figure 4.4: Plot of absorbance *vs* time for γ-globulin solution in pH 7.4

There was also an increase in the absorbance at 204 nm as stirring time proceeded up to 5 hours for protein solution in pH 9 buffer.

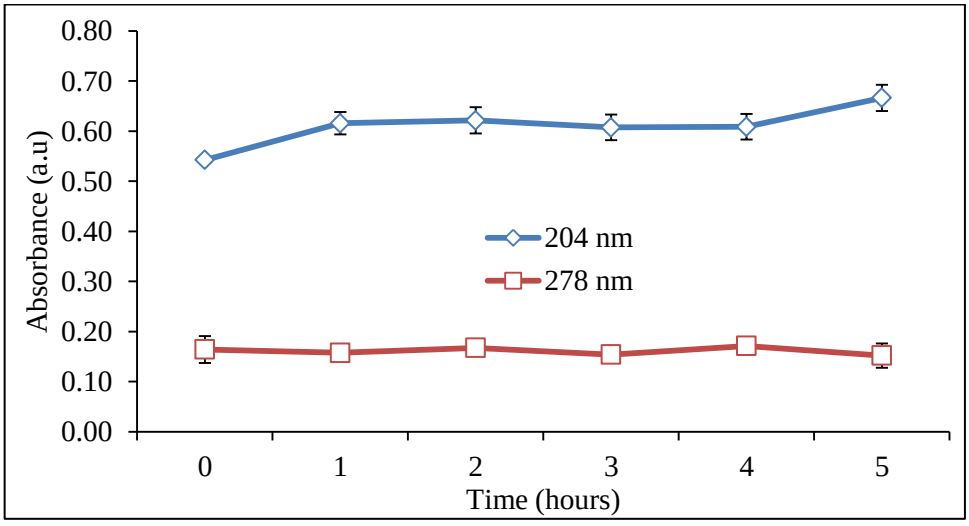

Figure 4.5: Plot of absorbance *vs* time for γ-globulin solution in pH 9

As presented in Figure 4.5 above, absorbance increased from 0.54 a.u. at 204 nm between 0 and 1 hour which then remained relatively stable up till 4 with a further increase towards the end of the experiment. Meanwhile, the absorbance recorded at 278 nm remained comparatively constant all throughout the experiment.

The minor variations in the absorbance observed at 204 and 278 nm with continuous stirring of the aqueous γ-globulin solution at pH 5, 6, 7.4 and 9 may suggest conformational changes to the protein structure. This could be attributed to either or the combination of agitation stress as a result of stirring and the pH of the aqueous solution [204]. With respect to mechanical stirring of protein solutions, there is evidence that this process can generate adequate stress required to overcome the stabilizing forces holding the protein structure together, leading to conformational changes such as unfolding of the protein's three-dimensional structure and exposure of the hydrophobic structural regions to the aqueous environment [204- 206]. The stirring stress provided in this work as a result of the procedure setup could also induce one or more of the following events including; (a) interfacial effects between γ-globulin and the stirrer bar/ glass bottom of the volumetric flask, (b) local thermal effects because of the friction between the stirrer bar and bottom of the flask, and (c) shearing [205, 206]. Agitation stress can also lead to cavitation described as the rapid formation of spaces or bubbles within the protein solution which can quickly breakdown and consequently produce shock waves, highly turbulent flow conditions, higher pressures and temperature which may lead to the production of hydroxyl and hydrogen radicals subsequently causing formation of protein aggregates [205, 206]. However, lack of visual evidence of aggregation in the protein samples suggests cavitation may not be the important mechanism in this case.

The solution pH is a major parameter in determining the rate of conformational change to the protein structure [207- 210]. The pH dictates the type and distribution of surface charges on proteins which consequently affects electrostatic intramolecular folding interactions and intermolecular protein-protein interactions that help stabilize their three-dimensional structure. Proteins are usually stable over a narrow pH range and may possibly unfold or aggregate outside these values. They are heavily charged at extremes of pH (acidic or basic) which increases the repulsive intramolecular and intermolecular interactions resulting in partial/complete unfolding of the protein because of a lower electrostatic energy in the unfolded state [204, 209- 210]. Hence, slight fluctuations in the absorbance values may

signify conformational changes but these differences may have also occurred simply due to the minor variations in sample concentrations.

To confirm the results obtained with UV analysis, further stability tests were carried out on fresh γ-globulin solutions by performing CD spectroscopy as discussed in the following section.

4.2 CD spectroscopy

A typical CD spectrum of γ-globulin is presented in Figure 4.6. It displays a positive intensity maximum at 201 nm and a negative intensity maximum at 218 nm, which is characteristic of β-sheets [201, 211]. This is dissimilar to the spectra recorded for highly α-helical proteins where a double minimum intensity is observed at 208 and 222 nm [212].

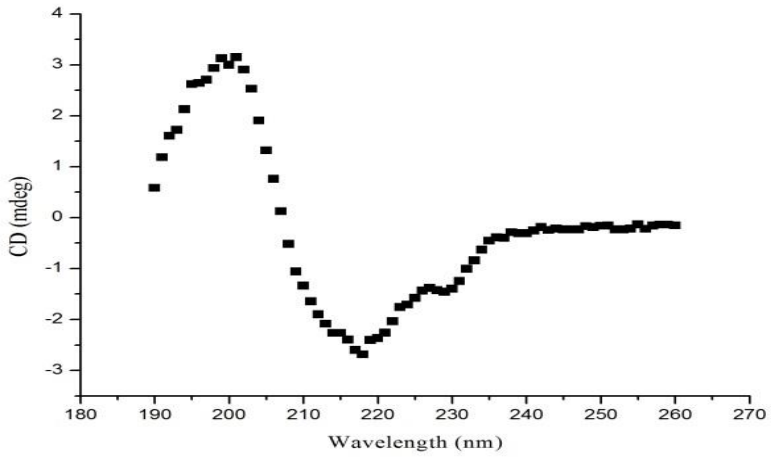

Figure 4.6: A typical CD spectrum for γ-globulin

It is understood that CD spectra in the far-UV region (180–250 nm) analyses the secondary structures of proteins, while the side-chain tertiary structures are observed in the near-UV region (usually from 250 to 350 nm) [201, 211]. In this work, CD spectra ranging from 190 to 260 nm were collected and used to monitor changes to the secondary structure of γ-globulin at pH 5, 6, 7.4 and 9, continuously stirred at 250 rpm for 5 hours at room temperature (23 ± 2 °C).

The CD spectra collected for γ-globulin solution at pH 5 with continuous stirring up to 5 hours is presented in Figure 4.7.

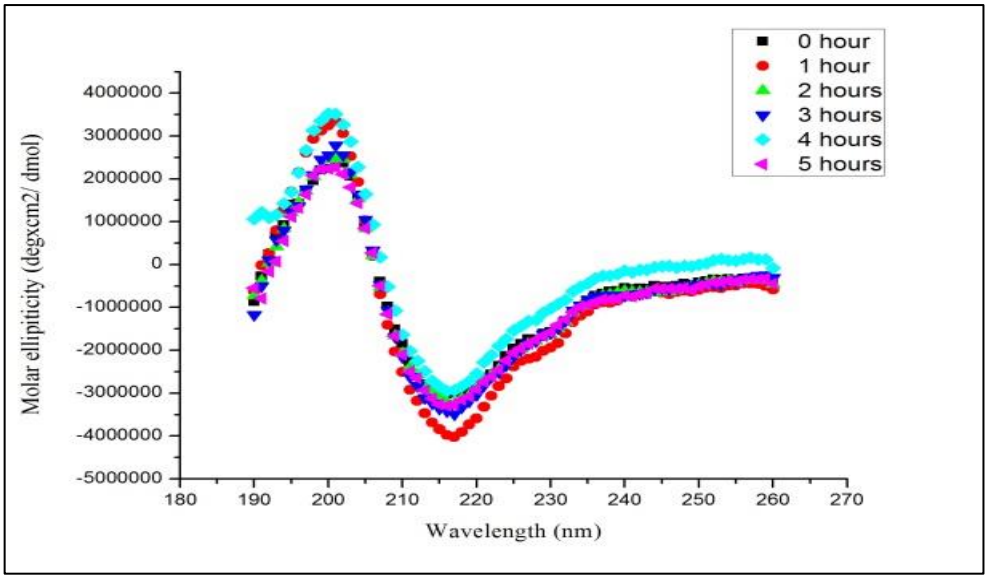

Figure 4.7: CD spectra for γ-globulin solution at pH 5 at times 0 to 5 hours

At pH 5, there was an initial increase in the maximum positive and negative ellipticity values between 0 and 1 hour which is not later observed when stirring is carried on for 2 hours. The recorded maximum values returned back to their initial state at 2 hours and remained relatively stable up to 4 hours. There was an increase and a decrease in the positive and negative maximum respectively at 5 hours. There was also a major change to the ellipticity values recorded between 190 and 195 nm at 4 hours, likely signifying either a rearrangement or loss of γ-globulin secondary structure [212]. Although, this occurrence might be temporary as the spectra returns back to its original shape at 5 hours of continuous stirring.

There were differences between the positive maximum values recorded for γ-globulin solution at pH 6 with continuous stirring up to 5 hours. As presented in Figure 4.8, there was an initial increase in the positive maximum between 1 and 2 hours, followed by a decrease as stirring proceeded to 3 hours, and then it remained relatively stable between 3 and 5 hours.

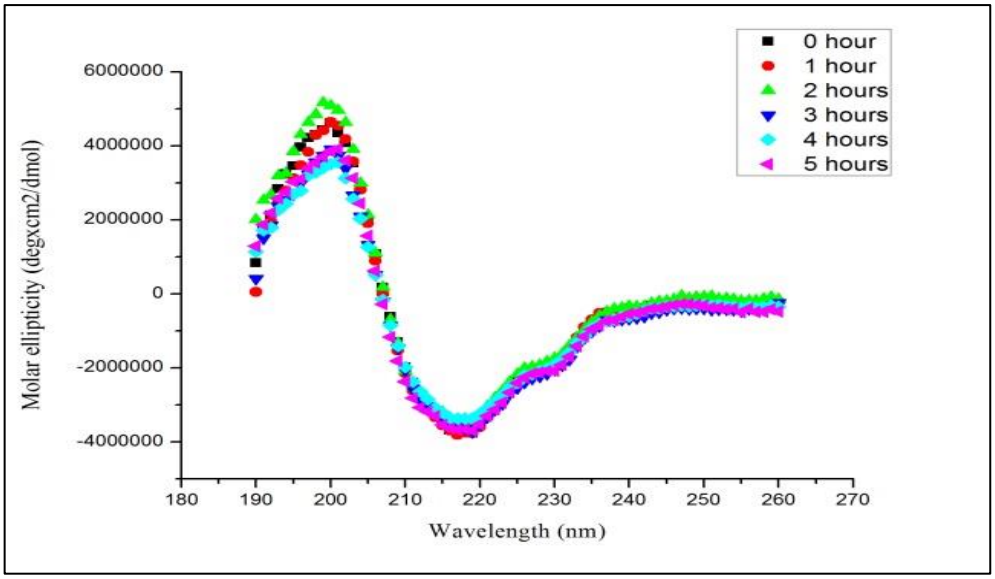

Figure 4.8: CD spectra for γ-globulin solution at pH 6 at times 0 to 5 hours

Aside from the aforementioned differences for γ-globulin solution at pH 6, the spectra generally remained unchanged with respect to the negative ellipticity values collected between times 0 and 5 hours. Similarly, the CD spectra collected for γ-globulin solution at pH 7.4 and 9 (Figure 4.9 and Figure 4.10 respectively) showed variations with time only for the positive ellipticity values recorded between 190 and 205 nm, with no differences between the data from 205 to 260 nm. However, the variations were more pronounced at pH 9 than pH 6 and 7.4, and less prominent at pH 6 than for pH 7.4 and 9.

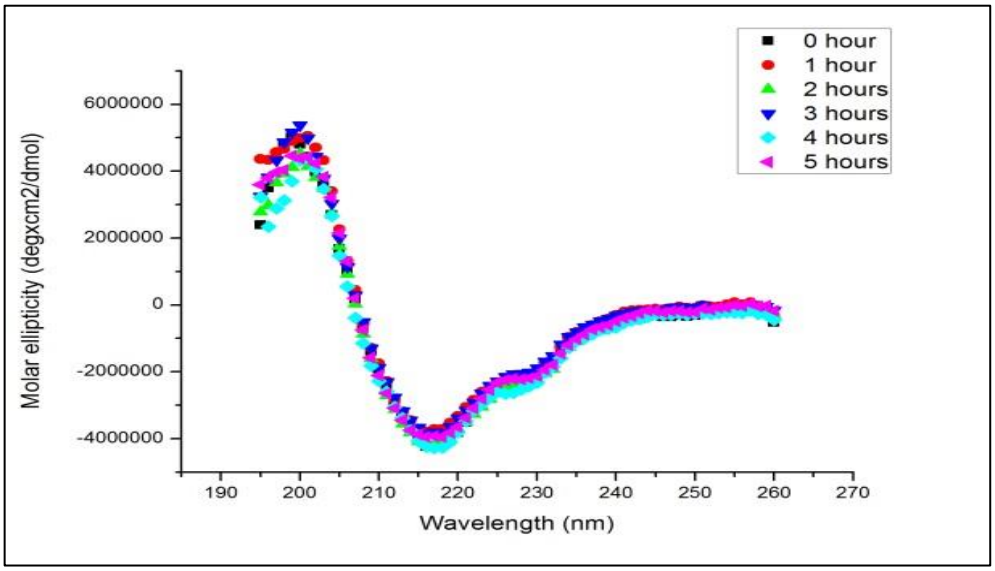

Figure 4.9: CD spectra for γ-globulin solution at pH 7.4 at times 0 to 5 hours

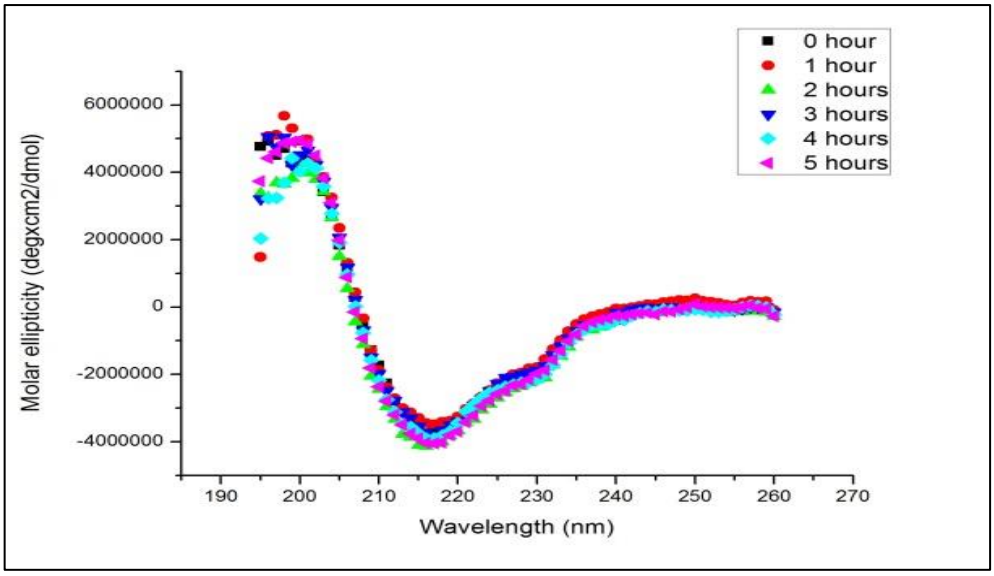

Figure 4.10: CD spectra for γ-globulin solution at pH 9 at times 0 to 5 hours

Based on the CD analysis, it could be stated that both the pH and mechanical stirring of γ-globulin solution play an important role in the rate at which conformational changes occur in the protein secondary structure. In comparison to the typical CD spectrum of γ-globulin, the initial spectra recorded at t= 0 for γ-globulin at pH 5, 6 and 7.4 showed no difference. Variations to the spectra were only observed after stirring was introduced to the protein solution and were more pronounced after 4 hours of continuous stirring. Meanwhile, the initial spectrum recorded at t = 0 for γ-globulin at pH 9 differed from those at pH 5, 6 and 7.4 indicating a difference in γ-globulin stability. As stated earlier, the agitation stress provided by stirring and the electrostatic influence of pH on the protein structure may result in the conformational changes that affect the stability of protein. These studies suggest that γ-globulin was most stable at pH 6 under stirring at room temperature.

In addition to γ-globulin stability, the iso-electric point of the protein was also considered in the design of SCDDS and is discussed in section 4.3.

4B. IEP determination

This section briefly discusses work carried out relating to IEP determination for γ-globulin.

4B.1 Aims and Objectives

The aim of this work was to understand the influence of pH on the net charge of the γ-globulin molecule. To achieve this, the Z-potential of γ-globulin in an aqueous media was studied across a range of pH values.

4B.2 Experimental

The steps involved in this process are described in section 2.4.

4B.3 Introduction

Proteins consist of charged amino acid residues covalently or tightly attached to them which are mostly present in the interior of their structure but also over the entire macromolecular surface. These residues can be positive, negative, neutral or polar in nature, and together give the protein its overall or net charge [213]. IEP of a protein is described as the pH at which the numbers of negative and positive charges are equalized allowing for a net neutral electrical charge [214, 215]. Accordingly, proteins will be positively charged when the pH is lower than IEP and negatively charged at a pH greater than their IEP. Therefore, IEP plays an important role in understanding the electrostatic state of proteins and consequently being able to influence the stability and immobilization of these macromolecules onto charged surfaces [204, 210, 214- 215]. Hence, the data derived from this work will be important in determining the ideal parameters for SCCDS formulation.

In relation to protein stability, conformational structural changes are said to be least likely to occur at or around the IEP. This is attributed to the fact that proteins have a net neutral charge at the IEP thus there will be no electrostatic contribution to protein stability [204, 210]. However, there is still evidence of attractive dipole protein-protein interactions at pH around the IEP as a result of the presence of oppositely charged groups which may lead to aggregation of the macromolecule [204, 209]. In relation to protein adsorption on a solid surface, the total amount of immobilized protein is generally perceived to be maximized at or around the IEP [214, 215]. This is attributed to the reduced electrostatic protein–protein repulsions and decreased protein-protein interactions which enable the molecules to closely

arrange themselves at the adsorbing surface resulting in higher packing density. The electrostatic state of the protein also governs how they interact with a charged adsorbent surface. Electrostatic attractions because of opposite charges on the protein (at pH > or < IEP) and adsorbent surface can result in an accelerated migration towards the surface, and consequently an increase in adsorption rates [214, 215]. The investigations carried out to determine the net charge of γ-globulin with respect to change in pH are briefly discussed as follows.

4B.4 Results and discussion

The plot of zeta-potential against pH for γ-globulin is presented in Figure 4.11.

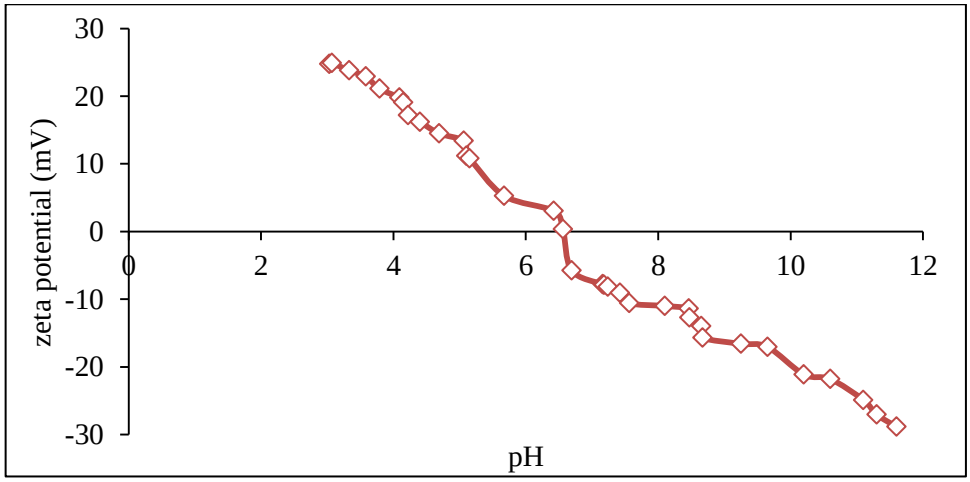

Figure 4.11: pH Titration curve for γ-globulin

As observed, the net charge for γ-globulin gradually changes with pH, remaining positive at lower pH (< 6.60) and turning negative at higher pH (> 6.60). Therefore, the IEP of γ-globulin was determined to be around pH 6.60. The IEP for γ-globulin reported in this study differs slightly from other work (between pH 7.2-7.8) and it may be attributed to the fact that γ-globulin sample analysed here is a mixture of different types of immunoglobulin (e.g. IgG, IgA, and IgM) as opposed to a single type (IgG) used in other work [216, 217].

As stated earlier, the net charge of a protein results from the presence of charged amino acid residues including cysteine, tyrosine and lysine. The amino acids contain ionizable carboxylic and amine groups, and ionization of these functional groups result from the reversible exchange of protons with the acid (*e.g.* HCl) or base (*e.g.* NaOH) in solution [213]. The net positive charge at pH below IEP occurs due to the protonation of the amide group (NH_3^+),

whereas deprotonation of the carboxyl group (COO^-) above I.E.P results in the net negative charge in the protein. At the IEP, amine groups present are assumed to be completely protonated and the carboxylic groups are also fully deprotonated resulting in a net neutral charge [213].

Additionally, the pH titration curve recorded for γ-globulin can be used to further understand the stability data discussed above in section A.4 where the protein was found to be least stable at pH 9. γ-globulin attains strong negative charge as pH reaches close to pH 9 resulting in the increase of repulsive inter/intra- molecular forces and consequently the partial or complete unfolding of the protein.

4.3 Conclusion

The influence of pH on the surface charge and stability of γ-globulin was successfully investigated. The protein molecule was found to be least stable at pH 7.4 and 9 when compared to pH 5 and 6. The IEP of γ-globulin was determined to be at pH 6.6, with a net positive and negative charge below and above it respectively. The increased instability of γ-globulin at pH values away from the IEP can be attributed to net negative charge. Based on the aforementioned results, a suitable pH can be selected to investigate the γ-globulin immobilization onto core particles which could be either below the IEP (pH 5), around the I.E.P (pH 6), and/or just above the I.E.P (pH 7.4 and 9). Although it has been established that γ-globulin is least stable at pH 7.4 and 9 but adsorption will still be carried out at these pH values to understand the effect of electrostatic interactions and its impact on protein adsorption on a solid surface. Furthermore, stirring of γ-globulin solution during adsorption experiments will be limited to 4 hours due to their reduced stability thereafter. The adsorption of γ-globulin onto solid core particles is discussed in Chapter 5.

Chapter 5

Protein adsorption studies for core particles

This chapter discusses the adsorption of γ-globulin onto inorganic silica particles (S_{AL}, S_{XDP}, S_{FP}, and MSU-H) and organic polymeric particles (PCL and PCL-ES100). The structural and surface characterization of protein-adsorbed particles is also discussed in this chapter.

5A. Protein adsorption studies

This section covers the studies investigating the immobilization of γ-globulin onto suitable core materials.

5A.1 Aims and Objectives

This aspect of the study focused on the immobilization of γ-globulin onto the solid surfaces of core materials. The following studies were carried out to determine the ideal parameters for protein adsorption (including pH and γ-globulin concentration) for each core particle. Additionally, the rate of γ-globulin immobilization at the determined ideal conditions was also studied for each particle.

5A.2 Experimental

Details of the experimental procedures for maximum adsorption studies are listed in section 2.5.1. The methods involved in the kinetic processes for the core particles are detailed in section 2.5.2. The adsorption experiments were limited to 4 hours due to the results of γ-globulin stability testing (section 4A.4).

5A.3 Introduction

Adsorption or immobilization is defined as the adhesion of substances or molecules to the surface of a particle [218]. The immobilization of protein molecules at a solid interface can simply occur when an aqueous solution of the macromolecule is introduced to a known amount of the adsorbent. A complete adsorption process consists of several stages including: (i) passage of adsorbate from bulk solution into the interfacial region, (ii) attachment of adsorbate at the sorbent surface, and (iii) optimization of adsorbate-surface interaction, which in this case can involve relaxation of attached protein molecules by structural changes. The degree of relaxation determines how easily the immobilized protein desorbs [218].

Nevertheless, protein adsorption onto a solid surface is a complicated process because unlike "small" molecules (*e.g.* nitrogen gas), these large molecules can reach sorbent surfaces by two different mechanisms [219]; direct adsorption and progressive exchange. Direct adsorption involves direct attachment of protein molecules onto the adsorbent surface. This continues until the surface including accessible pores become saturated with the adsorbing molecules. Progressive exchange on the other hand requires progressive removal of pre-adsorbed molecules before adsorption of protein molecules on the surface [219- 220]. Overall immobilization of protein molecules onto solid surfaces is known to be a dynamic exchange process, which can also be irreversible. Bentaleb *et al* proposes that three different populations of immobilized protein molecules can exist at the surface: (i) a rapidly interchangeable and/ or desorbable population, (ii) a population which is not exchangeable and can only slowly desorb from the surface, (iii) an irreversibly adsorbed population [220].

With regards to existing literature, one of the key driving forces affecting protein immobilization onto a solid particle are cohesive interactions between the protein and the adsorbing surface. The protein-surface interactions can include van der Waals, hydrogen bonding, electrostatic forces, and hydrophobic interactions [222, 223]. The protein immobilization can take place either by physical adsorption (physisorption) or chemical adsorption (chemisorption) [200]. The main properties of chemical/ physical adsorption are listed in Table 5.1. It is worth noting that protein immobilization can also occur by both mechanisms simultaneously. For instance, the molecule could first adsorb by physisorption and then later chemisorb on to the surface [200].

Table 5.1: Properties of physisorption and chemisorption [200]

Physisorption	**Chemisorption**
Normally *via* van der Waals forces, hydrophobic effect, electrostatic interaction or hydrogen bonding.	Usually stronger interactions than van der Waals such as covalent bonding.
Usually occurs rapidly.	Can occur rapidly or slowly.
Occurs at low temperatures.	Usually requires activation energy. The heat of adsorption is greater than that for physisorption.
Binding is reversible.	Binding is largely irreversible and often leads to chemical changes in the adsorbate molecules.
Can result in the formation of multilayers by intermolecular interactions with involving van der Waals forces.	Results only in the formation of a monolayer.

Protein molecules try to optimize their interaction with the adsorbing surface during the adsorption process which requires structural rearrangements to allow the macromolecule to relax/spread out thus increasing their points of contact with the surface. Changes to the protein's structure during immobilization are also known to contribute in entropic gain to promote their adsorption [135]. This occurrence is more likely to be observed with 'soft' proteins such as IgG, albumin and haemoglobin *etc.* [135]. This study will rely on the physisorption of protein molecules onto the surface of solid core particles.

5A.4 Results and discussion

The following sections discuss the data obtained for the maximum and kinetic studies for the adsorption of γ-globulin onto polymeric and silica core systems.

5.1 Maximum adsorption studies

This section discusses the results for experiments investigating the plateau amounts of γ-globulin adsorbed onto S_{AL}, S_{XDP}, S_{FP}, MSU-H, and PCL-ES100 particles. Adsorption isotherms are presented as plots of adsorbed protein amounts (mg/g) *vs* concentration (mg/ml) and related to the Langmuir and Freundlich models. Adsorption isotherms for PCL particles are not presented because of the lack of any protein adsorption onto these particles.

5.1.1 Adsorption isotherms

IgG can interact with a solid surface in various ways as presented in Figure 5.1. This may occur using their constant region (Fc) or antigen binding sites (Fab) or both. However, it has been shown that most of the structural changes are primarily limited to the Fc region [135, 224].

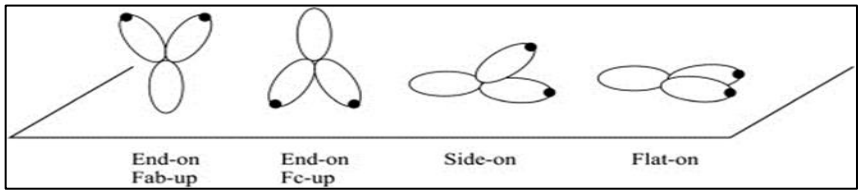

Figure 5.1: Modes of adsorption of IgG molecules [135]

Adsorption can be measured by the decrease in concentration of a protein solution of known concentration when an adsorbent surface is exposed to it. This difference is usually presented as the mass of protein molecules (mg) bound to one gram of adsorbent [135, 200, 224- 227].

An adsorption isotherm is a curve that relates the quantity of adsorbed protein to the equilibrium protein concentration. It is generally used to describe binding interactions between the adsorbate and adsorbent [135, 200, 224- 227]. Among the adsorption isotherm models present in literature, two are typically used to fit experimental results for protein adsorption; Langmuir (equation 5.11) and Freundlich (equation 5.12) [226]. The Langmuir's isotherm can be used to describe a dynamic protein adsorption process where it is assumed that (i) a monolayer is formed at the adsorbent surface (ii) there are no interactions amongst adsorbed molecules, and (iii) no conformational change occurs to the protein structure upon adsorption [226]. On the other hand, Freundlich's isotherm can be used to certify several immobilization processes permitting for one or more interactions either between adsorbed molecules or between the adsorbed molecules and sorbent surface [226].

$$Langmuir's\ model: \frac{C}{Q} = \frac{1}{bQ_m} + \frac{1}{Q_m}C \qquad \text{Equation 5.11}$$

$$Freundlich's\ model: \frac{Q}{Q_m} = kC^{1/n}\ or\ \ln Q = \frac{1}{n}\ln \mathrm{C} + \ln \mathrm{k}Q_m \qquad \text{Equation 5.12}$$

Where; C is the protein concentration, Q_m and Q are the maximum and actual amounts of adsorbed protein respectively, while b, n and k represent constants under specific conditions [226]. The adsorption isotherms for the studied core particles are presented below as plots of adsorbed γ-globulin (mg/g) vs protein concentration (mg/ml), followed by model fitting using Langmuir/ Freundlich's model (section 5.1.2).

The adsorption isotherms for S_{FP} particles as a function of pH are presented in Figure 5.2. The plots for S_{FP} show a well-defined plateau level for the immobilization of γ-globulin onto the surface of these solid particles.

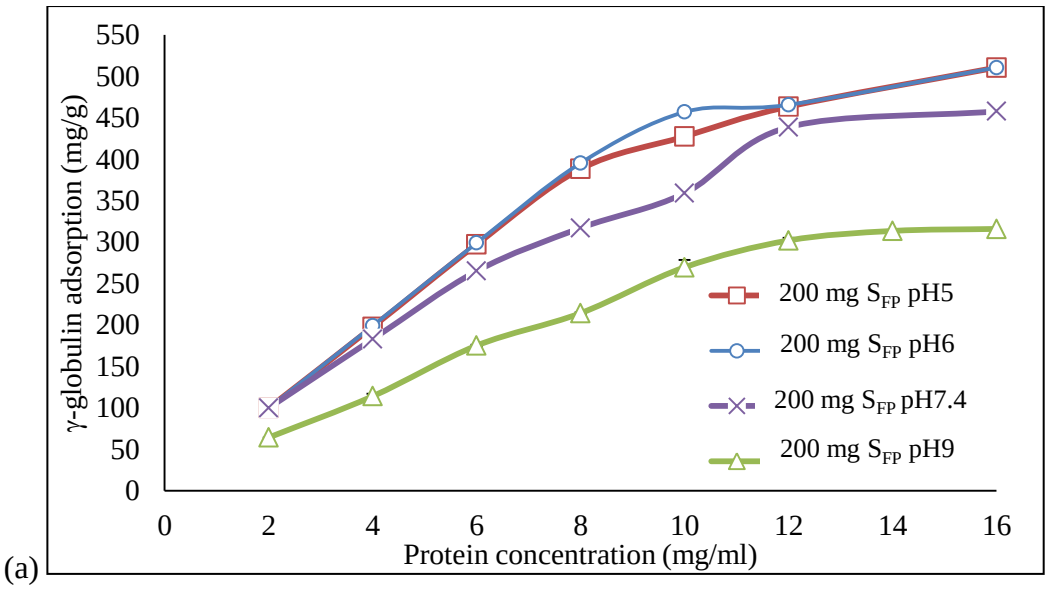

(a)

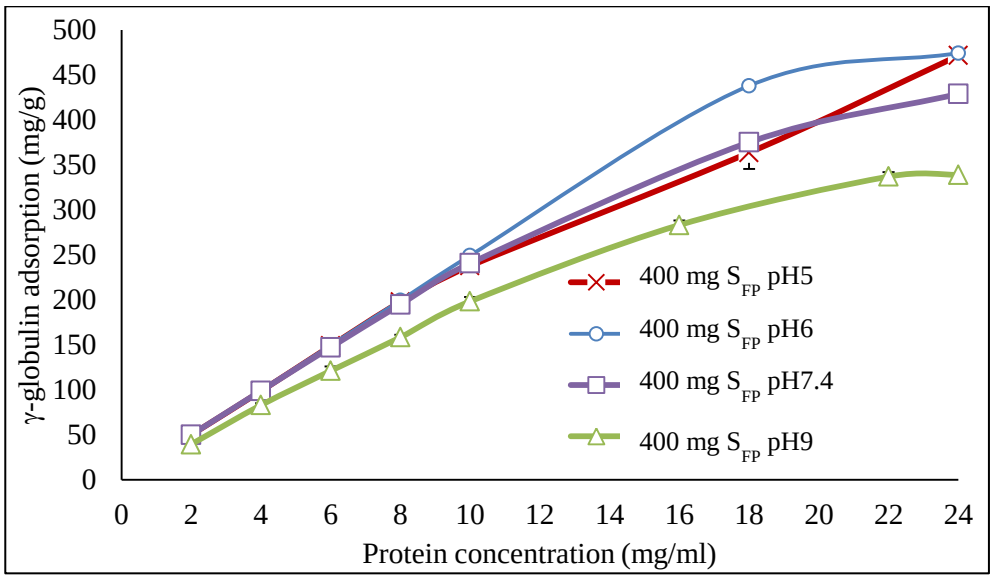

(b)

Figure 5.2: Adsorption of γ-globulin onto (a) 200mg and (b) 400 mg of S_{FP} particles

Adsorption isotherms with a well-defined plateau value are typical for immobilization of macromolecules on solid sorbent surfaces [135, 228- 229]. There is a transition from partial to full surface coverage with the adsorption of γ-globulin onto S_{FP} particles. As presented in Figure 5.2, at all pH values in relation to both amounts of S_{FP} (200 and 400mg) there was a sharp increase in the amount of adsorbed γ-globulin (mg/g) with a rise in initial protein concentrations (2 to 10 mg/ml). The adsorbed amount started to level off as the protein concentration approached higher values above 10 mg/ml. A plateau was achieved at or above 10 mg/ml with 200 mg S_{FP} for all pH values and 18 mg/ml with 400 mg S_{FP} at pH 6 and 7.4, and at 16 mg/ml for pH 9. Although a plateau was not obtained at pH 5 with 400 mg S_{FP}, the

experiment was halted at 24 mg/ml to allow for a comparative data with other pH values. It is understood that the rapid increase at initial concentrations (2 to 10 mg/ml) is associated with high affinity of protein for the sorbent surface. The plateau signifies saturation of the adsorbent surface with a closed-packed monolayer of macromolecules. Therefore, any additional rise in the protein concentration usually does not lead to further increase in adsorption. The comparative surface coverage at various concentrations can be established by estimating the amount of γ-globulin molecules per unit area of the S_{FP}. For instance, by using the particles' BET SSA (289 m^2/g), the estimated protein coverage of 0.17 mg/m^2 at 2 mg/ml and 1.51 mg/m^2 at the plateau (18 mg/ml) was obtained for 400 mg S_{FP} particles.

In line with results obtained for S_{FP} particles, the amount of γ-globulin (mg/g) adsorbed onto S_{XDP} (Figures 5.3a and b) rose quickly with increasing protein concentration at all pH before gradually reaching a plateau at 8 and 16 mg/ml for 200 and 400 mg S_{XDP} respectively. γ-globulin immobilization with S_{XDP} further indicates saturation of the particle surface at equilibrium protein concentration.

(a)

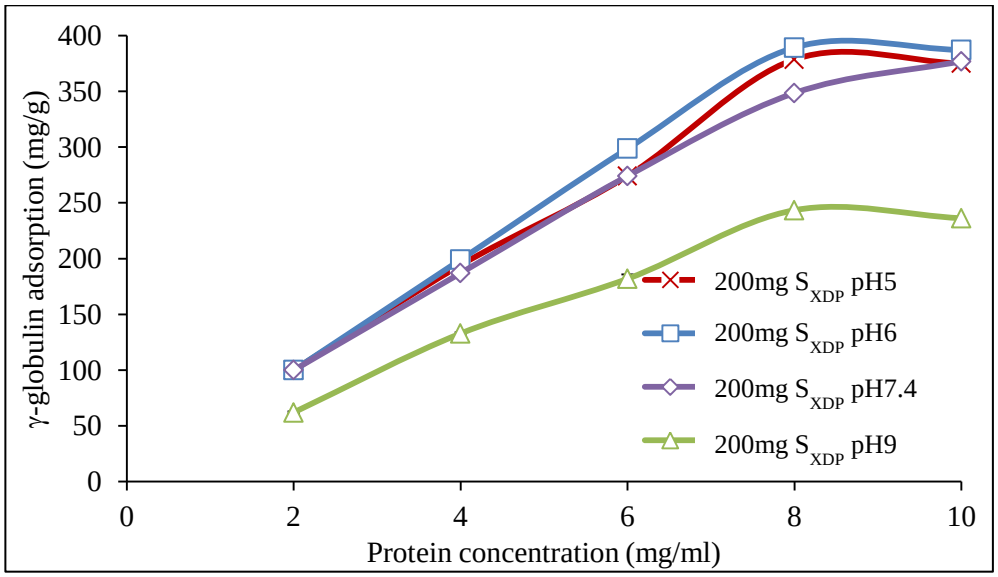

(b)

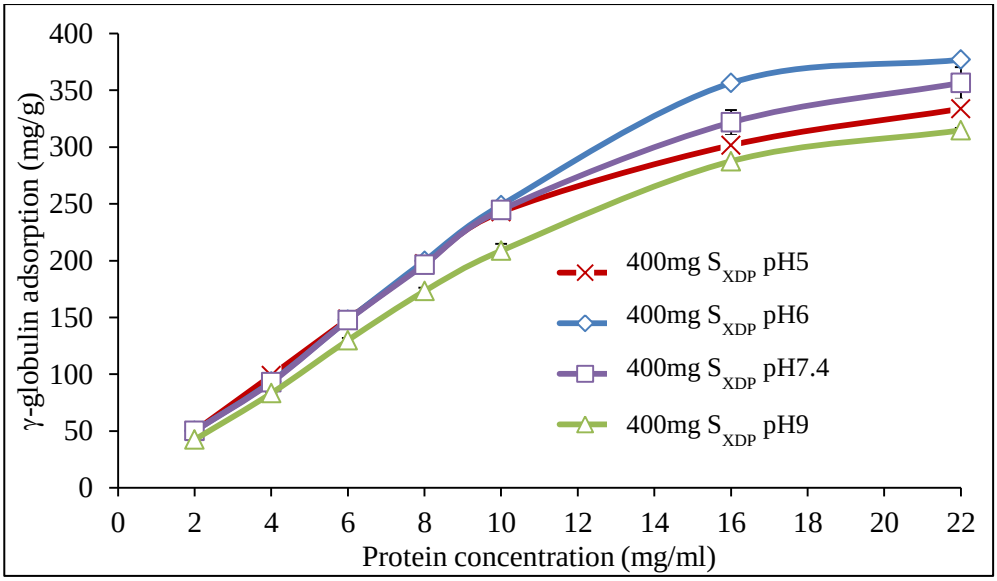

Figure 5.3: Adsorption of γ-globulin onto (a) 200mg and (b) 400 mg of S_{XDP} particles

Generally, for both S_{FP} and S_{XDP}, there was a reduction in the quantity of immobilized γ-globulin when the adsorbent mass was doubled to 400 mg. This could be explained by the difference in surface coverage as a result of the increase in effective surface area at the higher silica mass (400 mg). For example, γ-globulin adsorption at 2 mg/ml resulted in 100 mg/g (0.35 mg/m^2) of protein on 200 mg of S_{FP} in comparison to 50 mg/g (0.17 mg/m^2) with 400 mg at pH 6. A higher surface coverage at the lower adsorbate amount (200 mg) could be attributed to the orientation of immobilized γ-globulin molecules. As previously stated, protein molecules can undergo structural rearrangements on adsorption to optimize their interaction with the adsorbing surface [135]. This occurrence is less likely if adjacent adsorption sites are occupied by neighbouring protein molecules. The flexibility of the adsorbing protein molecule is not restricted when adjacent sites are not filled, and it has more space to relax at the surface [135]. It can be proposed that at lower γ-globulin concentrations (2 – 10 mg/ml) the probability of empty adjacent adsorption sites is greater with 400 mg S_{FP}/ S_{XDP} than 200 mg due to the higher ratio of particle to protein molecules. Therefore, at 400 mg S_{FP}/ S_{XDP} the protein molecules would be able to spread out, leading to higher surface coverage per molecule. The crowding of protein molecules at the surface in the case of experiments with 200 mg silica can be expected to result into different packing orientation and higher protein density at the surface [228, 230- 231].

The γ-globulin adsorption against protein concentration on 200 and 400 mg S_{AL} particles is presented in Figures 5.4a and b.

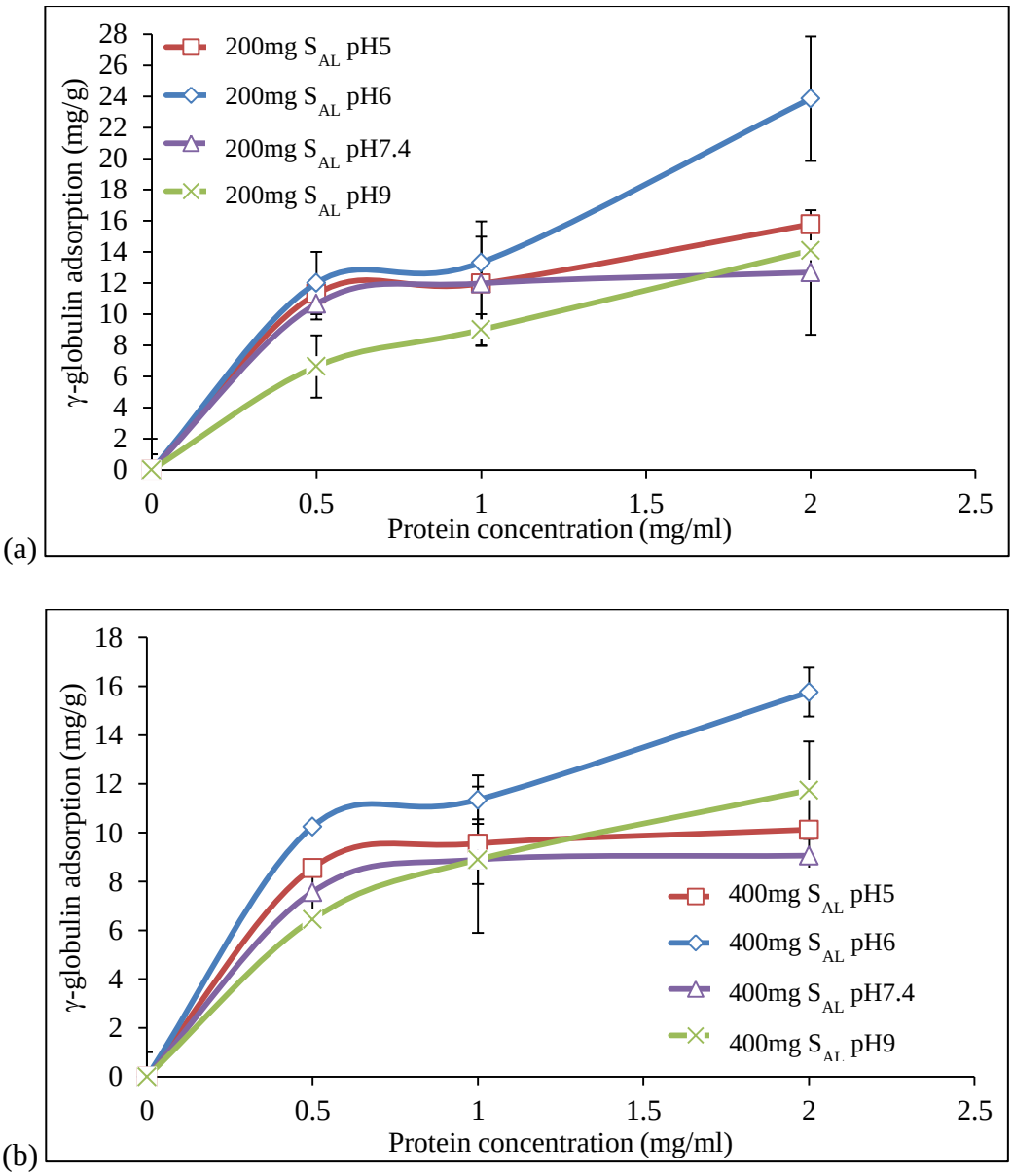

Figure 5.4: Adsorption of γ-globulin onto (a) 200mg and (b) 400 mg of S_{AL} particles

In contrast to both S_{FP} and S_{XDP} there was limited increase in the amount of adsorbed γ-globulin with increasing protein concentration (mg/ml). There was no increase in the amount of protein adsorption at pH 5, 7.4 and 9. However, a sudden surge in adsorbed protein could be seen at pH 6 with 2 mg/ml γ-globulin concentration which may suggest formation of multilayer [200]. The experiment was stopped at 2 mg/ml because over 70% of free protein was still present in solution after 4 hours. The quantity of protein adsorbed onto S_{AL} ranged from only 13 to 24 mg/g depending on γ-globulin concentration (0.5 to 2 mg/ml respectively) and pH. Thus, implying that immobilization of γ-globulin on S_{AL} may be limited due to its comparatively non-porous nature.

In general, the highest quantity of immobilized γ-globulin on the silica particles was observed at pH 5 and 6 while adsorption at pH 9 resulted in the least amount. This can be attributed to the influence of net charge on the protein and stability at this pH as discussed in Chapter 4. There was a reduced conformational stability of γ-globulin with increasing net charge on the molecule at pH 9 in comparison to the other pH values. This means higher surface coverage per molecule and consequently less adsorption can be expected due to high probability for structural rearrangements at pH 9 [231, 232]. The γ-globulin molecule has a comparatively higher net negative charge (~ -16 mV) at pH 9 than pH 7.4 (~ -9 mV). It is positively charged at pH 5 (~ +12 mV) and almost neutral at pH 6 (~ +3 mV). This would mean that in terms of possible electrostatic interactions with negatively-charged adsorbent (silica), pH 5 was more favoured due to opposite charges and least favoured at pH 9 owing to repulsion [233- 235]. However, it is worth noting that these electrostatic interactions are not primarily responsible for γ-globulin adsorption onto the silica particles as immobilization still occurs to a great extent for both S_{FP} and S_{XDP} at pH 6, 7.4 and 9 irrespective of their electrostatic state. Protein adsorption is generally known to be a net result of various interactions including van der Waals forces, hydrogen bonding, hydrophobic interactions and the electrostatic forces. This is attributed to the fact that proteins are large molecules with a number of active sites that can allow for these interactions to occur simultaneously [223].

In summary the highest γ-globulin adsorption was recorded for S_{FP} and the lowest with S_{AL} at all studied pH. Both S_{XDP} and S_{FP} particles adsorbed more than 10 times the amount of γ-globulin than S_{AL}. This suggests a correlation between the surface properties particularly porosity and pore size of the adsorbent and amount of protein adsorbed [236]. The comparatively low porosity and small pore sizes on S_{AL} particles was confirmed by BET as shown in Table 5.2.

Table 5.2: Physicochemical characteristics of silica core particles

	S_{FP}	S_{XDP}	S_{AL}
BET surface area (m^2/g)	289	258	767
BJH cumulative pore volume (ml/g)	1.35	1.44	0.40
Pore diameter (nm)	19.1	22.2	2.5

S_{FP} and S_{XDP} are mesoporous in nature with a comparatively high pore volume and large pores in comparison to S_{AL}. Therefore, it can be confirmed that the immobilization of γ-

globulin onto these inorganic materials was dependent on the porosity and type and size of pores along with pH.

The effect of surface porosity and pH on the immobilization of γ-globulin onto silica was further observed with MSU-H particles. Experiments with MSU-H were limited to pH 5, 6 and 7.4 due to low adsorption at pH 9. As presented in Figure 5.5, unlike adsorption isotherms for S_{FP} and S_{XDP}, the plot of adsorbed γ-globulin (mg/g) *vs* protein concentration (mg/ml) for MSU-H does not show a well-defined plateau at pH 6 and 7.4.

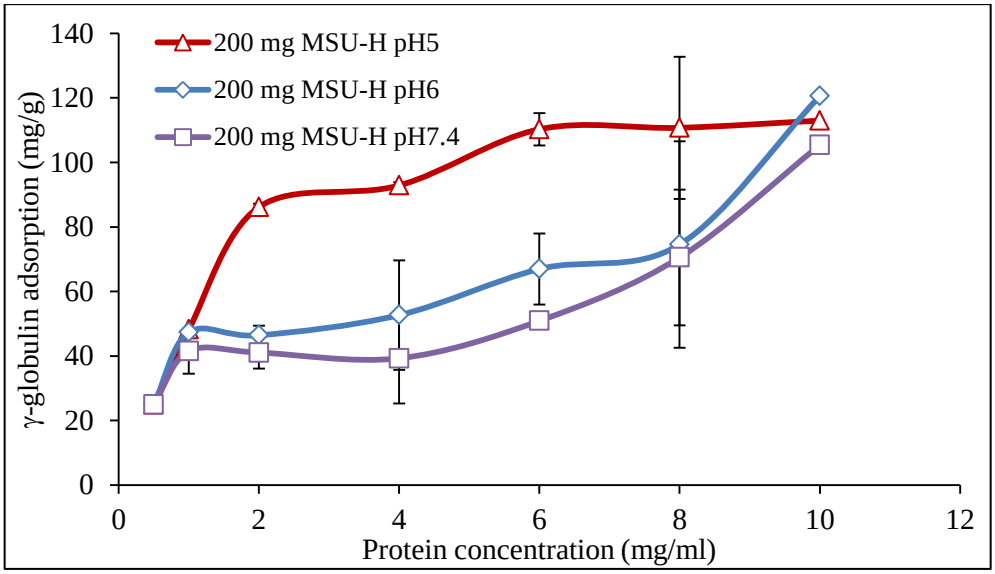

Figure 5.5: Adsorption isotherm for MSU-H particles at pH 5, 6 and 7.4

The isotherm for MSU-H (particularly at pH 6 and 7.4) suggested an initial immobilization on available spaces at the particle surface at lower concentrations (0.5 to 4 mg/ml) followed by the possible formation of multi-layer as the amount of free protein increases [237]. The plateau at pH 5 was achieved at 4 mg/ml which was lower when compared to S_{FP} and S_{XDP} particles. The quantity of immobilized protein increased from 25 mg/g at 0.5 mg/ml to ~ 45 mg/g at 1 mg/ml for pH 6 and 7.4. Thereafter adsorption increased by only 1 or 2 mg/g until free γ-globulin concentration was increased to 6 mg/ml. The total γ-globulin adsorption was lower at pH 6 and 7.4 between 0.5 to 8 mg/ml in comparison to pH 5. However, γ-globulin adsorption was similar at 10 mg/ml protein concentration for all three pH conditions.

The reduced γ-globulin adsorption obtained for MSU-H in comparison to S_{FP} and S_{XDP} further establishes the influence of pore diameter on protein adsorption. Even though MSU-H particles have a larger SSA (782 m^2/g) than both S_{FP} and S_{XDP} but it contains smaller pores of

5.7 nm. γ-globulin is a large molecule which cannot access small pores available on MSU-H particles. Hence, most adsorption occurs only on the particle surface and majority of the pores remain unfilled. The effect of pore sizes was evident from the fact that silica with largest pores according to BET (S_{FP} and S_{XDP}) resulted in highest amount of γ-globulin adsorption followed by MSU-H and S_{AL}.

Protein adsorption was also investigated on PCL and PCL-ES100 nanoparticles. Unfortunately, the lack of porosity on PCL nanoparticles resulted in insignificant protein adsorption at all studied conditions. Hence, protein adsorption was carried only on PCL-ES100 particles.

γ-globulin adsorption on PCL-ES100 (1:2 to 1:5 ratios) particles at pH 5 and 6 are presented in Figure 5.6. These experiments were limited to only pH 5 and 6 due to the high solubility of ES100 above pH 7. PCL-ES100 particles resulted in similar protein adsorption besides on 1:2 ratio particles. The protein immobilization was found to be higher at pH 5 than pH 6 for these particles which was different to S_{FP}, S_{XDP}, and MSU-H particles as previously discussed.

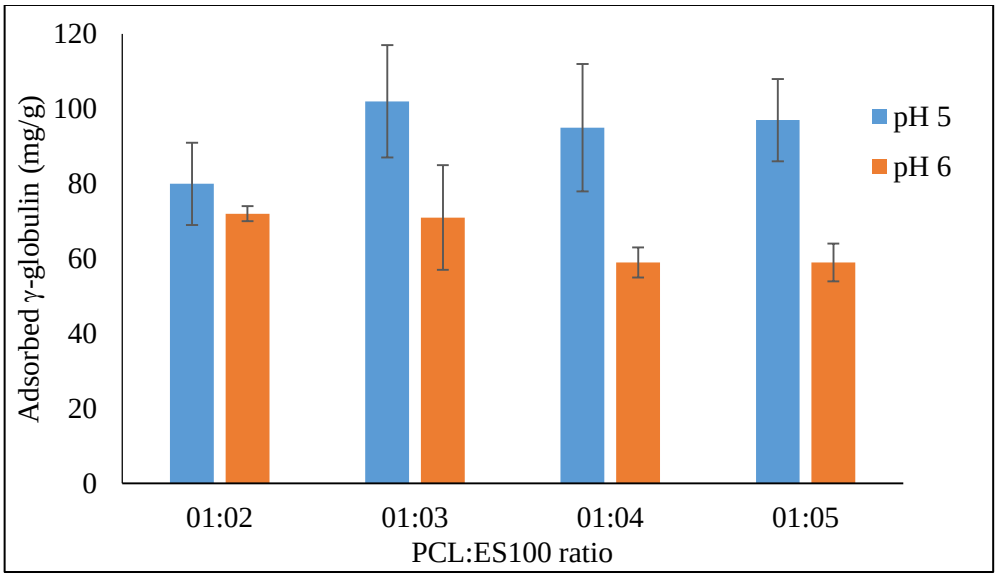

Figure 5.6: Immobilization of γ-globulin onto PCL-ES100 nanoparticles

The physicochemical nature of polymeric nanoparticles including size and surface charge play an important role in their interaction with macromolecules aside pH [238 – 241]. A higher immobilization capacity at pH 5 can be attributed to electrostatic interactions between the adsorbent surface and the adsorbing molecules in addition to other forces including hydrophobic interactions [238, 239]. A comparatively higher affinity of γ-globulin molecules

(IEP ~ 6.60) for PCL-ES100 can be expected at pH 5 due to the net positive charge on protein and net negative charge on the nanoparticles. Electrostatic interactions appear to play a much significant role in protein adsorption on PCL-ES100 than for silica particles. It is also worth considering that the PCL-ES100 stability may also reduce as the pH approaches close to neutral due to the solubility of ES100 thus affecting their capacity to successfully immobilize γ-globulin onto the surface at pH 6. Interestingly, both PCL and PCL-ES100 particles have comparatively small specific surface area as determined by BET but only the latter was able to adsorb γ-globulin. This could be attributed to the presence of pores on the surface of PCL-ES100 particles, unlike PCL particles which were completely non-porous.

In summary due to their pore diameter, the highest γ-globulin immobilization was observed with S_{FP} and S_{XDP} particles while S_{AL} and PCL core systems had little or no protein adsorption. The maximum immobilization was generally achieved at a pH closer to the I.E.P of γ-globulin except for PCL-ES100 particles. Nevertheless, it can be concluded that protein adsorption is a complicated process which is dependent on various factors including pH, surface porosity, and net/surface charge of both the protein and adsorbent. To further understand the adsorption process with silica particles, their isotherms were fitted using Langmuir and Freundlich models. The data obtained with PCL-ES100 was insufficient for the model fitting.

5.1.2 Langmuir and Freundlich model fitting

The adsorption data for S_{FP}, S_{XDP}, S_{AL} and MSU-H were fitted to Langmuir and Freundlich models (Appendix A.5) and the R^2 values are presented in Table 5.3 and 5.4 respectively.

Table 5.3: R^2 values for Langmuir model plots of silica particles

Material	pH 5	pH 6	pH 7.4	pH 9
S_{FP}	0.9748	0.9999	0.9964	0.9664
S_{XDP}	0.9928	0.9999	0.9871	0.8073
S_{AL}	0.9701	0.8326	0.9981	0.8984
MSU-H	0.9973	0.6377	0.6485	NA

Table 5.4: R^2 values for Freundlich model plots of silica particles

Material	pH 5	pH 6	pH 7.4	pH 9
S_{FP}	0.886	0.7432	0.9552	0.9309
S_{XDP}	0.6353	0.637	0.8915	0.8787
S_{AL}	0.8906	0.7572	0.997	0.9718
MSU-H	0.9053	0.7351	0.3978	NA

In general, the isotherms were a better fit to Langmuir model suggesting monolayer coverage of γ-globulin on the surface of these adsorbent particles [226, 229]. However, it is still worth noting that the Langmuir model does not consider conformational changes and lateral inter-molecular interactions related to protein immobilization on a solid surface [229]. R^2 values obtained for MSU-H suggested Langmuirian type surface adsorption at pH 5. Whereas, isotherms plotted at pH 6 and 7.4 did not fit to either Langmuir or Freundlich models. This once again indicates monolayer coverage at pH 5 and rejects the likelihood of multilayer coverage at higher pH values. Although the Langmuir and Freundlich equations are widely used to define the data for protein adsorption, there can be adsorbate-adsorbent systems such as that of the MSU-H that may not follow these models. This could be related to the fact that multiple interactions can occur in between the adsorbed macromolecules which are not fully considered whilst fitting data to these models [200].

In addition to the maximum γ-globulin adsorption studies on the core particles, the rate at which γ-globulin molecules are adsorbed at the plateau concentrations was also investigated which is discussed in the following section.

5.2 Kinetic adsorption measurements

As previously explained immobilization of protein molecules onto solid surfaces is a complex process and in many cases, can be time-consuming and irreversible. The period taken for an immobilization process to occur can be efficiently determined by kinetic adsorption isotherms. Understanding and consequently being able to control the rate at which protein molecules immobilize is beneficial especially during the design of drug delivery systems [242]. Overall, the primary adsorption rate is limited by the movement of adsorbing molecules toward the adsorbent surface and is further affected by on-going interactions between the adsorbate and the surface [243]. This section covers the results and discussion for kinetic adsorption measurements of γ-globulin onto silica and polymeric materials.

The high affinity of γ-globulin molecules for S_{FP} particles can be confirmed by their kinetic adsorption isotherms as presented in Figure 5.7.

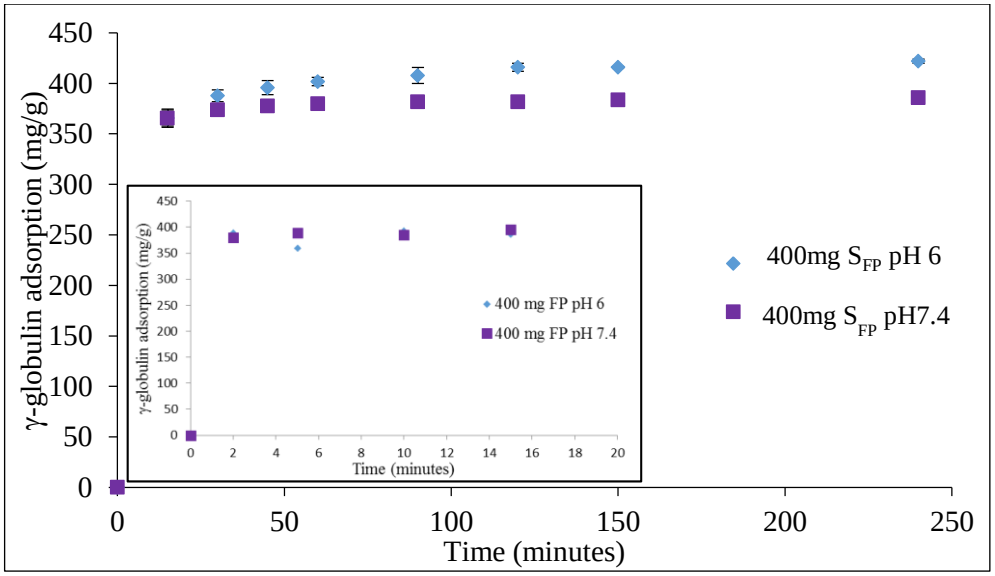

Figure 5.7: The rate of change of adsorption (mg/g) with time (minutes) for S_{FP} at (a) 240 minutes (inset) 15 minutes

The initial immobilization of γ-globulin on S_{FP} takes place rapidly with approximately 81 % of protein adsorption happening within the first 15 minutes. Minimal changes to the amount of adsorbed γ-globulin occurred as the experiment progressed to 240 minutes. Prior to surface saturation, the γ-globulin adsorption kinetics on S_{FP} is not primarily limited by the movement of the protein molecules towards the adsorbent surface but possibly by the initial quantity of γ-globulin or S_{FP} [244- 246]. Thus, assuming the kinetic process to be of a pseudo-second-order (Equation 5.13) and using the integrated equation (Equation 5.15) below a straight-line plot can be obtained (Appendix A.6). The adsorption rate constant (k) presented in Table 5.5 was estimated from the adsorption kinetic isotherm. Pseudo-second order kinetic rate law can be expressed as follows [244, 246];

$$\frac{dq_t}{dt} = k(q_c - q_t)^2 \qquad \text{Equation 5.13}$$

Where, k represents the rate constant of sorption ($g.mg^{-1}.min^{-1}$), q_c is the maximum amount of immobilized adsorbate (mg/g), and q_t is the quantity of adsorbed molecules on the adsorbent-surface at any time (mg/g).

Integration of the above equation gives Equation 5.14 and can also be re-arranged to give Equation 5.15, where *h* is known as the adsorption rate ($mg.g^{-1}.min^{-1}$) [244];

$$\frac{1}{(q_c - q_t)} = \frac{1}{q_c} + kt \qquad \text{Equation 5.14}$$

$$\frac{t}{q_t} = \frac{1}{h} + \frac{1}{q_c}t \qquad \text{Equation 5.15}$$

The values derived for S_{FP} (Table 5.5) indicate fast adsorption rate and high maximum capacity for kinetic experiments carried out at pH 6 in comparison to pH 7.4. This further supports the adsorption data discussed in section 5.1.1.

Table 5.5: Kinetic model fitting for S_{FP} particles

	Best model fitting	R^2 value	k (mg/min)	q_c (mg/g)
pH 6	Pseudo-2nd order	0.998	1.74	417
pH 7.4	Pseudo-2nd order	1.000	1.60	385

Unlike the kinetics for S_{FP}, γ-globulin adsorption onto S_{XDP} particles at pH 6 and 7.4 progressed steadily until a maximum protein immobilization was attained between 180 - 240 minutes as shown in Figure 5.8.

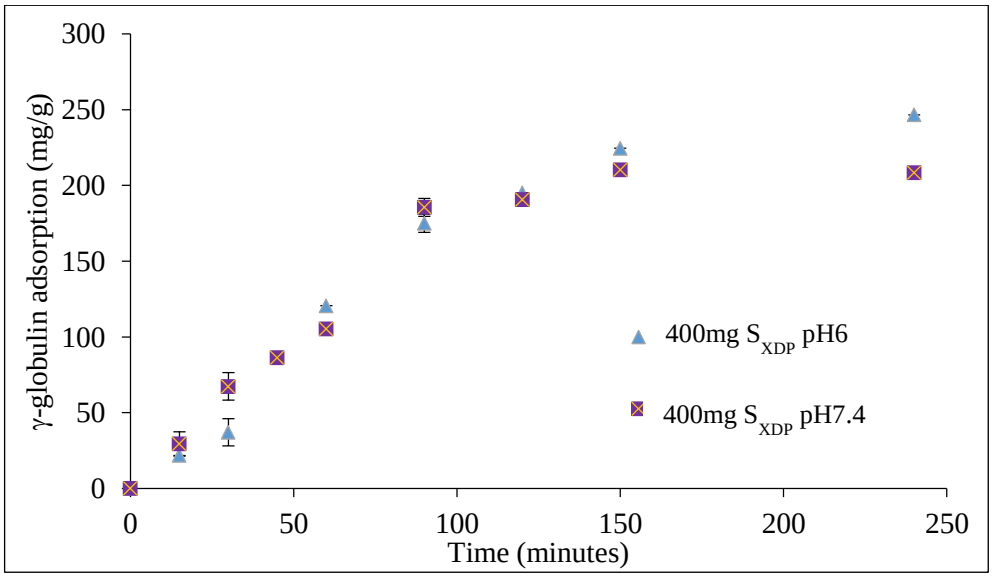

Figure 5.8: Kinetic curve for γ-globulin adsorption onto S_{XDP} particles

Within the first 90 minutes the quantity of adsorbed γ-globulin largely increased at a steady rate with approximately 74 % of free γ-globulin molecules adsorbed onto S_{XDP}. Thereafter, a slower approach to the rise in adsorbed protein was observed until equilibrium was achieved

at around 150 minutes. These results indicate that kinetic process with S_{XDP} can be assumed to be of the first-order depending primarily on the migration of γ-globulin to the adsorbent surface [208, 247]. The following equation describes the pseudo-first order rate process [247]:

$$\frac{dQ}{dt} = k(Q_m - Q) \qquad \text{Equation 5.16}$$

Integration of the above equation gives [247]:

$$\ln(Q_m - Q) = lnQ_m - kt \qquad \text{Equation 5.17}$$

Thus, the maximum amount of adsorbed protein (Q_m) or quantity adsorbed at a specific time (Q) can be calculated using Equation 5.17. A straight-line plot (Appendix A.6) was obtained for S_{XDP} when $ln\ (Q_m\text{-}Q)$ is plotted as a function of time, t. The rate constant (k) was then be determined from the kinetic isotherm and is presented in Table 5.6.

Table 5.6: Kinetic model fitting for S_{XDP} particles

	Best model fitting	R^2 value	k (mg/min)	Q_m (mg/g)
pH 6	Pseudo-1st order	0.9751	1.23	294
pH 7.4	Pseudo-1st order	0.9752	1.03	248

A slightly higher rate constant and larger Q_m was obtained for S_{XDP} at pH 6 in comparison to pH 7.4, suggesting a faster adsorption rate and higher adsorption capacity for γ-globulin at pH 6. However, this was not as explicit as S_{FP} particles presented earlier.

The adsorption kinetics for S_{AL} particles at pH 6 and 7.4 are presented in Figure 5.9 and it confirmed their limited ability to adsorb γ-globulin molecules at both pH conditions.

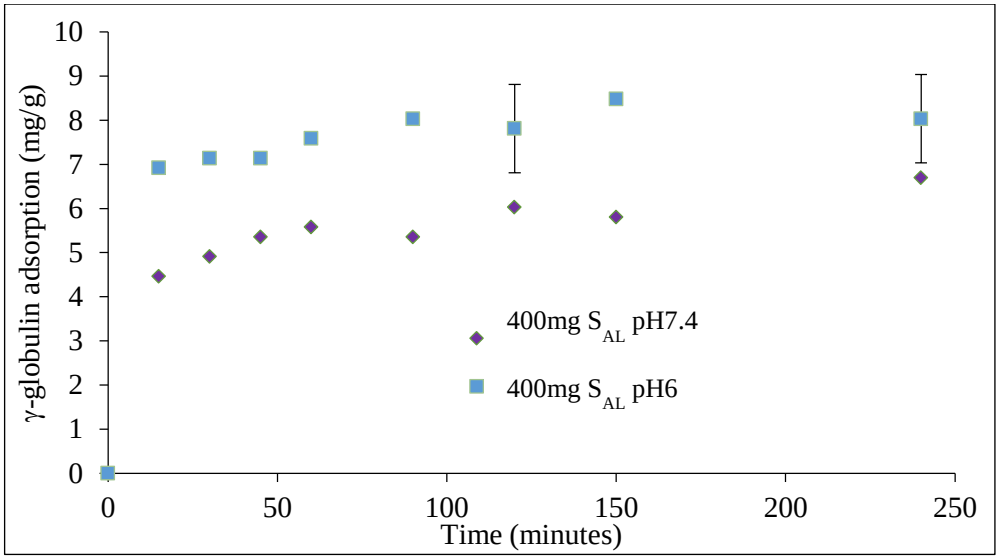

Figure 5.9: Kinetic curve for adsorption of γ-globulin onto S_{AL} particles

Although the initial adsorption process was rapid and occurred within the first 15 minutes, the amount of γ-globulin adsorbed within this period was minimal in comparison to S_{FP} and S_{XDP}. It also remained same until the end of the experiment at 240 minutes. Therefore, these results indicate that equilibrium is achieved for S_{AL} at 15 minutes with only a small amount of γ-globulin attached to the solid surface. The fast adsorption of γ-globulin on S_{AL} indicates strong affinity of protein for S_{AL} surface, however, effect of the lack of porosity on the total adsorption value is evident from the isotherm presented in Figure 5.9.

The adsorption results for S_{AL} were best fitted with a pseudo-second order plot (Appendix A.6) with the rate constant values listed in the table below. The rate constant and adsorption capacity are both just slightly higher at pH 6 in comparison to pH 7.4. This indicates that the effect of pH on protein adsorption on these particles was not as strong as for S_{FP} and S_{XDP} particles.

Table 5.7: Kinetic model fitting for S_{AL} particles

	Best model fitting	R^2 value	k (mg/min)	q_c (mg/g)
pH 6	Pseudo-2nd order	0.992	0.030	8
pH 7.4	Pseudo-2nd order	0.9848	0.025	6

The kinetic adsorption isotherm for MSU-H at pH 6 and 7.4 are presented in Figure 5.10.

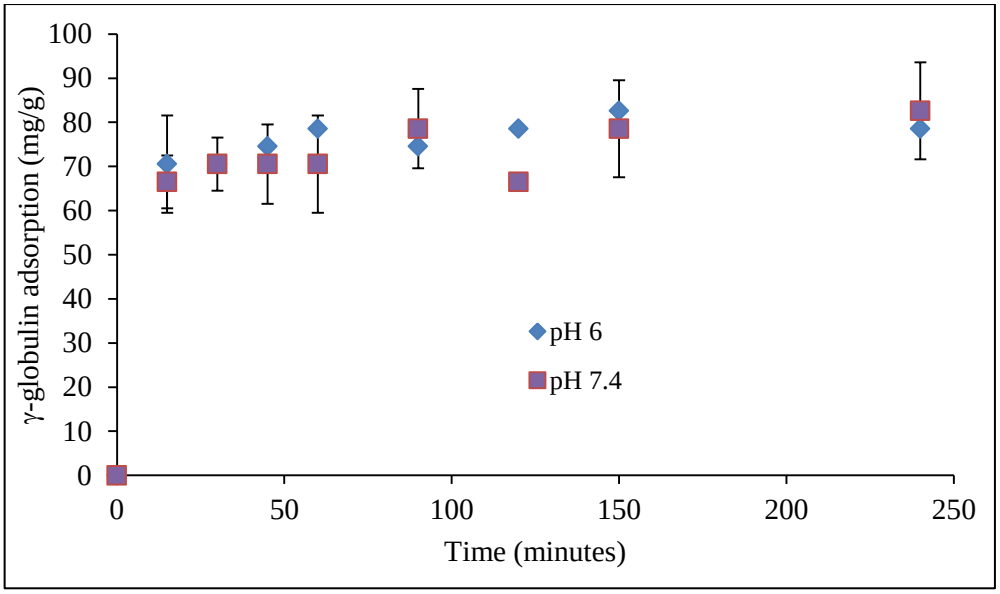

Figure 5.10: Kinetic γ-globulin adsorption plot for MSU-H particles

Similar to S_{FP} and S_{AL} particles, maximum γ-globulin adsorption (79 mg/g) was achieved within the first 15 minutes. There were variations to the quantity adsorbed after this period which possibly represent the dynamic exchange process of γ-globulin. In other words, adsorption and desorption seemed to occur simultaneously, where, the adsorbing molecules attached, detached, re-attached and re-orientated themselves to optimize their interaction with the surface [135].

The pseudo-second order model provided the best correlation for data obtained with MSU-H (Appendix A.6), with slightly higher R^2 value at pH 6 but similar adsorption rate and adsorption maxima at both pH values (Table 5.8).

Table 5.8: Kinetic model fitting for MSU-H particles

	Best model fitting	R^2 value	k (mg/min)	q_c (mg/g)
pH 6	Pseudo-2nd order	0.9983	0.33	80
pH 7.4	Pseudo-2nd order	0.9875	0.34	81

Generally, the kinetic data obtained with silica core particles suggested that the surface immobilization of γ-globulin occurred either in a step-wise manner as seen with S_{XDP} or the adsorbent-surface acted like a "sponge" imbibing significant amount of protein from solution within a relatively short period of time as observed with MSU-H, S_{FP} and S_{AL}.

The kinetic adsorption data for PCL-ES100 (1:3 ratio) at pH 5 is presented in Figure 5.11 and similar to S_{FP}, S_{AL}, and MSU-H, the immobilization of γ-globulin onto the surface of these particles occurs within a short period.

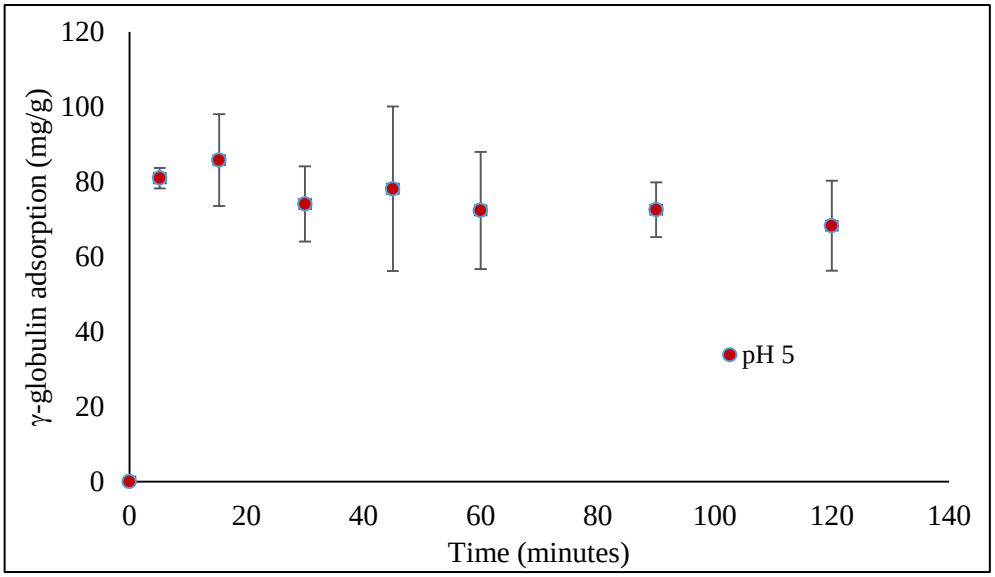

Figure 5.11: Kinetic γ-globulin adsorption plot for PCL-ES100 particles

Although the maximum adsorption capacity is achieved at 15 minutes but the quantity of adsorbed γ-globulin continued to fluctuate and decrease for the duration of the experiment. The pseudo-second order model gave the best correlation for the data obtained with PCL-ES100 (Appendix A.6) with the constant values noted in the Table 5.9.

Table 5.9: Kinetic model fitting for PCL-ES100 particles

	Best model fitting	R^2 value	k (mg/min)	q_c (mg/g)
pH 5	Pseudo-2nd order	0.9973	0.58	69

The total protein adsorption on these particles after 120 minutes was 69 mg/g which was lower than the initial value of 95 mg/g in 15 minutes. This could be either due to the realignment of protein molecules on the surface or possible deformation of these particles at pH 5. Hence, γ-globulin adsorption on PCL-ES100 in a short period of time may be beneficial to avoid both particle degradation and protein rearrangement.

In summary, the kinetic adsorption experiments confirmed strong affinity of γ-globulin for S_{FP}, S_{XDP}, MSU-H, and PCL-ES100 particles in comparison to S_{AL}. Further to these

adsorption experiments, the physico-chemical characteristics of protein adsorbed-core particles were measured as discussed in the following section to monitor any changes that may have occurred during the adsorption process.

5B. Characterization of protein adsorbed-core particles

This section covers the surface and structural characterization of γ-globulin adsorbed-core particles.

5B.1 Aims and Objectives

The following work was carried out to help confirm the presence of protein molecules at the surface of γ-globulin-adsorbed silica and PCL-ES100 particles. The data obtained from structural analysis of these systems also helped to study any changes to the conformation of immobilized γ-globulin.

5B.2 Experimental

Following the maximum adsorption studies, protein-adsorbed core particles were prepared and freeze-dried as described in section 2.5.1. BET analysis was performed according to the method described for PCL particles in section 2.2.2. The surface charge of protein-adsorbed silica particles (S_{FP}, S_{XDP}, S_{AL}, and MSU-H) was determined as per method in section 2.4. The zeta -potential of protein-adsorbed PCL-ES100 (1:3) particles was performed as described in section 2.2.1. ATR-FTIR analysis was also carried out on the γ-globulin-adsorbed core particles as described in section 2.2.3.

5B.3 Introduction

The immobilization of macromolecules onto solid surfaces is known to alter the surface properties and size of the adsorbent particle [79, 238, and 248]. These changes signify the presence of adsorbed molecules at the surface, and can help in explaining the interactions of adsorbate with adsorbent [238, 248]. Therefore, protein-adsorbed particles were analysed with respect to their surface charge, porosity and surface area as follows. The zeta-potential of loaded particles against pH was also analysed.

5B.4 Results and discussion

This section summarizes and explains the data obtained for experiments relating to the determination of surface properties, particle size and surface charge for protein-adsorbed core particles.

5.3 Specific surface area and porosity for protein-adsorbed silica

Nitrogen sorption isotherms for protein-adsorbed S_{FP}, S_{XDP}, and S_{AL} particles are presented in Appendix A.7. In general, there were no changes to the shape of the isotherms post γ-globulin adsorption. The plots for protein-loaded S_{FP} and S_{XDP} particles remained class Type IV indicating that they still retained their mesoporous nature after immobilization of γ-globulin. The isotherm for protein-adsorbed S_{AL} also remained the same (Type II) still appearing to be non-porous as before [176, 177]. However as recorded in Table 5.10, there was a decrease in the SSA, pore volume and diameter for γ-globulin-adsorbed S_{FP} and S_{XDP} particles, when compared to BET data obtained before protein immobilization.

Table 5.10: Surface characteristics for protein-adsorbed S_{FP}, S_{XDP}, and S_{AL} particles

Silica particle	**γ-globulin-adsorbed particle**	**S_{FP}**	**γ-globulin-adsorbed S_{FP}**	**S_{XDP}**	**γ-globulin-adsorbed S_{XDP}**	**S_{AL}**	**γ-globulin-adsorbed S_{AL}**
Quantity of adsorbed nitrogen (cm^3/g STP)		892	393	966	612	260	266
BET surface area (m^2/g)		289	161	258	187	767	703
BJH cumulative pore volume (ml/g)		1.35	0.60	1.44	0.93	0.40	0.42
BJH pore diameter (nm)		19.1	14.8	22.2	19.1	2.5	2.6

The quantity of adsorbed nitrogen molecules (cm^3/g STP) decreased by more than 50% for S_{FP} and about 40% for S_{XDP} after γ-globulin adsorption. In contrast to S_{FP} and S_{XDP}, the differences to the surface properties of S_{AL} were minimal, with the SSA reducing only by 8% post protein immobilization. In summary, amongst the three silica core particles, the differences recorded after γ-globulin immobilization was highest for S_{FP} and lowest for S_{AL} which also agrees with the protein adsorption data.

The changes observed to surface properties of the silica particles post-immobilization can be related to the presence of adsorbed protein molecules at the adsorbent surface [79, 248]. A reduction in the nitrogen adsorption and SSA for these protein adsorbed- silica particles would suggest that the adsorbing surface was now occupied by γ-globulin molecules and hence there was less room for nitrogen to adsorb to it. Similarly, the decrease in the pore volume after γ-globulin immobilization would also indicate reduced space or inaccessibility

of pores for nitrogen molecules due to the presence of protein molecules on the surface [227]. The importance of pore size and adsorbent surface was also clearly apparent from these results. Pores on S_{FP} (19 nm) and S_{XDP} (22 nm) could evidently accommodate γ-globulin molecules but S_{AL} (2.5 nm) and MSU-H (7.5 nm) could not. The estimated hydrodynamic radius of γ-globulin is known to be 5.29 nm indicating requirement of much larger spaces for it to be able to successfully adsorb onto available pores [249]. Nonetheless, proteins are macro-molecules meaning that the total calculated BET surface area could rarely match the accessible surface area for these onto adsorbent particles [227]. The maximum change in surface properties observed with S_{FP} is likely due to the highest protein adsorption on to its surface than other silica particles.

Interestingly, unlike S_{FP}, S_{XDP}, and S_{AL} particles, there was a change to the slope of the BET isotherm for MSU-H after γ-globulin adsorption (Appendix A.7). As discussed in section 3.3, the isotherm of MSU-H could be classed as a Type IV indicating mesoporous nature. However, H1 hysteresis loop for the protein-adsorbed MSU-H particles became smaller with the increase in γ-globulin concentration. The particles after adsorption at 10 mg/ml nearly lost its original slope and hysteresis. This suggests that there was a change to the mesoporous nature of MSU-H after γ-globulin immobilization. The presence of protein at the particle surface evidently reduces the accessibility of adsorbing nitrogen molecules as presented in Table 5.11.

Table 5.11: Summary of surface characteristics for protein-adsorbed MSU-H

Type of particle	Quantity of adsorbed nitrogen (cm^3/g STP)	BET surface area (m^2/g)	BJH cumulative pore volume (ml/g)	BJH pore diameter (nm)
MSU-H	651	782	0.99	5.7
γ-globulin-adsorbed MSU-H at 1 mg/ml	281	264	0.43	7.0
γ-globulin-adsorbed MSU-H at 2 mg/ml	27	25	0.04	7.4
γ-globulin-adsorbed MSU-H at 4 mg/ml	27	29	0.04	7.1
γ-globulin-adsorbed MSU-H at 6 mg/ml	34	26	0.05	8.3

γ-globulin-adsorbed MSU-H at 8 mg/ml	29	21	0.04	9.8
γ-globulin-adsorbed MSU-H at 10 mg/ml	11	9	0.002	11.9

Similarly, as compared to S_{FP} and S_{XDP}, there was a decrease in the BET surface area, pore volume and amount of nitrogen adsorbed to the surface of the MSU-H particles after immobilization of γ-globulin. The quantity of adsorbed nitrogen, SSA and pore size changed from 651 cm^3/g STP, 781.9 m^2/g and 0.99 ml/g pre-adsorption to 281 cm^3/g STP, 263.5 m^2/g and 0.43 ml/g respectively post adsorption at 1 mg/ml γ-globulin concentration. A further decrease was observed in these properties as protein concentration increases from 1 mg/ml to 2 mg/ml confirming the growing presence of γ-globulin at the particle surface. Interestingly, there was minimal change to the SSA, pore volume, and quantity of adsorbed nitrogen as protein concentration increased from 2 mg/ml to 10 mg/ml, thereby suggesting a concentration limit to the adsorption of γ-globulin by these silica particles. It can also be noted from Table 5.11 that the BJH pore diameter increased after immobilization of γ-globulin and continued rising with increasing protein concentration. As the BJH model is based on the cylindrical pore model and the pore diameter is calculated on the capillary condensation of the adsorbate molecules in the pores, it does not consider any changes to the surface morphology which can be caused by the adsorption of protein molecules [250, 251]. Therefore, it can be unreliable in some cases such as this where adsorbate molecule accessible imperfections created by protein adsorption could be misinterpreted as pores [250, 251].

In summary, analysis of surface properties for the protein-adsorbed core particles confirmed the presence of γ-globulin molecules at the surface of the adsorbing materials. The higher capacity for protein adsorption with S_{FP}, S_{XDP}, and MSU-H particles in contrast to S_{AL}, was confirmed by the decrease to their specific surface area and pore volume. The minimal changes to protein-adsorbed S_{AL} suggested a low quantity of γ-globulin on their surface confirming the particles' limited ability for γ-globulin adsorption. The net surface charge of these particles was also investigated as described in the following section.

5.4 Surface charge analysis for protein-adsorbed silica particles

The surface charge on protein-adsorbed S_{FP}, S_{XDP}, S_{AL}, and MSU-H particles were determined to establish how it changed from untreated core particles. The plot (Appendix A.8) of zeta-potential as a function of pH provided the point of zero charge (PZC) as presented in the table below;

Table 5.12: PZC for γ-globulin-adsorbed silica particles

	γ-globulin-adsorbed S_{FP}	γ-globulin-adsorbed S_{XDP}	γ-globulin-adsorbed S_{AL}	γ-globulin-adsorbed MSU-H
PZC	4.8	4.5	4.0	5.0

Prior to protein immobilization, the PZC for these core materials was determined to be in the range of pH 0.80 to 1.60, with MSU-H recording the lowest value while S_{XDP} gave the highest value. There was an upward shift to the PZC values after γ-globulin was immobilized suggesting that the surface-charge of the loaded-core materials was influenced by the presence of adsorbed protein molecules [238]. The surface charge on these particles appeared to be shifting closer to the IEP (pH 6.60) of γ-globulin confirming its presence on the surface.

In addition to these investigations, the surface area, porosity and surface charge of protein adsorbed-PCL-ES100 particles were also analysed as described in the following sections.

5.5 Specific surface area and porosity of protein-adsorbed PCL-ES100

Likewise, a decrease in specific surface area (m^2/g) and pore volume (ml/g) after γ-globulin immobilization onto PCL-ES100 (ratio 1:3) nanoparticles was also observed. A change was recorded from approximately 20 m^2/g and 0.06 ml/g before adsorption to 17 m^2/g and 0.03 ml/g after adsorption. There was no difference in the nitrogen sorption isotherms for these particles before and after γ-globulin immobilization (Appendix A.7). The surface charge of protein-adsorbed PCL-ES100 particles was characterized as follows.

5.6 Surface charge analysis for protein-adsorbed PCL-ES100

There was a change to surface charge of these particles after protein immobilization due to the influence of adsorbed γ-globulin molecules. Prior to γ-globulin adsorption, the zeta-potential varied from -36 to -39 mV. However, after immobilization the particles contained almost neutral charge ranging from +4 to -8 mV. The positive charge obtained was only present at

pH 5 and could be attributed to the variation in surface coverage between pH 5 and 6 [238]. There was higher amount of adsorbed γ-globulin at pH 5 onto these particles, which would mean that the surface charge was determined by the immobilized macromolecules. On the contrary, adsorption at pH 6 resulted in comparatively lower protein immobilization indicating zeta-potential value to be derived from the combination of both adsorbed protein and uncovered particle surface.

5.7 ATR-FTIR analysis of γ-globulin-adsorbed core particles

ATR-FTIR analysis was conducted on protein loaded core particles to assess γ-globulin immobilization and changes to the conformation of the protein that may arise due to its adsorption on the particle surface. Typically, the secondary structure of a protein can be predicted by FTIR analysis based on the absorption of infra-red (IR) radiation by their peptide bonds [252]. As discussed in Chapter 4, for the ATR-FTIR spectra of proteins, the amide I band ranging from wavenumbers of 1600 to 1700 cm^{-1} (mainly due to C=O stretching vibrations) and amide II band (primarily because of N-H bending, and C-H stretching vibrations) found between 1500 to 1600 cm^{-1} are typically monitored for studies relating to protein conformation [201, 202]. The amide I band is related to the secondary structure of protein, while the amide II N-H stretching mode is used to monitor the unfolding of the protein [201].

The ATR-FTIR spectra for native γ-globulin and protein-adsorbed silica particles are presented in Figure 5.12. The spectra for untreated silica was discussed in section 3.5.

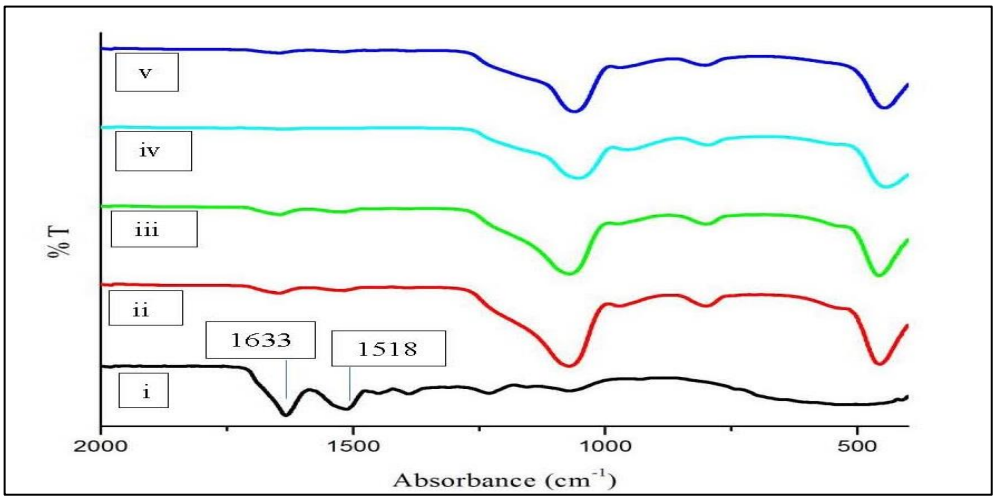

Figure 5.12: ATR-FTIR spectra for (i) γ-globulin, and protein-adsorbed (ii) S_{FP} (iii) S_{XDP} (iv) S_{AL} (v) MSU-H particles

For the free γ-globulin molecule, the amide I and II bands can be observed at 1633 and 1518 cm^{-1} respectively. Generally, the amide I band near 1650 to 1658 cm^{-1} represents an α-helical structure, whereas that for β-sheet structure exists between 1620-1640 cm^{-1} [253, 254]. Thus, indicating a secondary structural arrangement of primarily β-sheets for pure γ-globulin. The amide I band shifted to 1649 cm^{-1} upon interaction with S_{FP} and MSU-H. Whilst a band shift to 1647 and 1636 cm^{-1} was observed with S_{XDP} and S_{AL} particles respectively. The peak shift observed with S_{FP}, S_{XDP}, and MSU-H indicate changes in the hydrogen bonding involved in the peptide linkages found in the secondary structure of adsorbed γ-globulin [254]. As stated earlier, protein molecules can undergo conformational re-arrangements upon interaction with the solid surface. Hence, these changes can be interpreted as a conversion of the native β-sheet arrangement of γ-globulin to a possible α-helical structure [254]. This could be an issue if the protein does not reverse back to its original conformation upon desorption from the surface or if there is a loss of the protein's biological function.

In comparison to the native protein, there was also a reduction in peak intensity for amide I observed with protein-adsorbed silica particles. The reduction in intensity can be related to the surface concentration of γ-globulin as it rises with the increase in the adsorbed protein content ($S_{FP} > S_{XDP} >$ MSU-H $> S_{AL}$). An upward shift was observed for amide II band *i.e* 1525 cm^{-1} for S_{FP} and S_{XDP}, and to 1522 cm^{-1} for MSU-H particles. The amide II peak completely disappeared from the protein-adsorbed S_{AL} particles. This could simply be linked to comparatively low adsorption onto these particles.

Amide I and II peaks could not be observed for protein-adsorbed PCL-ES100 particles (A.9). This could once again be attributed to the poor signal intensity due to low surface adsorption of γ-globulin onto these particles.

The release of immobilized γ-globulin from the surface of the solid particles was investigated as the next step and it is discussed in Chapter 6 using only protein-adsorbed S_{FP}, S_{XDP}, MSU-H and PCL-ES100 core materials. The study on S_{AL} particles was discontinued due to their limited protein adsorption capacity.

5.8 Conclusion

The effect of pH and surface porosity on immobilization of protein onto solid surfaces was successfully investigated with the means of γ-globulin as a model adsorbate, and silica and polymeric particles as the solid adsorbent. Immobilization was successfully carried out with S_{FP}, S_{XDP}, S_{AL}, MSU-H and PCL-ES100 particles, with the maximum adsorbed amounts observed with S_{FP} and S_{XDP} (511 and 387 mg/g respectively). Protein adsorption with silica materials was more favourable at pH 6, while electrostatic interactions at pH 5 between protein and solid surface possibly influenced the quantity of protein immobilized onto PCL-ES100. The adsorption capacity was also established to be greater with mesoporous particles (S_{FP}, S_{XDP}, and MSU-H) when compared to non-porous materials (S_{AL}). The release of γ-globulin from the core particles was evaluated and is discussed in Chapter 6.

Chapter 6

Protein release studies for uncoated core particles

This chapter discusses γ-globulin release from uncoated protein adsorbed- S_{FP}, S_{XDP}, MSU-H and PCL-ES100 particles. The stability of desorbed γ-globulin is also covered in Part B of this chapter.

6A. Protein release studies

This section covers the work investigating the release of protein from uncoated γ-globulin-covered solid core particles.

6A.1 Aims and Objectives

This study was carried out to gain an understanding on the maximum rate at which immobilized γ-globulin can be released from the surface of protein-adsorbed solid materials formulated in Chapter 5. Thus, the ideal parameters (including pH and type of displacer) for desorption of protein from γ-globulin-adsorbed S_{FP}, S_{XDP}, MSU-H and PCL-ES100 particles was investigated as follows.

6A.2 Experimental

Desorption of γ-globulin from freeze-dried pre-adsorbed core particles (S_{FP}, S_{XDP}, MSU-H and PCL-ES100) was studied as described in section 2.6. The investigations were limited to 180 minutes for PCL-ES100 due to stability concerns regarding the polymeric particle.

6A.3 Introduction

In most systems, the immobilization of proteins onto solid surfaces is often considered irreversible as dilution/washing of the particle surface with chosen solvent does not usually lead to a substantial release [218, 229]. One of the main factors said to influence the reversibility of adsorption is the protein denaturation that occurs upon its attachment on the adsorbent [218]. Nevertheless, several ways to promote the release of immobilized proteins have been investigated successfully, and they include;

- Use of a displacer or surface-active substances such as surfactants can encourage desorption of the macromolecules by an exchange mechanism. The attached protein is

substituted from the surface in favour of immobilization of the added molecules [255 - 257].

- Replacement of adsorbed protein with molecules can also occur by an exchange mechanism between immobilized macromolecules and free protein in solution. This process can either be homo-molecular or hetero-molecular (such as the Vroman effect) [258, 259]. An example of hetero-molecular can be IgG with fibrinogen [259].
- The change in pH or ionic strength can also lead to displacement of adsorbed proteins due to the reduction in electrostatic affinity between the adsorbate and adsorbent surface [260- 262]. However, these changes can also lead to protein denaturation and or aggregation.

In summary, whichever method is used to detach the proteins from the solid surface, there is a need to quantify and predict the manner at which these molecules desorb for an efficient design of a drug delivery system [229]. In this study, the use of surface-active molecules (Tween 80, PF127, and SDS) as a displacer for desorption of immobilized γ-globulin was investigated as the preferred method. This was to mimic the surface active agents already present in the body fluid which may act as displacers in *in-vivo* conditions.

Table 6.1: Physicochemical characteristics of studied displacers [96, 263-264]

	SDS (or Sodium Lauryl sulfate, SLS)	PF127 (Poloxamer 407)	Tween 80 (Polyoxyethylene-sorbitan-monooleate)
Description	Anionic surfactant	Non-ionic triblock copolymer	Non-ionic surfactant
Structure	$CH_3(CH_2)_{11}SO_4Na$ 12-carbon tail group attached to an anionic sulfate head group.	$H(OCH_2CH_2)_X$-$(OCH_2CHCH_3)_y$-$(OCH_2CH_2)_2OH$ Triblock Hydrophilic poly (ethylene oxide) ends and hydrophobic poly (propylene oxide)	$C_{64}H_{124}O_{26}$ Hydrophobic carbon tail chain attached to poly-oxyethylene head groups.
M.W	288.378 g/mol	12600 kDa	1310 g/mol
Melting point (°C)	204 – 207	56	-20.6

The physicochemical characteristics of the surface-active molecules used in this study are summarized in Table 6.1 above and they are investigated as follows for desorption of γ-globulin.

6A.4 Results and discussion

The release kinetics for γ-globulin from the surface of S_{FP} particles in SIF (pH 6.8) and at pH 7.4 are presented in Figures 6.1 a and b.

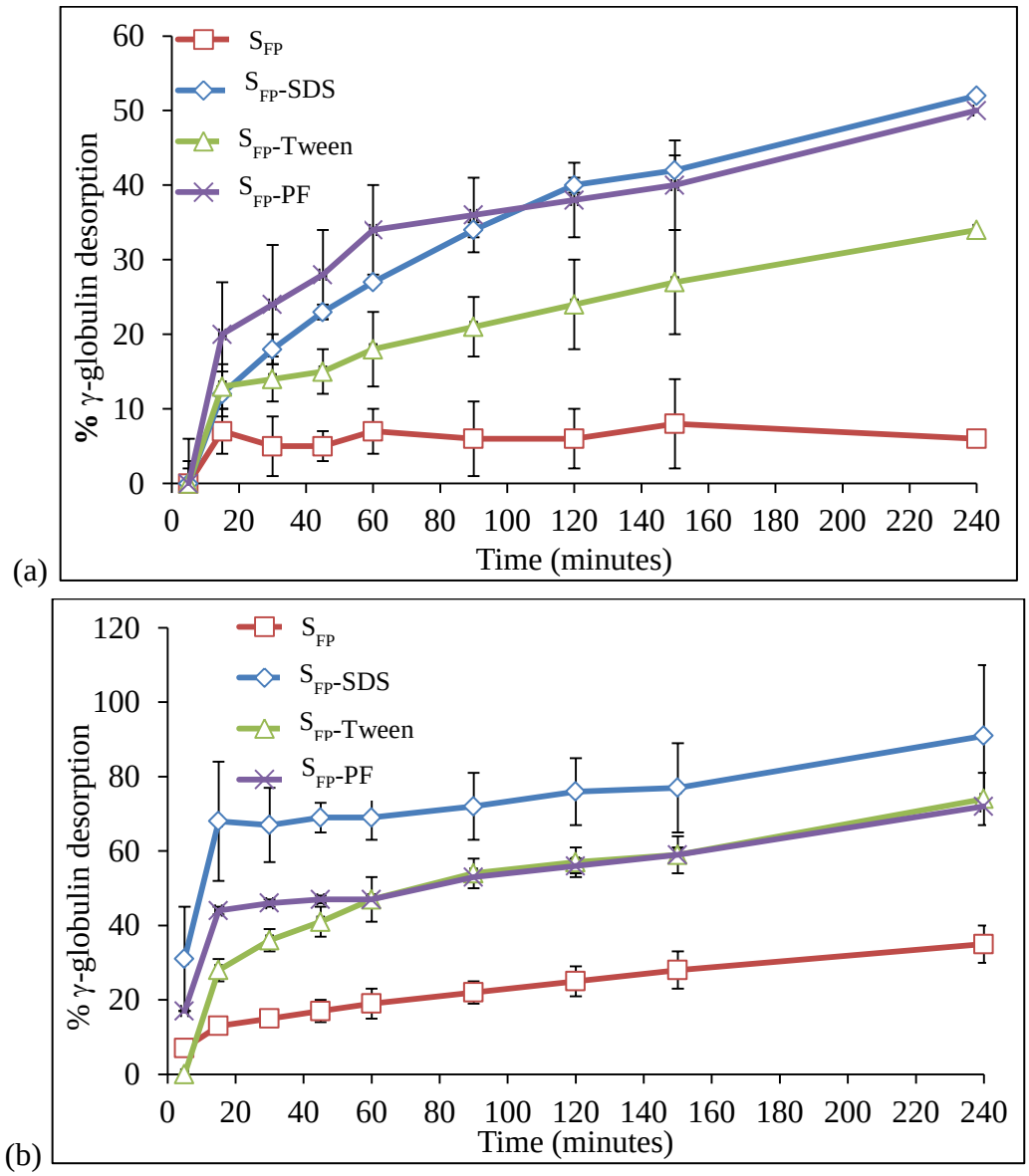

Figure 6.1: The % desorption of γ-globulin from S_{FP} with time at (a) pH 6.8 and (b) 7.4

In comparison to their adsorption kinetics, the detachment of protein from S_{FP} took place at a much slower rate. After 90 minutes, only 6 ± 3% and 22 ± 3% of γ-globulin was desorbed without the presence of a displacer in SIF and at pH 7.4 respectively. This finding not only confirmed the high affinity of γ-globulin for S_{FP}, but also suggested that protein adsorption on these particles might be irreversible. However, desorption rate was greatly improved with the presence of surface-active molecules in both media. The desorption results after 90 minutes

and at 240 minutes are summarized in Tables 6.2 a and b respectively. It can be noted from the table below that desorption rate improves with time and is faster at pH 7.4.

Table 6.2a: Desorption of γ-globulin from S_{FP} at 90 minutes

	pH	
Displacer	6.8	7.4
None	6 ± 3%	22 ± 3%
SDS	34 ± 0.1%	72 ± 9%
Tween 80	21 ± 5%	54 ± 4%
PF127	36 ± 6%	53 ± 1%

Table 6.2b: Desorption of γ-globulin from S_{FP} at 240 minutes

	pH	
Displacer	6.8	7.4
None	6 ± 6%	35 ± 5%
SDS	52 ± 2%	91 ± 19%
Tween 80	34 ± 7%	74 ± 7%
PF127	50 ± 6%	72 ± 0.1%

As previously stated, the use of surface-active molecules as a displacer is an established approach for protein desorption [255- 257]. The amount of protein detached by these molecules is typically dependent on the type and concentration of surfactant, along with the surface properties of the adsorbent [265, 266]. The initial surface loading conditions including protein concentration in the solution and its contact time with the solid surface also plays a role in their effectiveness [265, 266]. For the protein-adsorbed S_{FP} particles at 240 minutes (Table 6.2b), the highest desorption was obtained with 0.1% SDS in both SIF and at pH 7.4 with 52±2% and 91±19% respectively. Tween 80 provided the least protein desorption (34%) at pH 6.8, whereas there was minimal difference between the percentage release by both Tween 80 and PF127 (74 and 72% respectively) at pH 7.4. The variations between these surfactants in the percentage of γ-globulin desorbed could possibly be linked to their nature and molecular weight and volume. Anionic surfactant such as SDS with negatively charged head groups are known to promote high protein desorption[266]. Whereas, non-ionic molecules such as Tween 80 and PF127 have comparatively reduced effect on the desorption of immobilized protein [266]. The slight differences between protein desorption by PF127 and Tween 80 could be attributed to disimilarities in the hydrophobicity of their hydrocarbon chains [266].

The known mechanism of action for protein displacement by a surfactant molecule include; desorption by replacement or enhanced solubilization of macromolecules due to the presence of surface active agents. Removal of proteins by the replacement mechanism is said to occur when there is a significant interaction between the adsorbent surface and surfactant molecules in comparison to interactions between protein and surfactant [267]. As proteins typically have weak interactions with non-ionic entities like Tween 80 and PF127, desorption replacement could be the favoured mechanism instead of solubilization [267]. However, ionic surfactants like SDS may interact strongly with charged side-chains of the protein and result 'in part' desorption *via* solubilization [267, 268].

Similarly, the desorption of γ-globulin from S_{XDP} particles was also investigated with and without displacers and are presented in Figures 6.2a and b. Protein release without surfactants was only 2% and 28% at pH 6.8 and 7.4 respectively in 240 minutes.

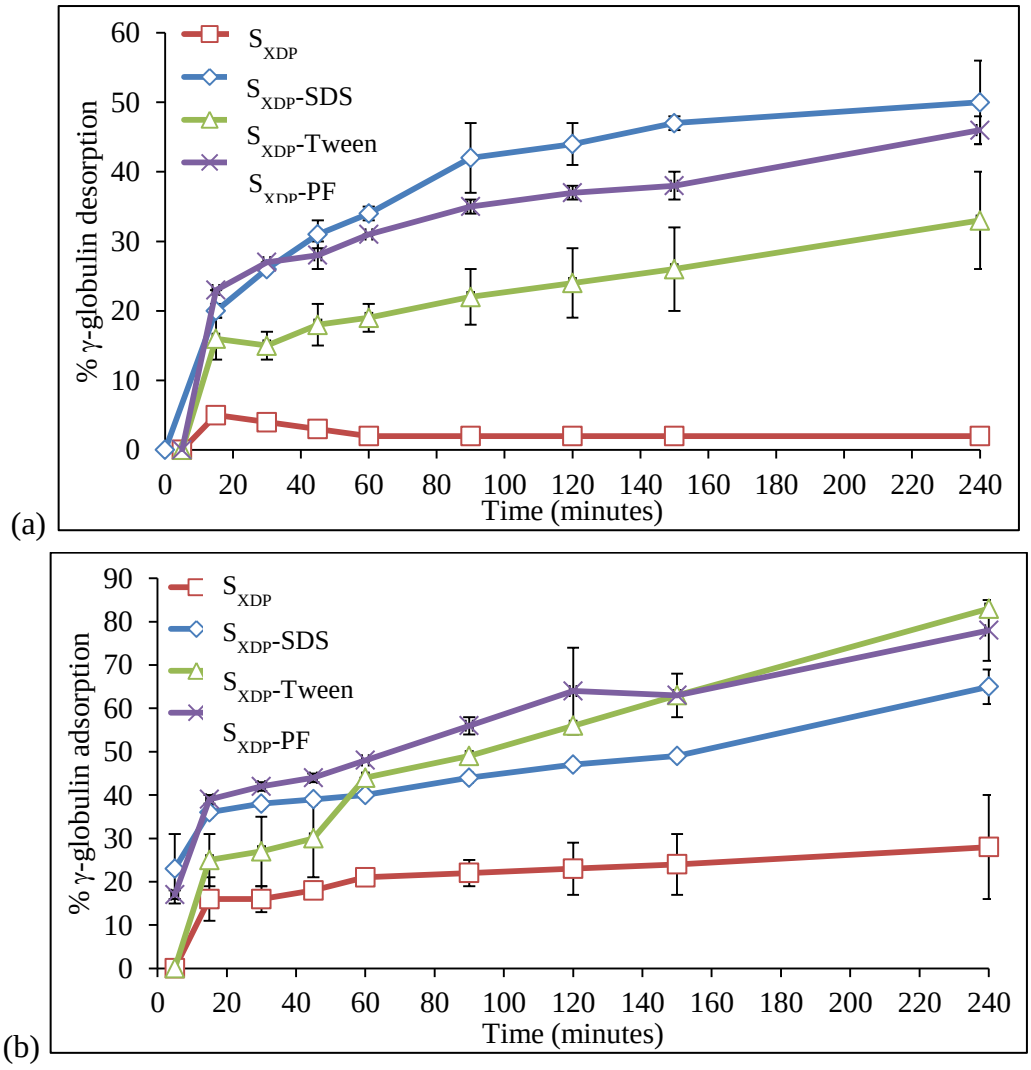

Figure 6.2: The % desorption of γ-globulin from S_{XDP} with time at (a) pH 6.8 and (b) 7.4

The release rate increased significantly with the addition of surfactants where a steady protein desorption was obtained with time. The desorption results after 90 minutes and at 240 minutes are summarized in Tables 6.3 a and b respectively.

Table 6.3a: Desorption of γ-globulin from S_{XDP} at 90 minutes

	pH	
Displacer	6.8	7.4
None	2 ± 1%	22 ± 3%
SDS	42 ± 5%	44 ± 1%
Tween 80	22 ± 4%	49 ± 1%
PF127	35 ± 1%	56 ± 2%

Table 6.3b: Desorption of γ-globulin from S_{XDP} at 240 minutes

	pH	
Displacer	6.8	7.4
None	2 ± 1%	28 ± 12%
SDS	50 ± 6%	65 ± 4%
Tween 80	33 ± 7%	83 ± 1%
PF127	46 ± 2%	78 ± 7%

Introduction of SDS in the media resulted in 50% and 65% desorption after 240 minutes at pH 6.8 and 7.4 respectively. Whereas, PF127 and Tween 80 containing buffer resulted in protein desorption of 46% and 33% at pH 6.8 respectively. A significant increase was observed at pH 7.4 with the final protein release reaching to 78% and 83% for PF127 and Tween 80 respectively. Like S_{FP} at pH 6.8, the higher desorption obtained for S_{XDP} was in the presence of SDS in comparison to PF127 and Tween 80. On the contrary, Tween 80 led to the maximum and SDS inclusion resulted in the lowest desorption percentage at pH 7.4. This trend at pH 7.4 does not fall in line with the one recorded for S_{FP}. Still, desorption from both particles was highest at pH 7.4 regardless of the presence and type of surfactant in the buffer. Therefore, suggesting that the release process from silica is definitely influenced by pH of the media and the inclusion of surfactant promotes this further. This increase in desorption rate could be related to the presence of the net charge on γ-globulin molecules at these pH [261]. For example, higher electrostatic repulsion between silica and protein could be expected at pH 7.4 due to net negative charge on the γ-globulin molecules.

The desorption from MSU-H was investigated using only PF127 as a result of conclusions made from the stability analysis on desorbed protein from S_{FP} and S_{XDP} particles as discussed in Part B. The protein desorption from MSU-H presented in Figure 6.3 confirmed higher desorption at pH 7.4 (34%) in comparison to pH 6.8 (26%) in 240 minutes, similar to S_{FP} and S_{XDP} particles.

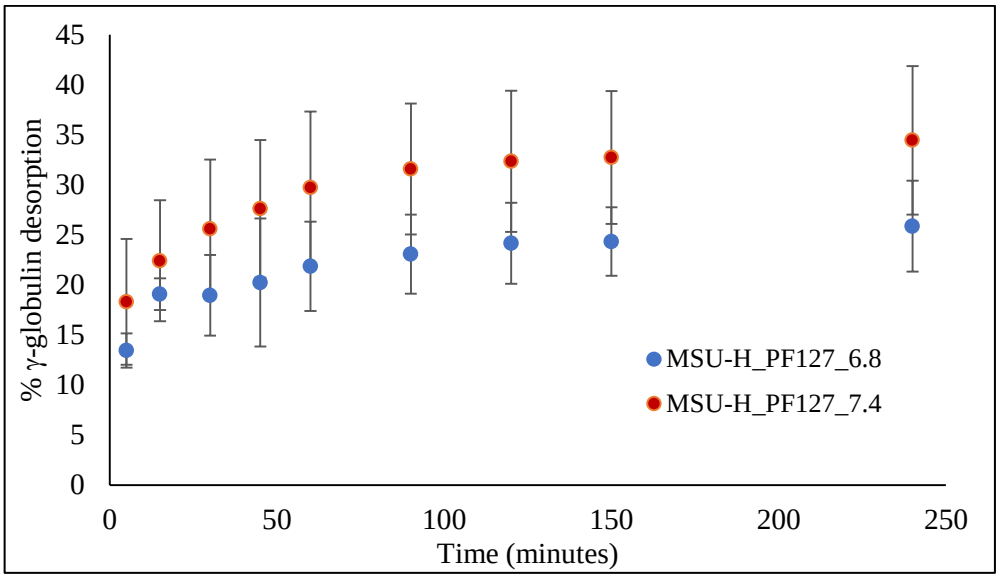

Figure 6.3: Plot of % desorption against time for protein adsorbed-MSU-H

The total γ-globulin release from MSU-H was comparatively lower than S_{FP} and S_{XDP} particles which could be due to the pore sizes of MSU-H. It could be possible that protein molecules occupying pores become inaccessible to the displacer molecules which may take much longer to desorb. The 26 to 34% desorption could be attributed to the displacement of surface γ-globulin with PF127.

The desorption experiments with PCL-ES100 (ratio 1:3) were limited to pH 6.8 media containing PF127 for 3 hours because of their reduced stability at pH 7.4. As noted in the Table 6.4, approximately 72% of immobilized γ-globulin was desorbed within the first hour. There was a minimal increase in the percent desorption as the experiment proceeded further upto 3 hours.

Table 6.4: Desorption data for protein-adsorbed PCL-ES100

Time (hour)	1	2	3
% desorbed	72 ± 11	70 ± 5	76 ± 5

In summary, protein desorption with a displacer at both pH 6.8 and 7.4 for all studied core particles resulted in a maximum of 91% γ-globulin desorption from S_{FP} in SDS containing pH 7.4 media. This confirms that there is always a population of protein molecules that are irreversibly adsorbed on the solid surface or inaccessible to the media [220]. The maximum γ-globulin desorption was obtained from S_{FP}, followed by S_{XDP} and PCL-ES100 particles. Experiments with MSU-H resulted in the least quantity of γ-globulin desorption. This could be linked to the adsorption of γ-globuin in the pores and/or the state of the adsorbed protein layer prior to desorption [266, 267]. In relation to the release of immobilized proteins from solid materials, it was observed that the core particles with higher protein population on the surface retained a smaller fraction when exposed to the buffer-displacer solution after 3 or 4 hours. This could be attributed to the protein's ability to adapt and improve its contact with the un-adsorbed surface thereby making its release more difficult [266]. The low protein desorption from MSU-H may also be due to the multilayer formation (Section 5.1) during adsorption which is known to be comparatively harder to disrupt with surfactant molecules [267]. Further experiments with an increase in surfactant concentration or contact time with desorption media may result in the higher γ-globulin desorption from MSU-H particles.

As discussed earlier, protein molecules usually change their conformation in order to easily adapt to the surface upon adsorption onto a solid [135]. Therefore there is a possibility that desorbed protein might not retain or reverse back to its orginal structure, and consequently loose its functional ability [257, 269 - 272]. Hence, the conformational intergrity of γ-globulin upon subsequent displacement was investigated using CD specstroscopy as discussed in Part 6B.

6B. Stability of γ-globulin in its desorbed state

This section covers studies investigating the structural stability of protein released from the core particles discussed in Part A.

6B.1 Aims and Objectives

This work was carried out to evaluate any conformational changes that may have occurred to the γ-globulin molecule upon subsequent release from the surface of the solid particles. The data obtained also provided information on the effect of release parameters such as pH and displacer type, on the structural stability of desorbed protein.

6B.2 Experimental

Protein-adsorbed core particles were prepared at concentrations (10 mg/ml for S_{FP} and S_{XDP}, 0.5 mg/ml for S_{AL}) that allowed for high surface content, except for MSU-H and PCL-ES100 (4 and 1 mg/ml respectively) where a plateau was not essentially derived. Protein desorbed from these surface-loaded particles were studied *via* CD spectroscopy as detailed in section 2.3.3. Data collected was evaluated and compared against that for the native γ-globulin.

6B.3 Introduction

The stability of a protein molecule plays a role in various other events aside funtional activity. These include displacement and recovery of active macromolecules from an adsorbent surface, the inhibition of aggregation of other protein molecules at the surface, and possible activation of certain biological actions such as immune responses [269]. Thus, there is a need to understand their conformational intergrity in relation to the adsorption/desorption process while designing relevant drug delivery systems [273]. The introduction of an adsorbent material into a protein solution encourages interactions between the non-polar region of a macromolecule with the adsorbent surface. Consequently, this may result into the reduction in the stabilizing effect due to the disruption of intramolecular hydrophobic interactions [274]. During the immobilization or displacement of protein onto/from a solid material, a number of factors can prompt these rearrangements to the protein's secondary structure as briefly discussed below;

I. Surface coverage: As stated earlier, surface-induced denaturation can occur upon the adsorption of macromolecules onto solid substrates [269]. For example, Felsovalyi

et al reported the loss of the α-helical content of lysozyme upon immobilization onto silica particles [229]. Surface-induced denaturation can be linked to degree of protein coverage of the adsorbent surface, where the probabiltiy of changes to their conformation decreases with a rising surface content [229, 257, 273- 274]. This is attributed to the fact that protein molecules are prone to relax and unfold at low surface coverages due to the availability of free space. On the other hand, surface crowding at high coverages leads to steric hindrance which prevents unfolding of a macromolecule and helps in retaining its conformation [229, 257]. However, denaturation can still occur in the latter case *via* other mechanisms such as enhanced possibility of protein-protein interactions on the surface due to the close proximity of other molecules [229].

II. pH: The environmental pH conditions during adsorption and desorption are known to affect protein stabiltiy [218, 274]. As discussed earlier in section 4A.4, the structural stability of a protein decreases at extremely high or low pH values [231, 232]. In general, it is believed that these macromolecules are less likely to undergo conformational rearrangements at pH values close to their IEP.

III. Molecular flexibility: As stated previously, protein molecules can be divided into two categories namely 'soft' and 'hard' proteins based on their molecular flexibility [135, 274]. Soft molecules like γ-globulin can sometimes undergo structural changes upon adsorption onto a solid surface if immobilization parameters are not established carefully [135, 274].

Other factors such as failure to use appropriate displacer (type and/or concentration) can also result in conformational changes after desorption. In this study, the secondary structure of γ-globulin molecules displaced from the surface of silica and PCL-ES100 particles were investigated as follows.

6B.4 Results and discussion

The secondary structure of desorbed γ-globulin using various displacer was confirmed by CD spectroscopy. The CD spectra for native γ-globulin was disscussed in section 4.2. Figures 6.4 and 6.5 present CD spectra of γ-globulin after desorption using SDS, Tween 80 and PF127 as displacer molecules.

Generally, the slope of spectra collected for γ-globulin desorbed from S_{FP} at pH 6.8 (Figure 6.4a) did not differ from that of the native protein. The maximum positive and negative ellipticity values at 201 and 218 nm respectively indicate that desorbed protein still retains its β-sheet conformation [275].

(a)

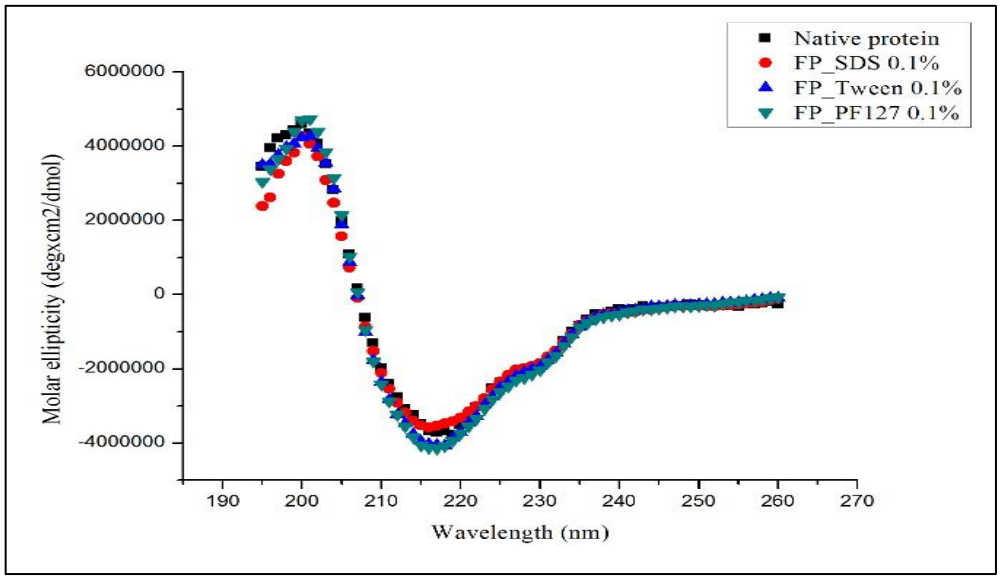

Figure 6.4a: CD spectra for γ-globulin desorbed at pH 6.8 from S_{FP}

Minor differences were observed in the ellipticity values for γ-globulin desorbed with SDS between 195- 200 nm, and also with Tween 80 and PF127 from 215- 220 nm. This may simply be attributed to slight irregularities in estimation of the γ-globulin concentration for the analyzed samples which impacts the CD absorbance data and consequently the corrected molar CD values [275].

Similar to S_{FP}, there were no differences observed to the slope of the spectra collected at pH 6.8 for γ-globulin desorbed from S_{XDP} with the use of SDS and PF127 (Figure 6.4b). However, in comparison to native protein, considerable changes were obtained for protein desorbed with Tween 80 where the shape of its spectra is nearly lost. This indicates a major change to conformation of desorbed γ-globulin in the presence of Tween 80.

(b)

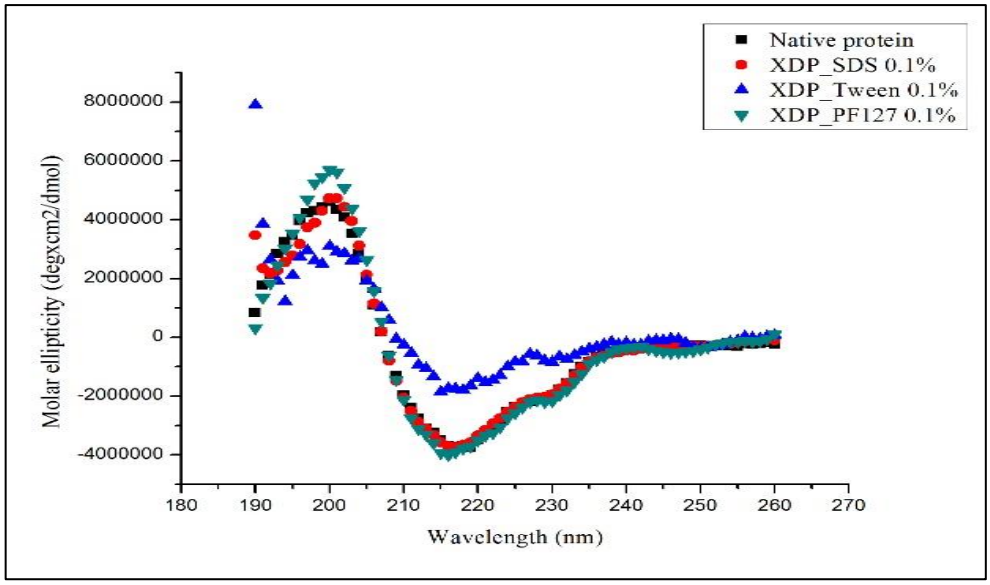

Figure 6.4b: CD spectra for γ-globulin desorbed at pH 6.8 for S_{XDP}

The slightly higher ellipticity values recorded for both SDS and PF127 between 190 and 205 nm could also be as a result of variations in sample concentration. Furthermore, changes to the ellipiticty values due to varying protein concentration could indicate aggregation of the macromolecule. However, as the minima and maxima peaks of the spectra for both SDS and PF127 are still present and do not shift from the original wavelengths of 218 and 201 nm respectively, it would suggest that desorbed γ-globulin still retains its native conformation in the presence of these displacers.

The spectra for protein desorbed from MSU-H at pH 6.8 is presented in Figure 6.4c. In comparison to native protein, the spectra for γ-globulin desorbed from MSU-H retained its original shape and consequently the β-sheet conformation of its original structure. Similar to S_{FP} and S_{XDP}, there were considerable differences between the molar ellipicity values of the spectra for desorbed γ-globulin from MSU-H and the native protein which may be attributed to dissimilarities in concentration as previously discussed.

(c)

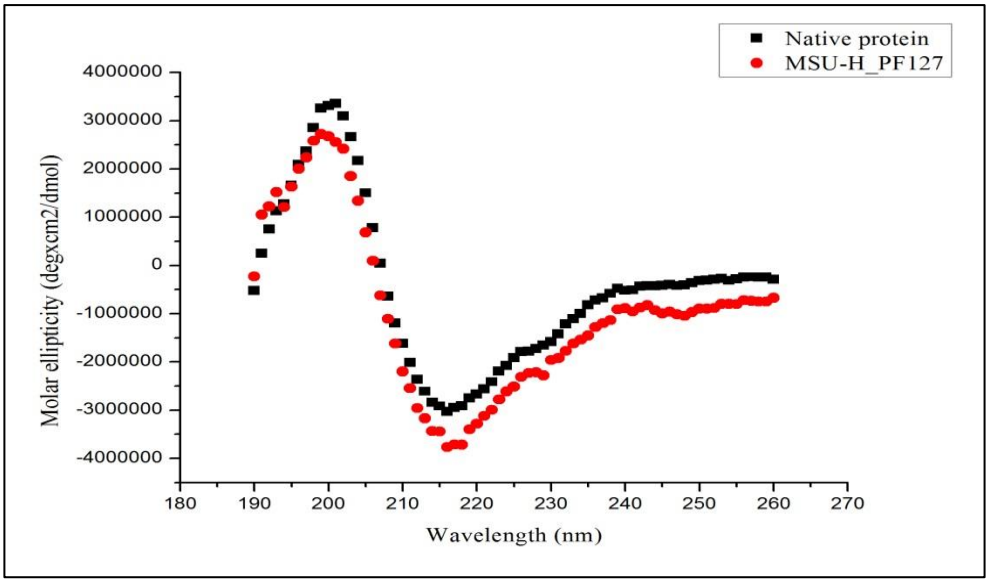

Figure 6.4c: CD spectra for γ-globulin desorbed at pH 6.8 for MSU-H

The CD spectra for protein desorbed at pH 7.4 from S_{FP}, S_{XDP}, and MSU-H with surface-active molecules are presented in Figures 6.5a to c.

(a)

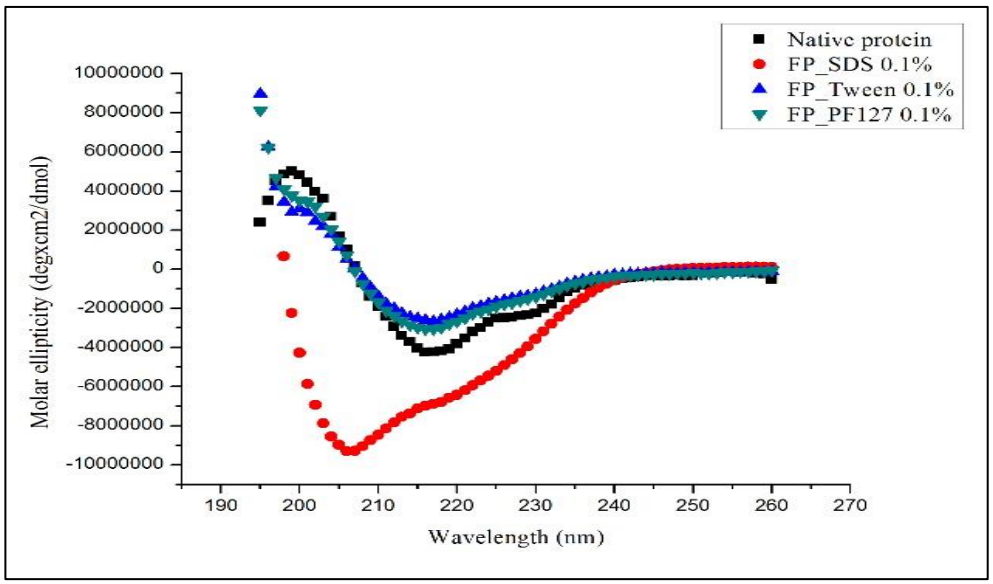

(b)

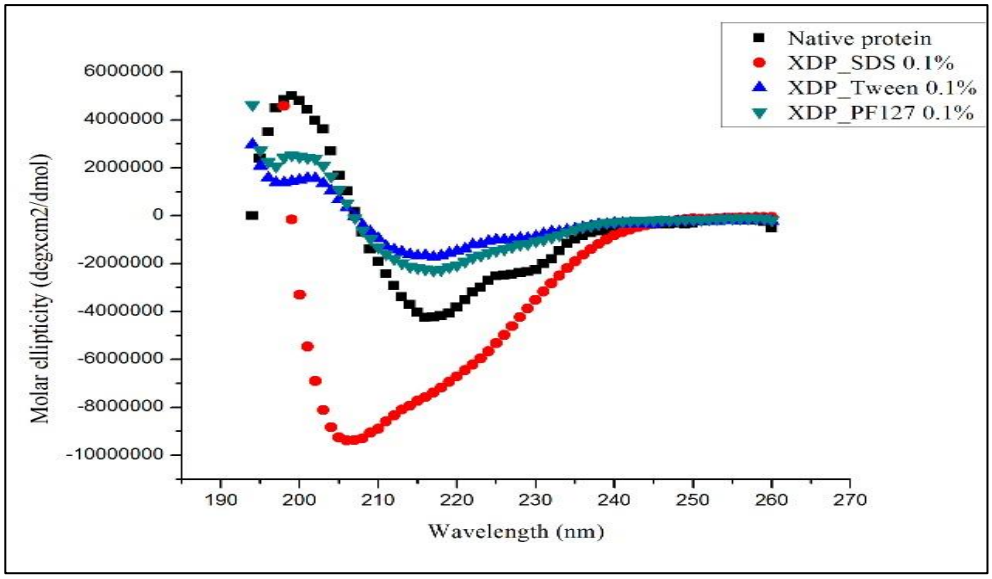

(c)

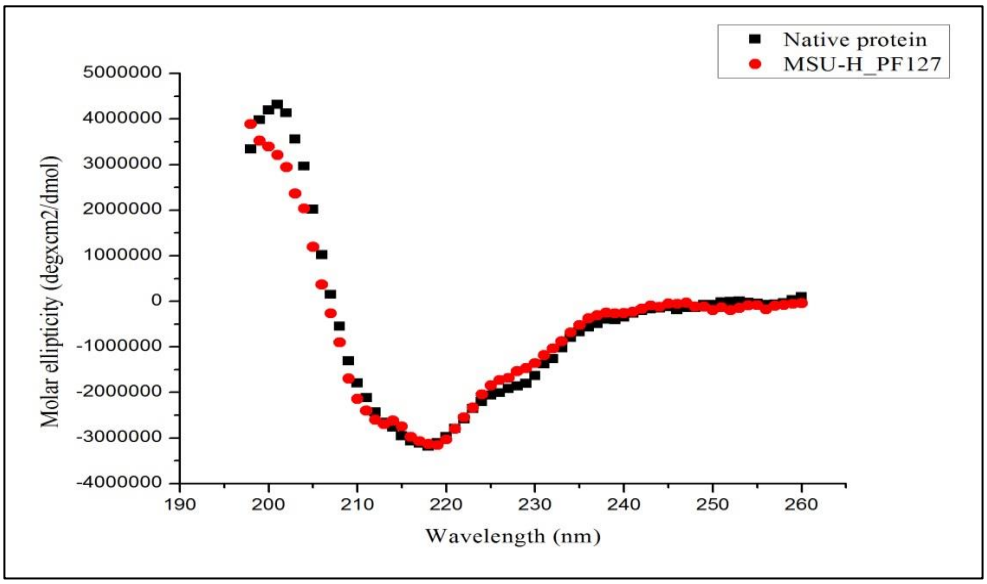

Figure 6.5: CD spectra for γ-globulin desorbed at pH 7.4 from (a) S_{FP}, (b) S_{XDP} and (c) MSU-H

Generally, in contrast to the data obtained at pH 6.8, the spectra for γ-globulin molecules desorbed from these silica particles at pH 7.4 considerably differed from that of the native protein. Aside from differences in the ellipticity values, for γ-globulin desorbed with PF127 and Tween 80, there was either a loss of the maxima peak at 201 nm (as seen with S_{FP} and MSU-H) or shift in this peak as observed with S_{XDP} particles. The minima peak at 218 nm for protein desorbed by both PF127 and Tween 80 retained its position when compared to the native spectra. On the other hand, the spectra for γ-globulin desorbed by SDS from S_{FP} and S_{XDP} completely lost its maxima peak and there was a significant shift in the position of the

minima peak. This indicated conformational changes to the secondary structure of released γ-globulin at this pH.

In summary, when compared to native γ-globulin, desorption by SDS at pH 7.4 resulted in the most pronounced changes to CD spectra followed by Tween 80 and PF127. This could be related to the interactions of released protein with surfactant molecules in the media. SDS is an anionic surfactant that strongly binds to the positively charged and the hydrophobic residues of proteins through its sulfate groups and alkyl chains respectively, which could result in the unfolding of the protein structure [276]. On the other hand, although non-ionic molecules like Tween 80 and PF127 could have weak hydrophobic interactions with released γ-globulin, they tend to interact more with each other rather than the protein thus limiting their denaturing effects on the structure of the macromolecule [276]. Furthermore, interactions of ampiphilic substances like PF127 and Tween 80 including masking of hydrophobic sites of the protein have been shown to have stabilizing effects on the protein structure by preventing aggregation and surface adsorption [276- 278]. Moreover, as the spectra deviations from native protein were more pronounced for protein desorbed at pH 7.4 than pH 6.8 it would seem that the pH also plays a role in the stability of released γ-globulin. As discussed earlier in section 4A.4, differences in the electrostatic state of protein with the change in pH can result in conformational alterations to the structure of the macromolecule.

CD spectra was also collected for γ-globulin desorbed from PCL-ES100 (1:3 ratio) with 0.1% PF127 in pH 6.8 buffer (Appendix A.10) and it shows a loss of the maxima peak and a shift in the minima peak. This indicates changes to the secondary structure of the protein and it may be related specifically to interactions of γ-globulin with the polymeric surface. With respect to the type of core particle, conformational changes to the protein were least pronounced for S_{FP} and more substantial for PCL-ES100. This suggests that the absorbent surface may play a role in the stability of the protein but a combined effect of core particles, pH and displacer must also be considered.

6.1 Conclusion

The release of immobilized γ-globulin was evaluated and found to vary with pH and the type of displacer present in the media. The highest percentage of released γ-globulin (91%) was obtained at pH 7.4 in the presence of SDS. However, the stability of desorbed γ-globulin was found to be better at pH 6.8 with molecules displaced by PF127. Based on these results,

protein adsorbed-S_{FP}, S_{XDP}, and MSU-H particles were selected for the formulation of SCDDS *via* supercritical fluid technology (SCFT) as discussed in chapter 7. The work with PCL-ES100 systems was discontinued due to the reduced stability of γ-globulin following its subsequent desorption from the particle surface.

Chapter 7

Formulation of SCDDS and drug release studies

This chapter covers the formulation of SCDDS and the release of immobilized protein from the coated core particles.

7A. Formulation of SCDDS

This section discusses the work relating to the preparation of SCDDS using γ-globulin-adsorbed S_{FP}, S_{XDP}, and MSU-H particles.

7A.1 Aims and Objectives

The aim of this study was to design a SCDDS that will allow for the adsorption and subsequent release of γ-globulin at the intestinal pH without compromising the integrity of the protein. The ideal solid core materials that will permit for the immobilization and subsequent release of γ-globulin have been investigated and discussed in Chapters 5 and 6. Further to this work, the appropriate shell material that can provide protection to the protein-adsorbed core particles against gastric pH will be studied as follows.

7A.2 Experimental

The experimental procedure involved in this work is detailed in section 2.7.

7A.3 Introduction

The rising interest in protein and peptide therapeutics has led to the growing research in the developments of novel carrier systems particularly for oral delivery [1]. However, several physicochemical and biological barriers pose as a challenge for the use of biomolecules as oral drug therapies [32]. This includes physiological factors of the G.I tract that can result in significant changes to the biologics such as denaturation of therapeutic proteins because of the acidic environment in the stomach [32]. Various delivery systems (as discussed in Chapter 1) have been established to overcome some of these limitations including the use of enteric materials that provide protection to the biomolecules against the harsh acidic environment of the G.I tract [53]. SCDDS involves the immobilization of the therapeutic drug molecule on the surface of a solid, followed by the coating of this drug core to achieve targeted/sustained release [73]. SCDDS in this work was prepared by immobilizing γ-globulin molecules onto

silica particles (S_{FP}, S_{XDP} and MSU-H) and their subsequent coating by FAs [Palmitic (PA), Stearic (SA) and Myristic acid (MA)] *via* melt deposition method in $scCO_2$. These FAs excipients and supercritical coating conditions were selected based on the work reported by Trivedi *et al* [73]. The work successfully established the role of FAs as a shell coating for bovine serum albumin adsorbed-core particles.

With respect to the formulation of DDS for biomolecules, the use of SCF has been established as a processing technique that can help ensure the stability of these molecules during coating procedures [279]. Conventional methods for coating usually involve one or more organic solvents that are not only toxic to the environment but can also lead to the degradation of therapeutic proteins [279, 280]. The possibility of a substantial amount of residual solvents being retained in formulated particles also means that they can be harmful to the patients. Additionally, conventional techniques such as hot-melt coating or fluid bed systems comprise of extreme temperatures that are not compatible with thermo-labile substances including peptides/proteins [279, 281]. Hence, the need to develop novel procedures that can help to avoid these concerns has led to the advancement of SCF technology in DDS design for biomolecules [279]. The application of SCFs, specifically $scCO_2$, as a processing media provides a coating technique that either reduces or excludes the need for organic solvents. The coating can also be performed in oxygen and moisture-free environment to minimize the chances of oxidation and hydrolysis. Furthermore, processing of excipients such as FAs in $scCO_2$ allows the opportunity for coating to be performed at comparatively lower temperatures due to the plasticizing effect of $scCO_2$ [282]. This helps to avoid the possibility of thermal denaturation of thermo-sensitive excipients such as protein or peptide.

In this work, SCDDS prepared using $scCO_2$-based technology was investigated for their selective ability to delay γ-globulin release at gastric pH (pH 1.2) and promote a controlled-release at intestinal conditions (either at SIF or pH 7.4). A schematic of the procedure involved in SCDDS design is presented in Figure 7.1.

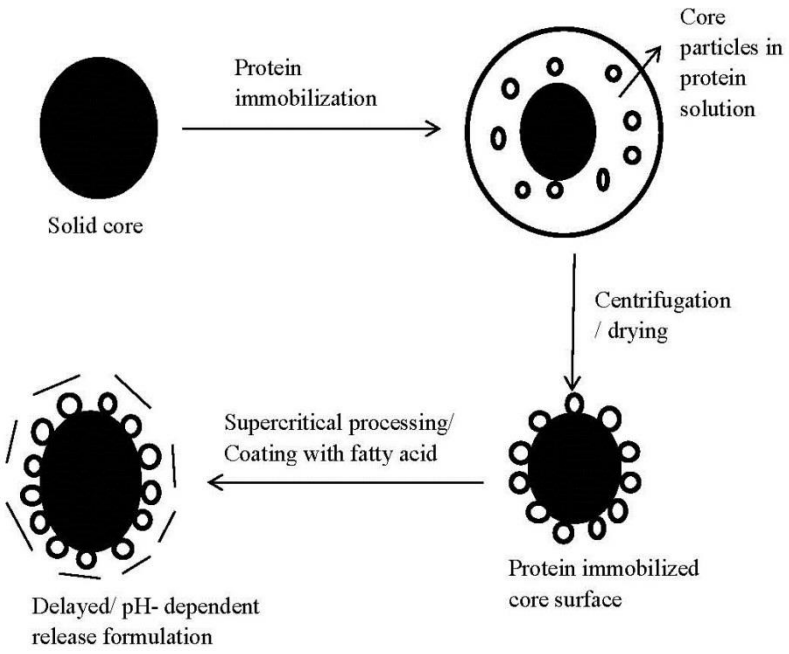

Figure 7.1: Schematic presentation of SCDDS design

During the $scCO_2$ coating process, the desired quantities of γ-globulin-immobilized particles and FA are introduced into a high pressure vessels at pre-determined temperature and pressure to allow melting of FAs. The protein-adsorbed core particles suspended in the FA melt are then mixed to achieve even coverage of coating around the particles. Depressurization of the vessel causes deposition of shell material on the surface of particles which can then be retrieved and potentially be used immediately as there are no further steps involved in the formulation process *i.e.* drying, solvent evaporation *etc*.

7A.4 Results and discussion

The γ-globulin-adsorbed S_{FP}, S_{XDP} and MSU-H particles were coated with MA, PA and SA by melt deposition in $scCO_2$. The silica to FA proportions were established after preliminary release studies from the formulations prepared with 1:2, 1:1, and 2:1 (silica: FA) ratios for all core particles. There was no protein release for formulations prepared with 1:2 and 1:1 ratios from SCDDS based on S_{FP} and S_{XDP} in SGF, SIF and pH 7.4 buffer. Whereas, MSU-H based formulations prepared with 2:1 ratio led to similar protein release as uncoated particles and 1:2 ratio formulations did not show any γ-globulin release. The formulations which did not provide sufficient protection and/or release of γ-globulin were excluded from further studies. In order to allow for sufficient particle surface coverage and protection to the protein by FAs,

the silica to FA ratios of 2:1 for S_{FP}/ S_{XDP} and 1:1 for MSU-H particles were chosen. The higher ratio of FA required for final formulations of MSU-H in comparison to both S_{FP} and S_{XDP} could be due to larger specific surface area of MSU-H *i.e.* 782 m^2/g for MSU-H than 289 and 258 m^2/g for S_{XDP} and S_{FP} respectively.

7B. Protein release studies for coated particles

This section covers *in-vitro* drug release studies carried out with formulated SCDDS in SGF and SIF, and in phosphate buffer pH 7.4 containing 0.1% PF127 as a displacer. The CD analysis of released protein is also discussed in this section.

7B.1 Aims and Objectives

The aim of this work was to study the rate of γ-globulin release from the FA coated particles. The data obtained from this work provided information on the influence of pH and type of shell material on the amount of γ-globulin released from these core materials. The effect of the processing method on the stability of γ-globulin was also studied from the CD analysis of released protein.

7B.2 Experimental

The experimental procedures involved in the protein release studies are detailed in section 2.7.1. CD analysis of release γ-globulin was performed as detailed in section 2.3.3.

7B.3 Results and discussion

This section covers the *in-vitro* release data obtained for SCDDS formulations prepared with 2:1 and 1:1 silica to FA ratios for S_{FP}/ S_{XDP} and MSU-H particles respectively.

7.1 γ-globulin release profiles from SCDDS formulated with PA

The release profile of γ-globulin from SCDDS prepared with protein adsorbed-S_{FP} particles and PA are presented in Figure 7.2. There was no release of γ-globulin from these particles during the first 120 minutes in SGF. On the other hand, by 135 minutes at SIF and pH 7.4, a release of 25% and 53% were obtained respectively.

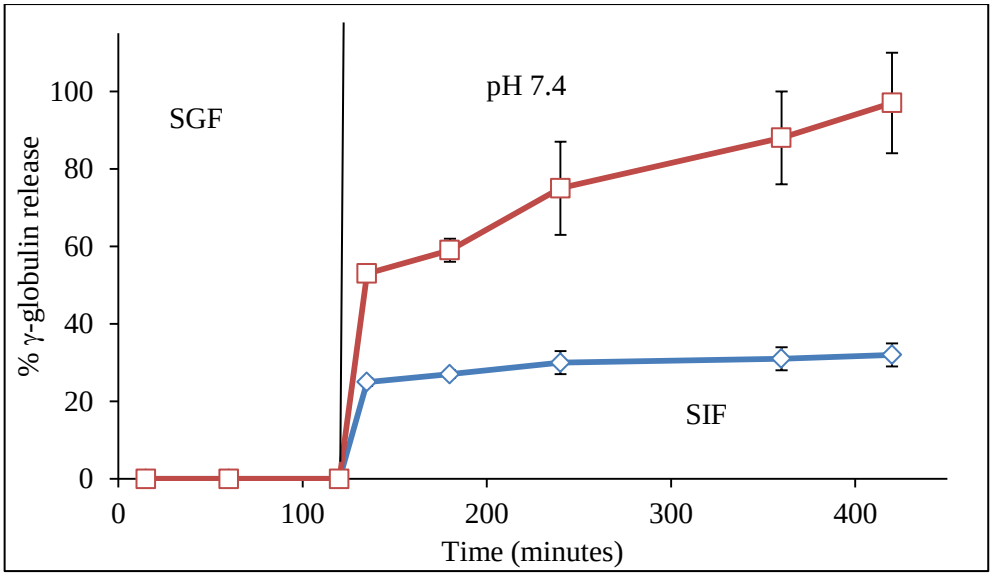

Figure 7.2: γ-globulin release profile for PA coated S_{FP}

The amount of γ-globulin released from these particles at pH 7.4 continued to rise rapidly reaching to 97% at 420 minutes. On the other hand, there was only a slight increase in the percentage of protein released at SIF conditions with just 32% in solution at 420 minutes. The initial experiments (between 0 and 120 minutes) in SGF (pH 1.2) represent the first stages of digestion that occurs in the stomach upon oral intake, and a lack of protein release indicate that PA successfully acted as an enteric coating at the acidic environment. The subsequent γ-globulin release in SIF and at pH 7.4 suggests that protein release from the coated PA particles occurs by the continuous erosion of PA. This can be attributed to the physico-chemical property of FAs with respect to their enhanced solubility at alkaline pH in comparison to acidic pH [97]. As the pH reaches close to neutral, the carboxylic acid group of PA become deprotonated which drives their dissolution. On the other hand, the protonation of FA molecules in SGF media makes them insoluble [97]. The dissolution of PA at the higher pH values would mean that the displacer (PF127) in the media can now have access to the solid surface and promote γ-globulin release by displacement mechanism. Additionally, as earlier discussed in section 6A.4, the faster release at pH 7.4 could also be attributed to the electrostatic repulsion between γ-globulin and silica at this condition.

Similar to S_{FP}, PA coating also prevented the release of γ-globulin from S_{XDP} coated particles in SGF (Figure 7.3).

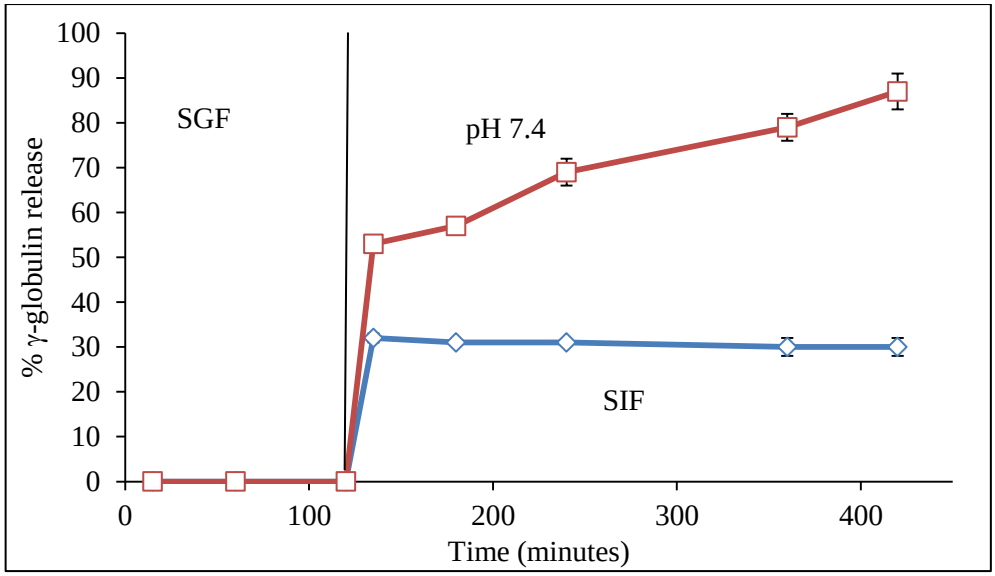

Figure 7.3: γ-globulin release profile for PA coated S_{XDP}

There was no protein release within the first 120 minutes. However, by 135 minutes, 32% and 53% of immobilized γ-globulin was released at SIF and pH 7.4 respectively. Although the release attained in SIF remained at 32% as the experiment proceeded to 420 minutes, but the percentage of γ-globulin released at pH 7.4 rapidly increased to 87%. Similar to S_{FP}, the data obtained with PA coated S_{XDP} particles also indicate a pH-dependent release of immobilized protein as a result of the solubility of the PA shell in alkaline conditions.

The protein release profile for PA coated MSU-H based SCDDS is presented in Figure 7.4. There was no γ-globulin release in SGF similar to S_{FP} and S_{XDP} based formulations. In contrast to both S_{FP} and S_{XDP}, γ-globulin release from the MSU-H coated particles was delayed until 240 minutes in SGF (21%) with a slight increase at 420 minutes to 25%. This delay was also observed at pH 7.4 where 27% protein release was obtained after 180 minutes with an increase to 33% at 420 minutes.

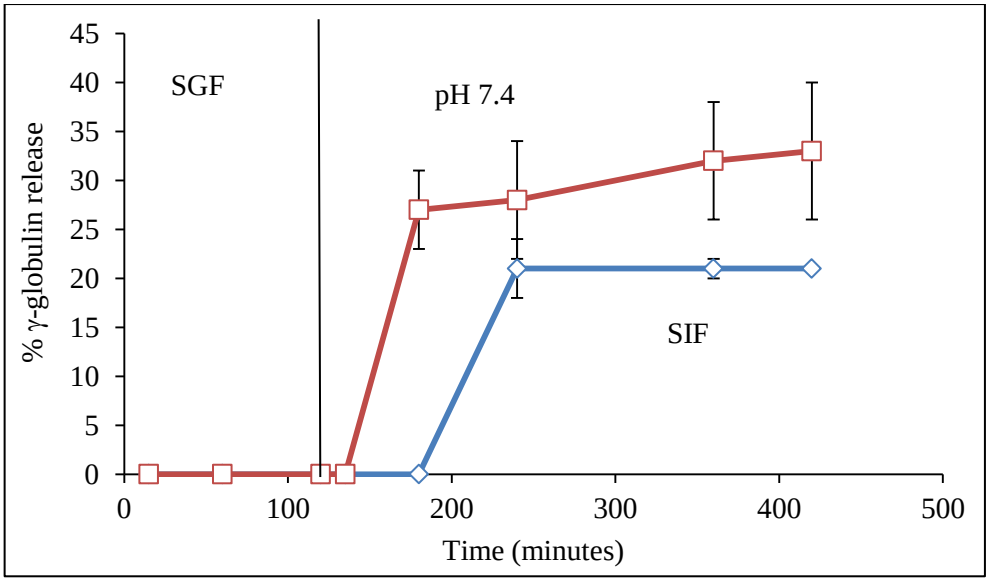

Figure 7.4: γ-globulin release profile for PA coated MSU-H

The total protein released from MSU-H based SCDDS was lower than that for S_{FP} and S_{XDP} based formulations which was also similar to the desorption results discussed in section 6A.4. Moreover, the difference between the release at pH 7.4 and in SIF for MSU-H formulations was also considerably smaller than for the other particles. This could be related to the comparatively smaller pore size for MSU-H particles resulting in a limited access to immobilized protein by the displacer molecules in the release media. Therefore, it may be possible that the amount of protein released from these particles relates mainly to γ-globulin adsorbed at the surface which is easily accessible to the desorbing FA molecules.

7.2 γ-globulin release profiles from SCDDS formulated with SA

The release profiles for SCDDS prepared by the SA coating of protein adsorbed-S_{FP} are presented in Figure 7.5. Similar to previous observations, the release of γ-globulin from these formulations was dependent on pH. The SA shell was able to prevent γ-globulin release in SGF and the release of γ-globulin was higher at pH 7.4 in comparison to pH 6.8. The percentage of immobilized protein released from the SA coated S_{FP} particles increased from 21 and 41% at 135 minutes to 25 and 72% at 420 minutes for SIF and pH 7.4 respectively.

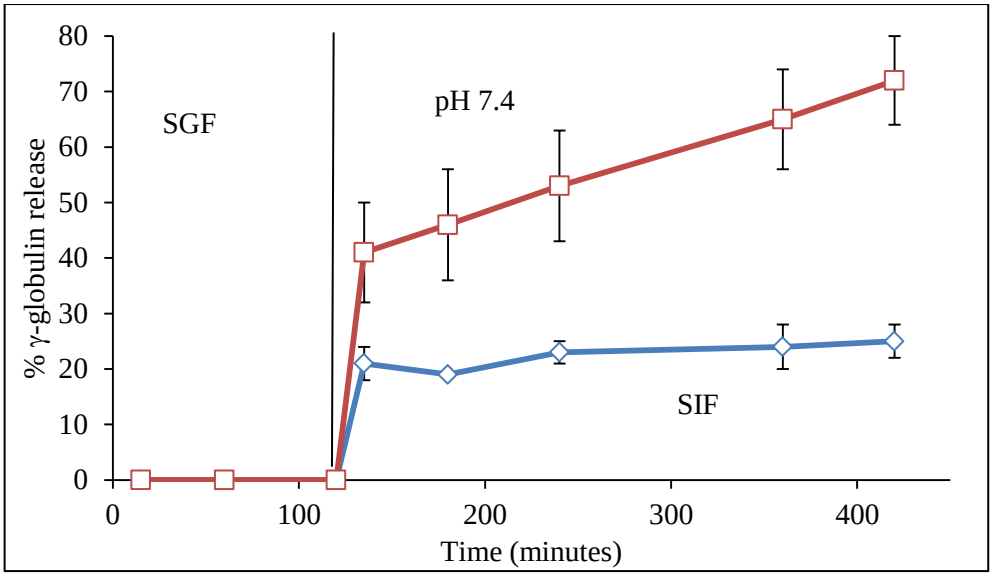

Figure 7.5: γ-globulin release profile for SA coated S_{FP}

The pH-dependent release of γ-globulin from SCDDS prepared by SA coating of S_{XDP} particles can also be observed in Figure 7.6.

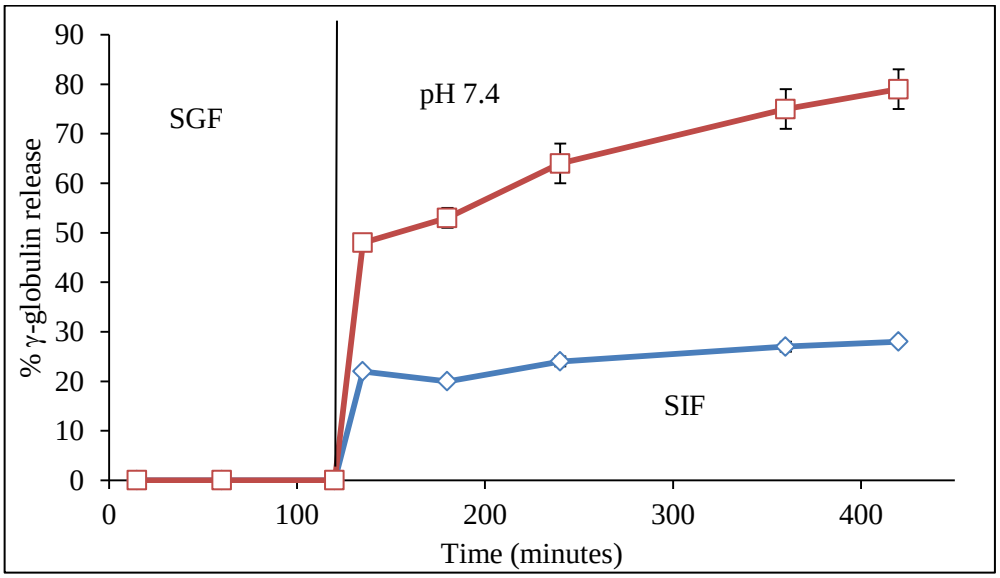

Figure 7.6: γ-globulin release profile for SA coated S_{XDP}

The release of γ-globulin from these S_{XDP} based formulations was low and slower in SIF, in comparison to pH 7.4. The γ-globulin release in SIF and pH 7.4 media was obtained to be 22% and 48% respectively at 135 minutes. A total release of 28% and 79% was determined at 420 minutes in SIF and pH 7.4 respectively.

The protein release profiles for SA coated MSU-H particles are presented in Figure 7.7. Similar to earlier observations, the release of γ-globulin from MSU-H based formulations was lower in comparison to both S_{FP} and S_{XDP}. The total amount of γ-globulin released was only 25% and 29% in SIF and pH 7.4 media respectively after 420 minutes.

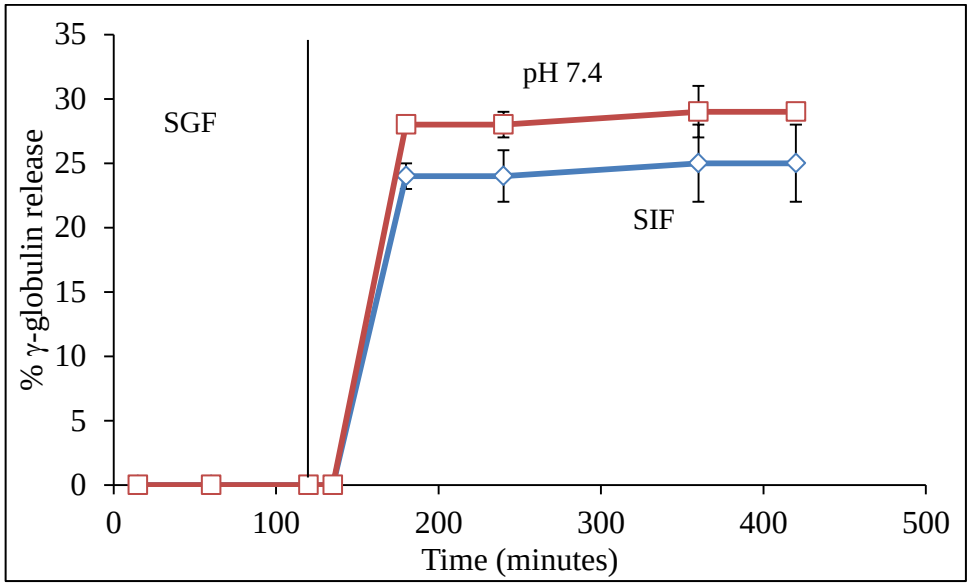

Figure 7.7: γ-globulin release profile for SA coated MSU-H

Generally, for all the SA coated silica particles the amount of protein released at pH 7.4 was higher than that in SIF. As discussed earlier, this could be related to the increased solubility of SA [97, 283], along with the higher electrostatic repulsion behaviour of γ-globulin and core particles at pH 7.4 [261].

7.3 γ-globulin release profiles from SCDDS formulated with MA

The release profile of γ-globulin from SCDDS formulations prepared using MA and S_{FP} particles is presented in Figure 7.8. MA coating on protein adsorbed S_{FP} also prevented the release of γ-globulin in SGF and resulted in 21% and 38% release at SIF and pH 7.4 respectively after 135 minutes. There was only a minimal rise in the released amount in SIF but values obtained at pH 7.4 increased rapidly to give a total γ-globulin release of 52% after 420 minutes.

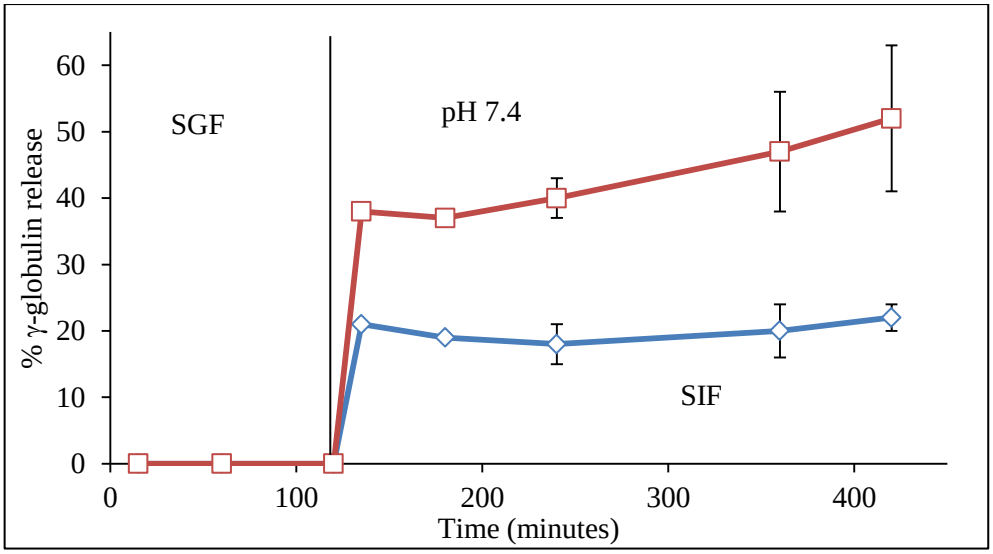

Figure 7.8: γ-globulin release profile for MA coated S_{FP}

Figure 7.9 presents protein release from MA coated S_{XDP} based formulations. There was no release in SGF and a total γ-globulin release of 35% and 77% was obtained after 420 minutes in SIF and pH 7.4 buffer respectively.

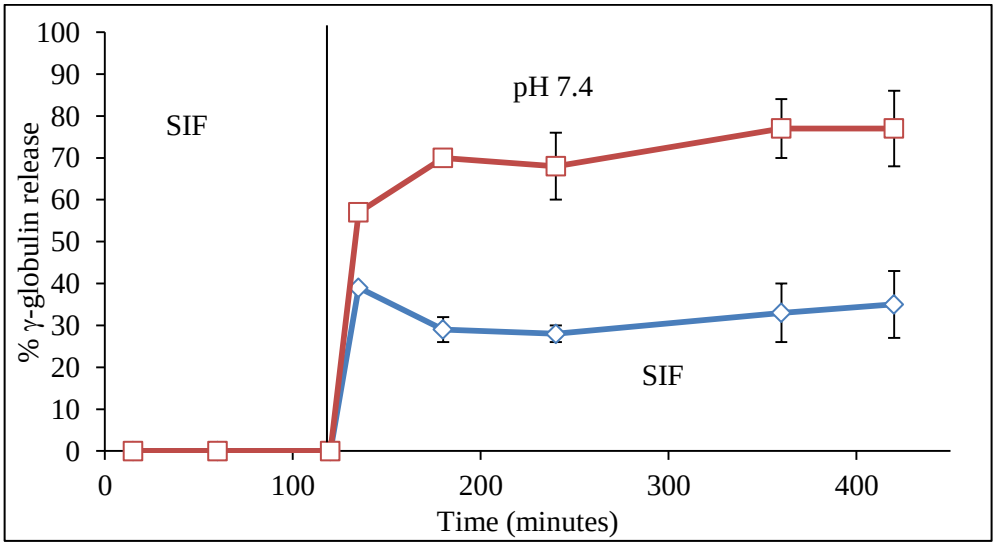

Figure 7.9: γ-globulin release profile for MA coated S_{XDP}

The protein release profile for MA and MSU-H based SCDDS is presented in Figure 7.10, where, zero release in SGF was followed by 21% and 30% protein release after 135 minutes in SIF and at pH 7.4 respectively. The amount of γ-globulin released in both media stayed relatively constant between 135 and 360 minutes. There was a sudden increase in γ-globulin

release between 360 and 420 minutes in pH 7.4 buffer resulting in total release of 42% after 420 minutes.

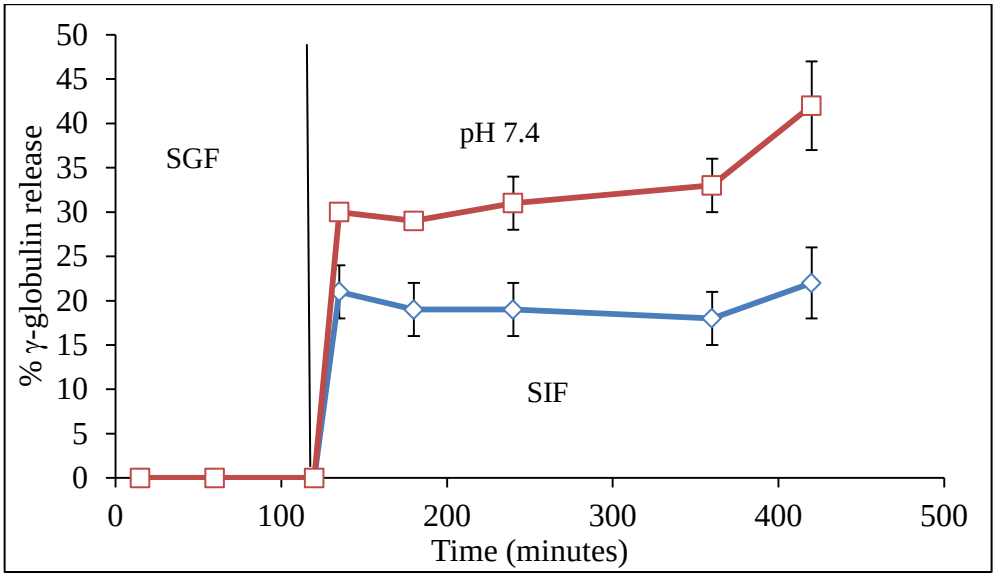

Figure 7.10: γ-globulin release profile for MA coated MSU-H

In summary, when compared to SIF the release of γ-globulin was higher for all FA coated silica formulations at pH 7.4. As protein release from these systems was as a result of the erosion of the FA coating, therefore it can be expected that it will follow a trend of MA > PA > SA [73, 98]. This is attributed to the reduction in solubility of FAs with the increase in carbon chain length [98]. However, this trend was not observed with the data obtained in this work. Although, for coated MSU-H particles the highest protein release was seen with MA but the same was not observed with S_{FP} and S_{XDP} preparations where PA coating provided higher γ-globulin release of 97% and 87% for S_{FP} and S_{XDP} respectively. Additionally, the release of protein from MA coated formulations happened at a more controlled manner than that from both PA and SA systems particularly at pH 7.4. It is not fully understood why this occurred but it is thought to be due to possible imperfections during the coating process and/or supersaturation of the dissolution media. With regards to the coating *via* $scCO_2$ processing, it is known that CO_2 interactions improve with decrease in carbon chain length of FA. This could possibly result in lower melt viscosity of MA in $scCO_2$ leading to better mixing and uniform surface coating with better control in the release of γ-globulin.

Tables 7.1a to 7.1c compare the release of γ-globulin from uncoated and FA-coated silica particles after 240 minutes.

Table 7.1a: γ-globulin release from uncoated and coated S_{FP} particles after 240 minutes

	uncoated	MA	PA	SA
SIF	50 ± 6%	18 ± 3%	30 ± 3%	23 ± 2%
pH 7.4	72 ± 0.1%	40 ± 3%	75 ± 12%	53 ± 10%

Table 7.1b: γ-globulin release from uncoated and coated S_{XDP} particles after 240 minutes

	uncoated	MA	PA	SA
SIF	46 ± 2%	28 ± 2%	31 ± 0.1%	24 ± 1%
pH 7.4	78 ± 7%	68 ± 8%	69 ± 3%	64 ± 4%

Table 7.1c: γ-globulin release from uncoated and coated MSU-H particles after 240 minutes

	uncoated	MA	PA	SA
SIF	26 ± 5%	19 ± 3%	21 ± 3%	24 ± 2%
pH 7.4	34 ± 7%	31 ± 3%	28 ± 6%	28 ± 1%

Generally, the amount of protein released from the uncoated S_{FP} and S_{XDP} particles at pH 7.4 and in SIF was higher than that from SCDDS. This suggests that the FA coating definitely slowed the release of γ-globulin from these systems along with the required enteric properties. This delay can be attributed to the fact that the release of protein from the coated particles first requires the solubilization of FA shell before coming in contact with the release media. The only exception was seen with PA coated S_{FP} particles where the percentage of γ-globulin released at pH 7.4 (75%) was similar to the uncoated particles at 72%. Although, this is difficult to explain however it could be due to a number of factors including surface features of S_{FP} along with the coating imperfections in this formulation. Likewise, MSU-H based SCDDS showed lower release in SIF for MA coated formulation but had limited effect of other FA coating as protein release for both uncoated and coated particles was very similar in both SIF and pH 7.4 buffer. Although, imperfect coating and differences in surface properties (surface area, pore size and volume) can be the possible reason but it is important to remember that adsorption of a macromolecule and desorption from a solid surface is a complex process.

As described in section 2.8, F1 and F2 contrast was made between the reference (uncoated particles) and various coated preparations in both SIF and at pH 7.4. The results obtained are presented in Tables 7.2a to c.

Table 7.2a: F1 and F2 calculations for FA coated S_{FP} particles

	S_{FP}: MA		S_{FP}: PA		S_{FP}: SA	
	SIF	pH 7.4	SIF	pH 7.4	SIF	pH 7.4
F1	55	39	36	3	51	25
F2	31	30	40	79	33	40

Table 7.2b: F1 and F2 calculations for FA coated S_{XDP} particles

	S_{XDP}: MA		S_{XDP}: PA		S_{XDP}: SA	
	SIF	pH 7.4	SIF	pH 7.4	SIF	pH 7.4
F1	24	12	22	13	45	20
F2	47	54	50	52	37	43

Table 7.2c: F1 and F2 calculations for FA coated MSU-H particles

	MSU-H: MA		MSU-H: PA		MSU-H: SA	
	SIF	pH 7.4	SIF	pH 7.4	SIF	pH 7.4
F1	20	9	12	17	3	15
F2	64	24	75	62	91	64

Two dissolution profiles can be regarded similar if the value of F1 is <15 and F2 is > 50 [284]. In general, for FA coated S_{FP} and S_{XDP} formulations, F1 values were higher than 15 and F2 values were lower than 50. Hence, suggesting that these coated preparations were not similar to the reference (uncoated) particles. The only exemptions were observed at pH 7.4 with PA coated S_{FP} and S_{XDP}, and MA coated S_{XDP} particles. These variations can be related to the pH solubility of the FA shell as earlier discussed. The higher solubility of FAs at pH 7.4 would mean that coated particles are more likely to quickly lose their FA shell, thus resulting in a release profile that is relatively similar to that of uncoated particles. On the other hand, the F1 and F2 values for FA coated MSU-H formulations (Table 7.2c) show that their release profiles at pH 7.4 and SIF are similar to that of the uncoated particles. For both uncoated and coated MSU-H preparations, the total γ-globulin release was comparatively lower than S_{FP} and S_{XDP}, and it was also limited to only a maximum of 33 to 34%. This could be due to the relatively smaller pore sizes of MSU-H particles as previously discussed in section 6A.4. The

inadequate protein release could be as a result of displacement of only surface γ-globulin by PF127. Additionally, the state of immobilized γ-globulin layer prior to desorption could also be linked to the limited release. Adsorbed protein molecules are less likely to desorb if they have undergone significant changes to their conformational state upon attachment to the solid surface [218, 266- 267].

Nevertheless, SCDDS prepared using silica and FA clearly possess important enteric properties but further investigations into the coating technique to achieve improved surface coverage may be required to enhance the potential of these systems to be used as oral DDS. The structural conformation of released γ-globulin was evaluated by CD spectroscopy as discussed in section 7.4.

7.4 Stability of desorbed γ-globulin

This section covers CD analysis to investigate any changes to the secondary structure of released γ-globulin from SCDDS.

The CD spectra for γ-globulin released in SIF and phosphate buffer pH7.4 from FA coated S_{FP} formulations are presented in Figures 7.11a and b. In comparison to native protein, lower ellipticity values were observed in the spectra for released γ-globulin. This may be attributed to the variations between the concentrations of released protein which could consequently result in differences in CD absorbance and molar ellipticity values [285].

(a)

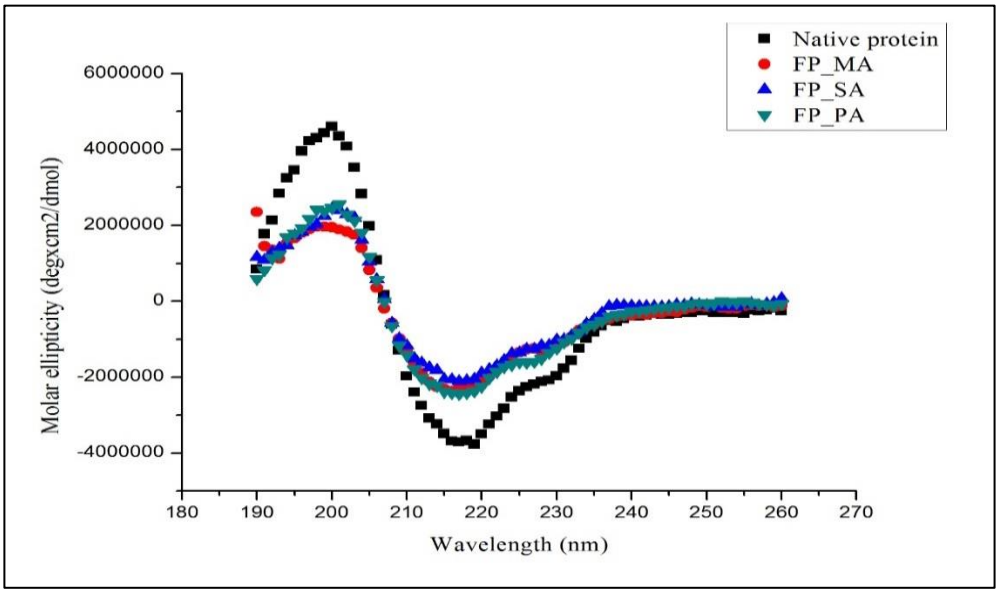

(b)

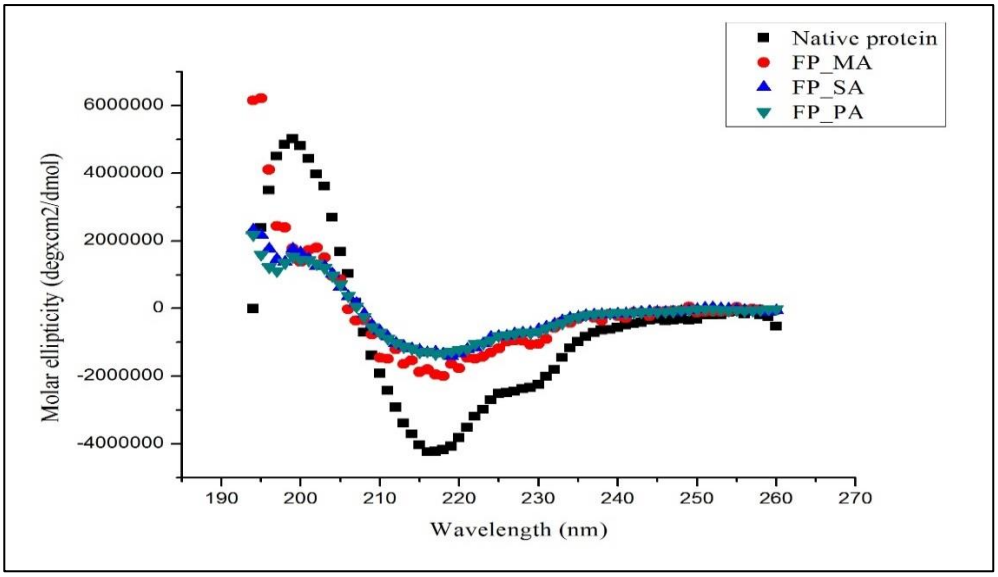

Figure 7.11: CD spectra for released γ-globulin from FA-S_{FP} in (a) SIF (b) pH 7.4

In comparison to native protein, there were no changes to the slope of the spectra for γ-globulin released from S_{FP} based formulations in SIF indicating that the protein retains its original β- sheet structural arrangement. On the other hand, there was nearly a complete loss of the shape of the spectra for γ-globulin released at pH 7.4 from all the FA coated S_{FP} particles. This suggests pH-induced changes to the conformation of released γ-globulin at pH 7.4 which could be attributed to the electrostatic state of the protein at this pH [209]. This pH-induced effect to protein stability was also observed after γ-globulin desorption as described in section 6B.4. As discussed earlier in section 5A.4, at higher pH values γ-globulin molecules attain higher charges which could affect the electrostatic inter-molecular and intra-molecular interactions that are responsible for maintaining its structural conformation.

The spectra for protein released from FA coated S_{XDP} particles are presented in Figures 7.12a and b. Similar to S_{FP}, aside from the differences in the ellipticity values there are no changes to the shape of the spectra for γ-globulin released in SIF. The loss to the slope of the spectra for γ-globulin released at pH 7.4 was also observed for these systems.

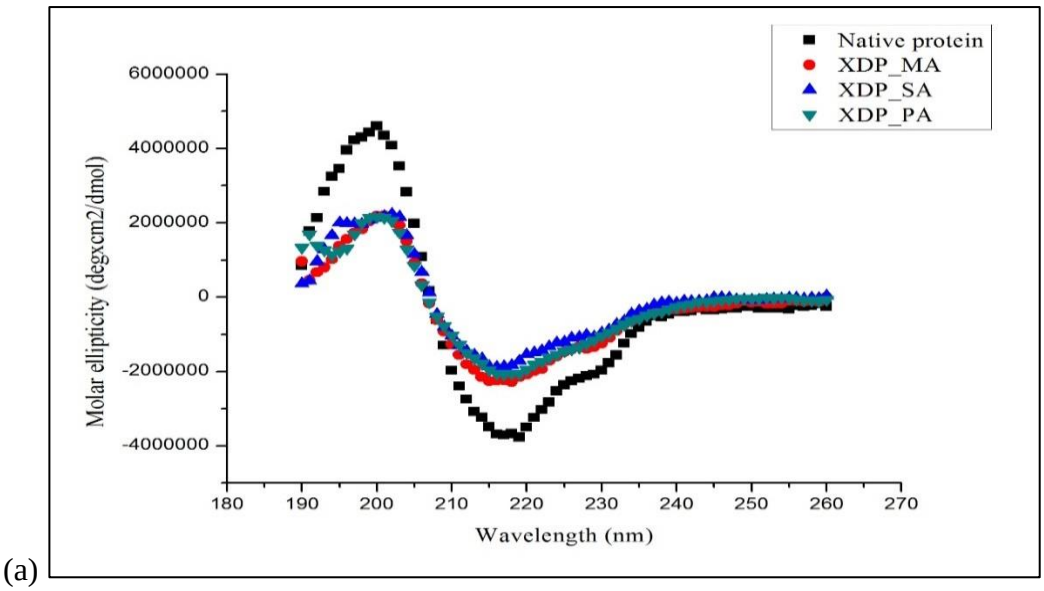

(a)

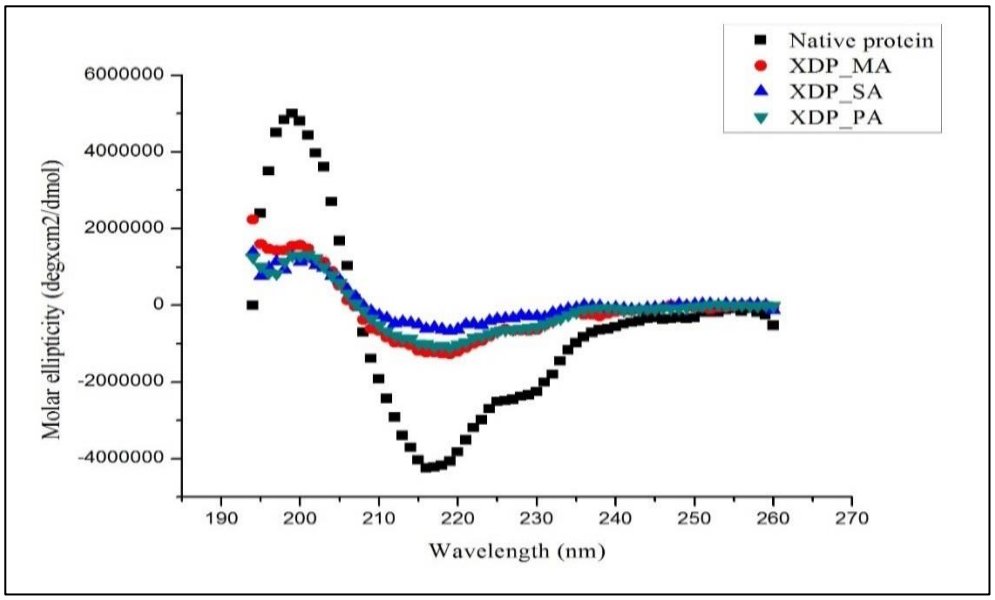

(b)

Figure 7.12: CD spectra for released γ-globulin from FA-S_{XDP} in (a) SIF (b) pH 7.4

CD spectra obtained for released protein from MSU-H formulations are presented in Figure 7.13a and b and they differed considerably from that of native protein.

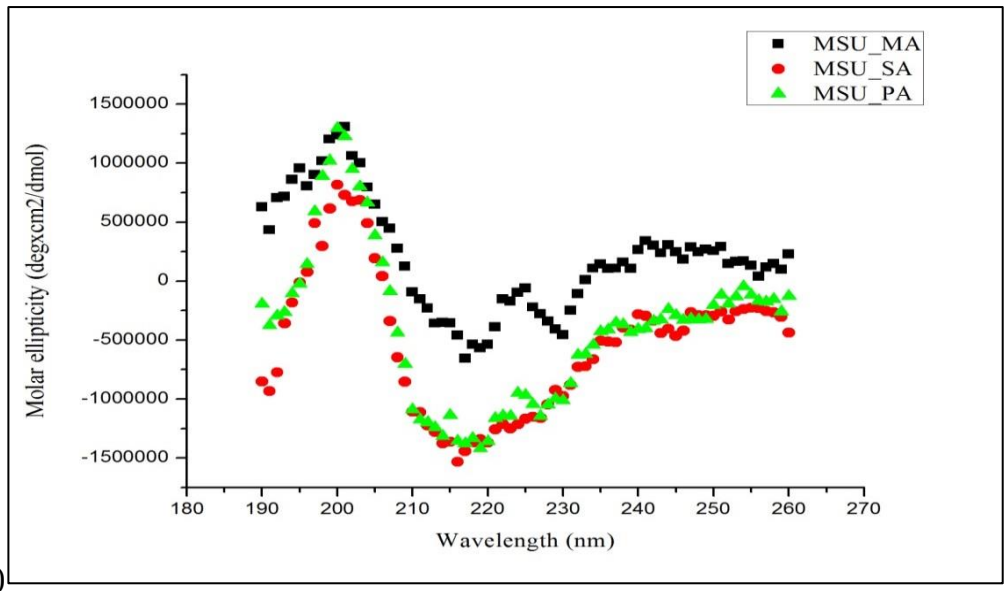

(a)

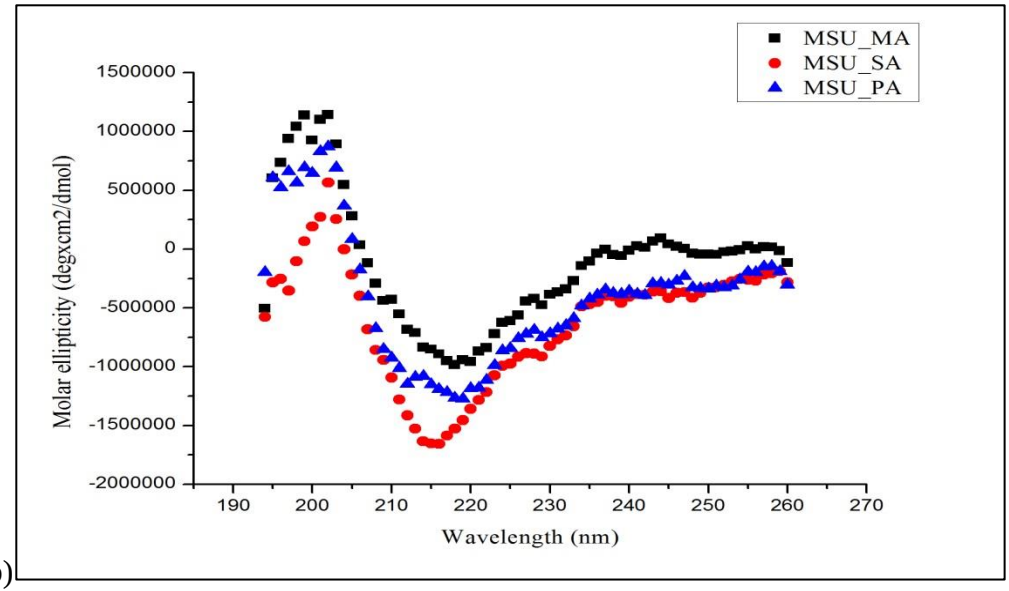

(b)

Figure 7.13: CD spectra for released γ-globulin from FA-MSU-H in (a) SIF (b) pH 7.4

The CD spectra collected for MSU-H based SCDDS indicate possible changes to the conformation of protein released from these formulations at both SIF and pH 7.4. However, it is worth noting that the amount of protein released from coated MSU-H particles (0.08 to 0.095 mg/ml) might not be sufficient to allow for an accurate CD analysis. The standard γ-globulin concentration used for CD analysis in this work usually ranged from 0.1 to 0.25 mg/ml. It is known that quality of CD spectrum can be influenced by the analyte concentration where data collected at low concentrations could provide inconclusive results due to high noise to signal ratio [285].

The results obtained for the coated formulations confirm earlier observations made in section 6B.4, where, pH-induced conformational change to the secondary structure of γ-globulin at pH 7.4 was also observed for all silica particles.

7.5 Conclusion

The aim of protein immobilization on solid surfaces and subsequent coating by SCF processing with FAs was successfully achieved. The formulated SCDDS effectively prevented the release of adsorbed protein in SGF consequently protecting the macromolecules against the possible denaturation by the acidic gastric conditions. Protein release was successfully achieved at alkaline pH with higher release obtained at pH 7.4 in comparison to SIF. Generally, larger amounts of immobilized γ-globulin were released from SCDDS formulations prepared with PA coating and S_{FP} and S_{XDP} particles whereas the least released quantities were recorded with MSU-H formulations. The stability of released γ-globulin was evaluated by performing CD spectroscopy and found to be better for experiments carried out in SIF. These results suggest that SCDDS have the potential to protect biomolecules from the harsh gastric environment and provide release in upper intestine without causing any denaturation of the protein/peptide based pharmaceutical actives.

Chapter 8

Summary and Future work

This section summarizes the key findings for this work and discusses future work related to this research.

8.1 Summary (Key findings)

I. Polymeric nanoparticles (PCL and PCL-ES100) were successfully formulated by solvent extraction from the organic phase of nano-emulsions either at atmospheric pressure or by $scCO_2$ processing. The solvent removal process was evaluated to be more efficient under $scCO_2$ conditions in the formulation of PCL nanoparticles, with complete solvent extraction occurring within 1 hour at a CO_2 flow rate of 10 g/min. The gas-like viscosity of $scCO_2$ coupled with high diffusivity facilitated faster extraction rate without particle agglomeration in comparison to solvent extraction at atmospheric pressure at the same temperature. PCL particles formulated by SFEE were monodisperse with negative surface charge and particle sizes ranging between 190 to 356 nm. PCL nano-emulsions prepared with the lowest polymer concentration (0.6% w/v) and higher surfactant amount (0.14% w/w) led to the formulation of particles with the smallest sizes. On the other hand, there was no correlation between rising polymer content and particle size for PCL-ES100 particles although the addition of ES100 to the PCL systems further resulted in a decrease in size (184 to 199 nm).

II. The physico-chemical characteristics of formulated polymeric systems and silica materials were evaluated by nitrogen sorption (BET and BJH), SEM, ATR-FTIR, and DSC. The SSA, and pore diameter and volume of these solid particles were determined by BET theory and BJH model respectively. S_{FP}, S_{XDP} and MSU-H particles were determined to be mesoporous in nature with the largest porosity obtained for S_{FP} and S_{XDP}, while S_{AL}, PCL and PCL-ES100 particles were largely non-porous. The lowest surface area and pore volume were recorded for PCL and PCL-ES100 particles and largest specific surface area was obtained for MSU-H and S_{AL} particles. DSC analysis confirmed the presence of PCL in the PCL-ES100 systems. The change of zeta-potential with pH was confirmed for native γ-globulin by titration experiments and the IEP was determined to be around pH 6.60.

III. The immobilization of γ-globulin was successfully evaluated with experiments involving S_{FP}, $S_{XDP,}$ S_{AL}, MSU-H and PCL-ES100. For the silica particles, protein adsorption followed the descending trend of S_{FP} > S_{XDP} > MSU-H > S_{AL}. The variations in adsorbed protein between these particles were related to their differences in surface porosity and pore sizes. A reduction in the immobilized γ-globulin (mg/g) was observed for S_{FP}, S_{XDP}, and S_{AL} particles when the quantity of silica was doubled to 400 mg and could be related to surface crowding at lower adsorbent amounts. Adsorption of γ-globulin was also successfully obtained on PCL-ES100 particles with minimal differences between varying ratios. In comparison to silica particles, electrostatic interactions between the adsorbent surface and the adsorbing molecules were suggested to largely influence γ-globulin immobilization on PCL-ES100.

IV. The release of immobilized protein from uncoated γ-globulin-covered S_{FP}, S_{XDP}, MSU-H and PCL-ES100 (1:3 ratio) particles was evaluated to be faster in the presence of a displacer (SDS/ Tween80/ PF127). The displacer molecules encouraged γ-globulin desorption from the adsorbent surface by an exchange mechanism. The anionic surfactant (SDS) resulted in the highest percentage for desorbed protein of 91% when compared to the non-ionic molecules (Tween80 and PF127). In comparison to SIF, desorption in pH 7.4 media led to the highest γ-globulin desorption. The stability of desorbed γ-globulin appeared to be compromised at pH 7.4 possibly due to the electrostatic state of the protein at this pH. Additionally, interactions of the desorbed protein with the displacer in the media (particularly SDS) resulted in further changes to their conformation.

V. SCDDS was successfully formulated by FA coating of protein-adsorbed S_{FP} and S_{XDP} particles (2:1 silica: FA ratio), and MSU-H (1:1 ratio) *via* melt deposition technique by $scCO_2$ processing. A pH-induced release of γ-globulin was observed with the SCDDS formulations where protein release was not obtained in SGF but achieved in both SIF and pH 7.4 media. This was attributed to the pH-dependent solubility of the FA shell. When compared to experiments carried out in SIF, the release of γ-globulin was also recorded to be highest at pH 7.4. This could be due to a number of factors including the higher solubility of FA, and the electrostatic interactions between the protein and adsorbent surface at this pH. There was no consistent correlation between the FA coating and the amounts of protein released. However, in addition to their enteric properties, coated formulations delayed γ-globulin release resulting in lower

protein release in 4 hours when compared to uncoated particles. Similar to earlier observations, when compared to the SIF media, the conformational stability of released γ-globulin was compromised at pH 7.4. Additionally, protein released from FA coated MSU-H particles also showed significant changes to their secondary structure. The collective data from this work indicate that S_{FP} and S_{XDP} particles can be used as carrier systems for large protein molecules, FAs as the shell material, and SCFT as the processing technique for the formulation of SCDDS.

8.2 Future work

Although, this research has effectively recognised the application of SCFT for the preparation of polymeric nanoparticles, there is a possible limitation with regards to detection of the presence of residual solvent in these preparations. It would be of particular interest to perform established method of analysis for residual solvent testing such as gas chromatography [286]. Gas chromatograph–based techniques including direct injection, headspace analysis, and solid-phase micro-extraction are the most common and are chemically specific for residual solvents [286].

Secondly, this work has successfully established the preparation of SCDDS with mesoporous silica particles for the delivery of γ-globulin but it can be extended to include other types of solid materials including carbon and iron oxide particles [287]. The use of polymeric nanoparticles for protein immobilization can be further investigated focusing particularly on processes that may improve their physico-chemical characteristics including their porosity. There are numerous methods to obtain porous structures but gas foaming using $scCO_2$ or use of a pore forming agent could be explored to assess if porous PCL particles could be prepared. The work carried out by Orsi, *et al* successfully produced hollow micro- and nano-polystyrene/ poly-(lactic-co-glycolic) acid (PLGA) particles by gas foaming technique in $scCO_2$ [288]. Prior to polymer processing at $scCO_2$ conditions, the polystyrene and PLGA particles were embedded in a barrier film that subsequently helped to contain the particles for ease of handling and to prevent loss of the blowing agent that encouraged the formation of pores. The gas foaming method is said to be simple and environmental friendly, and suitable for the production of a variety of pore structures [288]. A study published by Yang *et al* also proposed a simple double-emulsion method for the production of highly porous polymeric particles [289]. The introduction of an effervescent salt ammonium bicarbonate in the internal

aqueous phase helped to confer these favourable morphological properties in the formulated particles [289].

In this work, the amount of protein immobilized onto core materials (mg/g) was estimated using concentration equations as described in section 2.5.1. For further characterization, quantitative assessment techniques such as particle mass spectrometry can be employed to analyse γ-globulin adsorption onto the solid particles [290]. This method is inexpensive and simple and it quantifies protein immobilization based on mass variations of the core particles before and after adsorption. Additionally, its mass resolution is significantly adequate enough to differentiate between adsorbent materials with and without protein [290].

The use of FAs as coating materials for delivery of protein at simulated gastric and intestinal pH have been established by this work and can also be expanded to cover other enteric coating materials or systems including the use of other stimuli-responsive polymers. By using a double emulsion technique, Carpuso and Fahmy were able to encapsulate the interleukin-10 protein in an aqueous gelatine core which was subsequently coated with Eudragit® FS30D polymer [72]. The polymer coating helped to protect the encapsulated protein from the low pH at the stomach and target their delivery to the lower G.I. tract [72]. In addition to investigating other coating techniques, the drug release studies carried out in SIF can be prolonged to cover a period of 24 hours to further understand the release profile of the FA coated silica particles formulated in this work.

In this research, the conformation of release γ-globulin has been established by CD analysis. Additional techniques like fluorescence spectroscopy could also be employed to study the protein structure. Furthermore, it will be important to carry out protein assays to determine if the released γ-globulin still retains its biological functionality. For example, ELISA (enzyme-linked immunosorbent assay) is a plate-based assay procedure that is designed for quantifying and detecting antibodies such as immunoglobulins in biological samples [291].

Finally, this work doesn't address the important aspect of poor absorption of proteins when delivered *via* oral route due to their high hydrophilic properties. Fatty acids are known to act as penetration enhancer, hence, the coating in this work to prepare SCDDS can potentially serve dual purpose [292]. This could be investigated to establish cellular absorption or permeability of biologics released from SCDDS using standard cell lines such as Caco-2, HT-29, HT-29/MTX and T84 [293].

References

[1] Škalko-Basnet, N., Biologics: the role of delivery systems in improved therapy. *Biologics: Targets and Therapy*, 2014. **8**: p. 107–114.

[2] Renukuntla, J., Vadlapudi, A. D., Patel, A., Boddu, S., Mitra, A. K., Approaches for Enhancing Oral Bioavailability of Peptides and Proteins. *International Journal of Pharmaceutics*, 2013. **447**(0): p. 75-93.

[3] Cram, D. J. and Hammond, G. S., Organic Chemistry. 1959, New York: McGraw-Hill Book Company, Inc. p. 526-549.

[4] Carey, F. A., Organic Chemistry. 1987, New York: McGraw-Hill Book Company, Inc. p. 1085-1138.

[5] Nature Education, Protein Function. [cited 2019 2nd February]; Available at: http://www.nature.com/scitable/topicpage/protein-function-14123348.

[6] Genetics Home Reference, What are proteins and what do they do? [cited 2019 2nd February]; Available at: http://ghr.nlm.nih.gov/handbook/howgeneswork/protein.

[7] Jorgensen, L., Hostrup, S., Moeller, E. H., Grohganz, H., Recent trends in stabilising peptides and proteins in pharmaceutical formulation – considerations in the choice of excipients. *Expert Opinion Drug Delivery*, 2009. **6**(11).

[8] Bruice, P. Y., Organic Chemistry. 2nd ed. 1987, New Jersey: Prentice Hall. p. 907-952.

[9] Hua, L., Zhou, R., Thirumalai, D., Berne, B. J., Urea denaturation by stronger dispersion interactions with proteins than water implies a 2-stage unfolding. *Proceedings of the National Academy of Sciences*, 2008. **105**(44): p. 16928- 16933.

[10] D'Hondt, M., Bracke, N., Taevernier, L., Gevaert, B., Verbeke, F., Wynendaele, E., De Spiegeleer, B., Related Impurities in Peptide Medicines. *Journal of Pharmaceutical and Biomedical Analysis*, 2014. **101**: p. 2- 30.

[11] Wang, L., Liu, Y., Zhang, W., Chen, X., Yang, T., Ma, G., Microspheres and Microcapsules for Protein Delivery: Strategies of Drug Activity Retention. *Current Pharmaceutical Design*, 2013. **19** (35): p. 6340-6352.

[12] Dulal, P., Protein or Peptide drugs: Applications, Problems and Solutions. *Biotechnology Society of Nepal (BSN) E-bulletin*, 2010. **2**.

[13] Leader, B., Baca, Q. J., Golan, D. E., Protein therapeutics: a summary and pharmacological classification. *Nature review: Drug discovery*, 2008. **21** (7): p. 21-39.

[14] Carter, P. J., Introduction to current and future protein therapeutics: A protein engineering perspective. *Experimental Cell Research*, 2011. **317**: p. 1261-1269.

[15] Rosado, J. L., Solomons, N. W., Lisker, R., Bourges, H., Enzyme replacement therapy for primary adult lactase deficiency. Effective reduction of lactose malabsorption and milk intolerance by direct addition of β-galactosidase to milk at mealtime. *Gastroenterology*, 1984. **87**: p. 1072–1082.

[16] Abildgaard, C. F., Simone, J. V., Corrigan, J. J., Seeler, R. A., Edelstein, G., Vanderheiden, J., Schulman, I., Treatment of hemophilia with glycine-precipitated factor VIII. *New England Journal of Medicine*, 1966. **275**: p. 471–475.

[17] Roth, D. A., Kessler, C. M., Pasi, K. J., Rup, B., Courter, S. G., Tubridy, K. L., Human recombinant factor IX: safety and efficacy studies in hemophilia B patients previously treated with plasma-derived factor IX concentrates. *Blood*, 2001. **98**: p. 3600-3606.

[18] Corwin, H. L., Gettinger, A., Pearl, R. G., Fink, M. P., Levy, M. M., Shapiro, M. J., Corwin, M. J., Colton, T., Efficacy of recombinant human erythropoietin in critically ill patients: a randomized controlled trial. *Journal of the American Medical Association*, 2002. **288**: p. 2827–2835.

[19] Keizer, M. P., Aarts, C., Kamp, A. M., Caron, H. N., van de Wetering, M. D., Wouters, D., Kuijpers, T. W., Asparaginase inhibits the lectin pathway of complement activation. *Molecular Immunology*, 2018. 93: p. 189-192.

[20] Mease, P. J., Goffe, B. S., Metz, J., VanderStoep, A., Finck, B., Burge, D. J., Etanercept in the treatment of psoriatic arthritis and psoriasis: a randomised trial. *Lancet*, 2000. **356**: p. 385–390.

[21] Kaminski, M. S., Estes, J., Zasadny, K. R., Francis, I. R., Ross, C. W., Tuck, M., Regan, D., Fisher, S., Gutierrez, J., Kroll, S., Stagg, R., Tidmarsh, G., Wahl, R. L., Radioimmunotherapy with iodine ^{131}I tositumomab for relapsed or refractory B‑cell non-

Hodgkin lymphoma: updated results and long-term follow-up of the University of Michigan experience. *Blood*, 2000. **96**: p. 1259–1266.

[22] Campos-Neto, A., Rodrigues-Júnior, V., Pedral-Sampaio, D. B., Netto, E. M., Ovendale, P. J., Coler, R. N., Skeiky, Y. A. W., Badaró, R., Reed, S. G., Evaluation of DPPD, a single recombinant Mycobacterium tuberculosis protein as an alternative antigen for the Mantoux test. *Tuberculosis*, 2001. **81** (5/6): p. 353–358.

[23] Anassi, E., Ndefo, U. A., Sipuleucel-T (Provenge) Injection: The First Immunotherapy Agent (Vaccine) For Hormone-Refractory Prostate Cancer. *Pharmacy and Therapeutics*, 2011. **36** (4): p. 197-202.

[24] MacKenzie, I. Z., Bichler, J., Mason, G.C., Lunan, C. B., Stewart, P., Al-Azzawi F., De Bono, M., Watson, N., Andresen, I., Efficacy and safety of a new, chromatographically purified rhesus (D) immunoglobulin. *European Journal of Obstetrics and Gynecology and Reproductive Biology*, 2004. **117**: p. 154–161.

[25] Shi, L., Sings, H. L., Bryan, J. T., Wang, B., Wang, Y., Mach, H., Kosinski, M., Washabaugh, M. W., Sitrin, R., Barr, E., Gardasil: prophylactic human papillomavirus vaccine development -from bench top to bed-side. *Clinical Pharmacology and Therapeutics*, 2007. **81**: p. 259–264.

[26] Bruno, B. J., Miller, G. D., Lim, C. S., Basics and recent advances in peptide and protein drug delivery. *Therapeutic Delivery*, 2013. **4** (11): p. 1443-1467.

[27] Díaz, A., David, A., Pérez, R., González, M. L., Báez, A., Wark, S. E., Zhang, P., Clearfield, A., Colón, J. L. Nanoencapsulation of Insulin into Zirconium Phosphate for Oral Delivery Applications. *Biomacromolecules*, 2010. **11** (9): p. 2465-2470.

[28] Hamman, J. H., Enslin, G. M., Kotzé, A. F., Oral Delivery of Peptide Drugs: Barriers and Developments. *Biodrugs*, 2005. **19** (3): p. 165-177.

[29] Fonte, P., Araújo, F., Reis, S., Sarmento, B., Oral Insulin Delivery: How Far Are We? *Journal of Diabetes Science and Technology*, 2013. **7** (2): p. 520-531.

[30] Rafati, A., Boussahel, A., Shakesheff, K. M., Shard, A. G., Roberts, C. J., Chen, X., Scurr, D. J., Rigby-Singleton, S., Whiteside, P., Alexander, M. R., Davies, M. C., Chemical

and spatial analysis of protein loaded PLGA microspheres for drug delivery applications. *Journal of Controlled Release*, 2012. **162**: p. 321-329.

[31] Kumarn, G. P., Rajeshwarrao, P. Nonionic surfactant vesicular systems for effective drug delivery-an overview. *Acta Pharmaceutica Sinica*, 2011. **1** (4): p. 208-219.

[32] Mahato, R. I., Narang, A. S., Thoma, L., Miller, D. D., Emerging Trends in Oral Delivery of Peptide and Protein Drugs. *Critical Reviews in Therapeutic Drug Carrier Systems*, 2013. **20** (2&3): p. 153–214.

[33] Lodish, H., Berk, A., Zipursky, S. L., Molecular Cell Biology, Chapter 15, Transport across Cell Membranes. 4th ed. 2000, New York: W. H. Freeman. [cited 2019 20th February]; Available at: https://www.ncbi.nlm.nih.gov/books/NBK21525/.

[34] Pauletti, G.M., Gangwar, S., Knipp, G. T., Nerurkar, M. M., Okumu, F. W., Tamura, K., Siahaan, T. J., Borchardt, R. T., Structural requirements for intestinal absorption of peptide drugs. *Journal of Controlled Release*, 1996. **41**: p. 3-17.

[35] Zhou, X. H., Overcoming enzymatic and absorption barriers to non-parenterally administered protein and peptide drugs. *Journal of Controlled Release*, 1994. **29**: p. 239-52.

[36] Hochman, J., Artursson, P., Mechanisms of absorption enhancement and tight junction regulation. *Journal of Controlled Release*, 1994. **29**: p. 253-67.

[37] Levendoski, E. E., Leydon, C., Thibeault, S. L., Vocal Fold Epithelial Barrier in Health and Injury: A Research Review. *Journal of Speech, Language, and Hearing Research*, 2014. **57**: p. 1679–1691.

[38] Sharom, F. J., DiDiodato, G., Yu, X., Ashbourne, K. J. D., Interaction of the P-glycoprotein Multidrug Transporter with Peptides and Ionophores. *The Journal of Biological Chemistry*, 1995. **270** (17): p. 10334-10341.

[39] Sultatos, L., First-Pass Effect. *Elsevier Inc*., 2007. p. 1- 2.

[40] Shakweh, M., Ponchel, G., Fattal, E., Particle Uptake by Peyer's Patches: A pathway for Drug and Vaccine delivery. *Expert Opinion in Drug Delivery*, 2004. **1** (1): p. 141- 163.

[41] Ziv, E., Lior, O., Kidron, M., Absorption of Protein via the Intestinal Wall: A Quantitative Model. *Biochemical Pharmacology*, 1987. **36** (7): p. 1035-1039.

[42] Park, K., Kwon, I. C., Park, K., Oral protein delivery: current status and future prospects. *Reactive and Functional Polymers*, 2011. **71**(3): p. 280–287.

[43] Bernkop-Schnürch, A., The use of inhibitory agents to overcome the enzymatic barrier to perorally administered therapeutic peptides and proteins. *Journal of Controlled Release*, 1998. **52**: p. 1-16.

[44] Piper, D. W., Fenton, B. H., pH stability and activity curves of pepsin with special reference to their clinical importance. *Gut*, 1965. **6** (5): p. 506-508.

[45] Knarreborg, A., Jensen, S. K., Engberg, R. M., Pancreatic lipase activity as influenced by unconjugated bile acids and pH, measured in vitro and in vivo. *Journal of Nutritional Biochemistry*, 2003. **14** (5): p. 259–265.

[46] Hyun, H. H., Zeikus, J. G., General Biochemical Characterization of Thermostable Extracellular β-Amylase from Clostridium thermosulfurogenes. *Applied and Environmental Microbiology*, 1985. **49** (5): p. 1162-1167.

[47] Thanou, M., Verhoef, J. C., Junginger, H. E., Chitosan and its derivatives as intestinal absorption enhancers. *Advanced Drug Delivery Reveiws*, 2001. **50**: p. S91-S101.

[48] Schipper, N. G. M., Vårum, K. M., Stenberg P., Ocklind, G., Lennernäsa, H., Artursson, P., Chitosans as absorption enhancers of poorly absorbable drugs 3: Influence of mucus on absorption enhancement. *European Journal of Pharmaceutical Sciences*, 1999. **8** (4): p. 335-343.

[49] Schipper, N. G. M., Vårum, K. M., Artursson P., Chitosans as absorption enhancers for poorly absorbable drugs. 1: Influence of molecular weight and degree of acetylation on drug transport across human intestinal epithelial (Caco-2) cells. *Pharmaceutical Research*, 1996. **13** (11): p. 1686-692.

[50] Roberts, M. J., Bentley, M. D., Harris, J. M., Chemistry for peptide and protein PEGylation. *Advanced Drug Delivery Reveiws*, 2002. **54**: p. 459-476.

[51] Cefalu, W. T., Concept, strategies, and feasibility of noninvasive insulin delivery. *Diabetes Care*, 2004. **27**: p. 239-246.

[52] Borchardt, R. T., Optimising oral absorption of peptides using prodrug strategies. *Journal of Controlled Release*, 1999. **62**: p. 231-238.

[53] Russell-Jones, G. J., The potential use of receptor-mediated endocytosis for oral drug delivery. *Advanced Drug Delivery Reviews*, 1996. **20**: p. 83-97.

[54] Safari, J., Zarnegar, Z., Advanced drug delivery systems: Nanotechnology of health design A review. *Journal of Saudi Chemical Society*, 2014. **18**: p. 85-99.

[55] Peppas, N. A., Bures, P., Leobandung, W., Ichikawa, H., Hydrogels in pharmaceutical formulations. *European Journal of Pharmaceutics and Biopharmaceutics*, 2000. **50**: p. 27-46.

[56] Wood, K. M., Stone, G. M., Peppas, N. A., Wheat Germ Agglutinin Functionalized Complexation Hydrogels for Oral Insulin Delivery. *Biomacromolecules*, 2008. **9**(4): p.1293-1298.

[57] Peppas, N. A., Physiologically responsive hydrogels. *Journal of Bioactive and Compatible Polymers*, 1991. **6**: p. 241-246.

[58] Vakkalanka, S. K., Brazel, C. S., Peppas, N. A., Temperature- and pH-sensitive terpolymers for modulated delivery of streptokinase. *Journal of Biomaterials Science*, 1996. **8** (2): p. 119-129.

[59] Hoare, T. R., Kohane, D. S., Hydrogels in drug delivery: Progress and challenges. *Polymer*, 2008. **49**: p. 1993-2007.

[60] Patel, A. R., Vavia, P. R., Preparation and In Vivo Evaluation of SMEDDS (Self-Microemulsifying Drug Delivery System) Containing Fenofibrate. *American Association of Pharmaceutical Scientists Journal*, 2007. **9** (3): p. 41.

[61] Patel, R. B., Patel, M. R., Bhatt, K. K., Patel, B. G., Formulation consideration and characterization of microemulsion drug delivery system for transnasal administration of carbamazepine. *Bulletin of Faculty of Pharmacy, Cairo University*, 2013. **51**: p. 243-253.

[62] Li, X., Qi, J., Xie, Y., Zhang, X., Hu, S., Xu, Y., Lu, Y., Wu, W., Nanoemulsions coated with alginate/chitosan as oral insulin delivery systems: preparation, characterization, and hypoglycaemic effect in rats. *International Journal of Nanomedicine*, 2013. **8**: p. 23-32.

[63] Ye, T., Yuan, K., Zhang, W., Song, S., Chen, F., Yang, X., Wang, S., Bi, J., Pan, W., Prodrugs incorporated into nanotechnology-based drug delivery systems for possible improvement in bioavailability of ocular drugs delivery. *Asian Journal of Pharmaceutical Sciences*, 2013. **8**: p. 207-217.

[64] Kalepun, S., Manthina, M., Padavala, V., Oral lipid-based drug delivery systems – an overview. *Acta Pharmaceutica Sinica*, 2013. **3** (6): p. 361-372.

[65] Andros Pharmaceuticals Co., Ltd., Liposome [cited 2019 21st February]; Available at: http://www.androspharma.com/en/technology_en.htm.

[66] Martins, S., Sarmento, B., Ferreira, D. C., Souto, E. B., Lipid-based colloidal carriers for peptide and protein delivery – liposomes versus lipid nanoparticles. *International Journal of Nanomedicine*, 2007. **2** (4): p. 595-607.

[67]. Liu, X., Huang, G., Formation strategies, mechanism of intracellular delivery and potential clinical applications of pH-sensitive liposomes. *Asian Journal of Pharmaceutical Sciences*, 2013. **8**: p. 319-328.

[68] Gradauer, K., Barthelmes, J., Vonach, C., Almer, G., Mangge, H., Teubl, B., Roblegg, E., Dünnhaupt, S., Fröhlich, E., Bernkop-Schnürch, A., Prassl, R., Liposomes coated with thiolated chitosan enhance oral peptide delivery to rats. *Journal of Controlled Release*, 2013. **172** (3): p. 872-878.

[69] Shaji, J., Patole, V., Protein and Peptide Drug Delivery: Oral Approaches. *Indian Journal of Pharmaceutical Science*, 2008. **70** (3): p. 269-277.

[70] James, H. P., John, R., Alex, A., Anoop, K. R., Smart polymers for the controlled delivery of drugs – a concise overview. *Acta Pharmaceutica Sinica*, 2014. **4** (2): p. 120-127.

[71] Fogueri, L. R., Singh, S., Smart Polymers for Controlled Delivery of Proteins and Peptides: A Review of Patents. *Recent Patents on Drug Delivery & Formulation*, 2009. **3**: p. 40-48.

[72] Capurso, N. A., Fahmy, T. M., Development of a pH-Responsive Particulate Drug Delivery Vehicle for Localized Biologic Therapy in Inflammatory Bowel Disease. *Yale Journal of Biology and Medicine*, 2011. **84**: p. 285-288.

[73] Trivedi, V., Bhomia, R., Mitchell, J., The Preparation of Solid Core Drug Delivery Systems (SCDDS) for the Biomolecular Delivery. *14th European Meeting on Supercritical Fluids (EMSF), 18-21 May 2014, Marseille, France*. [cited 2019 21st February]; Available at: http://www.isasf.net/fileadmin/files/Docs/Marseille/HtmlDir/Papers/OLSH20.pdf.

[74] Yang, W., Pierstorff, E., Reservoir-Based Polymer Drug Delivery Systems. *Journal of Laboratory Automation*, 2012. **17** (1): p. 50-58.

[75] Lee, C., Lang, J., Yen, C., Shih, P., Lin, T., Mou, C., Enhancing Stability and Oxidation Activity of Cytochrome c by Immobilization in the Nanochannels of Mesoporous Aluminosilicates. *Journal of Physical Chemistry B*, 2005. **105**: p. 12277- 12286.

[76] Díaz, J. F., Balkus Jr, K. J., Enzyme immobilization in MCM-41 molecular sieve. *Journal of Molecular Catalysis B: Enzymatic*, 1996. **2**: p. 115- 126.

[77] Takahashi, H., Li, B., Sasaki, T., Miyazaki, C., Kajino, T., Inagaki, S., Immobilized enzymes in ordered mesoporous silica materials and improvement of their stability and catalytic activity in organic solvent. *Microporous and Mesoporous materials*, 2001. **44-45**: p. 755- 762.

[78] Vinu, A., Murugesan, V., Hartmann, M., Adsorption of Lysozyme over Mesoporous Molecular Sieves MCM-41 and SBA-15: Influence of pH and Aluminum Incorporation. *Journal of Physical Chemistry B*, 2004. **108**: p. 7323- 7330.

[79] Urabe, Y., Shiomi, T., Itoh, T., Kawai, A., Tsunoda, T., Mizukami, F., Sakaguchi, K., Encapsulation of Hemoglobin in Mesoporous Silica (FSM)—Enhanced Thermal Stability and Resistance to Denaturants. *ChemBioChem*, 2007. **8**: p. 668- 674.

[80] Washmon-Kriel, L., Jimenez, V. L., Balkus Jr, K. J., Cytochrome c immobilization into mesoporous molecular sieves. *Journal of Molecular Catalysis B: Enzymatic*, 2000. **10**: p. 453-469.

[81] Paul, W., Sharma, C. P., Inorganic nanoparticles for targeted drug delivery. *Woodhead Publishing limited*, 2010. p. 204- 235.

[82] AzoNano, Silicon Dioxide, Silica (SiO_2) Nanoparticles – Properties, Applications [cited 2016 2nd April]; Available at: https://www.azonano.com/article.aspx?ArticleID=3398.

[83] Liberman, A., Mendez, N., Trogler, W. C., Kummel, A. C., Synthesis and surface functionalization of silica nanoparticles for nanomedicine. *Surface Science Reports*, 2014. **69**: p. 132- 158.

[84] Kwon, S., Singh, R. K., Perez, R. A., Neel, E., Kim, H., Chrzanowski, W., Silica-based mesoporous nanoparticles for controlled drug delivery. *Journal of Tissue Engineering*, 2013. **4**: p. 1- 18.

[85] Radin, S., Chen, T., Ducheyne, P., The controlled release of drugs from emulsified, sol gel processed silica microspheres. *Biomaterials*, 2009. **30**: p. 850- 858.

[86] Klichko, Y., Liong, M., Choi, E., Angelos, S., Nel, A. E., Stoddart, J. F., Tamanoi, F., Zink, J. I., Mesostructured Silica for Optical Functionality, Nanomachines, and Drug Delivery. *Journal of American Ceramic Society*, 2009. **92** (S1): p. S2-S10.

[87] Meseguer-Olmo, L., Ros-Nicolàs, M. J., Vicente-Ortega, V., Alcaraz-Baños, M., Clavel-Sainz, M., Arcos, D., Ragel, C. V., Vallet-Regı´, M., Meseguer-Ortiz, C. I., A Bioactive Sol-Gel Glass Implant for In Vivo Gentamicin Release. Experimental Model in Rabbit. *Journal of Orthopaedic Research*, 2006. **24** (3): p. 454-460.

[88] Radin, S., El-Bassyouni, G., Vresilovic, E. J., Schepers, E., Ducheyne, P., In vivo tissue response to resorbable silica xerogels as controlled-release materials. *Biomaterials*, 2005. **26**: p. 1043-1052.

[89] Kortesuo, P., Ahola, M., Karlsson, S., Kangasniemi, I., Yli-Urpo, A., Kiesvaara, J., Silica xerogel as an implantable carrier for controlled drug delivery-evaluation of drug distribution and tissue effects after implantation. *Biomaterials*, 2000. **21**: p. 193-198.

[90] Peri, J. B., Hensley Jr., A. L., The surface structure of silica gel. *Journal of Physical Chemistry, 1968*. **72** (8): p. 2926- 2933.

[91] Owens, G. J., Singh, R. K., Foroutan, F., Alqaysi, M., Han, C., Mahapatra, C., Kim, H., Knowles, J. C., Sol–gel based materials for biomedical applications. *Progress in Materials Science*, 2016. **77**: p. 1- 79.

[92] Fu, C., Liu, T., Li, L., Liu, H., Chen, D., Tang, F., The absorption, distribution, excretion and toxicity of mesoporous silica nanoparticles in mice following different exposure routes. *Biomaterials*, 2013. **34**: p. 2565- 2575.

[93] Mahler, H. R., Cordes, E. H., Biological Chemistry. Harper International ed. 1966, New York: Harper & Row. p. 508- 524.

[94] Gurr, M. I., James, A. T., Lipid Biochemistry- An Introduction. 2nd ed. 1975, New York: John Wiley & Sons Inc. p. 18- 84.

[95] Mann, J., Truswell, A. S., Essentials of human nutrition. 4th ed. 2012, New York: Oxford University Press Inc. p. 49- 69.

[96] *Compound summary*, PubChem USA. [cited 2019 21st February]; Available at: https://pubchem.ncbi.nlm.nih.gov/.

[97] Cerchiara, T., Luppi, B., Bigucci, F., Petrachi, M., Orienti, I., Zecchi, V., Controlled release of vancomycin from freeze-dried chitosan salts coated with different fatty acids by spray-drying. *Journal of Microencapsulation*, 2003. **20** (4): p. 473- 478.

[98] Luppi, B., Bigucci, F., Cerchiara, T., Mandrioli, R., Pietra, A. M., Zecchi V., New environmental sensitive system for colon-specific delivery of peptidic drugs. *International Journal of Pharmaceutics*, 2008. **358**: p. 44- 49.

[99] Gill, P., Nanocarriers, nanovaccines, and nanobacteria as nanobiotechnological concerns in modern vaccines. *Scientia Iranica F*, 2013. **20** (3): p. 1003- 1013.

[100] Card, J. W., Magnuson, B. A., A review of the efficacy and safety of nanoparticle-based oral insulin delivery systems. *American Journal of Physiology- Gastrointestinal Liver Physiology*, 2011. **301**: p. G956- G967.

[101] Chuang, E., Lin, K., Su, F., Mi, F., Maiti, B., Chen, C., Wey, S., Yen, T., Juang, J., Sung, H., Noninvasive imaging oral absorption of insulin delivered by nanoparticles and its

stimulated glucose utilization in controlling postprandial hyperglycaemia during OGTT in diabetic rats. *Journal of Controlled Release*, 2013. **172**: p. 513- 522.

[102] Campardelli, R., Reverchon, E., Della-Porta, G., Biopolymer particles for proteins and peptides sustained release produced by supercritical emulsion extraction. *Procedia Engineering*, 2012. **42**: p. 239- 246.

[103] Yildirimer, L., Thanh, N., Loizidou, M., Seifalian, M. A., Toxicological considerations of clinically applicable nanoparticles. *Nano Today*, 2011. **6**: p. 585- 607.

[104] Azimi, B., Nourpanah, P., Rabiee, M., Arbab, S., Poly (ε-caprolactone) Fiber: An Overview. *Journal of Engineered Fibres and Fabrics*, 2014. **9** (3): p. 74- 90.

[105] Mahapatro, A., Singh, D. K., Biodegradable nanoparticles are excellent vehicle for site directed in-vivo delivery of drugs and vaccines. *Journal of Nanobiotechnology*, 2011. **9** (55): p. 1- 11.

[106] Seremeta, K. P., Chiappetta, D. A., Sosnik, A., Poly (ε-caprolactone), Eudragit® RS 100 and poly(ε-caprolactone)/Eudragit® RS100 blend submicron particles for the sustained release of the antiretroviral efavirenz. *Colloids and Surfaces B: Biointerfaces*, 2013. **102**: p. 441.

[107] Woodruff, M. A., Hutmacher, D.W., The return of a forgotten polymer-Polycaprolactone in the 21st century. *Progress in Polymer Science*, 2010. **35**: p. 1217.

[108] Karuppuswamy, P., Venugopal, J. R., Navaneethan, B., Laiva, A. L., Ramakrishna, S., Polycaprolactone nanofibers for the controlled release of tetracycline hydrochloride. *Material letters*, 2015. **141**: p. 180.

[109] Bilensoy, E., Sarisozen, C., Esendagli, G., Dogan, A. L., Aktas, Y., Sen, M., Mungan, N. A., Intravesical cationic nanoparticles of chitosan and polycaprolactone for the delivery of Mitomycin C to bladder tumors. *International Journal of Pharmaceutics*, 2009. **371**: p. 170.

[110] Payyappilly, S. S., Panja, S., Mandal, P., Dhara, S., Chattopadhyay, S., Organic solvent-free low temperature method of preparation for self-assembled amphiphilic poly(ε-caprolactone)–poly(ethylene glycol)block copolymer based nanocarriers for protein delivery. *Colloids and Surfaces B: Biointerfaces*, 2015. **135**: p. 510.

[111] Sinha, V. R., Bansal, K., Kaushik, R., Kumria, R., Trehan, A., Poly- ε -caprolactone microspheres and nanospheres: an overview. *International Journal of Pharmaceutics*, 2004. **278**: p. 1.

[112] Jameela, S. R., Suma, N., Misra, A., Raghuvanshi, R., Ganga, S., Jayakrishnan, A., Poly (ε-caprolactone) microspheres as a vaccine carrier. *Current Science*, 1996. **70**: p. 669.

[113] Youan, B., Benoit, M. A., Rollmann, B., Riveau, G., Gillard, J., Protein- loaded poly (ε-caprolactone) microparticles. II. Muramyl dipeptide for oral controlled release of adjuvant. *Journal of Microencapsulation*, 1999b. **16**: p. 601.

[114] Kadian, S. S., Harikumar, S. L., Eudragit and its Pharmaceutical Significance. *Pharmainfo.net*, 2009.

[115] Seremeta, K. P., Chiappetta, D. A., Sosnik, A., Poly(ε-caprolactone), Eudragit® RS 100 and poly(ε-caprolactone)/Eudragit® RS 100 blend submicron particles for the sustained release of the antiretroviral efavirenz. *Colliods and Surfaces B: Biointerfaces*, 2013. **102**: p. 441- 449.

[116] Evonik brochure: *Eudragit*®. [cited 2019 21st February]; Available at: https://healthcare.evonik.com/product/health-care/en/products/pharmaceutical-excipients/EUDRAGIT/.

[117] Gibaud, S., Al Awwadi, N. J., Ducki, C., Astier, A., Poly(ε-caprolactone) and Eudragit® microparticles containing fludrocortisone acetate. *International Journal of Pharmaceuics*, 2004. **269**: p. 491- 508.

[118] Obeidat, W. M., Price, J. C., Preparation and evaluation of Eudragit S 100 microspheres as pH-sensitive release preparations for piroxicam and theophylline using the emulsion-solvent evaporation method. *Journal of Microencapsulation*, 2006. **23** (2): p. 195- 202.

[119] Colomé, L. M., Raffin, R. P., Hoffmeister, C. R., Conrado, D. J., Pohlmann, A. R., Guterres, S. S., Eudragit S100 microparticles containing sodium pantoprazole: drug release, intestinal absorption and *in vitro/ex vivo* correlation. *Journal of Drug Delivery Science and Technology*, 2008. **18** (5): p. 323- 326.

[120] Bhamidipati, M., Scurto, A. M., Detamore, M. S., The Future of Carbon Dioxide for Polymer Processing in Tissue Engineering. *Tissue Engineering: Part B,* 2013. **19** (3): 221-232.

[121] Kemmere, M. Supercritical Carbon Dioxide for Sustainable Polymer Processes. *Supercritical Carbon Dioxide in Polymer Reaction Engineering*, 2005. Wiley-VCH Verlag GmbH & Co. KGaA: Weinheim.

[122] Goodship, V., Ogur, E., Polymer Processing with Supercritical Fluids. *Rapra series reviews,* 2005. **15**.

[123] Ginty, P. J., Whitaker, M. J., Shakesheff, K. M., Howdle, S. M., Drug delivery goes supercritical. *Materials Today*, 2005. **8** (8, Supplement 1): p. 42- 48.

[124] Sekhon, B. S., Supercritical Fluid Technology: An Overview of Pharmaceutical Applications. *International Journal of PharmTech Research,* 2010. **2**(1): p. 810- 826.

[125] Huang, Z., Sun, G., Chiew, Y. C., Kawi, S., Formation of ultrafine aspirin particles through rapid expansion of supercritical solutions (RESS). *Powder Technology*, 2005. **160**: 127- 134.

[126] Fages, J., Lochard, H., Letourneau, J., Sauceau, M., Rodier, E., Particle generation for pharmaceutical applications using supercritical fluid technology. *Powder Technology*, 2004. **141**: 219- 226.

[127] Knez, Z., Weidner, E., Particles formation and particle design using supercritical fluids. *Current Opinion in Solid State and Materials Science*, 2003. **7**: p. 353- 361.

[128] Kalani, M., Yunus, R., Effect of supercritical fluid density on nanoencapsulated drug particle size using the supercritical antisolvent method. *International Journal of Nanomedicine,* 2012. **7**: 2165- 2172.

[129] Kalani, M., Yunus, R., Application of supercritical antisolvent method in drug encapsulation: a review. *International Journal of Nanomedicine*, 2011. **6**: 1429- 1442.

[130] Vernau, W., Vernau, K. A., Bailey, C. S., Cerebrospinal fluid. 6th Ed. *Clinical Biochemistry of Domestic Animals*, 2008. Elsevier Inc. p. 769- 819.

[131] Encyclopedia.com, "Globulins". World of Microbiology and Immunology [cited 2019 21st February]; Available at: https://www.encyclopedia.com/science-and-technology/biochemistry/biochemistry/globulins.

[132] Spiegelberg, H. L., Biological Role of Different Antibody Classes. *International Archives of Allergy and Immunology*, 1989. **90**: p. 22-27.

[133] Schroeder H.W., Cavacini L. (2010) Structure and function of immunoglobulins. Journal of Allergy and Clinical Immunology, S41-S52.

[134] Wikimedia Commons, Immunoglobulin basic unit [cited 2019 21st February]; Available at: https://commons.wikimedia.org/wiki/File:Immunoglobulin_basic_unit.svg.

[135] Norde, W., Lyklema, J., Interfacial behaviour of proteins, with special reference to immunoglobulins. A physicochemical study. *Advances in Colloid and Interface Science*, 2012. **179-182**: p. 5-13.

[136] ThermoFisher Scientific, Immunoglobulin Structure and Classes. [cited 2019 21st February]; Available at: https://www.thermofisher.com/uk/en/home/life-science/antibodies/antibodies-learning-center/antibodies-resource-library/antibody-methods/immunoglobulin-structure-classes.html#.

[137] Kaneko, Y., Nimmerjahn, F., Ravetch, J. V., Anti-Inflammatory Activity of Immunoglobulin G Resulting from Fc Sialylation. *Science*, 2006. **313**: p. 670- 673.

[138] Immune Deficiency Foundation, Immunoglobulin Therapy & Other Medical Therapies for Antibody Deficiencies [cited 2019 21st February]; Available at: http://primaryimmune.org/treatment-information/immunoglobulin-therapy/.

[139] Jolles, S., Sewell, W. A. C., Misbah, S. A., Clinical uses of intravenous immunoglobulin. *Clinical and Experimental Immunology*, 2005. **142**: p. 1- 11.

[140] Perez, E. E., Orange, J. S., Bonilla, F., Chinen, J., Chinn, I. K., Dorsey, M., El-Gamal, Y., Harville T. O., Hossny, E., Mazer, B., Nelson, R., Secord, E., Jordan, S. C., Stiehm, E. R., Vo, A. A., Ballow, M., Update on the use of immunoglobulin in human disease: A review of evidence. *Journal of Allergy and Clinical Immunology*, 2016. **139** (3S): p. S1-S46.

[141] Prieto, C., Calvo, L., Supercritical Fluid Extraction of Emulsions for the Production of Vitamin E Nanocapsulates. XXI International Conference on Bioencapsulation, 2013. **14**.

[142] Brunauer, S., Emmett, P. H., Teller, E., Adsorption of Gases in Multimolecular Layers. *Journal of the American Chemical Society*, 1938. **60** (2): p. 309-319.

[143] Particle Analytical, BET, [cited 2019 21st February]; Available at: http://particle.dk/methods-analytical-laboratory/surface-area-bet-2/.

[144] Huang, X., Young, N. P., Townley, H. E., Characterization and Comparison of Mesoporous Silica Particles for Optimized Drug Delivery. *Nanomaterials and Nanotechnology*, 2014. **4** (2): p. 1-15.

[145] Pharmaceutical guidelines, Preparation of Buffer Solutions. [cited 2019 21st February]; Available at: https://www.pharmaguideline.com/2010/09/preparation-of-buffer-solutions.html.

[146] Kakade, A., Dissolution Analyses: Comparison of Profiles Using f2 Analysis Calculation. [cited 2019 21st February]; Available at: http://blog.eglifesciences.com/dissolution-analyses-comparison-of-profiles-using-f2-analysis-calculation.

[147] Solans, C., Morales, D., Homs, M., Spontaneous emulsification. *Current Opinion in Colloid and Interface Science*, 2016. **22**: p. 88- 93.

[148] Bouchemal, K., Briançon, S., Perrier, E., Fessi, H., Nano-emulsion formulation using spontaneous emulsification: solvent, oil and surfactant optimisation. *International Journal of Pharmaceutics*, 2004. **280**: p. 241.

[149] Lopez-Montilla, J. C., Herrera-Morales, P. E., Pandey, S., Shah, D. O., Spontaneous Emulsification: Mechanisms, Physicochemical Aspects, Modeling, and Applications. *Journal of Dispersion Science and Technology*, 2002. **23**(1-3): p. 219.

[150] Shahidzadeh, N., Bonn, D., Aguerre-Chariol, O., Meunier, J., Spontaneous emulsification: relation to microemulsion phase behaviour. *Colloids and Surfaces A: Physicochemical and Engineering Aspects*, 1999. **147**: p. 375.

[151] Falk, R. F., Randolph, T. W., Process Variable Implications for Residual Solvent Removal and Polymer Morphology in the Formation of Gentamycin-Loaded Poly(L-lactide) Microparticles. *Pharmaceutical Research*, 1998. **15**: p. 1233.

[152] Rao, J. P., Geckeler, K. E., Polymer nanoparticles: Preparation techniques and size-control parameters. *Progress in Polymer Science*, 2011. **36**: p. 887.

[153] Sapkale, G. N., Patil, S. M., Surwase, U. S., Bhatbhage, P. K., Supercritical fluid extraction- A review. *International Journal of Chemical Sciences*, 2010. **8** (2): p. 729- 743.

[154] Khaw, K., Parat, M., Shaw, P. N., Falconer, J. R., Solvent Supercritical Fluid Technologies to Extract Bioactive Compounds from Natural Sources: A Review. *Molecules*, 2017. **22** (1186): p. 1- 22.

[155] Donato, P., Dugo P., Mondello, L., Liquid Chromatography: Applications. Chapter 9.4.5: Supercritical Fluid Extraction. *Elsevier Incorporation*, 2013. p. 221- 222.

[156] Katayama, T., Ohgaki, K., Maekawa, G., Goto, M., Nagano, T., Isothermal vapor-liquid equilibria of acetone-carbon dioxide and methanol-carbon dioxide systems at high pressures. *Jounal of Chemical Engineering of Japan*, 1975. **8**: p. 89.

[157] Campardelli, R., Baldino, L., Reverchon, E., Supercritical fluids applications in nanomedicine. *Journal of Supercritical Fluids*, 2015. **101**: p. 193.

[158] Kazarian, S. G., Vincent, M. F., Bright, F. V., Liotta, C. L., Eckert, C. A., Specific Intermolecular Interaction of Carbon Dioxide with Polymers. *Journal of American Chemical Society*, 1996. **118**: p. 1729- 1736.

[159] Mawson, S., Johnston, K. P., Combes, J. R., DeSimone, J. M., Formation of Poly(1,1,2,2-tetrahydroperfluorodecyl acrylate) Submicron Fibers and Particles from Supercritical Carbon Dioxide Solutions. *Macromolecules*, 1995. **28** (9): p. 3182- 3191.

[160] Shieh, Y., Yang, H., Morphological changes of polycaprolactone with high-pressure CO_2 treatment. *Journal of Supercritical Fluids*, 2005. **33**: p. 183- 192.

[161] Fried, J. R., Li, W., High-pressure FTIR Studies of Gas-Polymer Interactions. *Journal of Applied Polymer Science*, 1990. **41** (5-6): 1123- 1131.

[162] Campardelli R., Porta G.D., Reverchon E. Solvent elimination from polymer nanoparticle suspensions by continuous supercritical extraction. *Journal of Supercritical Fluids*, 2012. **70**: p. 100.

[163] Santos, D. T., Martín, A., Meireles, M. A., Cocero, M. J., Production of stabilized sub-micrometric particles of carotenoids using supercritical fluid extraction of emulsions. *Journal of Supercritical fluids*, 2012. **61**: p. 167.

[164] Kwon, H., Lee J., Choi, S., Jang, Y., Kim, J., Preparation of PLGA nanoparticles containing estrogen by emulsification–diffusion method. *Colloids and Surfaces A: Physicochemical and Engineering Aspects*, 2001. **182**: p. 123.

[165] Galindo-Rodriguez, S., Alle´mann, E., Fessi, H., Doelker, E., Physicochemical Parameters Associated with Nanoparticle Formation in the Salting-out, Emulsification-Diffusion, and Nanoprecipitation Methods. *Pharmaceutical Research*, 2004. **21**: p. 1428.

[166] Pasquali, I., Bettini, R., Are pharmaceuticals really going supercritical. *International Journal of Pharmaceutics*, 2008. **364**: p. 176.

[167] Sharma, N., Madan, P., Lin, S., Effect of process and formulation variables on the preparation of parenteral paclitaxel-loaded biodegradable polymeric nanoparticles: A co-surfactant study. *Asian Journal of Pharmaceutical Sciences*, 2016. **11**: p. 404.

[168] Nanda, A. K., Wicks, D. A., The influence of the ionic concentration, concentration of the polymer, degree of neutralization and chain extension on aqueous polyurethane dispersions prepared by the acetone process. *Polymer*, 2006. **47**: p. 1805.

[169] Asasutjarit, R., Sorrachaitawatwong, C., Tipchuwong, N., Pouthai, S., Effect of Formulation Compositions on Particle Size and Zeta Potential of Diclofenac Sodium-Loaded Chitosan Nanoparticles. *International Journal of Medical, Health, Biomedical, Bioengineering and Pharmaceutical Engineering*, 2013. **7**: p. 568.

[170] Goloub, T., Pugh, R. J., The role of the surfactant head group in the emulsification process: Single surfactant systems. *Journal of Colloid and Interface Science*, 2003. **257**: p. 337.

[171] Hasani, F., Pezeshki, A., Hamishehkar, H., Effect of Surfactant and Oil Type on Size Droplets of Betacarotene-Bearing Nanoemulsions. *International Journal of Current Microbiology and Applied Sciences*, 2015. **4**: p. 146.

[172] Mu, L., Feng, S. S., A novel controlled release formulation for the anticancer drug paclitaxel (Taxol®): PLGA nanoparticles containing vitamin E TPGS. *Journal of Controlled Release*, 2003. **86**: p. 33.

[173] Feng, S., Huang, G., Effects of emulsifiers on the controlled release of paclitaxel (Taxol®) from nanospheres of biodegradable polymers. *Journal of Controlled Release*, 2001. **71**: p. 53.

[174] Jódar-Reyes, A. B., Martín-Rodríguez, A., Ortega-Vinuesa, J. L., Effect of the ionic surfactant concentration on the stabilization/destabilization of polystyrene colloidal particles. *Journal of Colloid and Interface Science*, 2006. **298**: p. 248.

[175] Furusawa, K., Sato, A., Shirai, J., Nashima, T., Depletion Flocculation of Latex Dispersion in Ionic Micellar Systems. *Journal of Colloid and Interface Science*, 2002. **253**: p. 273.

[176] Sing, K., Everett, D., Haul, R., Moscou, L., Pierotti, R., Rouquerol, J., Siemieniewska, T., Reporting physisorption data for gas/solid systems. *Pure Applied Chemistry*, 1985. **57** (4): p. 603- 619.

[177] Alothman, Z. A., A Review: Fundamental Aspects of Silicate Mesoporous Materials. *Materials*, 2012. **5**: p. 2874- 2902.

[178] Donohue, M. D., Aranovich, G. L., Classification of Gibbs adsorption isotherms. *Advances in Colloid and Interface Science*, 1998. **76-77**: p. 137- 152.

[179] Mahalingam, M., Krishnamoorthy, K., Fabrication and optimization of camptothecin loaded Eudragit S 100 nanoparticles by Taguchi L4 orthogonal array design. *International Journal of Pharmaceutical Investigation*, 2015. **5** (3): p. 147- 154.

[180] Beck, R. C. R., Lionzo, M. I. Z., Costa, T. M. H., Benvenutti, E. V., Ré, M. I., Gallas, M. R., Pohlmann, A. R., Guterres, S. S., Surface morphology of spray-dried nanoparticle-coated microparticles designed as an oral drug delivery system. *Brazilian Journal of Chemical Engineering*, 2008. **25** (2): 389- 398.

[181] Dubois, I. E., Holgersson, S., Allard, S., Malmström, M. E., Correlation between particle size and surface area for chlorite and K-feldspar. *Water-Rock Interaction - Proceedings of the 13th International Conference on Water-Rock Interaction, WRI-13 / [ed] P. Birkle, I.S. Torres-Alvorado*, 2010. p. 717-720.

[182] Doustgani, A., Vasheghani- Farahani, E., Soleimani, M., Hashemi-Najafabadi, S., Physical and Chemical Investigation of Polycaprolactone, Nanohydroxyapatite and Poly (Vinyl Alcohol) Nanocomposite Scaffolds. *World Academy of Science, Engineering and Technology International Journal of Materials and Metallurgical Engineering*, 2012. **6** (2): p. 172- 175.

[183] Abdelrazek, E. M., Hezma, A. M., El-khodary, A., Elzayat, A. M., Spectroscopic studies and thermal properties of PCL/PMMA biopolymer blend. *Egyptian Journal of Basic and Applied Sciences*, 2016. **3**: p. 10- 15.

[184] Smallwood, I. M., Handbook of Organic Solvents Properties. 1996, London: Hodder Headline Group, p. 1- 326.

[185] Sharma, M., Sharma, V., Panda, A. K., Majumdar, D. K., Development of enteric submicron particle formulation of papain for oral delivery. *International Journal of Nanomedicine*, 2011. **6**: p. 2097- 2111.

[186] Bansal, S., Beg, S., Asthana, A., Garg, B., Asthana, G. S., Kapil, R., Singh, B., QbD-enabled systematic development of gastroretentive multiple-unit microballoons of itopride hydrochloride. *Drug Delivery, Early Online*, 2014. p. 1- 15.

[187] Korang-Yeboah, M., Gorantla, Y., Paulos, S. A., Sharma, P., Chaudhary, J., Palaniappan, R., Polycaprolactone/maltodextrin nanocarrier for intracellular drug delivery: formulation, uptake mechanism, internalization kinetics, and subcellular localization. *International Journal of Nanomedicine*, 2015. **10**: p. 4763- 4781.

[188] Aliah, N. N., Ansari, M. N. M., Thermal analysis on Characterization of Polycaprolactone (PCL) – Chitosan Scaffold for Tissue Engineering. *International Journal of Scientific Research Engineering & Technology*, 2017. **6** (2): p. 76- 80.

[189] Rao, M. R. P., Yunusi, A., Shelar, S., Formulation and Evaluation of Floating Microcapsules of Cefpodoxime Proxetil. *Indian Journal of Pharmaceutical Education and Research*, 2014. **48** (Supplementary): p. 105- 113.

[190] Reda, R. I., Wen, M. M., El-Kamel, A. H., Ketoprofen-loaded Eudragit electrospun nanofibers for the treatment of oral mucositis. *International Journal of Nanomedicine*, 2017. **12**: p. 2335- 2351.

[191] Karthikeyana, K., Guhathakarta, S., Rajaram, R., Korrapati, P. S., Electrospun zein/eudragit nanofibers based dual drug delivery system for the simultaneous delivery of aceclofenac and pantoprazole. *International Journal of Pharmaceutics*, 2012. **438**: p. 117- 122.

[192] Illangakoon, U. E., Nazir, T., Williams, G. R., Chatterton, N. P., Mebeverine-Loaded Electrospun Nanofibers: Physicochemical Characterization and Dissolution Studies. *Journal of Pharmaceutical Sciences*, 2014. **103**: p. 283- 292.

[193] Bharti, C., Nagaich, U., Pal, A. K., Gulati, N., Mesoporous silica nanoparticles in target drug delivery system: A review. *International Journal of Pharmaceutical Investigation*, 2015. **5** (3): p. 124- 133.

[194] Watermann, A., Brieger, J., Mesoporous Silica Nanoparticles as Drug Delivery Vehicles in Cancer. *Nanomaterials*, 2017. **7** (189): p. 1- 17.

[195] Wang, Z., Liu, Q., Yu, J., Wu, T., Wang, G., Surface structure and catalytic behavior of silica-supported copper catalysts prepared by impregnation and sol–gel methods. *Applied Catalysis A: General*, 2003. **239**: p. 87- 94.

[196] Khdary, N. H., Ghanem, M. A., Abdesalam, M. E., Al-Garadah, M. M., Sequestration of CO_2 using Cu nanoparticles supported on spherical and rod-shape mesoporous silica. *Journal of Saudi Chemical Society*, 2018. **22**: p. 343- 351.

[197] Ashoka, S., Seetharamappa, J., Kandagal, P. B., Shaikh, S. M. T., Investigation of the interaction between trazodone hydrochloride and bovine serum albumin. *Journal of Luminescence*, 2006. **121**: p. 179- 186.

[198] Hoffmann, H., Pisch-Heberle, S., Analytical methods and stability testing of biopharmaceuticals. *Protein Formulation and Delivery, 2nd Edition*, 2007.

[199] Whitmore, L., Wallace, B. A., Protein Secondary Structure Analyses from Circular Dichroism Spectroscopy: Methods and Reference Databases. *Biopolymers*, 2007. **89** (5): p. 392- 400.

[200] Freifelder, D., Physical Chemistry for Students of Biology and Chemistry. 1982, Boston: Science Books International, Inc. p. 639- 650.

[201] Sekar, G., Kandiyil, S. T., Sivakumar, A., Mukherjee, A., Chandrasekaran, N., Binding studies of hydroxylated Multi-Walled Carbon Nanotubes to hemoglobin, gamma globulin and transferrin. *Journal of Photochemsitry & Photobiology, B: Biology*, 2015. **153**: p. 222- 232.

[202] Hayashi, T., Mukamel, S., Vibrational-Exciton Couplings for the Amide I, II, III, and A Modes of Peptides. *Journal of Physical Chemistry B*, 2007. **111**: p. 11032- 11046.

[203] Smith, E. L., Coy, N. H., The Absorption Spectra of Immune Proteins. [cited 2019 28th February]; Available at: http://www.jbc.org/content/164/1/367.full.pdf.

[204] Wang W., Nema, S., Teagarden, D., Protein aggregation—Pathways and influencing factors. *International Journal of Pharmaceutics*, 2010. **390**: p. 89- 99.

[205] Mahler, H. C., Friess, W., Grauschopf, U., Kiese, S., Protein Aggregation: Pathways, Induction Factors and Analysis. *Journal of Pharmaceutical Sciences*, 2009. **98** (9): p. 2909- 2934.

[206] Kiese, S., Papppenberger, A., Friess, W., Mahler, H. C., Shaken, Not Stirred: Mechanical Stress Testing of An IgG1 Antibody. *Journal of Pharmaceutical Sciences*, 2008. **97** (10): p. 4347- 4366.

[207] O'Brien, E. P., Brooks, B. R., Thirumalai, D., Effects of pH on proteins: Predictions for ensemble and single molecule pulling experiments. *Journal of American Chemical Society*, 2012. **134** (2): p. 979- 987.

[208] Di Russo, N. V., Estrin, D. A., Martı´, M. A., Roitberg, A. E., pH-Dependent Conformational Changes in Proteins and Their Effect on Experimental pKas: The Case of Nitrophorin 4. *PLOS, Computational Biology*, 2012. **8** (11): p. 1- 9.

[209] Chi, E. Y., Krishnan, S., Randolph, T. W., Carpenter, J. F., Physical Stability of Proteins in Aqueous Solution: Mechanism and Driving Forces in Nonnative Protein Aggregation. *Pharmaceutical Research*, 2003. **20** (9): p. 1325- 1336.

[210] Dill, K. A., Dominant Forces in Protein Folding. *Biochemistry*, 1990. **29** (31): p. 7133-7155.

[211] Thakur, R., Das, A., Sharma, V., Adhikari, C., Ghosh, K.S., Chakraborty, A., Interaction of different prototropic species of an anticancer drug ellipticine with HSA and IgG proteins: multispectroscopic and molecular modeling studies. *Physical Chemistry Chemical Physics*, 2015. **17** (26): p. 16937-16946.

[212] Swietnicki, W., Petersen, R., Gambetti, P., Surewicz, W. K., pH-dependent Stability and Conformation of the Recombinant Human Prion Protein PrP(90–231). *The Journal of Biological Chemistry*, 1997. **272** (44): p. 27517- 27520.

[213] Hook, F., Rodahl, M., Kasemo, B., Brzezinski, P., Structural changes in hemoglobin during adsorption to solid surfaces: Effects of pH, ionic strength, and ligand binding. *Proceedings of the Natural Academy of Sciences*, 1998. **95**: p. 12271- 12276.

[214] Biosynthesis, What is the isoelectric point. [cited 2019 28th February]; Available at: http://www.biosyn.com/faq/what-is-isoelectric-point.aspx.

[215] Gitlin, I., Carbeck, J. D., Whitesides, G. M., Why Are Proteins Charged? Networks of Charge–Charge Interactions in Proteins Measured by Charge Ladders and Capillary Electrophoresis. *Angewandte Chemie Int. Ed*., 2006. **45**: p. 3022- 3060.

[216] Mizerska, U., Fortuniak, W., Pospiech, P., Chojnowski, J., Slomkowski, S., Gamma Globulins Adsorption on Carbofunctional Polysiloxane Microspheres. *Journal of Inorganic and Organometallic Polymers and Materials*, 2015. **25**: p. 507- 514.

[217] HCC Learning Web, Protein. [cited 2019 28th February]; Available at: https://learning.hccs.edu/faculty/james.jabbur/biotechnical-applications-and-theoretical-considerations/proteins.

[218] Norde, W., Giacomelli, C. E., BSA structural changes during homomolecular exchange between the adsorbed and the dissolved states. *Journal of Biotechnology*, 2000. **79**: p. 259-268.

[219] Ball, V., Huetz, P., Elaissari, A., Cazenave, J. P., Voegel, J. C., Schaaf, P., Kinetics of exchange processes in the adsorption of proteins on solid surfaces. *Proc. Natl. Acad. Sci. USA*, 1994. **91** (15): p. 7330- 7334.

[220] Bentaleb, A., Ball, V., Haïkel, Y., Voegel, J. C., Schaaf, P., Kinetics of the Homogeneous Exchange of Lysozyme Adsorbed on a Titanium Oxide Surface. *Langmuir*, 1997. **13** (4): p. 729- 735.

[221] Brash, J. L., Samak, Q. M., Dynamics of Interactions between Human Albumin and Polyethylene Surface. *Journal of Colloid and Interface Science*, 1978. **65** (3): p. 495- 504.

[222] Kulikova, G. A., Parfenyuk, E. V., Surface properties of modified nanosized silica and their influence on human serum albumin immobilization. *Protection of Metals and Physical Chemistry of Surfaces*, 2010. **46** (5): p. 546- 549.

[223] Haynes, C. A., Norde, W., Globular proteins at solid-liquid interfaces. *Colloids Surfaces B: Biointerfaces*, 1994. **2** (6): p. 517- 566.

[224] Buijs, J., Norde, W., Changes in the Secondary Structure of Adsorbed IgG and F(ab')$_2$ Studied by FTIR Spectroscopy. *Langmuir*, 1996. **12**: p. 1605- 1613.

[225] Kondo, A., Oku, S., Higashitani, K., Structural Changes in Protein Molecules Adsorbed on Ultrafine Silica Particles. *Journal of Colloid and Interface Science*, 1991. **143** (1): p. 214- 221.

[226] Li, S., Hu, J., Liu, B., A study on the adsorption behaviour of protein onto functional microspheres. *Journal of Chemical Technology and Biotechnology*, 2005. **80**: p. 531- 536.

[227] Carlsson, N., Gustafsson, H., Thörn, C., Olsson, L., Holmberg, K., Åkerman, B., Enzymes immobilized in mesoporous silica: A physical-chemical perspective. *Advances in Colloid and Interface Science*, 2014. **205**: p. 339- 360.

[228] Hlady, V., Buijs, J., Jennissen, H. P., Methods for Studying Protein Adsorption. *Methods in Enzymology*, 1999. **309**: p. 402- 409.

[229] Felsovalyi, F., Mangiagalli, P., Bureau, C., Kumar, S., Banta, S., Reversibility of the adsorption of lysozyme on silica. *Langmuir*, 2011. **27**: p. 11873- 11882.

[230] Joshi, O., Lee, H. J., McGuire, J., Finneran, P., Bird, K. E., Protein concentration and adsorption time effects on fibrinogen adsorption at heparinized silica interfaces. *Colloids and Surfaces B: Biointerfaces*, 2006. **50**: p. 26- 35.

[231] Elgersma, A. V., Zsom, R. L. J., Norde, W., Lyklema, J., The Adsorption of Bovine Serum Albumin on Positively and Negatively Charged Polystyrene Latices. *Journal of Colloid and Interface Science*, 1990. **138** (1): p 145- 156.

[232] Quiquampoix, H., Staunton, S., Baron, M.-H., Ratcliffe, R. G., Interpretation of the pH dependence of protein adsorption on clay mineral surfaces and-its relevance to the understanding of extracellular enzyme activity in soil. *Colloids and Surfaces A: Physicochemical and Engineering Aspects*, 1983. **75**: p. 85- 93.

[233] Liu, B., Cao, S., Deng, X., Li, S., Luo, R., Adsorption behavior of protein onto siloxane microspheres. *Applied Surface Science*, 2006. **252**: p. 7830- 7836.

[234] Kondo, A., Oku, S., Higashitani, K., Adsorption of γ-Globulin, a Model Protein for Antibody, on Colloidal Particles. *Biotechnology and Bioengineering*, 1991. **37** (6): p. 537- 543.

[235] Demanèche, S., Chapel, J., Monrozier, L. J., Quiquampoix, H., Dissimilar pH-dependent adsorption features of bovine serum albumin and α-chymotrypsin on mica probed by AFM. *Colloids and Surfaces B: Biointerfaces*, 2009. **70**: p. 226- 231.

[236] Clemments, A. M., Botella, P., Landry, C. C., Protein Adsorption from Biofluids on Silica Nanoparticles: Corona Analysis as a Function of Particle Diameter and Porosity. *Applied Materials and Interfaces*, 2015. **7** (39): p. 21682- 21689.

[237] Deere, J., Magner, E., Wall, J. G., Hodnett, B. K., Adsorption and activity of proteins onto mesoporous silica. *Catalysis Letters*, 2003. **85** (1-2): p. 19- 23.

[238] Zhang, T., Zhu, G., Lu, B., Zhang, C., Peng, Q., Concentration-dependent protein adsorption at the nano–bio interfaces of polymeric nanoparticles and serum proteins. *Nanomedicine*, 2017. **12** (2): p. 2757- 2769.

[239] Welsch, N., Lu, Y., Dzubiella, J., Ballauff, M., Adsorption of proteins to functional polymeric nanoparticles. *Polymer*, 2013. **54**: p. 2835- 2849.

[240] Spada, G., Gavini, E., Giunchedi, P., Protein Delivery from Polymeric Nanoparticles. *World Academy of Science, Engineering and Technology International Journal of Pharmacological and Pharmaceutical Sciences*, 2011. **5** (4): p. 172- 176.

[241] Lindman, S., Lynch, I., Thulin, E., Nilsson, H., Dawson, K. A., Linse, S., Systematic Investigation of the Thermodynamics of HSA Adsorption to N-iso-Propylacrylamide/ N-tert-Butylacrylamide Copolymer Nanoparticles. Effects of Particle Size and Hydrophobicity. *Nano Letters*, 2007. **7** (4): p. 914- 920.

[242] Fang, F., Satulovsky, J., Szleifer, I., Kinetics of Protein Adsorption and Desorption on Surfaces with Grafted Polymers. *Biophysical Journal*, 2005. **89**: p. 1516- 1533.

[243] Buijs, J., Hlady, V., Adsorption Kinetics, Conformation, and Mobility of the Growth Hormone and Lysozyme on Solid Surfaces, Studied with TIRF. *Journal of Colloid and Interface Science*, 1997. **190**: p. 171- 181.

[244] Ho, Y. S., McKay, G., Pseudo-second order model for sorption processes. *Process Biochemistry*, 1999. **34**: p. 451- 465.

[245] Liu, Y, Liang, S., From Langmuir Kinetics to First- and Second-Order Rate Equations for Adsorption. *Langmuir*, 2008. **24**: p. 11625- 11630.

[246] Ma, Z., Bai, J., Wang, Y., Jiang, X., Impact of Shape and Pore Size of Mesoporous Silica Nanoparticles on Serum Protein Adsorption and RBCs Hemolysis. *Applied Materials and Interfaces*, 2014. **6**: p. 2431- 2438.

[247] Kalavathy, M. H., Swaroop, G., Padmini, E., Miranda, L. R., Moringa Oleifera, A Biosorbent for Resorcinol Adsorption-Isotherm and Kinetic Studies. *Carbon Letters*, 2009. **10** (1): p. 23- 32.

[248] Schlossbauer, A., Schaffert, D., Kecht, J., Wagner, E., Bein, T., Click Chemistry for High-Density Biofunctionalization of Mesoporous Silica. *Journal of American Chemical Society*, 2008. **130**: p. 12558- 12559.

[249] Armstrong, J. K., Wenby, R.B., Meiselman, H. J., Fisher, T. C., The Hydrodynamic Radii of Macromolecules and Their Effect on Red Blood Cell Aggregation. *Biophysical Journal*, 2004. **87**: p. 4259- 4270.

[250] Horikawa, T., Nicholson, D., Capillary condensation of adsorbates in porous materials. *Advances in Colliod and Interface Science*, 2011. **169**: p. 40- 58.

[251] De Lange, M. F., Vlugt, T. J. H., Gascon, J., Kapteijn, F., Adsorptive characterization of porous solids: Error analysis guides the way. *Microporous and Mesoporous Materials*, 2014. **200**: p. 199- 215.

[252] Gallagher, W., FTIR Analysis of Protein Structure. [cited 2019 03rd March]; Available at: https://www.chem.uwec.edu/chem455_s05/pages/manuals/FTIR_of_proteins.pdf.

[253] Haris, P. I., Can infrared spectroscopy provide information on protein–protein interactions? *Biochemical Society Transactions*, 2010. **38** (4): p. 940- 946.

[254] Haris, P. I., Chapman, D., Does Fourier-transform infrared spectroscopy provide useful information on protein structures? *Elsevier Science Publications (UK),* 1997. p. 328- 333.

[255] Norde, W., Anusiem, A. C. I., Adsorption, desorption and re-adsorption of proteins on solid surfaces. *Colloids and Surfaces*, 1992. **66**: p. 73- 80.

[256] Norde, W., MacRitchie, F., Nowicka, G., Lyklema, J., Protein Adsorption at Solid-Liquid Interfaces: Reversibility and Conformation Aspects. *Journal of Colloid and Interface Science*, 1986. **112** (2): p. 447- 456.

[257] Norde, W., Favier, J. P., Structure of adsorbed and desorbed proteins. *Colloids and surfaces*, 1992. **64**: p. 87- 93.

[258] Brash, J. L., Uniyal, S., Pusineri, C., Schmitt, A., Interaction of Fibrinogen with Solid Surfaces of Varying Charge and Hydrophobic-Hydrophilic Balance. *Journal of Colloid and Interface Science*, 1983. **95** (1): p. 28- 36.

[259] Huetz, P., Ball, V., Voegel, J.-C., Schaaf, P., Exchange Kinetics for a Heterogeneous Protein System on a Solid Surface. *Langmuir*, 1995. **11**: p. 3145- 3152.

[260] Galisteo, F., Norde, W., Protein adsorption at the AgI-Water Interface. *Journal of Colloid and Interface Science*, 1995. **172**: p. 502- 509.

[261] Krivosheeva, O., Dedinaite, A., Claesson, Per M., Salt- and pH-induced desorption: Comparison between non-aggregated and aggregated mussel adhesive protein, *Mefp-1*, and a synthetic cationic polyelectrolyte. *Journal of Colloid and Interface Science*, 2013. **408**: p. 82- 86.

[262] Ye, H., Huang, L., Li, W., Zhang, Y., Zhao, L., Xin, Q., Wang, S., Lin, L., Ding, X., Protein adsorption and desorption behavior of a pH-responsive membrane based on ethylene vinyl alcohol copolymer. *Royal Society of Chemistry Advances*, 2017. **7**: p. 21398- 21405.

[263] Sigma-Aldrich UK, *Materials Safety Data Sheet*, [cited 2019 04th March]: Available at: https://www.sigmaaldrich.com/catalog/product/sigma/p2443?lang=en&region=AE&utm_term=pluronic&utm_medium=cpc&utm_content=SIGMA/P2443&utm_source=bing&utm_campaign=Sigma%20Position%20Support%20Global%20(Bing%20ebizpfs).

[264] BASF, *Materials Safety Data Sheet*, [cited 2019 04th March]: Available at; https://worldaccount.basf.com/wa/NAFTA~en_US/Catalog/ChemicalsNAFTA/doc4/BASF/PRD/30089187/.pdf?asset_type=ti/pdf&language=EN&urn=urn:documentum:eCommerce_sol_EU:09007bb280095950.pdf.

[265] Welin-Klinström, S., Askendal, A., Elwing, H., Surfactant and Protein Interactions on Wettability Gradient Surfaces. *Journal of Colloid and Interface Science*, 1993. **158** (1): p. 188- 194.

[266] Rapoza, R. J., Horbett, T. A., The Effects of Concentration and Adsorption Time on the Elutability of Adsorbed Proteins in Surfactant Solutions of Varying Structures and Concentrations. *Journal of Colloid and Interface Science*, 1990. **136** (2): p. 480- 493.

[267] Wahlgren, M., Arnebrant, T., Removal of lysozyme from methylated silicon oxide surfaces by a non-ionic surfactant, pentaethylene glycol mono *n*-dodecyl ether (C_{12} E_5). *Colloids and Surfaces B: Biointerfaces*, 1996. **6**: p. 63- 69.

[268] Otzen, D., Protein-surfactant interactions: A tale of many states. *Biochimica et Biophysica Acta*, 2011. **1814**: p. 562- 591.

[269] Sethuraman, A., Vedantham, G., Imoto, T., Przybycien, T., Belfort, G., Protein Unfolding at Interfaces: Slow Dynamics of α-Helix to β-Sheet Transition. *Proteins: Structure, Function, and Bioinformatics*, 2004. **56**: p. 669- 678.

[270] Zoungrana, T., Findenegg, G. H., Norde, W., Structure, Stability, and Activity of Adsorbed Enzymes. *Journal of Colloid and Interface Science*, 1997. **190**: p. 437- 448.

[271] Lewis, D., Whateley, T. L., Adsorption of enzymes at the solid-liquid interface. *Biomaterials*, 1988. **9**: p. 71- 75.

[272] Schmidt, C. F., Zimmermann, R. M., Gaub, H. E., Multilayer adsorption of lysozyme on a hydrophobic substrate. *Biophysical Journal*, 1990. **57**: p. 577- 588.

[273] Kondo, A., Murakami, F., Higashitani, K. O., Circular Dichroism Studies on Conformational Changes in Protein Molecules upon Adsorption on Ultrafine Polystyrene Particles. *Biotechnology and Bioengineering*, 1992. **40**: p. 889- 894.

[274] Norde, W., Zoungrana, T., Surface-induced changes in the structure and activity of enzymes physically immobilized at solid/liquid interfaces. *Biotechnology and Applied Biochemistry*, 1998. **28**: p. 133- 143.

[275] Greenfield, N., Using circular dichroism spectra to estimate protein secondary structure. *Nature Protocols*, 2006. **1** (6): p. 2876- 2890.

[276] Jafari, M., Mehrnejad, F., Rahimi, F., Asghari, S. M., The Molecular Basis of the Sodium Dodecyl Sulfate Effect on Human Ubiquitin Structure: A Molecular Dynamics Simulation Study. *Scientific Reports*, 2018. **8** (2150): p. 1- 15.

[277] England, J. L., Stabilization and Release Effects of Pluronic F127 in Protein Drug Delivery. *Journal of Undergraduate Sciences*, 2015. **5** (2): p. 17- 24.

[278] Mollmann, S. H., Elofsson, U., Bukrinsky, J. T., Frokjaer, S., Displacement of Adsorbed Insulin by Tween 80 Monitored Using Total Internal Reflection Fluorescence and Ellipsometry. *Pharmaceutical Research*, 2005. **22** (11): p. 1931- 1941.

[279] Ribeiro Dos Santos, I., Richard J., Thies, C., Pech, B., Benoit, J. P., A supercritical fluid-based coating technology. 3: Preparation and characterization of bovine serum albumin particles coated with lipids. *Journal of Microencapsulation*, 2003. **20** (1): p. 110-128.

[280] Ogawa, Y., Injectable microcapsules prepared with biodegradable poly(α-hydroxy) acids for prolonged release of drugs. *Journal of Biomaterials Science, Polymer Edition*, 1997. **8** (5): p. 391 – 409.

[281] Kampen, A., Kohlus, R., Systematic process optimisation of fluid bed coating. *Powder Technology*, 2017. **305**: p. 426- 432.

[282] Yu, Z., Singh, B., Rizvi, S. S. H., Solubilities of Fatty Acids, Fatty Acid Esters, Triglycerides, and Fats and Oils in Supercritical Carbon Dioxide. *The Journal of Supercritical Fluids*, 1994. **7**: p. 51- 59.

[283] Vorum, H., Brodersen, R., Kragh-Hansen, U., Pedersen, A. O., Solubility of long-chain fatty acids in phosphate buffer at pH 7.4. *Biochimica et Biophysica Acta*. I, 1992. **1126**: p. 135- 142.

[284] Boddeda, B., Kumari, P.V.K., Chowdary, K.P.R., Formulation and evaluation of glipizide sustained release tablets. *International Journal of Pharmaceutical and Biomedical Research*, 2012. **3** (1): p.44- 48.

[285] Kelly, S. M., Jess, T. J., Price, N. C., How to study proteins by circular dichroism. *Biochimica et Biophysica Acta*, 2005. **1751**: p. 119- 139.

[286] B'Hymer, C., Residual Solvent Testing: A Review of Gas-Chromatographic and Alternative Techniques. *Pharmaceutical Research*, 2003. **20** (3): p. 337- 344.

[287] Gisbert-Garzarán, M., Manzano, M., Vallet-Regí, M., pH-Responsive Mesoporous Silica and Carbon Nanoparticles for Drug Delivery. *Bioengineering*, 2017. **4** (3): p. 1- 27.

[288] Orsi, S., Di Maio, E., Iannace, S., Netti, P. A., Hollow micro- and nano-particles by gas foaming. *Nano Research*, 2014. **7** (7): p. 1018- 1026.

[289] Yang, Y., Bajaj, N., Xu, P., Ohn, K., Tsifansky, M. D., Yeo, Y., Development of highly porous large PLGA microparticles for pulmonary drug delivery. *Biomaterials*, 2009. **30**: p. 1947- 1953.

[290] Xiong, C., Zhou, X., Zhang, N., Zhan, L., Chen, S., Wang, J., Peng, W., Chang, H., Nie, Z., Quantitative Assessment of Protein Adsorption on Microparticles with Particle Mass Spectrometry. *Analytical Chemistry*, 2014. **86** (8): p. 3876- 3881.

[291] Coleman, J.W., Yeung, J.H.K., Tingle, M.D., Park, B.K., Enzyme-linked immunosorbent assay (ELISA) for detection of antibodies to protein-reactive drugs and metabolites: criteria for identification of antibody activity. Detection and hapten specificity of anti-DNP, anti-captopril and anti- sulphanilamidobenzoic acid. *Journal of Immunological Methods*, 1986. **88**: p. 37- 44.

[292] Ibrahim, S.A., Li, S. K., Efficiency of Fatty Acids as Chemical Penetration Enhancers: Mechanisms and Structure Enhancement Relationship. *Pharmaceutical Research*, 2010. **27** (1): p. 115- 125.

[293] Jochems, P. G. M., Garssen, J., van Keulen, A. M., Masereeuw, R., Jeurink, P. V., Evaluating Human Intestinal Cell Lines for Studying Dietary Protein Absorption. *Nutrients*, 2018. **10** (322): p. 1- 15.

Appendix

A.1 PDI and zeta-potential for PCL particles at varying PCL-Tween 80 ratios

Table 1.1S: PDI and Z-potential of PCL particles before and after SFEE for PCL-Tween 80 (1:1 ratio) samples

PCL concentration (% w/w in acetone)	PDI ± SD before SFEE	PDI ± SD after SFEE	Z-potential (mV) ± SD after SFEE
0.6	0.14 ± 0.10	0.13 ± 0.08	-13 ± 3
1	0.10 ± 0.04	0.21 ± 0.03	-16 ± 2
2	0.18 ± 0.11	0.17 ± 0.09	-18 ± 2
4	0.25 ± 0.10	0.27 ± 0.09	-28 ± 3
6	0.35 ± 0.02	0.25 ± 0.02	-28 ± 5
8	0.36 ± 0.17	0.33 ± 0.08	-32 ± 1
10	0.38 ± 0.03	0.37 ± 0.05	-32 ± 1

Table 1.2S: PDI and Z-potential of PCL particles before and after SFEE for PCL-Tween 80 (2:1 ratio) samples

PCL concentration (% w/w in acetone)	PDI ± SD before SFEE	PDI ± SD after SFEE	Z-potential (mV) ± SD after SFEE
0.6	0.13 ± 0.07	0.12 ± 0.10	-10 ± 1
1	0.14 ± 0.05	0.19 ± 0.04	-17 ± 3
2	0.11 ± 0.04	0.17 ± 0.03	-21 ± 3
4	0.15 ± 0.05	0.19 ± 0.08	-22 ± 4
6	0.09 ± 0.02	0.23 ± 0.01	-28 ± 2
8	0.13 ± 0.06	0.25 ± 0.10	-28 ± 2
10	0.18 ± 0.05	0.20 ± 0.05	-31 ± 3

Table 1.3S: PDI and Z-potential of PCL particles before and after SFEE for PCL-Tween 80 (4:1 ratio) samples

PCL concentration (% w/w in acetone)	PDI ± SD before SFEE	PDI ± SD after SFEE	Z-potential (mV) ± SD after SFEE
0.6	0.12 ± 0.03	0.03 ± 0.02	-17 ± 1
1	0.19 ± 0.06	0.09 ± 0.07	-12 ± 1
2	0.09 ± 0.04	0.14 ± 0.07	-19 ± 3
4	0.19 ± 0.08	0.22 ± 0.02	-29 ± 2
6	0.29 ± 0.05	0.23 ± 0.01	-29 ± 3
8	0.27 ± 0.04	0.28 ± 0.00	-29 ± 4
10	0.27 ± 0.04	0.29 ± 0.05	-33 ± 2

Table 1.4S: PDI and Z-potential of PCL particles before and after SFEE for PCL-Tween 80 (8:1 ratio) samples

PCL concentration (% w/w in acetone)	PDI ± SD before SFEE	PDI ± SD after SFEE	Z-potential (mV) ± SD after SFEE
0.6	0.10 ± 0.04	0.07 ± 0.02	-20 ± 0
1	0.08 ± 0.05	0.07 ± 0.03	-19 ± 3
2	0.09 ± 0.07	0.16 ± 0.08	-15 ± 2
4	0.14 ± 0.08	0.19 ± 0.08	-21 ± 3
6	0.26 ± 0.04	0.21 ± 0.02	-29 ± 2
8	0.31 ± 0.06	0.23 ± 0.01	-31 ± 6
10	0.29 ± 0.07	0.29 ± 0.07	-33 ± 3

Table 1.5S: PDI and Z-potential of PCL particles before and after SFEE for PCL-Tween 80 (16:1 ratio) samples

PCL concentration (% w/w in acetone)	PDI ± SD before SFEE	PDI ± SD after SFEE	Z-potential (mV) ± SD after SFEE
0.6	0.13 ± 0.06	0.07 ± 0.02	-19 ± 4
1	0.06 ± 0.03	0.05 ± 0.01	-17 ± 3
2	0.14 ± 0.06	0.10 ± 0.03	-24 ± 7
4	0.17 ± 0.04	0.22 ± 0.04	-27 ± 6
6	0.23 ± 0.03	0.25 ± 0.02	-32 ± 5
8	0.19 ± 0.04	0.26 ± 0.09	-29 ± 3
10	0.27 ± 0.05	0.24 ± 0.03	-34 ± 4

A.2 Nitrogen sorption isotherms for PCL-ES100 particles

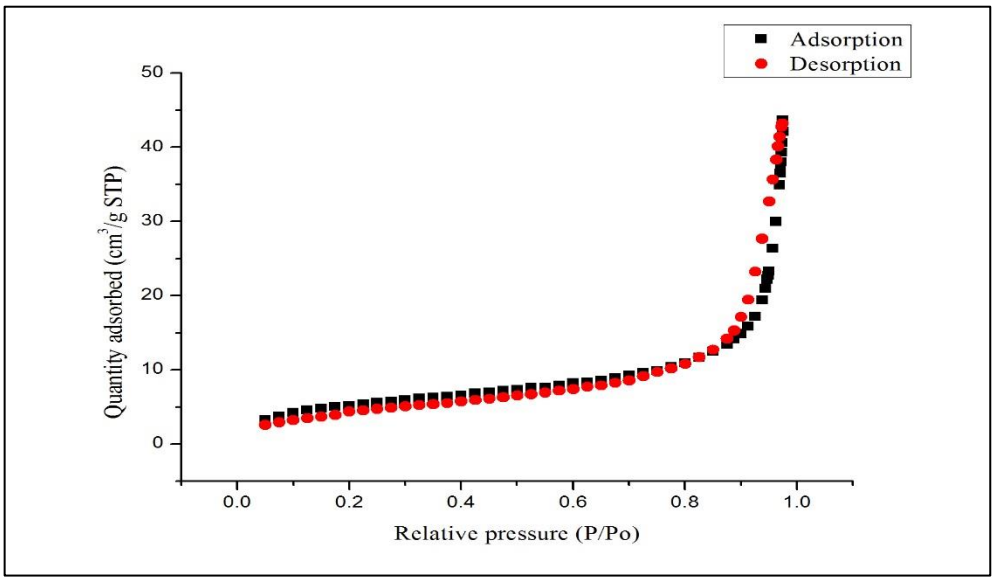

Figure 2.1S: Nitrogen sorption isotherm for PCL-ES100 (1:3 ratio) particles

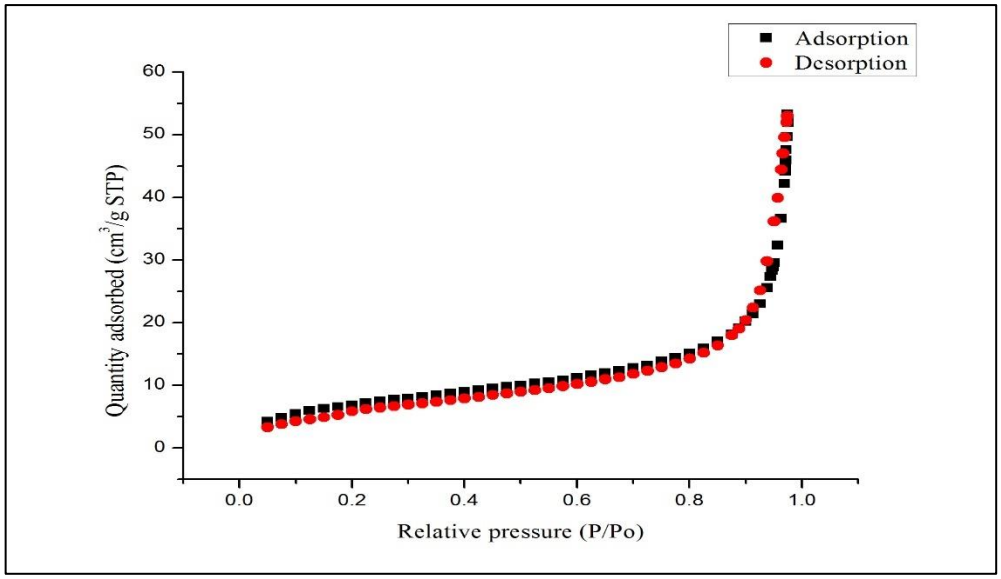

Figure 2.2S: Nitrogen sorption isotherm for PCL-ES100 (1:4 ratio) particles

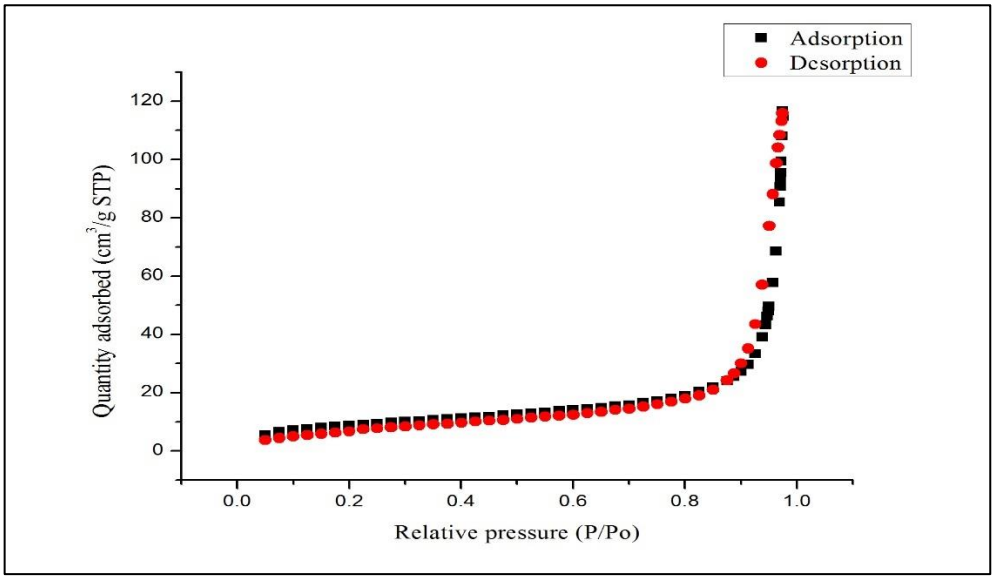

Figure 2.3S: Nitrogen sorption isotherm for PCL-ES100 (1:4 ratio) particles

A.3 ATR-FTIR analysis for PCL-ES100 particles

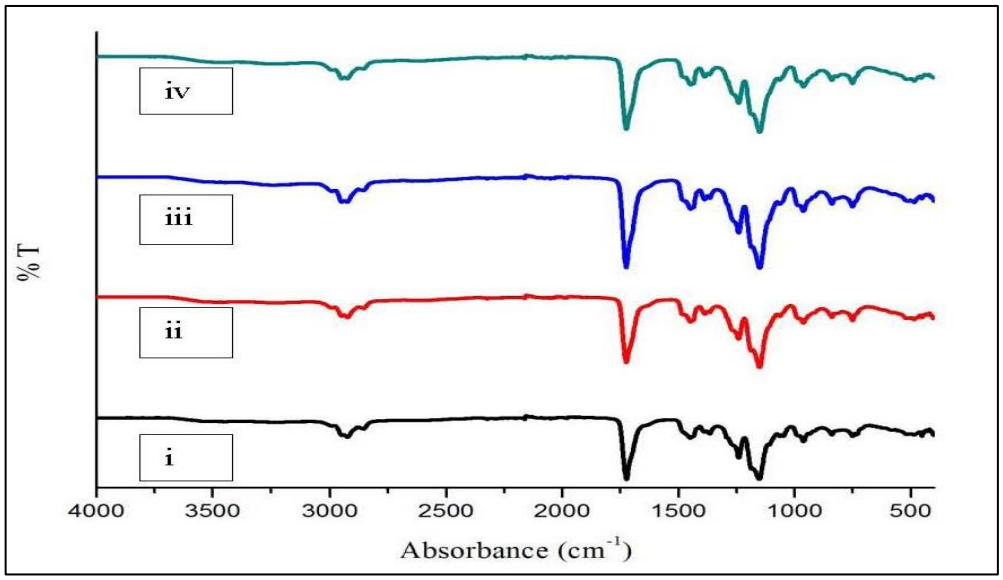

Figure 3.1S: ATR-FTIR spectra for PCL-ES100 particles (i) 1:2 (ii) 1:3 (iii) 1:4 and (iv) 1:5 ratios.

A.4 DSC analysis for PCL-ES100 particles at varying ratios

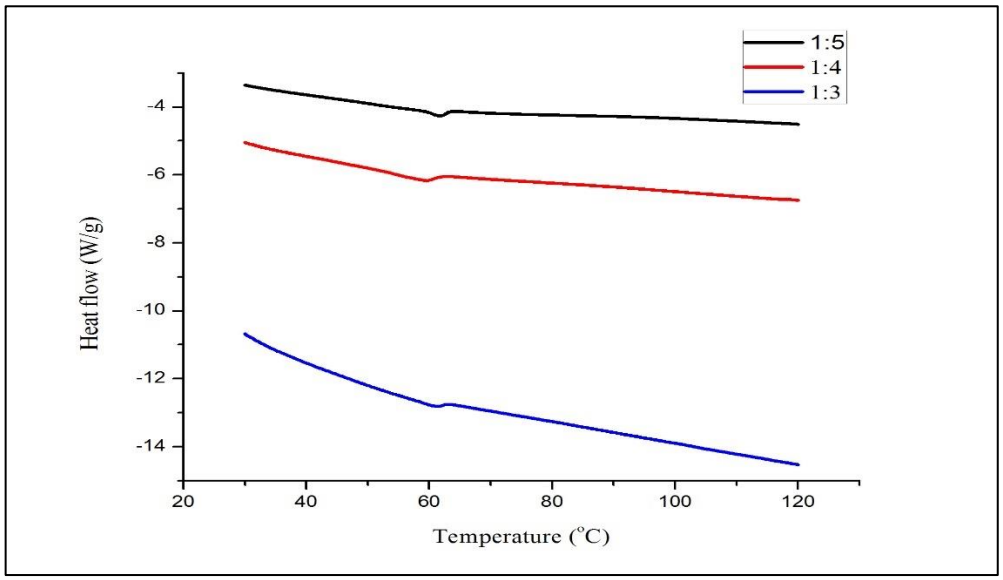

Figure 4.1S: DSC thermograms for PCL-ES100 particles

A.5 Langmuir and Freundlich model fitting for silica particles

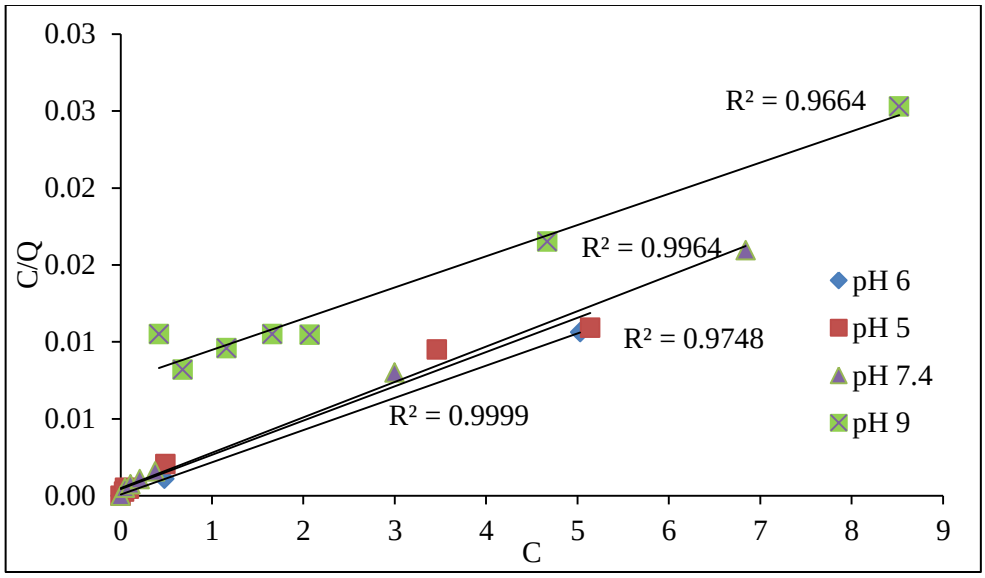

Figure 5.1S: Langmuir plot for γ-globulin adsorption onto S_{FP} particles

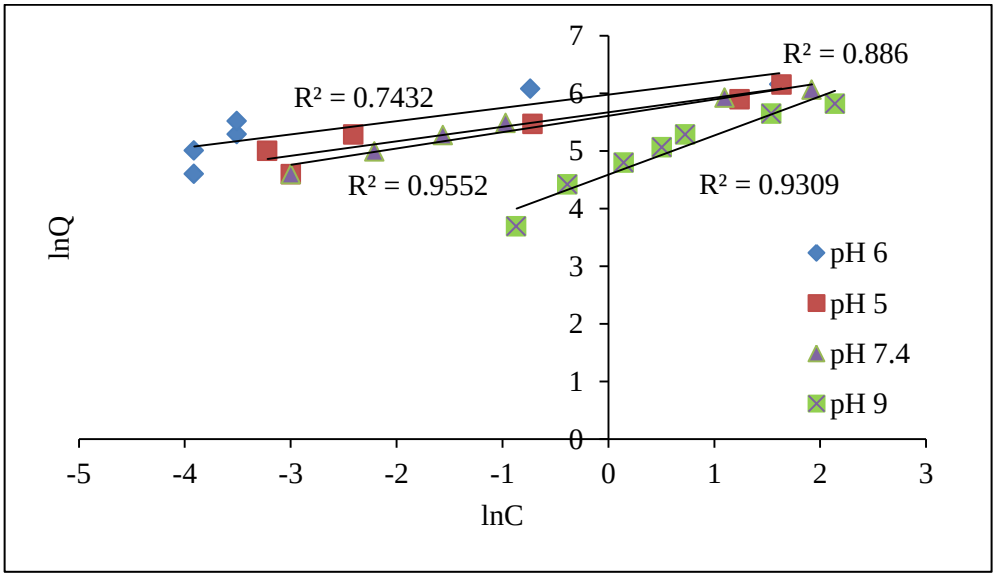

Figure 5.2S: Freundlich plot for γ-globulin adsorption onto S_{FP} particles

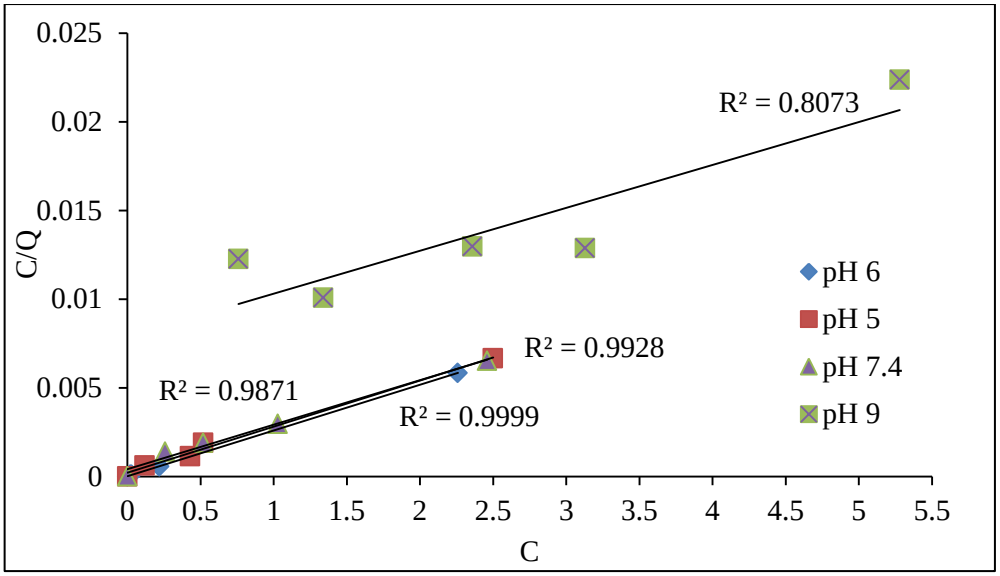

Figure 5.3S: Langmuir plot for γ-globulin adsorption onto S_{XDP} particles

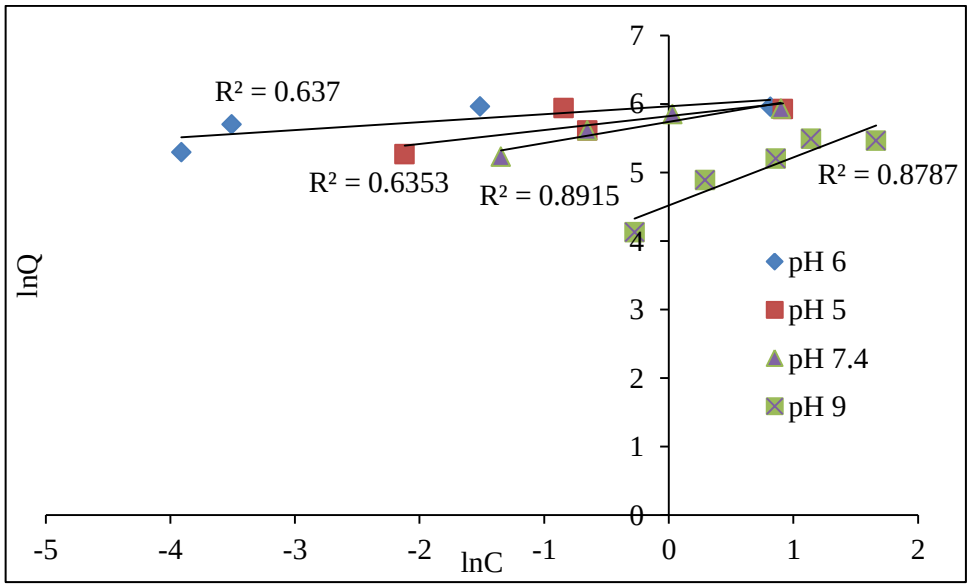

Figure 5.4S: Freundlich plot for γ-globulin adsorption onto S_{XDP} particles

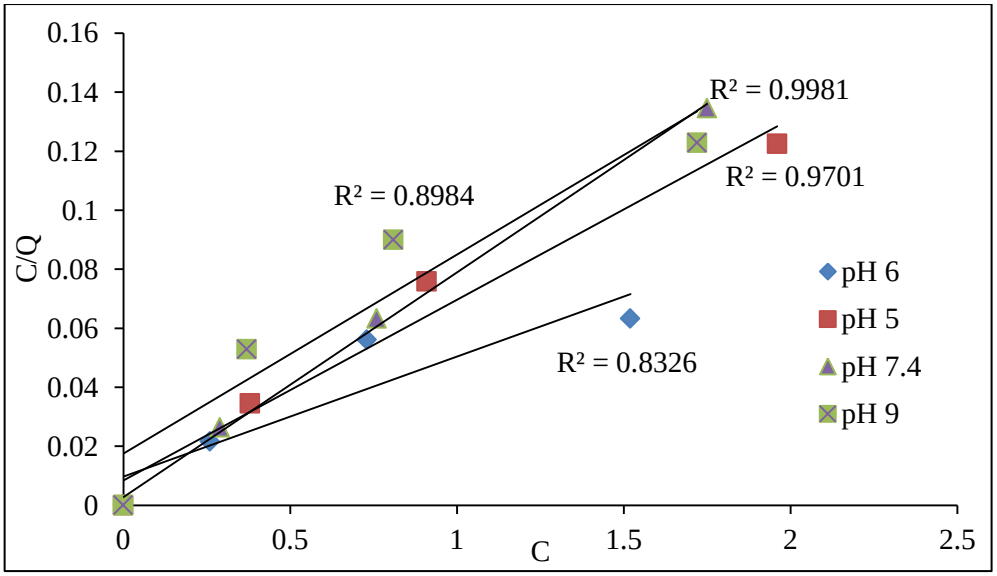

Figure 5.5S: Langmuir plot for γ-globulin adsorption onto S_{AL} particles

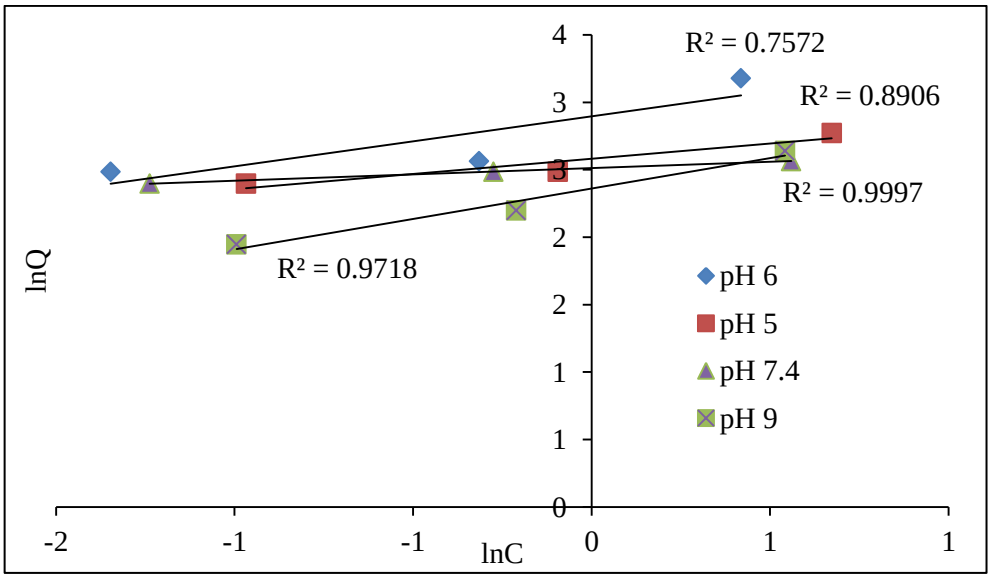

Figure 5.6S: Freundlich plot for γ-globulin adsorption onto S_{AL} particles

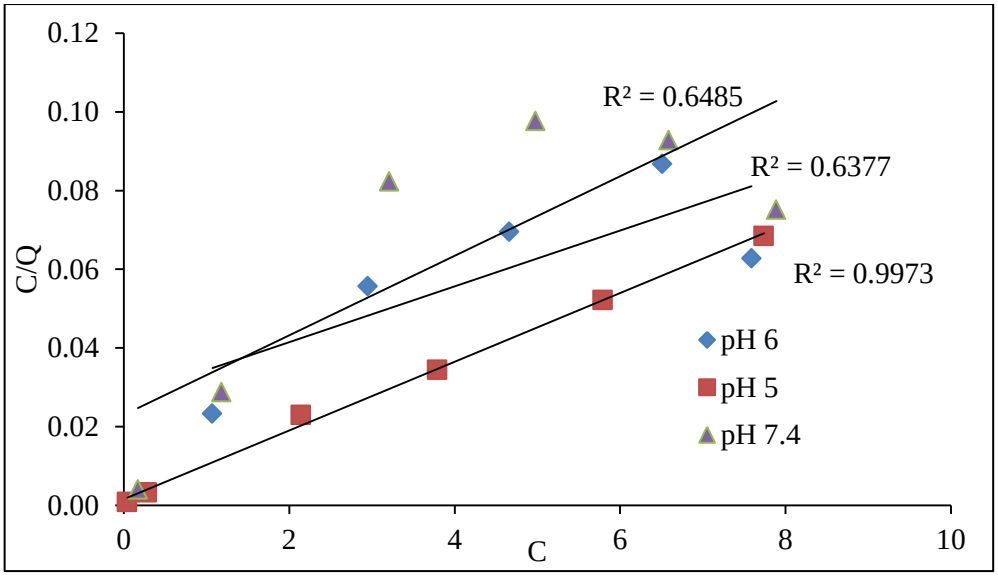

Figure 5.7S: Langmuir plot for γ-globulin adsorption onto MSU-H particles

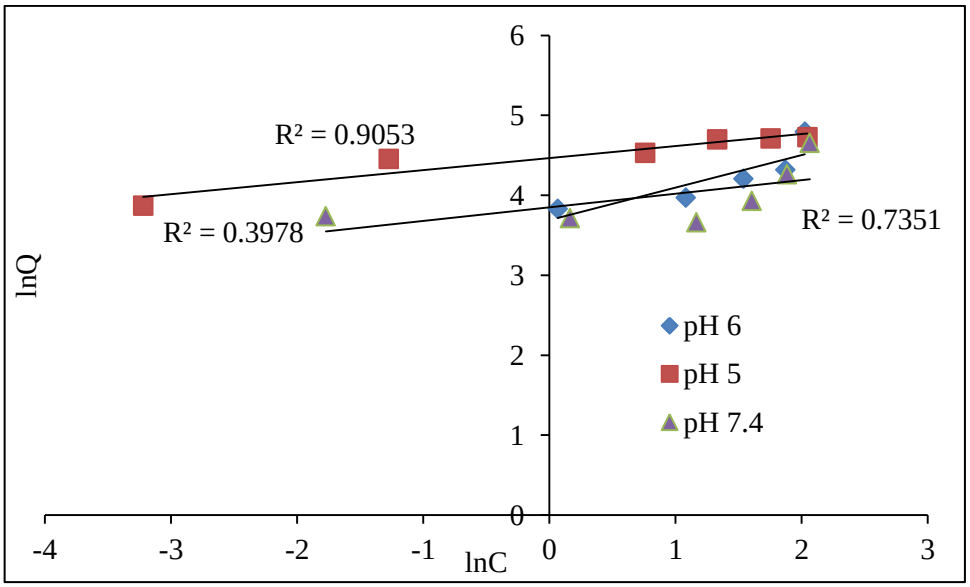

Figure 5.8S: Freundlich plot for γ-globulin adsorption onto MSU-H particles

A.6 Kinetic-order plots for γ-globulin immobilization on core particles

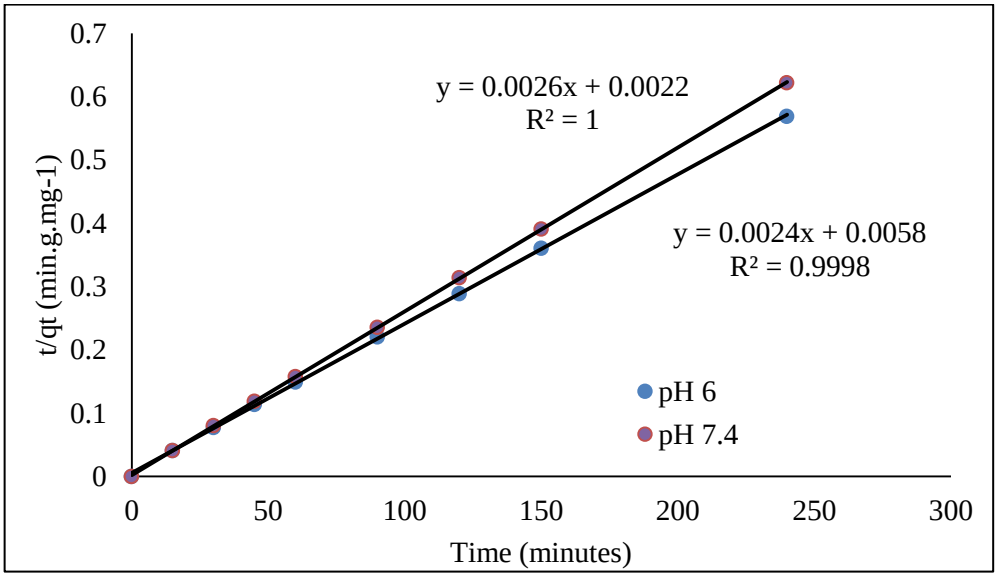

Figure 6.1S: Pseudo-second order kinetic curve for γ-globulin adsorption onto S_{FP}

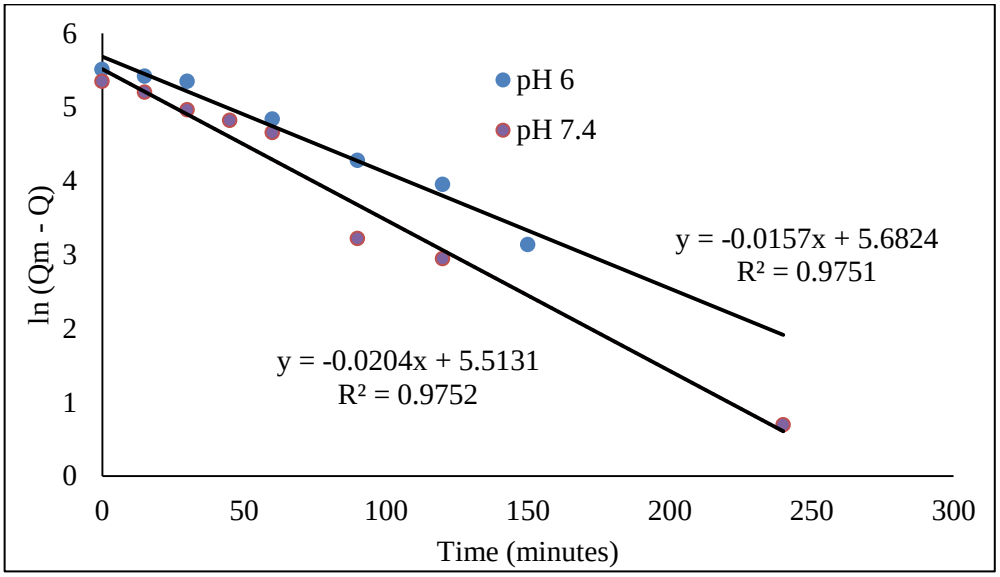

Figure 6.2S: Pseudo-first order kinetic curve for γ-globulin adsorption onto S_{XDP}

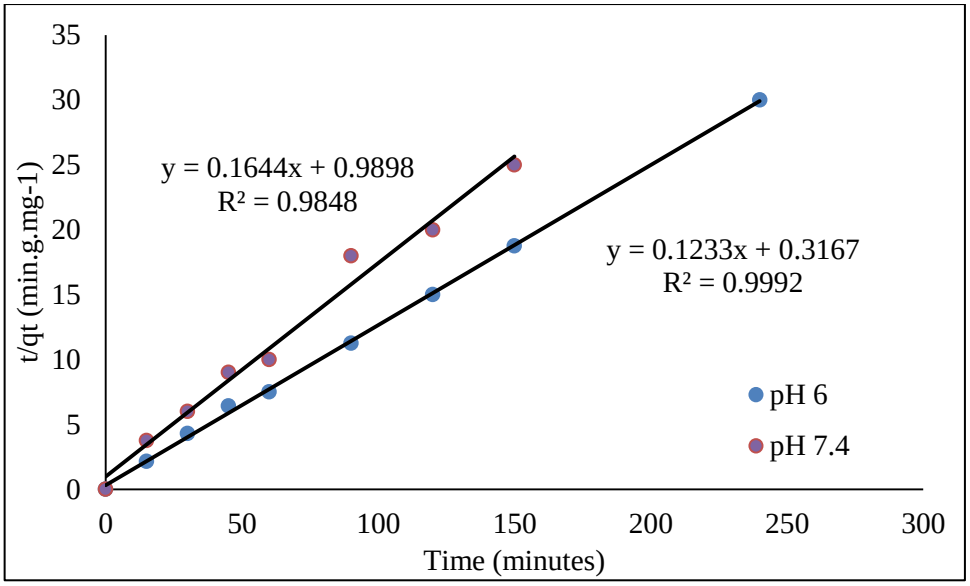

Figure 6.3S: Pseudo-second order kinetic curve for γ-globulin adsorption onto S_{AL}

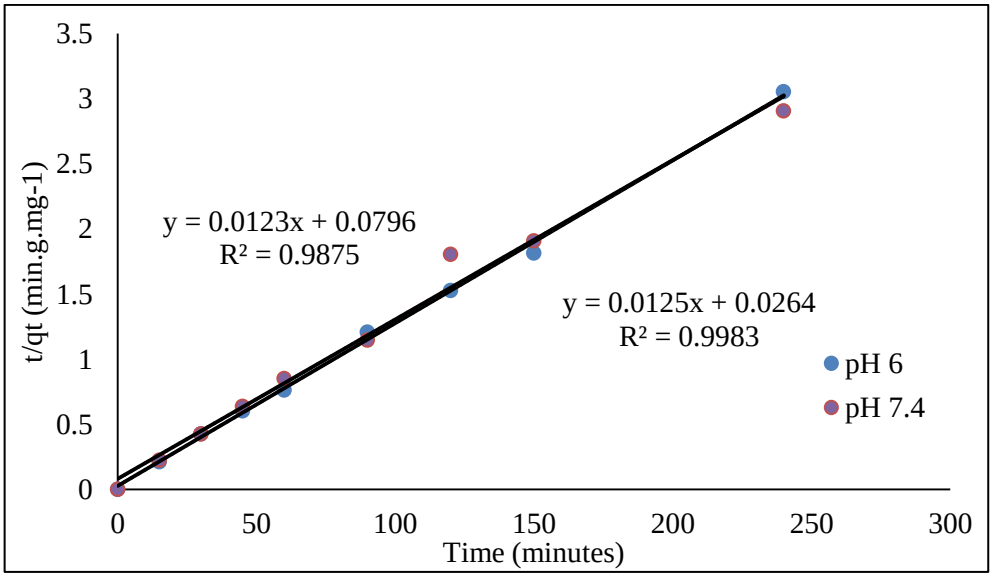

Figure 6.4S: Pseudo-second order kinetic curve for γ-globulin adsorption onto MSU-H

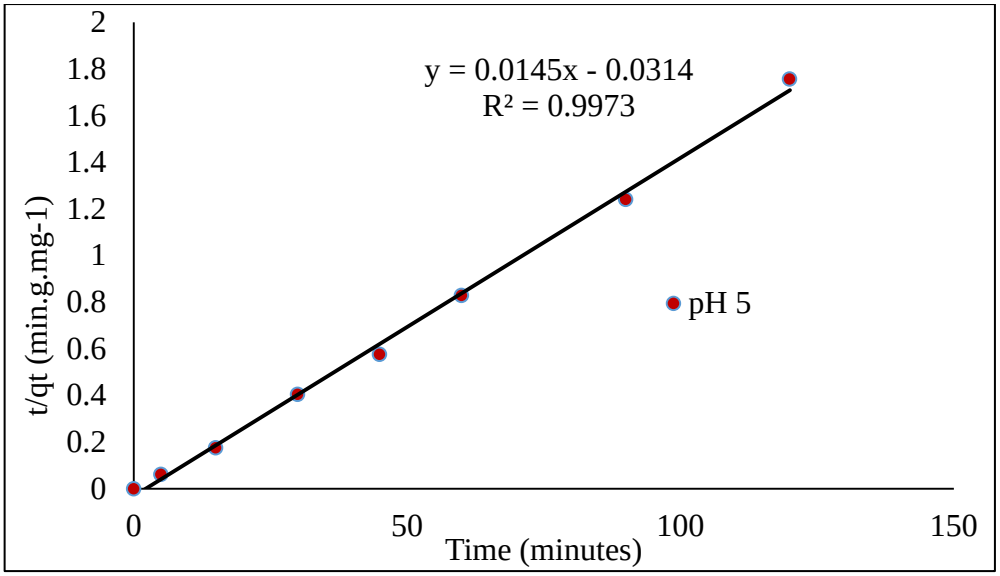

Figure 6.5S: Pseudo-second order kinetic curve for γ-globulin adsorption onto PCL-ES100 (1:3 ratio)

A.7 Nitrogen sorption isotherms for protein-adsorbed core particles

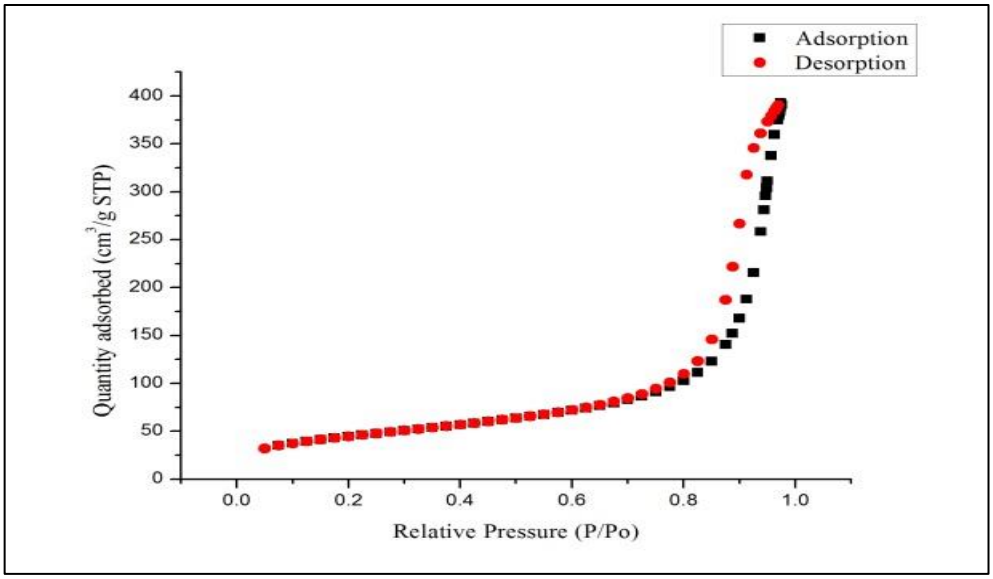

Figure 7.1S: Nitrogen sorption isotherm for protein-adsorbed S_{FP} particles

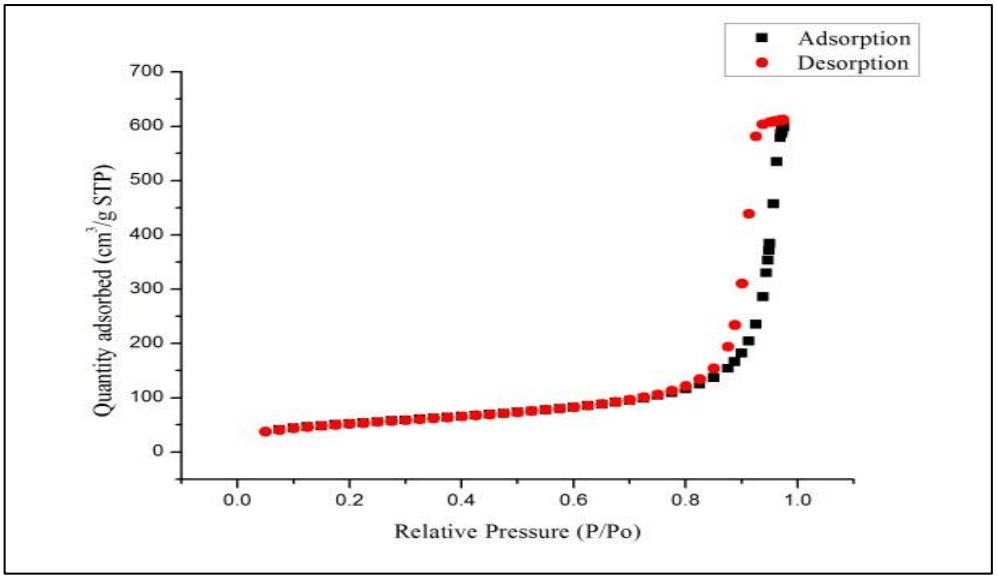

Figure 7.2S: Nitrogen sorption isotherm for protein-adsorbed S_{XDP} particles

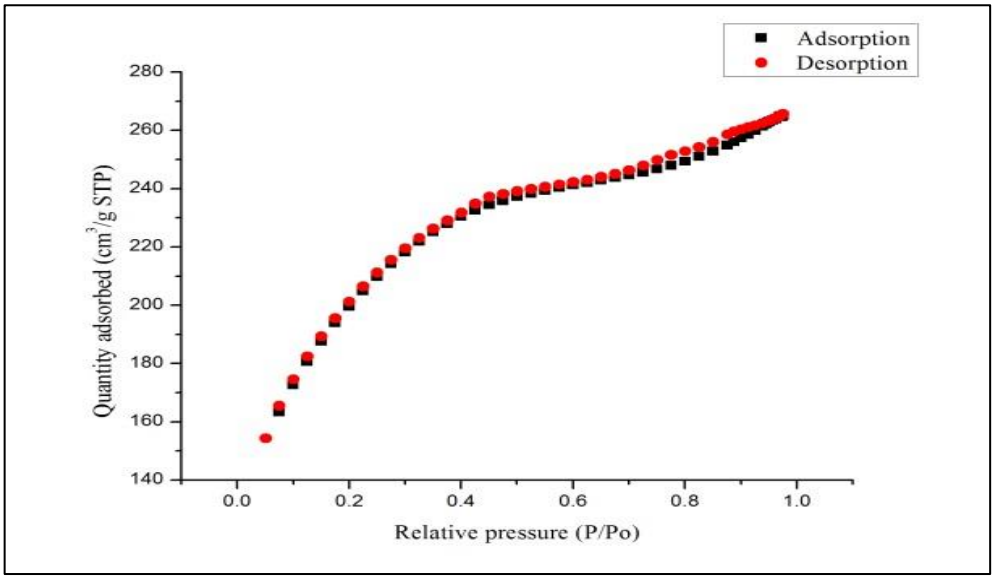

Figure 7.2S: Nitrogen sorption isotherm for protein-adsorbed S_{AL} particles

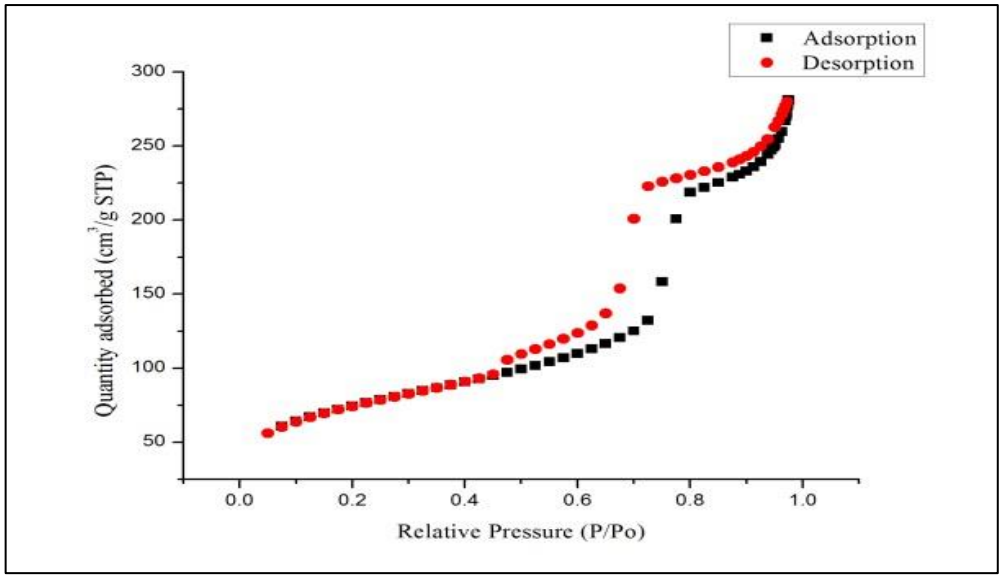

Figure 7.3S: Nitrogen sorption isotherm for protein-adsorbed MSU-H at 1 mg/ml

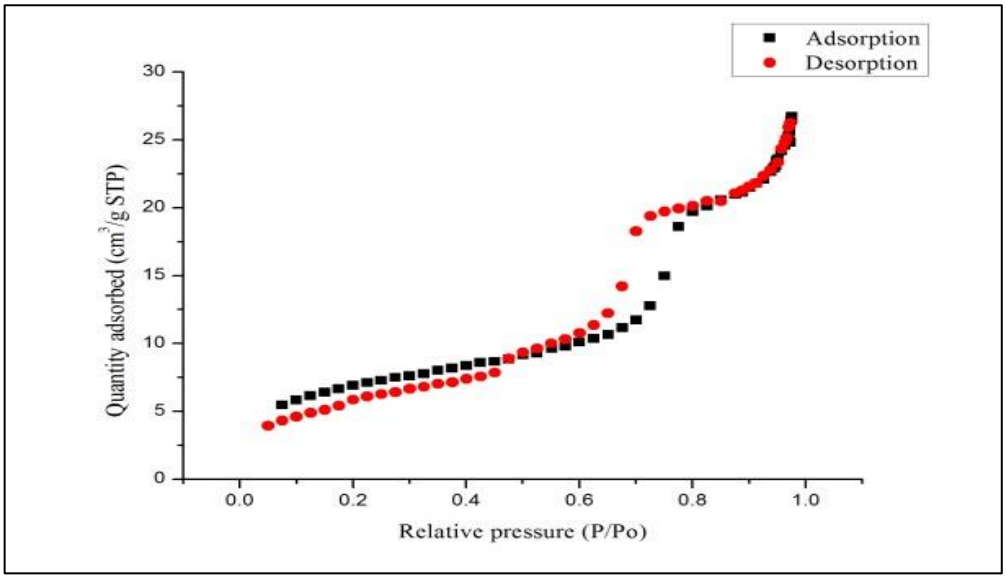

Figure 7.4S: Nitrogen sorption isotherm for protein-adsorbed MSU-H at 2 mg/ml

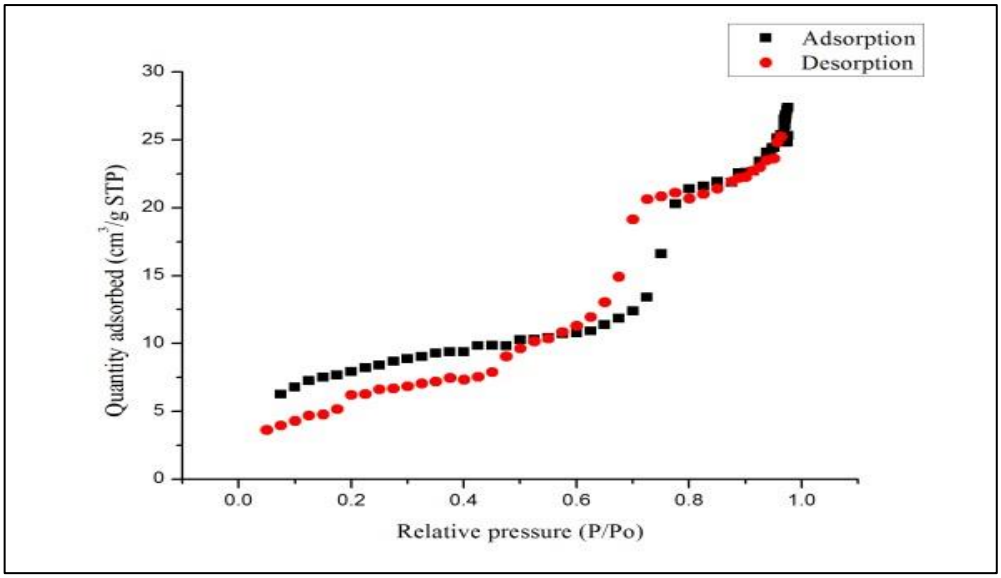

Figure 7.5S: Nitrogen sorption isotherm for protein-adsorbed MSU-H at 4 mg/ml

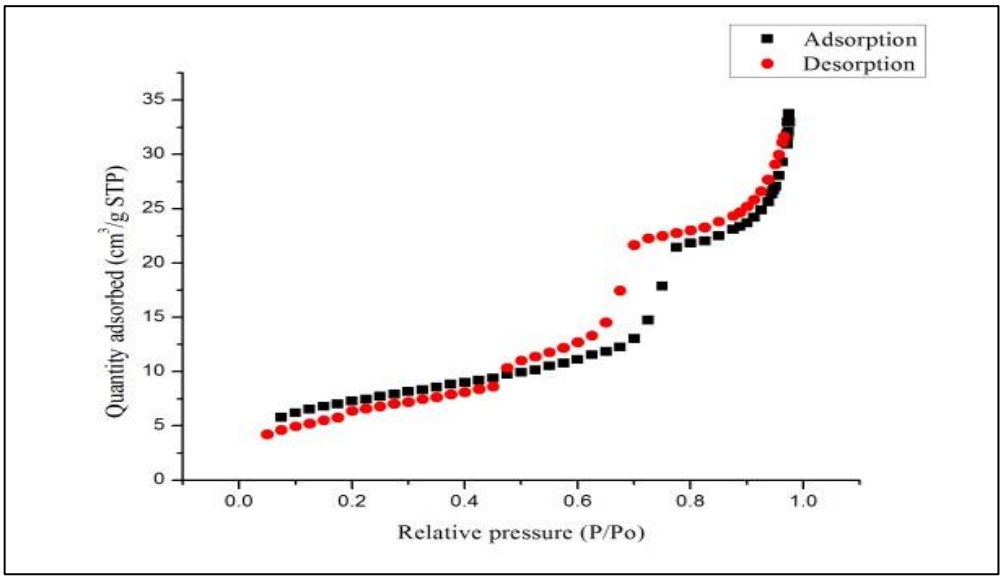

Figure 7.6S: Nitrogen sorption isotherm for protein-adsorbed MSU-H at 6 mg/ml

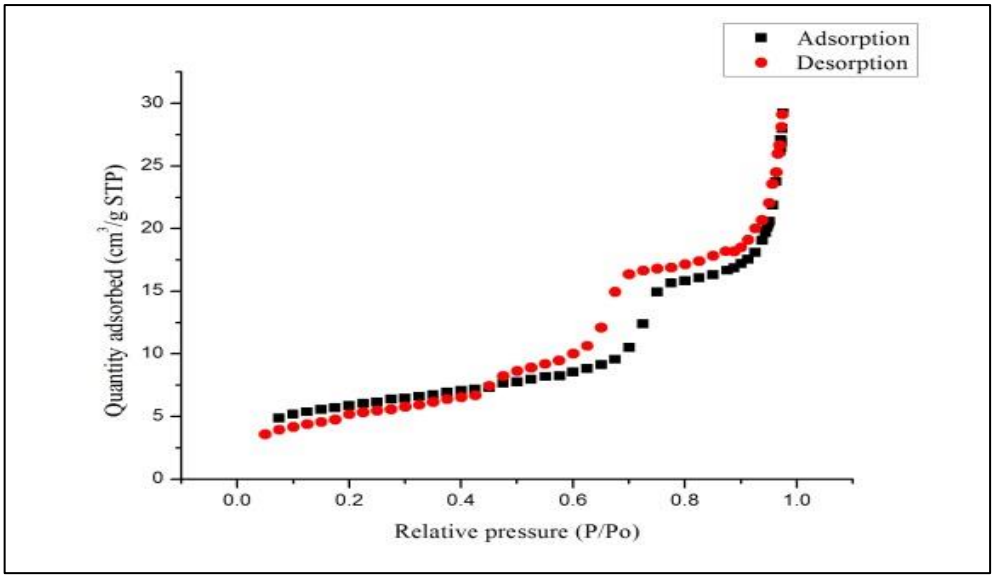

Figure 7.7S: Nitrogen sorption isotherm for protein-adsorbed MSU-H at 8 mg/ml

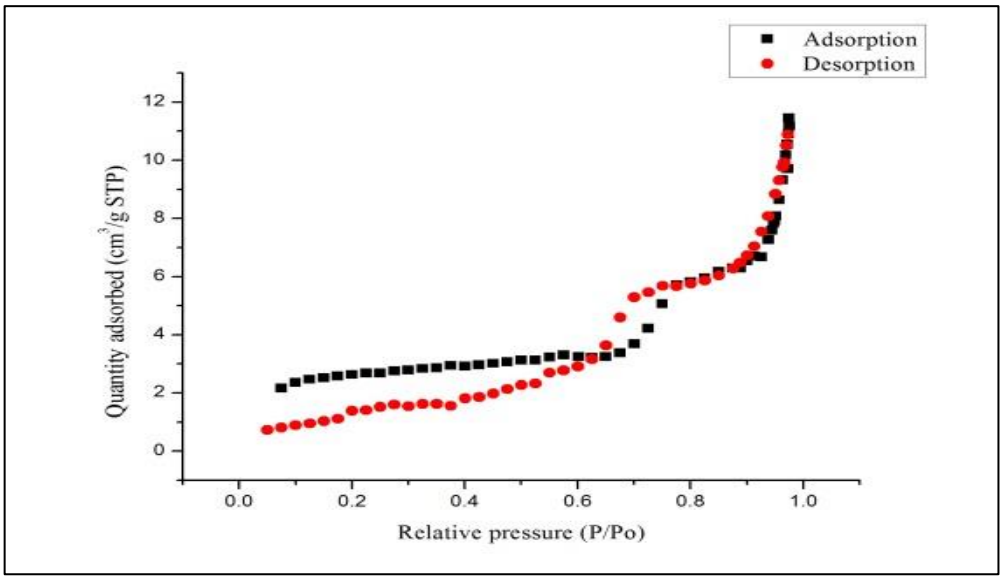

Figure 7.8S: Nitrogen sorption isotherm for protein-adsorbed MSU-H at 10 mg/ml

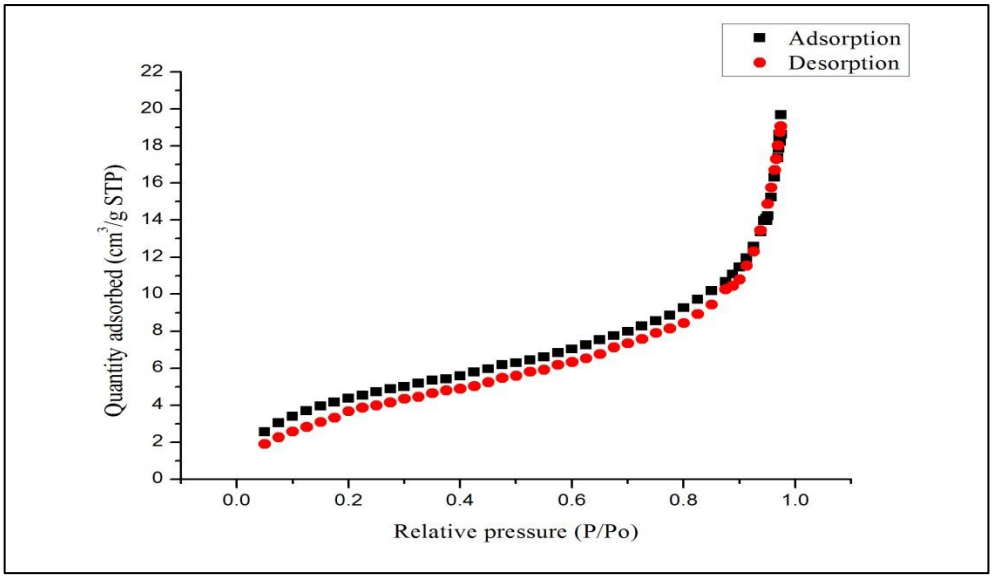

Figure 7.9S: Nitrogen sorption isotherms for protein-adsorbed PCL-ES100 particles

A.8 Surface charge analysis for protein-adsorbed silica

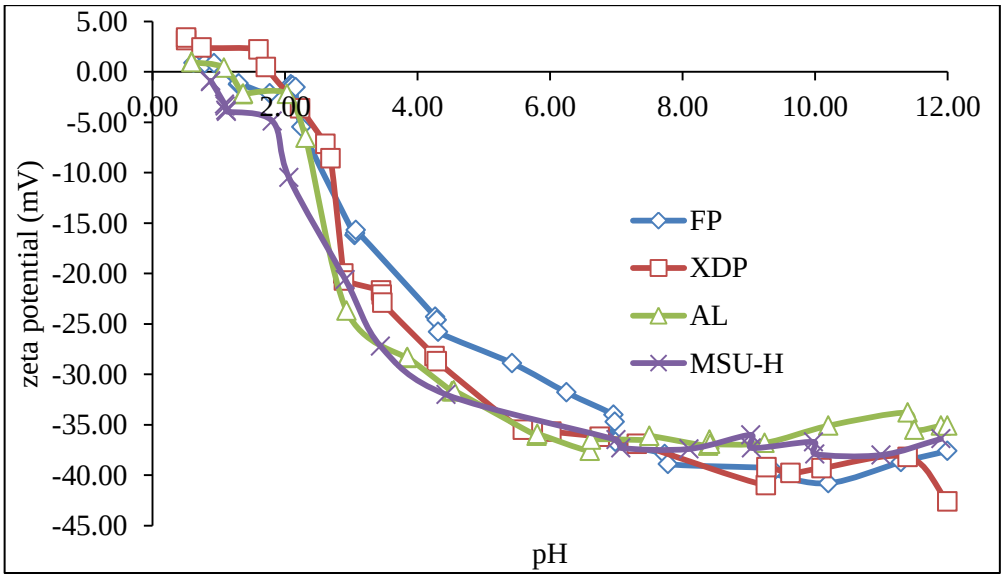

Figure 8.1S: Plot of zeta potential *vs* pH for untreated silica particles

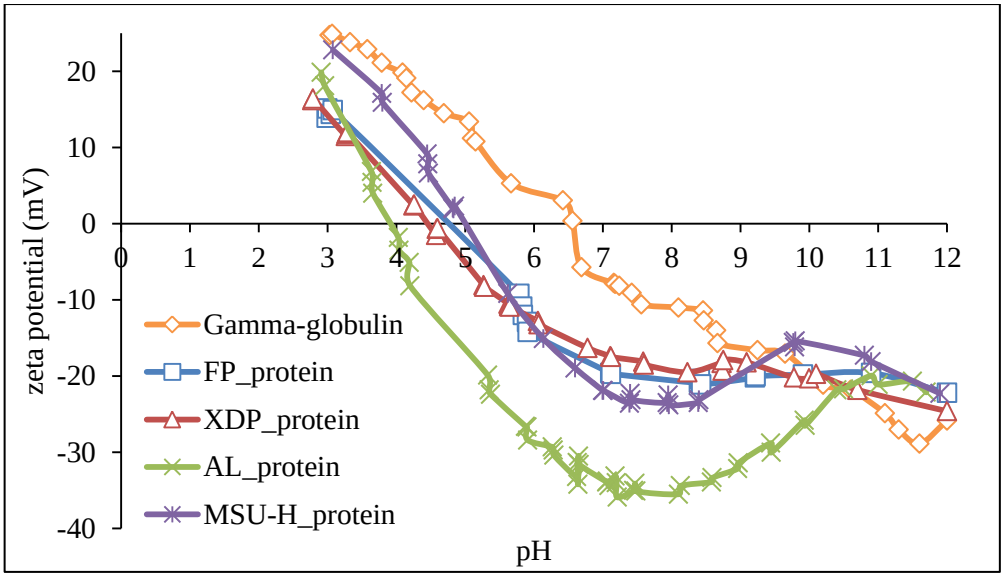

Figure 8.2S: Plot of zeta potential *vs* pH for protein-adsorbed silica particles

A.9 FTIR analysis for desorbed γ-globulin

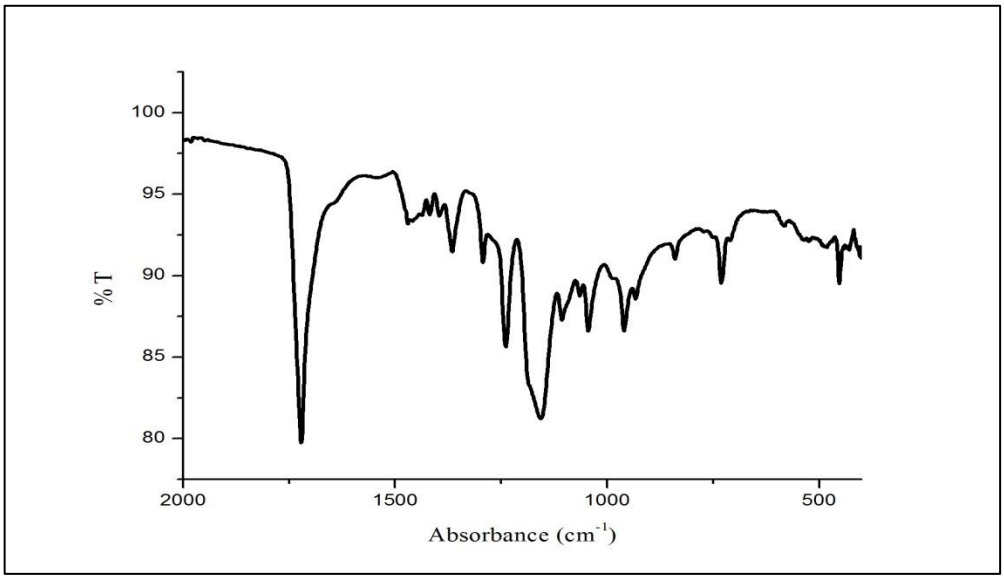

9.1S: FTIR spectra for protein adsorbed-PCL-ES100 (1:3)

A.10: CD analysis for desorbed protein

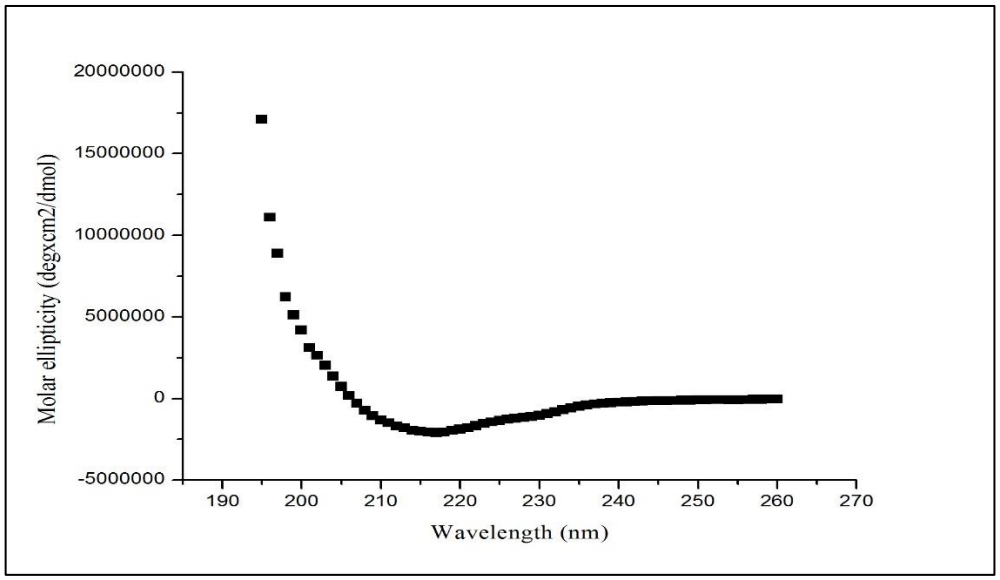

Figure 10.1S: CD spectra for desorbed γ-globulin from PCL-ES100

Drug Deliv. and Transl. Res.
DOI 10.1007/s13346-017-0422-3

ORIGINAL ARTICLE

Preparation of polycaprolactone nanoparticles via supercritical carbon dioxide extraction of emulsions

Adejumoke Lara Ajiboye[1] · Vivek Trivedi[1] · John C. Mitchell[1]

© The Author(s) 2017. This article is an open access publication

Abstract Polycaprolactone (PCL) nanoparticles were produced via supercritical fluid extraction of emulsions (SFEE) using supercritical carbon dioxide ($scCO_2$). The efficiency of the $scCO_2$ extraction was investigated and compared to that of solvent extraction at atmospheric pressure. The effects of process parameters including polymer concentration (0.6–10% *w*/*w* in acetone), surfactant concentration (0.07 and 0.14% *w*/*w*) and polymer-to-surfactant weight ratio (1:1–16:1 *w*/*w*) on the particle size and surface morphology were also investigated. Spherical PCL nanoparticles with mean particle sizes between 190 and 350 nm were obtained depending on the polymer concentration, which was the most important factor where increase in the particle size was directly related to total polymer content in the formulation. Nanoparticles produced were analysed using dynamic light scattering and scanning electron microscopy. The results indicated that SFEE can be applied for the preparation of PCL nanoparticles without agglomeration and in a comparatively short duration of only 1 h.

Keywords Solvent extraction · Polycaprolactone · Nanoparticles · Supercritical carbon dioxide · Supercritical fluid extraction of emulsions

Introduction

The use of drug delivery systems, particularly the micro- and nano-scale intelligent systems for therapeutic molecules has rapidly increased over the years because they can successfully maximise the efficacy of the drug molecules [1]. Nanoparticles are particles with a diameter range from 1 to 100 nm, even though the dynamic range can cover the whole nanometre scale [2]. As a drug delivery system, nanoparticles can entrap drugs or biomolecules into their internal structures and/or adsorb these drugs or biomolecules onto their external surfaces [3].

Due to their particle size, nanoparticles can move freely through the body via the smallest capillary vessels, cell and tissue gaps in order to reach their target organs [4]. These properties of nanoparticles help to modify the biodistribution and pharmacokinetic properties of the adsorbed/entrapped drug molecules leading to an improvement in the efficacy of the drug, decrease in unwanted side-effects and increase in patient compliance [5]. Nanoparticles can be prepared from inorganic or polymeric materials. Polymeric nanoparticles are more common and appropriate as they can be chemically modified to be biodegradable and biocompatible [6]. Biodegradable substances are broken down in vivo either enzymatically or non-enzymatically or both, to give rise to toxicologically safe by-products which are further removed by the normal metabolic pathways. The use of biodegradable polymers has greatly increased over the past decade, and they can generally be classified as either (1) synthetic biodegradable polymers which include relatively hydrophobic materials for example poly-lactic-co-glycolic acid (PLGA), polycaprolactone (PCL) and others, or (2) naturally occurring polymers such as chitosan, hyaluronan, etc. [7]. Principally, synthetic polymers have many inherent advantages since their structures can be manipulated to generate specialised carriers to suit particular applications [8].

PCL is a semi-crystalline polyester that is hydrophobic, biodegradable and biocompatible. When compared to other polymers, the biodegradation of PCL is slow; hence, it can

✉ Vivek Trivedi
V.Trivedi@greenwich.ac.uk

[1] Faculty of Engineering and Science, University of Greenwich, Central Avenue, Chatham Maritime, Kent ME4 4TB, UK

Published online: 21 August 2017